CELL-TYPE-SPECIFIC CONTRIBUTIONS OF THE TRANSCRIPTION FACTOR FOXP1 TO STRIATAL DEVELOPMENT AND FUNCTION

Ashley Grace Anderson

APPROVED BY SUPERVISORY COMMITTEE:

Said Kourrich, Ph.D. (Chair)

_____

Genevieve Konopka, Ph.D. (Mentor)

_____

Joseph Takahashi, Ph.D.

_____

Kimberly Huber, Ph.D.

_____

DEDICATION

First and foremost, I would like to thank my mentor Dr. Genevieve Konopka for being an exceptional scientific role model and for championing me even during my first years as a technician in her laboratory. She has helped guide my career with patience and invaluable insight while also allowing me the space to mature into an independent scientist. I am forever grateful for her mentorship. I would also like to thank my committee members for all their support and guidance.

This work is dedicated to the force of nature that was my grandmother, Elizabeth Jean Ozan Anderson. She was a pillar of strength for me, an inspiration, and her presence is missed every day. I also dedicate this work to my grandfather, Dr. Robert E. Anderson, an extraordinary grandpa and scientist. His not-so-subtle brainwashing, from giving me PH paper strips to play with as a toddler to working in his lab as a teenager, likely influenced my decision to become a scientist (correlation only). I would not be where I am now without the support from my grandparents and I owe them my deepest gratitude. Finally, I would like to dedicate this work to Dr. Grant Holland, the love of my life, and Mabel Anderson-Holland, the light of my life, for their unwavering support and love.

CELL-TYPE-SPECIFIC CONTRIBUTIONS OF THE TRANSCRIPTION FACTOR FOXP1 TO STRIATAL DEVELOPMENT AND FUNCTION

By

ASHLEY GRACE ANDERSON

DISSERTATION

Presented to the Faculty of the Graduate School of Biomedical Sciences at

The University of Texas Southwestern Medical Center

In Partial Fulfillment of the Requirements for the Degree of

DOCTOR OF PHILOSOPHY

The University of Texas Southwestern Medical Center

Dallas, Texas

August 2019

Copyright

By

Ashley Grace Anderson, 2019

All Rights Reserved

CELL-TYPE-SPECIFIC CONTRIBUTIONS OF THE TRANSCRIPTION FACTOR FOXP1 TO STRIATAL DEVELOPMENT AND FUNCTION

Publication No. _____

Ashley Grace Anderson, Ph.D.

The University of Texas Southwestern Medical Center, 2017

Supervising Professor: Genevieve Konopka, Ph.D.

ABSTRACT

Mutations in *FOXP1*, a member of the forkhead box protein (FOXP) family of transcription factors, have been identified as among the most significantly recurring *de novo* mutations associated with autism spectrum disorder (ASD). ASD is a genetically complex disorder, however, recent studies have identified distinct neuronal cell-types particularly vulnerable in this disorder. These cell-types include deep layer cortical neurons and dopamine receptor 1 (D1) and 2 (D2) expressing striatal spiny projection neurons (SPNs) where FOXP1 is highly expressed. However, the role of Foxp1 within these cell-types was largely unknown.

Using a *Foxp1* heterozygous mouse model and a human *in vitro* model system, I reported that FoxP1 regulates conserved pathways within the striatum based on a module preservation analysis between human and rodent gene co-expression networks. I also

found a cell-type-specific functional consequence of reduced Foxp1 expression in *Foxp1* heterozygous mice, whereby D2 SPNs had increased intrinsic excitability with no significant changes in dSPNs. Together, these data strongly support a conserved, cell-type-specific role for Foxp1 in striatal development and function.

The striatum is a critical forebrain structure for integrating cognitive, sensory, and motor information from diverse brain regions into meaningful behavioral output. Therefore, the overarching goal of my project is to investigate the cell-type specific molecular pathways regulated by Foxp1 within distinct striatal SPNs and link these molecular pathways to functional and behavioral outcomes. To do this, I generated mice with deletion of *Foxp1* from D1 SPNs, D2 SPNs, or both populations, and used a combination of single-cell RNA-sequencing (scRNA-seq), serial-two-photon tomography, and behavioral assays to delineate the contribution of Foxp1 to striatal development and function. I show that Foxp1 is crucial for maintaining the cellular composition of the striatum, especially D2 SPN specification, and proper formation of the striosome-matrix compartments at early postnatal and adult timepoints. I uncover downstream targets regulated by Foxp1 within D1 and D2 SPNs and connect these molecular findings to cell-type-specific deficits in motor and limbic system-associated behaviors, including motor-learning, ultrasonic vocalizations, and fear conditioning. Moreover, I identify non-cell autonomous molecular and functional effects produced by disruption of Foxp1 within one SPN subpopulation and the molecular compensation that occurs. Using the scRNA-seq data, I also examined gene expression changes within neuronal and non-neuronal cell-types of the developing striatum.

Using my above findings, I attempted to pharmacologically rescue motor-learning deficits in *Foxp1 cKO* mice by targeting dopaminergic and mTOR-regulated pathways. Finally, I discuss the current challenges and future strategies for therapeutic intervention in cases of *FOXP1* mutations. Overall, the findings presented in this thesis provide an important molecular window into striatal development and furthers our understanding of striatal circuits underlying ASD-relevant phenotypes.

TABLE OF CONTENTS

PRIOR PUBLICATIONS

1. **Anderson, A.G.,** Kulkarni, A., Harper, M., and Konopka, G. (2019). Single-cell analysis of Foxp1-driven mechanisms essential for striatal development. ***Under review***

2. Kulkarni, A., **Anderson, A.G.**, Merullo, D., Konopka, G. (2019) Beyond bulk: A review of single cell transcriptomics methodologies and applications. *Current Opinions in Biotechnology*, 58: 129-136.

3. Shimada, I.S, Somatilaka, B.N, Hwang, S., **Anderson, A.G.**, Shelton, J.M., Rajaram V., Konopka, G., Mukhopadhyay, S. (2019) Derepression of sonic hedgehog signaling upon Gpr161 deletion unravels forebrain and ventricular abnormalities. *Developmental Biology*, 450 (1):47-62

4. Araujo, D., Toriumi, K., Escamilla, C., Kulkarni, A., **Anderson, A.G.**, Harper, M., Usui, N., Birnbaum, S., Tucker, H., Powell, C., and Konopka, G. (2017). Foxp1 in forebrain pyramidal neurons controls gene expression required for spatial learning and synaptic plasticity. *J Neurosci.*, 37(45): 10917-10931.

5. Araujo, D.*, **Anderson, A.G.*** Berto, S., Runnels, W., Harper, M., Ammanuel, S., Reiger, M.A., Huang, H.C., Rajkovich, K., Tucker, H., Dougherty, J.D., Gibson, J.R., and Konopka, G. (2015). FoxP1 orchestration of ASD-relevant signaling pathways in the striatum. *Genes and Development*, 29(20): 2081-2096. **equal authorship contributions*

6. Ortega, S.B., Noorbhai, I., Poinsatte, K., Kong, X., **Anderson, A.G.**, Monson, N.L., and Stowe, A. (2015) Stroke induces a rapid adaptive autoimmune response to novel neuronal antigens. *Discovery Medicine* 19 (106): 381-392.

7. Lepp, S., **Anderson, A**., and Konopka, G. (2013) Connecting signaling pathways underlying communication to ASD vulnerability. *International Review of Neurobiology: Neurobiology of Autism* (Ed. G. Konopka), Elsevier: 113:97-133.

8. Li, F., Marchette, L.D., Brush, R.S., Elliott, M.H., Henry, K.A., **Anderson, A.G**., and Anderson, R.E. (2010). High levels of retinal docosahexaenoic acid do not protect photoreceptor degeneration in *VPP* transgenic mice. *Molecular Vision* 16:1669-79.

9. Li, F., Marchette, L.D., Brush, R.S., Elliott, M.H., Henry, K.A., **Anderson, A.G**., Zhao, C., Sun, X., Zhang, K., and Anderson, R.E. (2009). DHA does not protect *ELOVL4* transgenic mice from retinal degeneration. *Molecular Vision* 15:1185-1193.

LIST OF ABBREVIATIONS

ASD – autism spectrum disorder

ChIP-seq – chromatin immunoprecipitation sequencing

D1R – dopamine receptor 1 expressing cells

D2R – dopamine receptor 2 expressing cells

DEG – differentially expressed gene

dSPN – direct pathway spiny projection neuron

iSPN – indirect pathway spiny projection neuron

eSPN – eccentric spiny projection neuron

Foxp1^{CTL} – *Foxp1$^{loxP/loxP}$* (control, *Cre* negative mice)

Foxp1^{D1} – *Drd2$^{tg/-}$;Foxp1$^{loxP/loxP}$* mice (*Cre* positive)

Foxp1^{D2} – *Drd2$^{tg/-}$; Foxp1$^{loxP/loxP}$* mice (*Cre* positive)

Foxp1^{DD} – *Drd1$^{tg/-}$; Drd2$^{tg/-}$; Foxp1$^{loxP/loxP}$* mice (*Cre* positive)

FOXP – notation for human gene/transcript (e.g. *FOXP1*) or protein (e.g. FOXP1)

Foxp – notation for mouse gene/transcript (e.g. *Foxp1*) or protein (e.g. Foxp1)

FoxP – notation for multiple species gene/transcript (e.g. *FoxP1*) or protein (e.g. FoxP1)

GO – gene ontology

hNP – human neural progenitors

ID – intellectual disability

NDD – neurodevelopmental disorder

scRNA-seq – single-cell RNA-sequencing

SFARI – Simmons Foundation Autism Research Initiative

SPN – spiny projection neuron

STR – striatum

TF – transcription factor

CHAPTER 1: INTRODUCTION

PART I: THE FOXP FAMILY OF TRANSCRIPTION FACTORS

Discovery of the FOXP family

The Forkhead Box Binding Proteins 1-4 (FOXP1-4) belong to a subclass of an evolutionarily ancient family of forkhead box (FOX) transcriptional regulators characterized by a canonical forkhead or 'winged helix' DNA binding domain (DBD) (Clark et al., 1993; Hannenhalli and Kaestner, 2009). There are 19 classes of Fox proteins, categorized from FoxA to FoxS, with over 40 members within mammals (Hannenhalli and Kaestner, 2009). FOXP members share distinct sequence motifs including a zinc finger, leucine zipper, and forkhead DBD (Li et al., 2003; Shu et al., 2001; Wang et al., 2003). FOXP1, FOXP2, and FOXP4 are highly expressed within distinct regions of the central nervous system (CNS), unlike FOXP3 that shows limited expression in the CNS.

The FOX protein motif was first discovered in *D. melanogaster*, where mutations in the *fork head* (*fkh*) gene produced ectopic head structures in the foregut and hindgut of the drosophila embryo (Weigel et al., 1989). The authors found that *fkh* was a nuclear protein that bore no sequence similarity to known DNA-binding motifs (Weigel et al., 1989). Other studies in rat identified the *hepatocyte-enriched transcription factor HNF-3A* (known as *FOXA1*) in liver nuclear extracts (Costa et al., 1989). These authors then cloned and sequenced the *FOXA1* gene and showed that it bound DNA within a distinct region; however, the DNA-binding region was again unlike any other known DNA-binding motifs (Lai et al., 1990). Subsequently, *HNF-3A* was found to have a striking 92%

sequence similarity to the drosophila *fkh* within a ~110 amino acid DNA-binding region and termed forkhead binding proteins (Weigel and Jäckle, 1990).

Structure of the forkhead DNA-binding domain

The first high-resolution crystal structure of the forkhead DBD bound to DNA was of FOXA3 (Clark et al., 1993). The structural features of the forkhead DBD include two C-term "wings" or loop regions (W1 and W2), three α-helixes (H1, H2, and H3), and three β-sheets (S1, S3, and S3) (Clark et al., 1993). The third helix (H3) is flanked by two disordered polypeptide chains, W1 and W2, and these structures together encompass the 'winged helix' DNA-binding motif. H3 directly contacts the major groove of DNA while W1 and W2 bind substantially to the minor grooves (Cirillo and Zaret, 2007; Clark et al., 1993).

Multiple structures of the forkhead DBD within various Fox protein families have since been solved, including FOXD3, FOXK1, FOXP1, FOXP2, and FOXP3 (Chu et al., 2011; Cirillo and Zaret, 2007; Clark et al., 1993; Jin et al., 1999; Stroud et al., 2006; Tsai et al., 2006). Interestingly, the FOXP subclass contains a highly divergent forkhead DBD sequence and is located at the C-terminus of the protein instead of the N-terminus (Bandukwala et al., 2011; Lalmansingh et al., 2012; Li and Tucker, 1993; Stroud et al., 2006). The crystal structure of FOXP2 showed that the conventional FOX W1 was truncated and W2 contained a fifth α-helix (H5), which has also been observed in FOXD1 and FOXK1a but diverged noticeably in sequence (Stroud et al., 2006). Since the wing motifs in the FOXP subclass are shorter, they have limited contact with DNA and studies have found the FOXP forkhead DBD binds to DNA with lower affinity compared to other

FOX subclasses (Clark et al., 1993; Stroud et al., 2006). The forkhead DBD of FOXP1 shares high sequence identity with the forkhead domain in FOXP2, FOXP3, and FOXP4 (88%, 76%, and 89% respectively) (Chu et al., 2011). FOXP1 and FOXP2 also share the most full-length sequence similarity (~60%) spanning the two longest isoforms of both proteins amongst the FOXP subclass (Shu et al., 2001).

While most FOX proteins bind DNA as monomers, a unique structural feature of the FOXP subclass is the formation of domain-swapped dimers, where two monomers exchange α-helix H3 and β-strands S2 and S3 (Bandukwala et al., 2011; Stroud et al., 2006). The FOXP2 DBD structure further showed that FOXP2 existed in both monomeric and dimeric forms with a slow exchange rate. The property of domain-swapping in the FOXP subclass compared to other FOX proteins was found to be mediated by a highly conserved proline residue substituted to an alanine (P539A) residue in FOXP family members (Stroud et al., 2006). Another study using nuclear magnetic resonance spectroscopy (NMR) further confirmed this finding within the FOXP1 DBD. When the alanine in the FOXP1 DBD was switched back to proline (A539P), only monomers were formed in solution (Chu et al., 2011). The FOXP3 forkhead structure further revealed that FOXP3 can form stable domain-swapped dimers that can bridge DNA in the absence of co-factors (Bandukwala et al., 2011). This information lead to mechanistic insights into the gene regulatory mechanisms of the FOXP family, which found that FOXP members can mediate long-rage chromatin interactions to regulate gene expression (Bandukwala et al., 2011; Chen et al., 2015b; Stroud et al., 2006). In the full length FOXP-proteins, a conserved zinc finger/leucine zipper domain located ~50 residues N-terminal to the forkhead DBD is critical for dimerization and transcription activity of FOXP proteins (Wang

et al., 2003). These findings suggest that FOXP proteins have evolved unique properties with functional significance.

FOXP family members share the common FOX DNA binding core consensus sequences: 5'-RYMAAYA-3' (R=A/G; Y=C/T; M=A/C) (Stroud et al., 2006; Wang et al., 2003). Mouse Foxp1 was found to bind preferentially to a modified forkhead consensus sequence: 5'-TATTTRTRTT-3'. The leucine zipper (LZ) is an essential domain for mediating the homo- and heterodimerization of FOXP proteins, which is required for DNA-binding and the transcriptional activity of FOXP-proteins (Li et al., 2003; Shu et al., 2001; Wang et al., 2003). To a lesser extent, the zinc finger domain also regulates the transcriptional activation and dimerization ability of FOXP proteins (Li et al., 2003; Wang et al., 2003). While studies have shown the polyglutamine tract in FOXP proteins is not required for transcriptional activation, we still do not fully understand the functional properties of this domain. Polyglutamine tracts have been shown in other proteins to regulate protein-protein interactions that could alter selectivity and sensitivity of DNA-binding and FOXP2 has the longest naturally occurring polyglutamine tract within the human proteome (Hachigian et al., 2017).

When the FoxP class was first characterized, studies noted that several isoforms of Foxp1 and Foxp2 were expressed within a variety of different tissues and cell-types with different isoforms enriched in certain tissues (Shu et al., 2001). In whole brain tissue, three Foxp1 isoforms ranging in size were uncovered: Foxp1A (7.5kb), Foxp1B (3 kb), and Foxp1C (1.8 kb). The authors found higher levels of Foxp1A expression relative to the other Foxp1 isoforms specifically in heart and brain tissue (Shu et al., 2001). The longest isoform of Foxp2 was predominantly expressed in the brain compared to other

isoforms. The number of isoforms and expression patterns of Foxp1 and Foxp2 within tissues suggests a diversity of roles played by the Foxp family.

FOXP family association of with disease

The FOXP transcription factors are associated with several human developmental disorders and are known to regulate essential developmental processes within various organ systems, including the lung, heart, nervous and adaptive immune systems.

FOXP3 mutations and IPEX syndrome

Heterozygous mutations in *FOXP3* cause a rare, lethal syndrome called IPEX (immune-dysfunction, polyendocrinopathy, enteropathy, and X-linked inheritance) (Bennett and Ochs, 2001; Bennett et al., 2001). Most reported mutations in *FOXP3* disrupt the forkhead binding domain, however mutations outside the DBD have been found that disrupt known other domains, such as the leucine zipper and polyglutamine tract (Bacchetta et al., 2018; Ziegler, 2006). IPEX is primarily characterized by dysfunction of regulatory T_H1 lymphocytes (T_{regs}) causing immune dysregulation and multiorgan autoimmunity (Agakidis et al., 2019). Clinical presentations include severe diarrhea, eczema, type-1 diabetes, and thyroiditis with symptoms developing early in infancy and generally lethal within the first two years of life (Bacchetta et al., 2018).

Similarly, disruption of the murine *Foxp3* gene was found to be the genetic cause of the *scurfy* mouse phenotype (Brunkow et al., 2001). *Scurfy* mice are characterized by scaly and ruffled skin, reddened eyes, enlarged spleen and lymph nodes. These mice die prematurely at around postnatal (PN) day twenty-one (Brunkow et al., 2001). The *scurfy* mouse carries a 2-by insertion that results in a truncated Foxp3 protein that deletes the

forkhead DBD (Brunkow et al., 2001). FoxP3 is critical for thymus-derived T_{regs} cells and mutations in *Foxp3* leads to hyperproliferation of T_{regs} that cannot inhibit the production of cytokines thought to be responsible for the autoimmune damage in both IPEX and *scurfy* (Bacchetta et al., 2018). Mutations in human and mouse *FoxP3* show highly concordant phenotypes, indicating that FoxP3 likely regulates highly conserved pathways in the immune system. The role of Foxp3 within the brain has not been studied given its limited expression and will not be further discussed in subsequent sections.

FOXP2 mutations and verbal dyspraxia

FOXP2 was the first gene associated with a speech and language disorder in a large multigenerational family, termed the KE family (Lai et al., 2001). The first report describing the KE family classified the speech disorder of the affected family members as developmental verbal dyspraxia, which followed an autosomal dominant pattern of inheritance (Hurst et al., 1990). Affected family members were described as language-impaired rather than language-delayed and had extreme difficulty organizing and coordinating the high-speed movements required to produce intelligible speech (Hurst et al., 1990). Both the expression and comprehension of speech was delayed, with expressive language ability more severely affected. Problems with articulation and constructing grammatical sentences were also reported (Hurst et al., 1990). While affected members could position the tongue and lips properly for simple movements, they failed when a sequence of movements was required (Hurst et al., 1990). Comprehension was delayed in understanding comparative sentences (e.g “the knife is longer than the pencil” or “the girl is chased by the horse”) (Hurst et al., 1990). The affected family members did not have difficulties feeding as infants, few neonatal problems were

reported, and both hearing and intelligence quotient (IQ) were within the normal range (Hurst et al., 1990). In addition to confirming the above findings, another study found that affected KE family members had severe extralinguistic orofacial dyspraxia (Vargha-Khadem et al., 1995). Affected members performed significantly worse on tests assessing oral and facial movements (e.g., “bite your lip” or “close your left eye”) compared to non-affected members (Vargha-Khadem et al., 1995). Simultaneous or successive movements (e.g., closing the lips, then opening the mouth, then protruding the tongue) were more impaired than single movements in affected members (Vargha-Khadem et al., 1995). These studies emphasize that affected members have greater difficulty performing sequential orofacial movements (Hurst et al., 1990; Vargha-Khadem et al., 1995). While there was no IQ deficit of affected members when compared to the general population (Hurst et al., 1990), the affected members were behind unaffected members on both verbal and performance by 18-19 IQ points (Vargha-Khadem et al., 1995). Importantly, the KE affected members were still described as “sociable, amicable, and persevering in their efforts to be understood” (Watkins et al., 2002a).

The autosomal dominant inheritance pattern of the KE family’s speech disorder enabled researchers to map the responsible locus to a 5.6 cM interval of region 7q31 on chromosome 7 designated SPCH1 (Fisher et al., 1998). Additionally, a patient (CS) unrelated to the KE family with a similar speech and language disorder was found to have de novo translocation breakpoints within the SPCH1 locus (Lai et al., 2000). Subsequently, a missense mutation (R553H) in *FOXP2* was identified to be the causative mutation in the affected KE family members (Lai et al., 2001). This mutation resides in the forkhead domain within the highly conserved α-helix H3 that directly contacts DNA

and disrupts the DNA binding ability of FOXP2. Functionally, the R553H missense mutation disrupts the nuclear localization, DNA-binding ability, and transactivation capacity of FOXP2 (Vernes et al., 2006). These functional consequences were similar to another forkhead box protein, FOXC1, with a corresponding substitution (Saleem et al., 2003).

Early brain imaging studies of the KE family found bilateral regions with abnormal activity and grey matter density in affected members (Belton et al., 2003; Vargha-Khadem et al., 1998; Watkins et al., 2002b). The first study used positron electron tomography (PET) and magnetic resonance imaging (MRI) to examine difference in both brain activity and structure, respectively, between KE affect members and control subjects while participants repeated words heard over headphones (Vargha-Khadem et al., 1998). Though the PET scan analysis had low N (two KE affected members and four control subjects), they found that affected KE members had significantly underactive cortical regions in the left hemisphere relative to baseline (repetition of a specified word in response to hearing words reversed) that included the cingulate, sensorimotor, and middle temporal cortices (Vargha-Khadem et al., 1998). Overactive regions in KE affected members were also localized to the left hemisphere, which included the head and tail of the caudate nucleus, premotor, and ventral prefrontal cortical areas (Vargha-Khadem et al., 1998). A functional MRI study of the KE family a few years later (5 affected KE, 5 unaffected KE, and age-matched control participants) confirmed these differences in cortical and subcortical activity in affected members during both covert (responses were thought not spoken) and overt (responses were spoken) language tasks (Liégeois et al., 2003). This study measured brain regions activated during both covert and overt

language tasks and found the putamen (but not the caudate nucleus) consistently activated in control groups. Comparisons between control and affected KE members found the putamen consistently underactive during these tasks. Moreover, the authors found an increase in bilateral brain activity in affected members during language tasks, compared to strong left hemisphere activity in control language regions (Liégeois et al., 2003).

The KE affected members also showed changes in grey matter density across various cortical and subcortical regions. Of particular interest to this thesis, less grey matter was found in the right and left caudate nucleus, while more grey matter was found in both hemispheres of the lentiform nucleus, which includes both the putamen and globus pallidus (Vargha-Khadem et al., 1998). A subsequent MRI study from the same group with more subjects included in the analysis (6 affected KE members, 7 unaffected KE members, and 17 age-matched controls) confirmed the previous structural findings, whereby KE affected members had significant bilateral decrease in grey matter within the head of the caudate nucleus and an increase within the putamen (Watkins et al., 2002b). The reduction in volume of the caudate nucleus significantly correlated with the performance of affected KE members on oromotor control tests (Watkins et al., 2002b). This study also reported the first structural changes within the cerebellum of affected KE members (Watkins et al., 2002b). Interestingly, the striatum was the only region found to have both functional and structural differences within the KE affected members that correlated with their language impairments. These studies point to dysfunction of cortico-striatal circuitry as playing a prominent role in the both the orofacial and verbal dyspraxia of KE affected members.

Studies of the KE family were invaluable to our current understanding of the molecular mechanisms and circuitry underlying language ability at both the cognitive and motor-systems level. Many mutations across the *FOXP2* coding region have since been reported in individuals with verbal dyspraxia (Adegbola et al., 2015; Feuk et al., 2006; Laffin et al., 2012; Lennon et al., 2007; Moralli et al., 2015; Palka et al., 2012; Reuter et al., 2017; Rice et al., 2012; Shriberg et al., 2006; Tomblin et al., 2009; Turner et al., 2013; Zeesman et al., 2006; Zilina et al., 2012), including a *FOXP2* nonsense mutation (R328X) that co-segregated with speech deficits in a multiplex family (MacDermot et al., 2005). Additionally, de novo variants in *FOXP2* have also been implicated in autism spectrum disorder (ASD) (Satterstrom et al., 2018), in which a core phenotype is impairment in language/communication and social interaction. More recently, a genome wide association study (GWAS) study further implicated FOXP2 in attention-deficit/hyperactivity disorder (ADHD) (Demontis et al., 2019). Studies investigating the molecular and functional mechanisms regulated by FoxP2 across various model systems will be discussed in future sections.

FOXP1 mutations link to autism spectrum disorder and intellectual disability

Several years after the discovery of the KE mutation in *FOXP2*, reports identifying mutations in *FOXP1*, the closest paralogue of *FOXP2*, began surfacing in children with neurodevelopmental disorders (NDDs). In 2009, the first report linking a mutation in *FOXP1* to a neurodevelopmental disorder was found in a 23-month-old child with a *de novo* 785kb deletion of the 3p14.1p13 region (Pariani et al., 2009). This deletion encompassed 4 genes: 89% of *FOXP1* through the N-terminus and complete deletion of *EIF4E3*, *PROK2*, and *GPR27*. The child was developmentally delayed, speech delayed,

with muscle contractures, hypertonia, and eyelid abnormalities (Pariani et al., 2009). Early MRI and EEG studies before 17 months of age were normal. However, upon examination at 23 months, an MRI analysis found mild enlargement of the ventricles and sulci, which the authors noted was consistent with minor atrophy (Pariani et al., 2009). While this report implicated the deletion of *FOXP1* as the underlying cause of this disorder, several other genes were affected and therefore *FOXP1* could not directly be linked to the reported phenotypes.

A year later, three reports were published detailing mutations specifically affecting the *FOXP1* locus (Carr et al., 2010, Horn et al., 2010, Hamdan et al., 2010). The first report described a patient with a *de novo* ~1 Mb interstitial deletion of the 3p14.1 region that encompassed only *FOXP1* (Carr et al., 2010). Similar to the previous report (Pariani et al., 2009), gross motor skills and speech were delayed within this patient. An MRI at 26 months showed a dysmorphic corpus callosum, mild hypoplasia of the cerebellar vermis, and a Chiari I malformation (a herniation of the cerebellar tonsils into the foramen magnum) (Carr et al., 2010). The authors noted that Chiari I malformations could alter motor and speech development. Thus, while the previous study had genetic confounders, the Chiari I malformation in this patient confounded the interpretation of the *FOXP1* deletion on speech and motor development.

The next published study was the first to link mutations in *FOXP1* to intellectual disability (ID) (Horn et al., 2010). Gudrun Rappold and Tim Strom's group performed a study the examine the genetics underlying unexplained ID in a German cohort of 1523 unrelated patients. They performed a genome-wide microarray scan for copy number variations (CNVs) and found three overlapping deletions at chromosome 3p14.1 affecting

only the *FOXP1* gene in three unrelated individuals (Horn et al., 2010). Two of these deletions were confirmed to be *de novo*. Interestingly, all patients were speech delayed (first words at 3.5 years of age) and had poor speech articulation and dysgrammatism. Two patients had non-verbal, oromotor difficulties with lip protrusions. No MRI or EEG abnormalities were reported (Horn et al., 2010). To test for significance, the group also searched for CNVs within the *FOXP1* region in the Database of Genomic Variants (DGV) (Iafrate et al., 2004) and in 4104 ancestrally matched controls from various studies (Horn et al., 2010). They did find a 1.3 Mb deletion encompassing *FOXP1*, *EIF4E3*, *PROL2*, and *GPR27* in one individual from a control study. While this individual did not meet the criteria for mental retardation (IQ ranging 70-20), detailed clinical data was not available for further investigation. This report again confirmed previously described characteristics mutations in *FOXP1* could be linked to speech and language disorders.

The last report published in 2010 by Jaques Michaud and Guy Rouleau's group was the first to directly link mutations in *FOXP1* to ASD (Hamdan et al., 2010). The speech and language delays mentioned in the previous reports of patients with *FOXP1* mutations (Carr et al., 2010; Horn et al., 2010; Pariani et al., 2009) were exceedingly interesting given the sequence similarity of *FOXP1* to the well-established "language gene" *FOXP2* (Lai et al., 2001; Shu et al., 2001). However, no pathogenic mutations in *FOXP1* were found by sequencing individuals with developmental verbal dyspraxia (Vernes et al., 2009). Therefore, this study wanted to search for *FOXP1* mutations in other developmental disorders that are associated with language impairment, such as ASD and ID. The group searched for CNVs in patients diagnosed with ASD (n=80) and/or non-syndromic ID (NSID, n=30), as well as both parents, using genome-wide SNP arrays

(Hamdan et al., 2010). They also sequenced all the coding exons and intron-exon boundaries of the longest *FOXP1* isoform (*FOXP1A*) in 110 NSID, 84 ASD, and 51 NSID and ASD cases, as well as 570 controls (Hamdan et al., 2010). Two patients (patient A and patient B) with distinct *FOXP1* mutations were discovered. Patient A was diagnosed with NSID and had a *de novo* intragenic deletion of *FOXP1* that encompassed exons 4-14, including the translation initiation site, leucine zipper, and zinc finger domains. Patient B was diagnosed with both NSID and ASD and had *de novo* nonsense mutation (p.R525X) in *FOXP1* that abolished the last 152 amino acids, including part of the forkhead DBD and nuclear localization signal (Hamdan et al., 2010). Functionally, the p.R525X mutation disrupted the transcriptional repression ability of *FOXP1* in vitro (Hamdan et al., 2010). Both patients were developmentally delayed with severe expressive language impairments. Patient A could not clearly pronounce any word until age 3 and patient B said his first word at age 6, with no deficits in oromotor coordination. They both displayed significant behavioral problems, including irritability, impulsivity, mood lability, and physical aggression (Hamdan et al., 2010). These findings further implicated FOXP1 in regulating more global neurodevelopmental processes underlying cognitive ability, compared to the more selective language deficits seen with *FOXP2* mutations.

A whole exome sequencing study of sporadic ASD cases (n=20) and their parents found *de novo* mutations in several genes, including a single-base pair insertion in *FOXP1* that introduced a frameshift and premature stop codon (p.Ala339SerfsX4) (O'Roak et al., 2011a). The authors found this mutation caused nonsense-mediated decay (NMD) of the *FOXP1* transcript. Additionally, this proband carried an inherited *CNTNAP2* missense

variant at a highly conserved residue (p.His275Arg) predicted to be functionally disruptive. Clinically, this individual had a high ASD severity score and other comorbidities including language delay, moderate intellectual disability, and nonfebrile seizures (O'Roak et al., 2011a). This study was one of the first to demonstrate that *de novo* genetic disturbances may contribute significantly to the etiology of ASD.

Another study examined the presence of balanced chromosomal abnormalities (BCAs), such as inversions, excision/insertions, and translocation, genome-wide at nucleotide resolution in patients with neurodevelopmental disorders (NDD) (n=19,556 NDD cases, n=14,017 no clinical indication for NDD, n=13,991 control cases) (Talkowski et al., 2012). They found 5 individuals with *FOXP1* gene duplications and 1 individual with a deletion of *FOXP1*, all with either developmental delays or intellectual disability. This study was the first to identify a possible dosage increase of *FOXP1* (compared to the previously reported heterozygous deletions) as an underlying cause of the neurodevelopmental phenotype reported and they highlight that dosage sensitivity could be an important genetic mechanism underlying NDD.

Subsequently, several large-scale and high-throughput sequencing studies found that *de novo,* likely gene disrupting (LGD) mutations in *FOXP1* are among the most significantly recurrent mutations found in cohorts of individuals with ASD and/or ID/NDD (Coe et al., 2019; 2014; Iossifov et al., 2014; Stessman et al., 2017). A multi-group collaborative study led by Michael Wigler (Iossifov et al., 2014) used whole-exome sequencing of ~2800 families from the Simons Simplex Collection (SSC) (Fischbach and Lord, 2010) to uncover the contribution of *de novo* coding mutations in ASD (n=2,508 affected children, n=1,911 unaffected siblings and parents) (Iossifov et al., 2014). They

found that *FOXP1* was a the recurrently hit genes in the affected cohort. Two individuals with both ASD and ID carried LGD mutations in *FOXP1* (Iossifov et al., 2014).

Genetic studies from Evan Eichler's group have further confirmed that mutations in *FOXP1* are significantly linked to neurodevelopmental disorders (Coe et al., 2014; Stessman et al., 2017; Coe et al., 2019). The first study from the Eichler group combined both published and unpublished CNV datasets with single-nucleotide variant (SNV) data to construct a CNV morbidity map for detection of potentially causative genes underlying NDD in a large cohort of children (n=29,085) and healthy controls (n=19,584) (Coe et al., 2014). NDD affected children included diagnoses of ASD, ID, and/or developmental delay (DD). They found both CNV duplications (n=6), CNV deletions (n=2), and an LGD frameshift mutation in *FOXP1*. Importantly, CNV duplications (n=2), but not deletions, were also found in control cases (Coe et al., 2014). Two subsequent studies from the Eichler group examined the role of *de novo* mutations in protein-coding genes associated with NDDs using several high-throughput sequencing techniques (Coe et al., 2019; Stessman et al., 2017). In the first, they examined gene-disrupting mutations in NDD samples collected from an international consortium (>11,730 cases and >2,867 controls) by using single-molecule molecular inversion probes to sequence the coding and splicing portions of 208 potential NDD risk-genes identified from previous studies (Stessman et al., 2017). They found 68 genes that reached *de novo* significance for LGD mutations, including *FOXP1* (Stessman et al., 2017). Interestingly, the study also correlated a subset of these genes with clinical data from these individuals and found a strong negative correlation between genes associated with either ASD or ID, with *FOXP1* amongst those correlating strongly with ID.

In the latest study, the Eichler group performed a meta-analysis combining exome sequencing and CNV data from another NDD cohort (Turner et al., 2017b) and found that *FOXP1* was among the top genes to reach genome-wide significance for an excess of *de novo* LGD and missense mutations (Coe et al., 2019). Moreover, these significantly recurrently hit genes had cell-specific expression enrichments in distinct neuronal cell-types, including dopamine-receptor 1 (D1) and 2 (D2) spiny projection neurons (SPNs) of the striatum (Coe et al., 2019). Given the genetic and phenotypic heterogeneity of neurodevelopmental disorders, these large-scale genetic studies are critical for narrowing down commonly disrupted genes for future functional studies and ultimately therapeutic interventions.

Most recently, investigators from the Autism Sequencing Consortium (ASC) released a pre-print of the largest exome sequencing study to date (n=35,584) that examined *de novo* and case-control mutations in ASD (Satterstrom et al., 2018). Out of the 99 ASD risk-genes the authors found, *FOXP1* mutations were among the top 5 most significantly associated with ASD with a family-wise error rate (FWER) ≤ 0.05. Moreover, the authors reported that frequencies of *FOXP1* mutations were higher in subjects with severe neurodevelopmental delay compared to the other ASD-risk genes (Satterstrom et al., 2018). Together, these findings indicate that mutations in *FOXP1* affect broader neurodevelopmental pathways.

FOXP1 syndrome as a recognizable neurodevelopmental disorder

Distinctive neurodevelopmental phenotypes associated with mutations in *FOXP1* have emerged from the many subsequently published case-reports (Le Fevre et al., 2013; Mutlu-Albayrak and Karaer, 2019; Palumbo et al., 2013; Sollis et al., 2017; 2016; Song et

al., 2015; Thevenon et al., 2014; Urreizti et al., 2018; Vuillaume et al., 2018; Yamamoto-Shimojima et al., 2019). Two recent studies performed meta-analyses of both molecular and clinical data from individuals with *FOXP1* mutations and have described a recognizable “FOXP1 syndrome” (Meerschaut et al., 2017; Siper et al., 2017).

In the first study, the authors combined data from 25 new and 23 previously reported individuals with *FOXP1* mutations and correlated types of mutations (e.g., deletions/truncations vs missense) to distinct phenotypes (Meerschaut et al., 2017). The common neurological features they found across all cases were developmental delay (100%), neuromotor delay (95%), speech and language delay (100%), articulation problems or dysarthria (100%), and mild to moderate ID (96%). Autistic features were present in 75% of cases and behavioral problems, including hyperactivity, aggression, mood liability, and obsessive behaviors, in 69% (Meerschaut et al., 2017). When comparing the phenotypes of individuals with missense mutations or truncation of *FOXP1*, the authors found no significant differences in neurological features. The only feature significantly different between these cohorts was the higher prevalence of “prominent finger pads” within the cohort with missense mutations (Meerschaut et al., 2017).

In the second study, Joseph Buxbaum and Alexander Kolevzon’s group comprehensively examined clinical and genetic data from 9 individuals with *FOXP1*-specific mutations in a standardized environment in an effort to eliminate reporting bias (Siper et al., 2017). Similar to the first study, all individuals were developmentally delayed, displayed fine and gross motor coordination deficits, speech delay, poor articulation, and mild to moderate ID. These authors also noted the presence of visual-motor integration

deficits in all but one patient. While all of the individuals displayed ASD symptoms, only 25% of patients meet the official criteria for an ASD diagnoses. All patients had clinically significant ADHD symptoms of inattention, hyperactivity, and impulsivity with various degrees of severity. Deficits in expressive and receptive language skills, with more severe receptive language abilities, were found in every case (Siper et al., 2017). This conflicts with the first study that found expressive language ability more affected than receptive language ability (Meerschaut et al., 2017).

Combining reports from both studies, 61% of individuals with reported *FOXP1* mutations had brain imaging abnormalities (Meerschaut et al., 2017; Siper et al., 2017). Few shared structural abnormalities were observed across patients other than enlarged lateral ventricles or abnormalities around the ventricles (e.g., partial cavum septum pellucidum and diffuse periventricular leukomalacia). Other structural features ranged from cerebral/cerebellar atrophy, cortical and subcortical white matter abnormalities, to arachnoid cysts in the left hemisphere and cerebellum (Meerschaut et al., 2017; Siper et al., 2017).

While strongly linked to ASD in large-scale sequencing studies, the majority of individuals with *FOXP1* mutations are subthreshold for a DSM-5 ASD-diagnosis even though autistic features are always present. The core phenotypes associated with FOXP1 syndrome are broader than an ASD-diagnosis and include delays in motor and language milestones, mild to moderate ID, ASD symptoms, and ADHD traits such as anxiety, compulsive behaviors, attention deficits, and externalizing problems (Meerschaut et al., 2017; Siper et al., 2017). More comprehensive (e.g., larger N) studies of individuals with

FOXP1 mutations will be needed to further characterize the effects of different mutations on the phenotypic spectrum seen within the syndrome.

Of interest in this thesis is the overlapping phenotypes of *FOXP1* and *FOXP2* mutations that give rise to expressive and receptive language impairments, speech delay, and articulation problems. Previous studies have shown that FOXP1 and FOXP2 can heterodimerize to regulate transcriptional targets. This creates the interesting possibility that FOXP1 and FOXP2 could co-regulate molecular pathways underlying these shared phenotypes. In the next section, I will discuss the developmental expression pattern of FOXP1 and FOXP2 in the CNS to discern which brain regions and/or cell-types might be critical for mediating these co-regulated mechanisms. I will also review what is currently known about the functional consequences of manipulating FoxP1 and FoxP2 in the brain across various experimental systems.

FOXP4: a tentative association with developmental delay

In 2016, James Lupski's group from Baylor College of Medicine published a whole exome sequencing study of consanguineous Arab family and found 12 novel candidate disease genes, including a recessive mutation in *FOXP4* (Charng et al.). The affected child had a homozygous frameshift variant in *FOXP4*, but also carried two additional homozygous mutations in *LRRC1* and *ZNF514*. The child was developmentally delayed and had laryngeal hypoplasia, feeding problems, and ventricular septal defect (a hole in the heart). Additional studies identifying mutations in *FOXP4* will be needed to confirm this disease association.

Developmental expression of FOXPs in the CNS

The region- and cell-type specific expression patterns of FoxP1, FoxP2, and FoxP4 have been appreciated since the earliest studies characterizing the FoxP subclass (Lu et al., 2002; Shu et al., 2001). In mice, several studies examining the developing spinal cord and forebrain have noted the distinctive developmental patterning of these transcription factors (Dasen et al., 2008; Ferland et al., 2003a; Hisaoka et al., 2010; Pearson et al., 2018; Rousso et al., 2008; Takahashi et al., 2003; 2008; Tamura et al., 2004; 2003). Foxp proteins are first detected within the spinal cord where they follow a sequential expression pattern during motor neuron differentiation. Foxp2 and Foxp4 are expressed earliest at E8.5 followed by Foxp1 at E10.5 (Rousso et al., 2012). Each factor is enriched within distinct zones of the spinal cord with Foxp2 highly expressed in the neural progenitor (NP) rich ventricular zone (VZ), Foxp4 in the intermediate zone (IZ), and Foxp1 in the post-mitotic mantle zone (MZ) (Rousso et al., 2008).

Foxp1 expression in the murine forebrain begins at E12.5 within the lateral ganglionic eminence/striatum, cortical plate and layers II-VIa of the postnatal cortex, hippocampus, thalamus, deep cerebellar nuclei, superior colliculus, and inferior olive (Ferland et al., 2003a). Foxp2 expression is also detected at E12.5 in the lateral ganglionic eminence/striatum, subplate and layer VI of the postnatal cortex, Purkinje neurons of the cerebellum, olfactory bulb, amygdala, thalamus, hypothalamus, superior and inferior colliculus, substantia nigra, and inferior olive (Ferland et al., 2003a). Foxp1 is uniquely expressed in upper cortical layers and the hippocampus, whereas Foxp2 is uniquely enriched in Purkinje neurons of the cerebellum and distinct midbrain nuclei. In the rat developing forebrain, *Foxp4* expression overlaps with both *Foxp1* and *Foxp2*

within the cortex, LGE/striatum, thalamus, hippocampus, and Purkinje neurons of the cerebellum (Takahashi et al., 2003; 2008). In postnatal development, *Foxp4* expression in the striatum and cortex declines compared to *Foxp1* and *Foxp2* levels (Takahashi et al., 2008).

Murine and human *FoxP1*, *FoxP2,* and *FoxP4* have highly concordant expression patterns (Kang et al., 2011; Lai et al., 2003; Miller et al., 2014; Onorati et al., 2014; Vargha-Khadem et al., 2005). Using the human BrainSpan data (Miller et al., 2014), the expression of *FOXP1*, *FOXP2,* and *FOXP4* peaks embryonically across most brain regions (**Figure 1.1**). *FOXP4* expression peaks slightly earlier than *FOXP1* and *FOXP2* in human brain development (Kang et al., 2011; Miller et al., 2014). Compared to other *FOXP* members, *FOXP1* is more highly expressed in the striatum during fetal and post-natal development (**Figure 1.1**). *FOXP2* expression is highest throughout development in the thalamus and has the highest expression peak during fetal cerebellar development. *FOXP4* is highly expressed in the striatum and cerebellum during fetal development and *FOXP1* expression is maintained at higher levels than *FOXP2* postnatally in most regions except the thalamus (**Figure 1.1**).

One of the few brain regions where all *FOXP* transcription factors have shared, high expression is the developing and early postnatal striatum. The striatum is a critical region for both fine and gross motor control that is activated during human speech and language tasks (Liégeois et al., 2003). Since individuals with *FOXP1* or *FOXP2* mutations share certain phenotypes (e.g., deficits in expressive language abilities), understanding their role in the striatum could help illuminate common molecular pathways disrupted across both disorders. FOXP members can heterodimerize to regulate transcriptional

activity and a longstanding question in the field remains: what are the downstream targets regulated by either hetero- or homo-dimerization of FOXP family members? Studying the molecular pathways specifically in the striatum, a region with high FOXP expression overlap, might help the field begin to address this question (discussed in **Chapter 5**). The role of FoxP1 specifically within the striatum will be the primary focus of **Chapter 2-3** and I will discuss the potential compensation by Foxp2 or Foxp4 within this brain region in **Chapter 5**.

Cell-type specific expression of FOXPs in the forebrain

FoxP proteins are expressed in distinct and overlapping cellular populations with the forebrain. FoxP1 has the highest expression within the striatum relative to other brain regions (Precious et al., 2016) and, in mice, is one of the top most enriched genes (Heiman et al., 2008) (**Figure 1.2**). In situ hybridization (ISH) and immunohistochemistry (IHC) experiments have shown that expression of Foxp1, Foxp2, and Foxp4 are specific to spiny projection neurons (SPNs) and do not colocalize with known interneuron markers (Fong et al., 2018; Precious et al., 2016; Tamura et al., 2004). Single-cell RNA-sequencing (scRNA-seq) studies in the murine striatum have also confirmed the enrichment of *Foxp1*, *Foxp2*, and *Foxp4* in SPNs, not interneuron populations (Gokce et al., 2016; Saunders et al., 2018). I have also confirmed this at the transcript level in postnatal day 9 single-cell RNA-sequencing data, discussed further in **Chapters 2** and **3**. Several reports have found that *Foxp1* transcript is expressed in striatal microglia, however, Foxp1 protein has not yet been detected (see **Chapter 4**) (Saunders et al., 2018; Tang et al., 2012).

SPNs are classically divided into two distinct subtypes: SPNs expressing dopamine receptor 1 (D1) that project along the direct pathway (dSPNs) and dopamine receptor 2 (D2) that project along the indirect pathway (iSPNs). Striatal cell-type composition and circuitry is discussed in detail in **Chapter 1: Part II**. IHC and scRNA-seq studies have found that Foxp2 is more enriched within dSPNs compared to iSPNs, while Foxp1 is highly expressed in both subtypes (Saunders et al., 2018; Vernes et al., 2011). *Foxp4* expression is low in the postnatal striatum (**Figure 1.2**) and might be more specific to sparse, non-canonical SPNs, such as "eccentric" SPNs (eSPNs, discussed further in **Chapter 3**) (Saunders et al., 2018; Takahashi et al., 2008). Comparing the expression profiles of the canonical SPN subtype markers (*DRD1* and *DRD2*) with the FOXP family across human developmental timepoints, we see that *FOXP1* and *FOXP2* peak before *DRD1* and *DRD2* (8-13 pcw) expression and that these genes follow a similar co-expression pattern over development (**Figure 1.2**). Relative to the other gene expression profiles, *FOXP4* follows an almost opposite expression pattern (e.g., decreasing between 8-12 pcw) (**Figure 1.2**). Interestingly, *FOXP2* expression peaks before *DRD1* expression and *FOXP1* expression peaks before *DRD2* expression. I will further discuss the relationship between FoxP2 and DRD1 in a subsequent section and the critical role that *FOXP1* plays in striatal development, particularly of D2 SPNs in **Chapters 3** and **4**.

In the cortex, FoxP proteins in both human and mouse are confined to excitatory projection neurons in layer-specific clusters and absent from interneuron populations. In the hippocampus, *Foxp1* is highly enriched in the pyramidal cell layer of the CA1/2 and subiculum (**Figure 1. 3**). While *Foxp1* transcript has also been detected in the dentate

gyrus (DG), no Foxp protein expression has been detected (Araujo et al., 2017; Ferland et al., 2003a; Saunders et al., 2018). *Foxp4* is lowly expressed in both CA1/2 and the subiculum and Foxp2 is expressed sparsely within the subiculum (Ferland et al., 2003a; Saunders et al., 2018). CA1 pyramidal cells densely project to the subiculum, which in turn projects to many different brain regions including thalamic nuclei, prefrontal cortex, nucleus accumbens, and amygdala. The subiculum is therefore described as the "heart" of the extended hippocampal system (Aggleton and Christiansen, 2015). Hippocampal scRNA-seq data from Nelson Spruston's lab (Cembrowski et al., 2018; 2016) shows that *Foxp1* is expressed in subiculum neurons that project to three regions they profiled: the nucleus accumbens, amygdala, and prefrontal cortex. *Foxp2* and *Foxp4* are enriched in a rare excitatory subtype in the subiculum located in the deepest layer of cells across the long axis of the hippocampus that did not send projections to those profiled regions. The authors suggest this population might correspond to local excitatory neurons or project to other regions (Cembrowski et al., 2018).

Foxp4 in the CNS

Studies examining the role of Foxp4 in neurodevelopment have been few compared to Foxp1 and Foxp2. *Foxp4* KO^{neo} strains were first generated by Edward Morrissey's lab in 2004 by replacing exons 12-13 with a neomycin cassette (Li et al., 2004b). These mice died embryonically at E12.5 due to severe cardiac defects, earlier than *Foxp1* KO. Subsequently, *Foxp4* conditional KO mice were developed in collaboration with the Morrisey lab and used to study the effects of *Foxp4* deletion during lung and immune system development (Li et al., 2012; Wiehagen et al., 2012).

Currently, two studies have examined the role of Foxp4 in neurodevelopment (Rousso et al., 2012; Tam et al., 2011). The first examined the role of Foxp4 in cerebellar development. They found Foxp4 expression in the developing and mature cerebellum beginning at E12.5 in the subventricular zone of the cerebellum primordium and in migrating and mature Purkinje cells (PCs). siRNA silencing of *Foxp4* in organotypic cerebellar slices at P10, a phase of rapid dendritic growth in PCs, significantly reduced the dendritic arborization of PCs and Bergmann glial fibers, which are important for guiding PC dendritic development. *Foxp2* knockdown in cerebellar slices and *in vivo* within the mouse cerebellum produced similar PC arborization defects (French et al., 2007; Fujita et al., 2008; Shu et al., 2005; Usui et al., 2017b). This suggests that both *Foxp2* and *Foxp4* co-regulate molecular pathways important for PC development.

The second study from Bennett Novitch's lab used two *Foxp4* KO mouse strains to examine the role of *Foxp4* in neural tube and forebrain development (Rousso et al., 2012). They used previously published *Foxp4* KO^{neo} mice (Li et al., 2004b) and another strain that carries a LacZ-stop cassette between exons 5-6, *Foxp4* KO^{LacZ}. Both strains were embryonic lethal between embryonic day 10.5 and 12.5. The authors found that both *Foxp4* null strains resulted in gross neural tube defects, holoprosencephaly, spina bifida, and occasionally notochord and floor plate duplications (Rousso et al., 2012). The study also found that Foxp4 was important for repressing N-cadherin-based adherens junction components that form between neighboring neural progenitor cells (NPCs). Furthermore, they showed that both Foxp2 and Foxp4 act in opposition to NPC maintenance transcription factor, Sox2, to promote neural differentiation (Rousso et al., 2012).

Both studies indicate that Foxp2 and Foxp4 regulate common pathways in regions where they share overlapping expression. An important future study will be finding the transcriptional targets regulated by Foxp4 in distinct brain regions or cell-types and examining brain-specific deficits using the conditional *Foxp4* strain.

Foxp2 in the CNS

Foxp2 knockout and mutant mice display altered vocal behavior

The link between FOXP2 and verbal dyspraxia was the first molecular clue towards understanding human language development. Since its discovery, researchers have been studying the functional role of FoxP2 in multiple species and experimental systems. Several *Foxp2* deletion or mutation mouse models and knockdown studies in songbirds have shown that Foxp2 regulates aspects of vocal behaviors in multiple species. In 2005, the Buxbaum lab published the first *Foxp2* KO mouse using a construct that replaced forkhead DNA binding exons 12-13 with a neomycin cassette (Shu et al., 2005). They found that homozygous mutants died postnatally around 3 weeks of age (~P21) and had severe cerebellar morphological defects. They also found that both the heterozygous (*Foxp2*$^{+/-}$) and homozygous *Foxp2* mutants produced fewer pup ultrasonic vocalizations (USVs) and exhibited motor behavior deficits, as measure by the righting reflex. Furthermore, they tested learning and memory using the *Foxp2*$^{+/-}$ mice and found no deficits in Morris water maze performance. In another study, the vocal behavior of the same *Foxp2*$^{+/-}$ mice was assessed over juvenile and adult development and they found that *Foxp2*$^{+/-}$ mice vocalized less, produced shorter and abnormal syllables, and did not

follow the same developmental trajectory as *Foxp2*$^{+/+}$ (WT) vocalizations (Castellucci et al., 2016).

Simon Fisher's lab first developed two mouse strains carrying patient-relevant *Foxp2* mutations produced using an ENU mutagenesis screen (Groszer et al., 2008): 1) *Foxp2-R552H* strain harboring an equivalent KE mutation, arginine to histidine mutation within the DNA-binding domain, and 2) *Foxp2-S321X* strain containing a premature stop codon similar to the human R328X nonsense mutation found in a second family with a segregating FOXP2 mutation (MacDermot et al., 2005). *Foxp2-R552H* mice produced Foxp2 transcript and protein, however *Foxp2-S321X* mice produce no detectable Foxp2 protein effectively producing a null allele. Both mouse strains produced abnormal pup USVs, however these pups could produce multiple call types with complex structures which suggests the underlying neural mechanisms to produce speech are still intact (Gaub et al., 2010).

Aberrant striatal activity and motor-behavior with Foxp2 mutations

Studies from several labs have shown that Foxp2 is critical for motor-learning. *Foxp2-R552H* heterozygous mice (*Foxp2*$^{R552H/+}$) have deficits on the accelerating rotarod paradigm (French et al., 2012; Groszer et al., 2008) and have increased striatal firing activity freely behaving animals (French et al., 2012). Moreover, during a running task, negative modulation of striatal activity was observed in *Foxp2*$^{R552H/+}$ mice compared to control animals that exhibit an increase firing activity during this motor task. (French et al., 2012). Interestingly, a striatal-specific *Foxp2 cKO* mouse did not have overt motor-learning deficits on the rotarod, but displayed subtle deficits in lever pressing and ladder crossing (French et al., 2019).

Foxp2 is known to be enriched in dSPNs (Heiman et al., 2008; Saunders et al., 2018; Vernes et al., 2011). In songbird, FoxP2 regulates the expression of both D1R and Darpp32 expression, while also modulating songs through D1R-specific pathways (Murugan et al., 2013). However, in rodents, no cell-type specific manipulation of Foxp2 in dSPNs or examination of dSPNs specifically within *Foxp2* mutant or *KO* systems has been reported. An important future direction will be to fully characterize the cell-type specific role of Foxp2 in striatal SPNs. In **Chapter 3**, I discuss the striatal cell-type expression of Foxp2 in SPNs and the role Foxp2 might play in compensating for loss of Foxp1 in dSPNs.

Foxp1 in the CNS

Generation of Foxp1 knockout and conditional knockout mice

In 2004, the Tucker lab at UT Austin generated and characterized the first *Foxp1* knockout (KO) strain (Wang et al., 2004). The targeting construct used for homologous recombination in ES cells replaced exons encoding the forkhead DNA-binding domain (exons 12-14) with a neomycin selection cassette. The authors found that complete loss of *Foxp1* led to embryonic lethality at E14.5 due to cardiac failure. Interestingly, the authors found that embryonic age of lethality depended on the mouse strain, where 92% of *Foxp1*$^{-/-}$ mice on a pure C57BL/6 background died by E18.5, but only 59% *Foxp1*$^{-/-}$ on a C57BL6/129SV background died by E18.5. This suggested the penetrance of the cardiac defects underlying *Foxp1*$^{-/-}$ lethality were regulated by strain-specific modifier genes (Wang et al., 2004). Importantly, all *Foxp1* mouse experiments presented in **Chapters 2-4** are backcrossed several generations to C57BL/6J mice. Another group, in

collaboration with Dr. Tucker, generated a second *Foxp1* KO mouse to study the role of Foxp1 in B-cell development (Hu et al., 2006). This *Foxp1* targeting construct was designed to replace the N-terminal two thirds of the Foxp1 gene (exons 2-13), including the entire forkhead binding domain, with a lacZ and neomycin cassette (Hu et al., 2006). These *Foxp1* KO mice are used for experiments in **Chapter 2** where I characterize the molecular and behavioral phenotypes of *Foxp1* heterozygous (*Foxp1*$^{+/-}$) mice.

Several years later, another Tucker lab collaboration generated a conditional *Foxp1* mouse strain (Feng et al., 2010a). The construct was designed to insert loxP sites flanking exons 11-12 that encompass the DNA-binding domain and Frt sites flanking a pgk-neomycin cassette. This targeting strategy produced 2-site-specific *in vivo* recombination events: 1) Flp recombinase to delete the neomycin cassette from the germline and 2) Cre-recombinase to delete exons 11-12 (Feng et al., 2010a). Given the embryonic lethality of *Foxp1* KO mice, generation of the *Foxp1* conditional knockout (cKO) strain has been essential for studying the role of *Foxp1* in postnatal development. This *Foxp1 cKO* strain has been used to examine the role of Foxp1 in the CNS in several papers from our lab and others. In **Chapter 3**, I use this *Foxp1 cKO* line to characterize the role of Foxp1 in striatal projection neurons.

Characterization of brain-specific Foxp1 cKO mice

In 2014, Gudrun Rappold's lab published the first study characterizing a brain-specific *Foxp1* KO mouse (Bacon et al., 2015a). Preceding this study, Foxp1 had only been studied *in vivo* within a Huntington's disease (HD) mouse model or the spinal cord. A human FOXP1 construct was overexpressed in the striatum of an HD mouse strain and a microarray analysis found that differentially expressed genes were involved in

neuroinflammatory pathways (Tang et al., 2012). In the spinal cord, Foxp1 was shown to regulate Hox-protein and projection patterning of distinct spinal motor neurons (Rousso et al., 2008).

To achieve brain-wide deletion of *Foxp1*, the Rappold group used a *Nestin-Cre* transgenic strain crossed to *Foxp1 cKO* mice (*Nestin-Foxp1 cKO*) (Feng et al., 2010a). The most striking morphological features of the *Nestin-Foxp1 cKO* brain were a significant decrease in striatal area and enlarged lateral ventricles (Bacon et al., 2015a). They performed a microarray analysis on control and *Nestin-Foxp1 cKO* striatal tissue at P1 and found 85 significant differentially regulated genes (DEGs) (61 upregulated and 24 downregulated) that were enriched in pathways such as nucleosome, chromatin assembly, and DNA replication. They also found that E15 primary striatal neurons cultured from *Nestin-Foxp1 cKO* samples formed more elaborate dendritic arborization that controls. Hippocampal morphology and electrophysiology were also disrupted in *Nestin-Foxp1 cKO* mice. Neurons within the CA1 region were less densely packed and CA1 neurons (P21) had a reduced firing rate and increase spontaneous miniature excitatory postsynaptic currents (mEPSCs). No change in input resistance, capacitance, paired-pulse ratio, or long-term potential at the Shaffer collateral CA2 synapses were observed. They found that apical dendrites clustered in closer proximity to the soma in *Nestin-Foxp1 cKO* CA1 neurons and basal dendrite and total dendritic length was not affected (Bacon et al., 2015a). The authors did not examine the electrophysiological properties of striatal spiny projection neurons.

Nestin-Foxp1 cKO mice also exhibited disease-relevant behaviors (Bacon et al., 2015a). They were hyperactive in the open field, with increased repetitive behaviors as

scored by jumping and wall scrabbling. They exhibited impaired short-term memory in novel object and novel object location tasks and had impaired social interactions as measured by anogenital exploration, approach/following, and social retreat. Deficits in nest building behavior were also observed in *Nestin-Foxp1 cKO* mice, where *cKO* mice made no attempt at building a nest with the provided material. Sensorimotor gating as measured by the startle response in the pre-pulse inhibition (PPI) test was significantly decreased in *Nestin-Foxp1 cKO* animals. Rappold's group also examined vocalization behavior of *Nestin-Foxp1 cKO* mice and found they had significantly reduced pup ultrasonic vocalizations (USVs) (Fröhlich et al., 2017). Importantly, the authors found that heterozygous *Nestin-Foxp1* mice were not significantly different from controls in all behaviors tested. We found that full body *Foxp1* heterozygous animals displayed certain overlapping behavioral deficits, such as hyperactivity and altered pup USVs (described in **Chapter 2**). These findings present the interesting question of whether the timing of *Foxp1* deletion and/or the role of Foxp1 in regions outside the brain might contribute to these behavioral phenotypes.

Cortical and hippocampal role of Foxp1

The *Nestin-Foxp1 cKO* study established that Foxp1 is a critical regulator of global brain development and ASD-relevant behaviors. However, in which brain regions and cell-types could Foxp1 be regulating these behaviors? And what downstream molecular pathways are altered in a region or cell-type specific way? To begin examining the role of Foxp1 in a region specific way, Xue Li et al. performed knockdown (KD) experiments by electroporating *Foxp1* or scrambled shRNAs with a reporter construct to label transfected neurons at E14.5 into the somatosensory cortex (Li et al., 2015). They found that

knockdown of *Foxp1* in the cortex caused an accumulation of electroporated cells in the intermediate zone (IZ) and fewer cells in the cortical plate (CP) at E17.5, indicating that Foxp1 regulates the radial migration of cortical neurons. The authors found a similar phenotype at early postnatal timepoints (P2, P4, P7, and P14) and that overexpressing Foxp1 rescued the migration phenotype. *Foxp1* KD also reduces the polarity of newborn neurons, which likely contributes to radial migration defects. *Foxp1* KD neurons did not alter cell division, neural progenitor specification, and neuronal differentiation. Moreover, this study found that *Foxp1* KD reduced axonal and dendritic growth of cortical neurons *in vitro* (Li et al., 2015).

Noriyoshi Usui and Daniel Araujo from the Konopka lab further investigated the region-specific role of Foxp1 in the brain by characterizing mice with neocortical and hippocampal deletion of *Foxp1* (Araujo et al., 2017; Usui et al., 2017a). Using the *Emx1-Cre* driver line (Gorski et al., 2002), Foxp1 was completely deleted from both forebrain regions, further evidence that Foxp1 expression is restricted to excitatory neuronal populations. Usui et al. found that *Emx1-Foxp1 cKO* mice produced fewer postnatal ultrasonic vocalizations and had defects in cortical lamination. Lower cortical layer 6 (Foxp2+ layer) thickness decreased while upper layer thickness (Cux1+) increased in *Foxp1 cKO* mice. Ectopic upper layer cells (Cux1+) were also found in layers 5-6 (Usui et al., 2017a). Using bulk RNA-sequencing, they uncovered molecular targets of Foxp1 in the neocortex at postnatal day 1 and 7 (Araujo et al., 2017; Usui et al., 2017a). Many of the differentially expressed genes shared at both timepoints are associated with the synapse and synaptic transmission. Moreover, both up and down regulated targets were enriched for ASD-associated genes (Usui et al., 2017a).

Another study from the Konopka lab examined *Emx1-Foxp1* cKO mice at adult timepoints and found severe impairments in autism and intellectual-disability-relevant behaviors (Araujo et al., 2017) (see **Appendix B**). These mice had deficits in adult vocalizations, where male mice produced fewer courtship calls that were shorter in length and less complex when exposed to a female mouse. Social interaction was also impaired during a juvenile social interaction paradigm. *Foxp1* cKO mice spent less time in the interaction zone with the unfamiliar mouse compared to controls. Nest building was also disrupted in *Emx1-Foxp1* cKO mice. These social deficits notably overlap with phenotypes from the whole-brain (*Nestin-Foxp1 cKO*) mice and suggest that cortical-hippocampal circuits might be mediating these behaviors.

Emx1-Foxp1 cKO mice were also significantly impaired in spatial learning tasks, such as the Morris Water Maze and T-Maze task, that depend heavily on hippocampal circuits. Molecular characterization of the hippocampus found that Foxp1 regulated targets involved in synaptic transmission (e.g., *Scn9a, Scn9a2,* and *Slc24a4*) similar to the finding in the early postnatal cortex of these animal. Functional characterization of the hippocampus of *Emx1-Foxp1* cKO mice found a significantly reduced maintenance of long-term potentiation in the CA1 region in response to high frequency stimulation of Schaffer collaterals (Araujo et al., 2017). These studies were the first to dissect the region-specific roles of Foxp1 during brain development at the molecular, functional, and behavioral levels. **Chapter 3** will further examine the function of Foxp1 at the cellular level within the striatum.

PART II: STRIATAL DEVELOPMENT AND CIRCUITRY

Overview of basal ganglia circuitry

The striatum is the main input nucleus of an interconnected collection of subcortical nuclei termed the basal ganglia. The components of the basal ganglia include the striatum, globus pallidus external (GPe), globus pallidus internal (GPi), subthalamic nucleus (STN), substantia nigra pars reticulata (SNr) and pars compacts (SNc) (Gerfen and Bolam, 2016). Together these nuclei are critical for proper motor coordination, learning, and planning. Glutamatergic inputs from thalamic nuclei and cortical regions, densely from layer 5 and sparsely from layer 2/3, project onto the striatum (**Figure 1.4 A**). Moreover, corticofugal projections from layer 6 also form excitatory collaterals onto the striatum. Additionally, the striatum also receives neuromodulatory inputs from dopaminergic neurons in the ventral tegmental area and substantia nigra pars compacta heavily target the striatum (Gerfen and Bolam, 2016). These inputs synapse onto two distinct populations of GABAergic striatal spiny projection neurons (SPNs) that send projections along separate pathways: 1) the direct/striatonigral pathway SPNs (dSPNs, dopamine-1 receptor expressing) or 2) the indirect/striatopallidal pathway SPNs (iSPNs, dopamine-2 receptor expression) (Gerfen and Bolam, 2016). These SPN subtypes propagate incoming excitatory signals to the output nuclei of the basal ganglia: the GPi and SNr. Both GPi and SNr send GABAergic projections to the thalamus to inhibit excitatory thalamic modulation of the cortex. Direct pathway SPNs project to the GPi and the SNr to directly inhibit the inhibitory tone onto the thalamus to enhance thalamo-cortical excitatory inputs. Indirect pathway SPNs project to the GPe to ultimately enhance the inhibitory tone onto the thalamus to decrease thalamo-cortical strength. This complex

loop relies on the STN also providing excitatory inputs onto the GPi and SNr (**Figure 1.4**) (Gerfen and Bolam, 2016).

The striatum is composed of the several subregions known as the caudate nucleus (Ca), putamen (Pu), nucleus accumbens (NAc), and olfactory tubercles. In mice the caudate nucleus (Ca) and putamen (Pu) are one structure, while in humans the Ca and Pu are separated by the white matter tract called the internal capsule (**Figure 1.2 A-B**) that becomes prominent between 8 -11 gestation week (Onorati et al., 2014). From primate studies, researchers have found this anatomical separation of the caudate and putamen also results in the separation of inputs, whereby the caudate largely receives prefrontal cortical inputs and the putamen receives motor and somatosensory inputs (Gerfen and Bolam, 2016). Another major anatomical difference between rodent and primate basal ganglia is the location of the GPi. In primates, the GPi is situated adjacent to the GPe, whereas, in rodents, the GPi (also called the entopeduncular nucleus, EP) is located in internal capsule fiber tracts (Gerfen and Bolam, 2016).

Major differences between direct and indirect pathway SPNs

dSPNs and iSPNs are intermingled throughout the striatum, with no clear morphological identifier or organizational pattern. Therefore, the advent of transgenic mice carrying bacterial artificial chromosomes (BAC) driving the expression of fluorescent proteins under *Drd1* or *Drd2* promoters enabled researchers to better understand the molecular, morphological, and electrophysiological differences between direct and indirect pathways (Gong et al., 2007; 2003). iSPNs have smaller dendritic trees and fewer primary dendrites than dSPNs and are more excitable than dSPNs over a broad range of

intrasomatic current amplitudes in both younger and older animals (Ade et al., 2008; Cepeda et al., 2008; Day et al., 2008; Kreitzer and Malenka, 2007). This difference in dendritic surface area is believed to explain the differences observed in intrinsic excitability between SPN subtypes (Gertler et al., 2008). dPSNs also have less distal action potential back propagation compared to iSPNs (Day et al., 2008).

The striosome and matrix compartments

The striatum is also divided into distinct neurochemical compartments called the striosome and matrix. The striosome-matrix compartments are enriched for distinct neuropeptides and contribute differentially to striatal connectivity and behavior (Crittenden et al., 2016). Striosomes are defined histochemically by enriched expression of well-established markers, such as mu-opioid receptor (MOR) and pro-dynorphin (PDYN). The matrix compartment is enriched for enkephalin (PENK) and calbindin 1 (CALB1) (Crittenden et al., 2011). An analysis of brain-wide direct inputs onto striosomes and matrix compartments have shown that each compartment receives differential inputs from other brain regions (Smith et al., 2016). The matrix receives preferential input from the motor and visual cortex, while the striosomes receive significantly more projections from limbic associated regions, such as the amygdala, bed nucleus stria terminalis, and hypothalamus (Smith et al., 2016). Moreover, striosome and matrix compartments have been shown to regulate different behaviors associated with cost-benefit decision-making (Friedman et al., 2015).

SPNs that populate the striosome or matrix compartments are specified during early embryonic development. Striosome neurons are born earlier than matrix SPNs,

between E10-E12, while matrix SPNs are born through E13-E18 (Kelly et al., 2018) (Crittenden and Graybiel, 2011; Malach and Graybiel, 1986). SPNs that are born at E18 localize to an annular compartment that surrounds striosome patches (Kelly et al., 2018). Both striosome and matrix progenitor cells give rise to both dSPNs and iSPNs. dSPNs and iSPNs are specified independently from one another embryonically (e.g., dSPNs do not give rise to iSPNs) (Tinterri et al., 2018). Striosome SPNs begin to form detectable patch-like clusters as early as E16.5 (Hagimoto et al., 2017).

Excitatory inputs onto the striatum

Comprehensive maps of cortical and thalamic input onto the striatum has shown that corticostriatal inputs cluster into four large subdivisions with clear boundaries (Hunnicutt et al., 2016; Oh et al., 2016). Three boundaries correspond to the traditional divisions of dorsomedial, dorsolateral, and ventral striatal domains. These regional divisions have been shown to play a role in goal-directed, habitual, and affective control of behaviors, respectively (Hunnicutt et al., 2016). The dorsomedial region receives dense projections from the lateral orbital, ventral and dorsal anterior cingulate, and visual cortex. The dorsolateral region is the largest striatal subregion and receives dense inputs from the frontal association, motor, and sensorimotor cortex and the amygdala. The ventral striatal region receives dense projections from insular cortices, the prelimbic and infralimbic cortex, and the hippocampal subiculum (Hunnicutt et al., 2016). Additionally, a fourth subdivision in the posterior striatum was found that receives preferential inputs from auditory, visual, and rhinal cortices and the amygdala (Hunnicutt et al., 2016). Since the thalamus in the major target of basal ganglia output nuclei, this study also examined

thalamocortical and basal ganglia-thalamic projection patterns to better understand the organization of cortico-thalamo-basal ganglia circuits. The authors found that thalamic nuclei that receive dense projections from the basal ganglia project primarily back to the motor or lateral/ventral orbital cortex (Hunnicutt et al., 2016).

Another study comprehensively mapped the inputs from cortical regions onto either dSPNs or iSPNs (Wall et al., 2013). The authors found that dSPNs received preferential inputs from sensorimotor and limbic structures, including the primary somatosensory, prelimbic, and entorhinal cortex. They also found that amygdalar projections densely targeted dSPNs with very few identified on iSPNs (Wall et al., 2013).

Molecular development of the striatum and SPN specification

The molecular development of direct and indirect pathway SPNs is intertwined with the development of the striosome and matrix compartments. The molecular specification of dSPNs and iSPNs occurs during early embryonic development (Tinterri et al., 2018). Mature dSPNs and iSPNs have distinct molecular profiles based on expression studies using FACS followed by microarrays, translating ribosomal affinity purification, and, more recently, single-cell RNA-sequencing approaches in adult animals (Gokce et al., 2016; Heiman et al., 2008; Lobo et al., 2006a; Maze et al., 2014; Saunders et al., 2018). These studies have uncovered enriched transcripts in each SPN subpopulation and have provided a molecular window into their cellular identity and molecular specification. Several key transcription factors (TFs) have been identified for both pan SPN and d/iSPN sub-specification (**Figure 1.5**). *Gsx2* and *Ascl1* are TFs crucial for specifying the LGE neural progenitors early during development (Corbin et al., 2000; Kim et al., 2008a;

Toresson et al., 2000; Wang et al., 2009; Yun et al., 2001). *Dlx1/2* are important for specifying later born SPNs that occupy the matrix compartment of the developing striatum (Anderson et al., 1997; Long et al., 2009). *Ctip2* is reported to be expressed in most SPNs and regulates their differentiation and striosome-matrix organization (Arlotta et al., 2008). *Ebf1* and *Isl1* are transcription factors selectively expressed in dSPNs and specify either matrix or striosome dSPNs, respectively (Ehrman et al., 2013; Garel et al., 1999; Lobo et al., 2006a; 2008; Lu et al., 2014). *Foxo1* has been shown as an important downstream effector of *Isl1* during dSPN development (Waclaw et al., 2017). *Sp9 and Sp8* has been linked to the generation and survival of iSPNs (Xu et al., 2018; Zhang et al., 2016) by regulating the expression of *Six3*, another TF important for iSPN development (Xu et al., 2018). In addition, *G9a*, a chromatin modifier, was found to mediate a dSPN to iSPN identity switch (Maze et al., 2014). The transcriptional programs underlying SPN specification are still being unraveled. An important question is how these TFs might cooperate to regulate distinct SPN subpopulations and how the development of one SPN subtype influences the development of the other remains largely unknown. In **Chapter 3**, I examine the role of *Foxp1* in specifying iSPNs and the molecular compensation that occurs in other cell-types and discuss the possibility that Foxp2 may compensate for loss of Foxp1 in dSPNs.

QUESTIONS ADDRESSED IN THIS THESIS

In the following chapters, I will address these overarching questions:

1) What is the region-specific role of FOXP1 in the brain? I will address this question broadly in **Chapter 2** by finding the genes regulated by Foxp1 in the cortex, hippocampus, and striatum of Foxp1 heterozygous (*Foxp1*$^{+/-}$) mice using bulk RNA-sequencing (RNA-seq) and use weighted gene network co-expression analysis (WGCNA) for insights into the molecular pathways altered in a region-specific manner. I also perform an *in vitro* chromatin-immunoprecipitation sequencing (ChIP-seq) and RNA-seq experiments in human neural progenitors overexpressing FOXP1 to find both direct and indirect targets of FOXP1. We performed an analysis of module preservation on both human and mouse WGCNA networks and found that striatal modules were more conserved in human compared to hippocampal samples. We also found that *Foxp1*$^{+/-}$ mice produced fewer ultrasonic vocalizations and exhibited cell-type specific functional changes within indirect pathway (D2R) striatal neurons.

2) What is the cell-type specific role of Foxp1 in striatal projection neurons? I will address this question in **Chapter 3** by characterizing *Foxp1* conditional knockout mice crossed to D1R and/or D2R-Cre BAC transgenic mice to delete *Foxp1* from the direct, indirect, or both pathways. I use single-cell RNA-sequencing to find cell-type specific downstream targets of Foxp1 and link these molecular changes to deficit in behaviors and projection patterns of spiny projection neurons. In **Chapter 4**, I further characterize the role of Foxp1 within the striatum by examining changes in striatal cellular composition and additional clinically-relevant behaviors within these mice.

FIGURES

FIGURE 1.1. Expression patterns of *FOXPs* over human brain development.

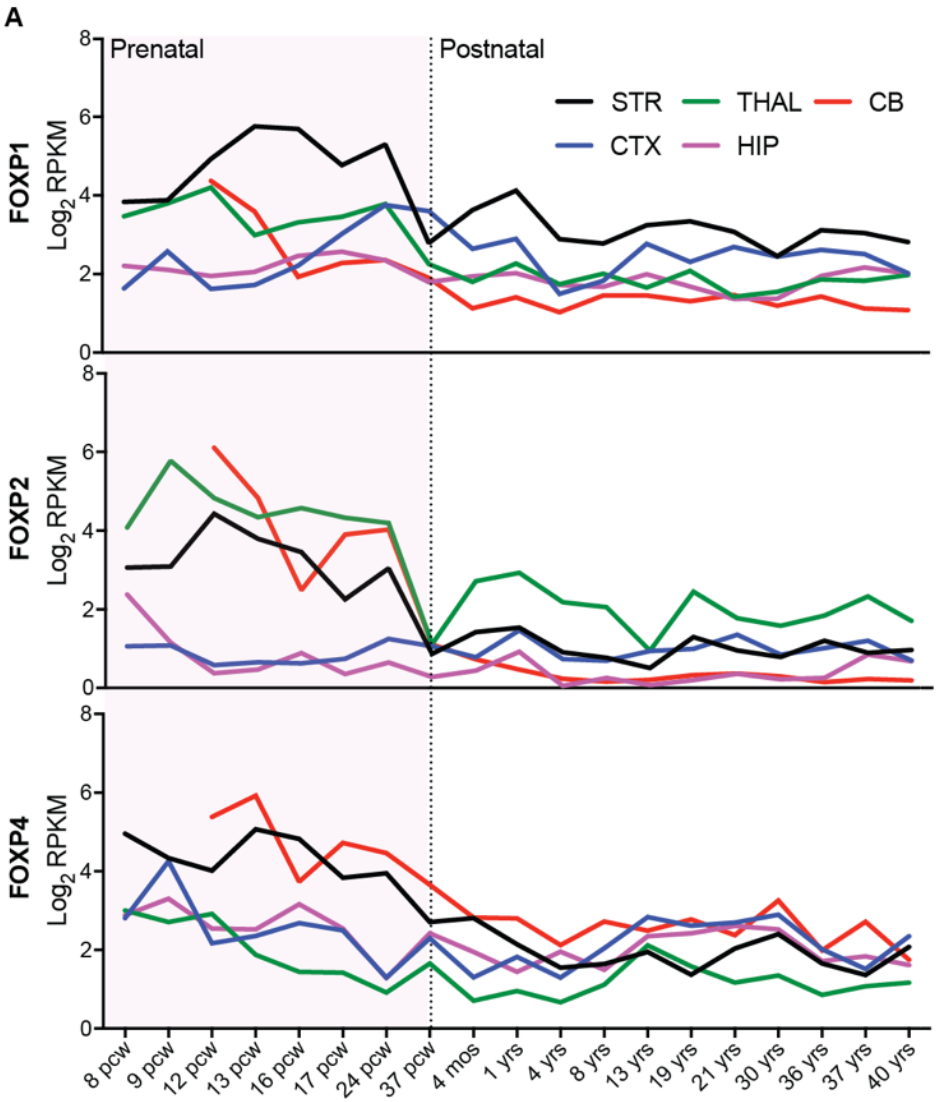

A) Using RNA-seq data from BrainSpan Atlas of the Developing Human Brain (Miller et al., 2014, Li et al., 2018), log-transformed reads per kilobase of transcript per million mapped reads (RPKM) values were plotted at each timepoint for each brain region with known expression of FOXP1, FOXP2, or FOXP4 (STR= striatum, CTX= dorsolateral prefrontal cortex, THAL= dorsal thalamus, HIP= hippocampus, CB= cerebellum). Pink overlay indicates fetal timepoints ending at the dotted line.

FIGURE 1.2. Cell-type specific expression of FoxP transcript in forebrain regions

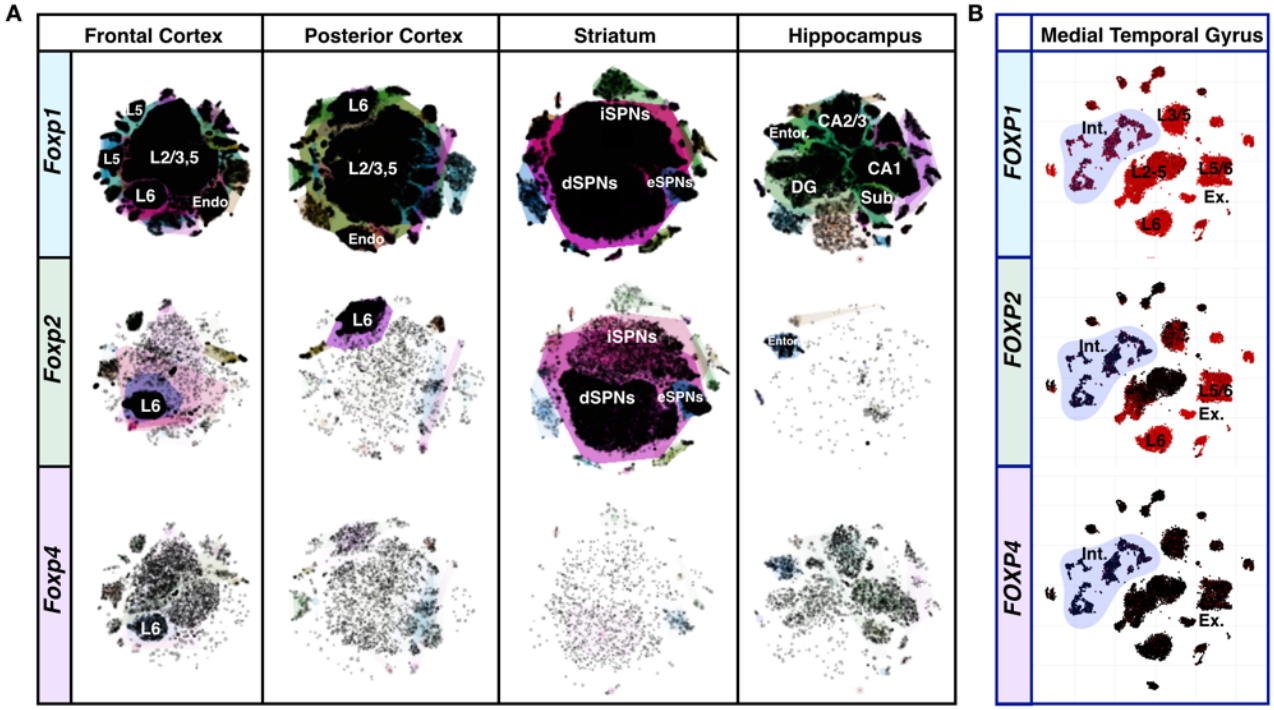

A) Visualization of adult mouse single-cell RNA-seq data from Saunders et al. Cell 2018. Visualization of *Foxp1*, *Foxp2*, and *Foxp4* expression within the frontal and posterior cortex, striatum, and hippocampus using the DropViz tool (http://dropviz.org). Expression is shown in black with enriched clusters shaded in color. B) Adult human cortical scRNA-seq data showing the expression of *FOXP1*, *FOXP2*, and *FOXP4* within the medial temporal gyrus from the Allen Brain Atlas tool (https://celltypes.brain-map.org/rnaseq/human). Red indicates high expression, black indicate no expression.

FIGURE 1.3. Expression of *FoxPs* and *Drds* in the developing human and mouse striatum

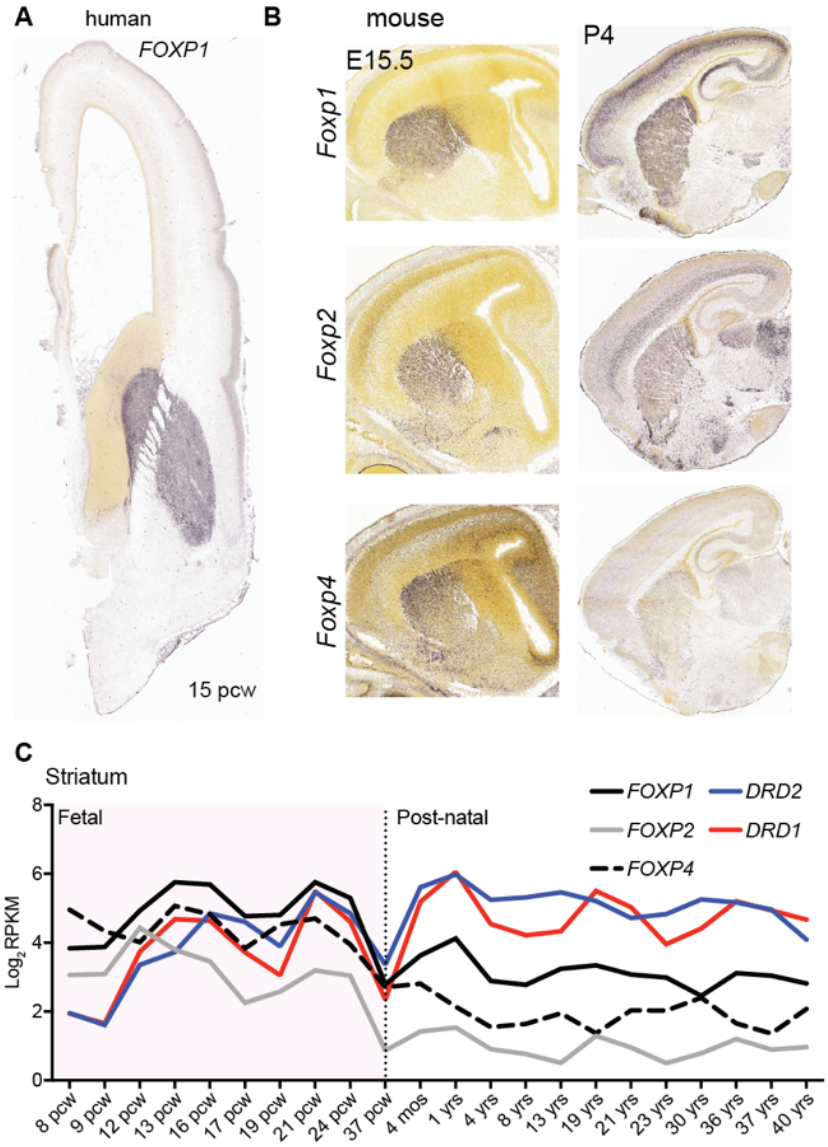

A) In situ hybridization (ISH) image from the BrainSpan Atlas of the Developing Human Brain (Miller et al., 2014, Li et al., 2018) showing FOXP1 expression at 15 post-conceptional weeks (pcw). **B**) Developing Mouse Brain ISH data from the Allen Brain Atlas showing expression of Foxp1 from sagittal sections at developmental timepoints E15.5 and P4. **C**) Striatal RNA-seq data of *FOXP1*, *FOXP2*, *DRD1*, and *DRD2* expression levels over fetal and post-natal development.

FIGURE 1.4. Diagram of basal ganglia circuits

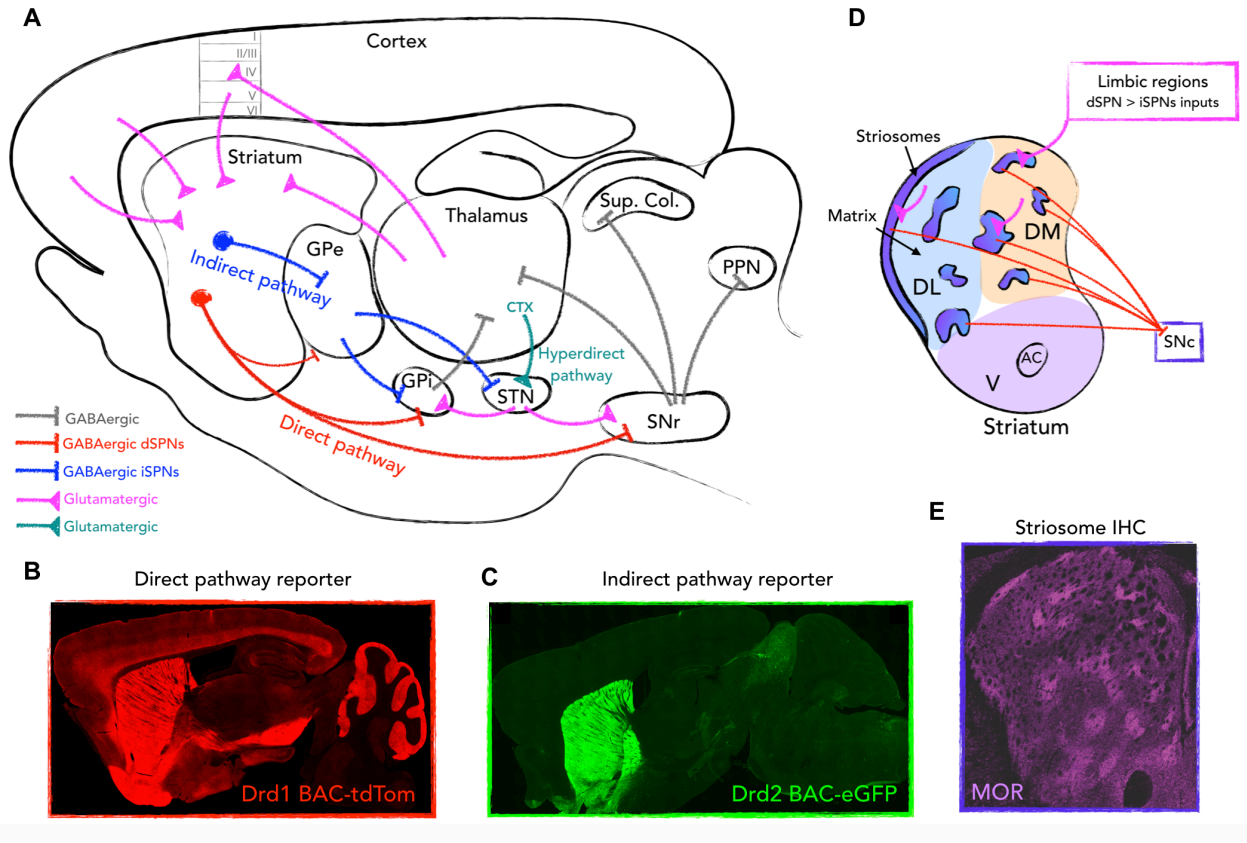

A) Stylized schematic of basal ganglia circuitry in the rodent brain from a sagittal perspective. Glutamatergic (pink) projections from layer 5 of the cortex and thalamus innervate the striatum. GABAergic projections along the "direct" (red) pathway innervate the GPi and SNr. GABAergic projections along the "indirect" (blue) pathway innervated the GPe, which projects inhibitory projections to the GPi and STN. The GPi and SNr project GABAergic projections back to the thalamus and other mid- and hind-brain nuclei, like the superior colliculus and pedunculopontine (PPN) nucleus. The subthalamic nucleus (STN) is modulated by GPi projections and cortical "hyperdirect" pathway. The STN modulates the output nuclei (GPi and SNr) with excitatory inputs. **B**) BAC transgenic mice expressing td-tomato under the *Drd1* promoter to label the direct pathway SPN projections (Ade et al., 2011). **C**) BAC mice expressing eGFP under the Drd2 promoter to label indirect pathway SPNs (Gong et al., 2003). **D**) The neurochemical division of the striatum into the striosome (filled) or matrix compartment and divisions between the dorsal

medial (DM), dorsal lateral (DL), and ventral (V). Direct pathway SPNs with striosomes send unique projections to the substantia nigra pars compacta (SNc) and receive preferential inputs from limbic brain regions.

FIGURE 1.5. Transcription factors important for striatal development and SPN specification

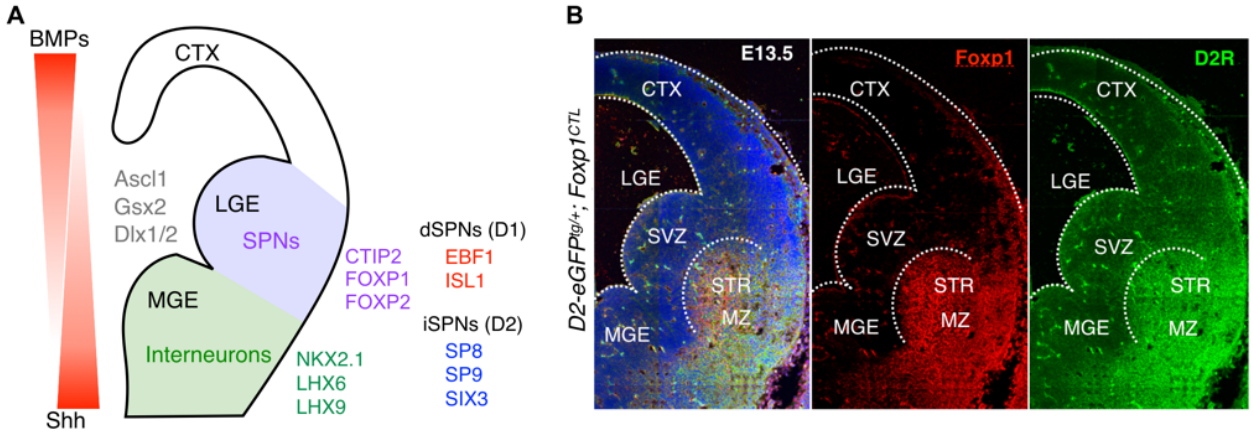

A) Schematic of the embryonic cortex (CTX), lateral and medial ganglionic eminences (LGE and MGE) from a coronal section. The gradients of ventral sonic hedgehog (Shh) and dorsal bone morphogenic proteins (BMPs) establish the transcriptional patterning of the developing brain. Cortical and striatal interneuron populations are generated from the MGE, where expression of transcription factors (TFs) are critical for interneuron development, like Nkx2.1, Lhx6, and Lhx9. SPNs are generated from the LGE and key TFs factors are important for SPN specification and sub-specification. Certain TFs are critical for generating both LGE and MGE, such as Ascl1, Gsx2, and Dlx1/2. B) Immunohistochemistry for Foxp1 (red) from an E13.5 embryo from a control mouse crossed into the D2-eGFP reporter (D2R) strain to label iSPNs (green). Foxp1 expression is restricted to the post-mitotic mantle zone (MZ) within the LGE.

CHAPTER 2: FOXP1 ORCHESTRATION OF ASD-RELEVANT SIGNALING PATHWAYS IN THE STRIATUM

Adapted from: Araujo, D.*, **Anderson, A.G.*** Berto, S., Runnels, W., Harper, M., Ammanuel, S., Reiger, M.A., Huang, H.C., Rajkovich, K., Tucker, H., Dougherty, J.D., Gibson, J.R., and Konopka, G. (2015). FoxP1 orchestration of ASD-relevant signaling pathways in the striatum. **Genes and Development**, 29(20): 2081-2096.

**equal authorship contributions*

ABSTRACT

Mutations in the transcription factor Forkhead box p1 (FOXP1) are causative for neurodevelopmental disorders such as autism. However, the function of FOXP1 within the brain remains largely uncharacterized. Here, we identify the gene expression program regulated by FoxP1 in both human neural cells and patient-relevant heterozygous Foxp1 mouse brains. We demonstrate a role for FoxP1 in the transcriptional regulation of autism-related pathways as well as genes involved in neuronal activity. We show that Foxp1 regulates the excitability of striatal medium spiny neurons and that reduction of Foxp1 correlates with defects in ultrasonic vocalizations. Finally, we demonstrate that FoxP1 has an evolutionarily conserved role in regulating pathways involved in striatal neuron identity through gene expression studies in human neural progenitors with altered FOXP1 levels. These data support an integral role for FoxP1 in regulating signaling pathways vulnerable in autism and the specific regulation of striatal pathways important for vocal communication.

INTRODUCTION

Autism spectrum disorder (ASD) denotes a group of heterogeneous neurodevelopmental conditions that are all characterized by diminished sociability, impaired communication, restricted interests, and stereotypic behaviors. While there is a strong genetic component to ASD, this is divided among several hundred genes, each with only a small contribution to the prevalence of the disorder (Geschwind and State 2015). Furthermore, many autism risk genes are thought to exert their effects during early brain development (State and Sestan 2012; Xu et al. 2014; Parikshak et al. 2015). Transcription factors play a key role in orchestrating the spatial and temporal gene expression patterns important for this process. Therefore, the identification of gene networks regulated by transcription factors implicated in both ASD and brain development should provide insight into the complex developmental brain mechanisms at risk in autism.

The transcription factors Forkhead box P1 (FOXP1) and FOXP2 have been implicated in neurodevelopmental disorders such as ASD and developmental verbal dyspraxia (DVD), respectively (Bacon and Rappold 2012). Foxp1 is a member of the Fox family of transcription factors, for which there is a designated protein nomenclature (uppercase for primates, lowercase for rodents, and mixed case for other species) (Kaestner et al. 2000). Foxp1 is highly enriched within the developing and mature neocortex, hippocampus, and striatum (Ferland et al. 2003; Teramitsu et al. 2004). Numerous studies have identified heterozygous deletions, point mutations, and duplications of FOXP1 as being causal for ASD (Bacon and Rappold 2012). In particular, recent large-scale exome sequencing efforts have identified FOXP1 as a gene with recurrent de novo mutations associated with ASD (Iossifov et al. 2014). Therefore,

understanding how FOXP1 functions within the brain should allow for key insights into the molecular pathways at risk in ASD. Several reports have begun to elucidate a role for Foxp1 in the brain (Rousso et al. 2012; Tang et al. 2012), and recent work has shown that mice with brain-specific loss of Foxp1 have altered hippocampal electrophysiology, striatal morphology, and social behaviors (Bacon et al. 2015). However, the region-specific transcriptional profile of Foxp1 in the mouse brain, how well this profile is conserved in human-relevant Foxp1 haploinsufficient models, and the behavioral consequences of disrupting these regional gene networks remain largely unknown.

FOXP2 is a paralog of FOXP1, and mutations in the FOXP2 gene lead to a number of brain and cognitive deficits, including DVD (Fisher and Scharff 2009; Bacon and Rappold 2012). In addition to being able to heterodimerize with Foxp2, Foxp1 expression overlaps with Foxp2 expression in the GABAergic medium spiny neurons (MSNs) of the striatum, a brain region critically involved in human language, vocal imitation in zebra finches, and rodent ultrasonic vocalizations (USVs) (Ferland et al. 2003; Li et al. 2004; Teramitsu et al. 2004; Fisher and Scharff 2009). Additionally, Foxp2 mutant mice demonstrate disruptions in mouse USVs as well as alterations in the electrophysiological and projection properties of MSNs (Shu et al. 2005; Enard et al. 2009; Vernes et al. 2011; French et al. 2012). Given the role for both Foxp1 and Foxp2 in the striatum, we hypothesized that Foxp1 regulates regional gene expression patterns in the brain and that normal levels of Foxp1 are crucial for mouse vocalization behavior. To test this hypothesis, we took advantage of a heterozygous (*Foxp1*$^{+/-}$) mouse model and a human neural progenitor (hNP) cellular model with altered expression of FOXP1. Using high-throughput sequencing technologies, we used these two systems to identify a conserved

role for FoxP1 in regulating autism-risk genes. We showed that Foxp1 differentially regulates the excitability of dopamine receptor 1-positive (D1) versus (D2) MSNs. We also demonstrated reduced USVs in *Foxp1*$^{+/-}$mice, similar to that seen in *Foxp2*$^{+/-}$ mice (Shu et al. 2005). This similarity in behavioral phenotype is reflected at the genomic level, as Foxp1-regulated genes in the striatum overlap with genes regulated by Foxp2 in the striatum. Finally, we found that FoxP1 regulates conserved pathways involved in striatal identity in both humans and mice. Taken together, these results suggest that FoxP1 plays a critical role in regulating striatal function and vocal communication, which, when disrupted, contributes to phenotypes characteristic of ASD.

RESULTS

Foxp1 gene regulation within distinct brain regions

In order to assess the ASD-relevant role of Foxp1 within the brain, we took advantage of a Foxp1 animal model. As Foxp1 knockout mice are embryonic-lethal at embryonic day 14.5 (E14.5) due to a developmental heart defect (Wang et al. 2004) and as most patients with FOXP1 mutations are haploinsufficient, we carried out analyses on Foxp1 heterozygous (*Foxp1*$^{+/-}$) mice (Hu et al. 2006). We tested the specificity of an antibody recognizing FoxP1 using hNPs with forced FOXP1 expression as well as whole brains from E13.5 Foxp1 knockout embryos. We identified expression of two Foxp1 isoforms (A and D), previously shown to be expressed in mouse brains (Wang et al. 2003), both of which were absent in brain tissue from knockout embryos (Supplemental Fig. 1A). Three brain regions relevant to ASD with substantial levels of Foxp1 expression are the striatum, hippocampus, and neocortex (Ferland et al. 2003; Maloney et al. 2013). We quantitatively

determined an ~50% reduction in total Foxp1 protein levels (isoforms A and D) in the *Foxp1*$^{+/-}$ hippocampus or striatum compared with control littermates (Fig. 1A, B). Interestingly, neocortical expression of Foxp1 (either total protein or isoform-specific expression) was not reduced to 50% in *Foxp1*$^{+/-}$mice, suggesting a homeostatic up-regulation of Foxp1 in the neocortex of these animals (Fig. 1A, B; Supplemental Fig. 1B, C).

We ascertained potential transcriptional targets of Foxp1 in vivo using RNA sequencing (RNA-seq) in the hippocampus or striatum of *Foxp1*$^{+/-}$mice and control littermates. To identify differentially expressed genes (DEGs), we filtered using a false discovery rate (FDR) of <0.05 and an absolute log fold change of ≥0.3 (Supplemental Table 1). As a control, RNA-seq was also conducted in the neocortex, and, not unexpectedly, we did not observe significant changes in gene expression in this brain region (data not shown).

Foxp1 regulation of ASD-associated pathways in the striatum and hippocampus

To characterize the identified Foxp1 targets with respect to ASD etiology, we compared the list of Foxp1 DEGs with the current list of annotated ASD genes in the SFARI database (667 genes) (http://www.sfarigene.org). We found that in vivo Foxp1-regulated genes significantly overlap with ASD genes in both the hippocampus and striatum (Fig. 1C). The SFARI database stratifies genes based on the strength of their association with ASD, and when we removed the genes in categories #5 and #6 (hypothesized support and not supported, respectively) and repeated our analyses, we obtained a similar result (17 genes [P = 0.057] for striatum and 39 genes [P = 0.0001] for

hippocampus, hypergeometric tests) (data not shown). Using quantitative RT–PCR (qRT–PCR), we confirmed 11 of 12 selected targets from the overlap between the *Foxp1*$^{+/-}$ striatal data set and the ASD genes in independent samples (Fig. 1D).

Mouse Foxp1 targets were further prioritized with respect to neurodevelopmental human diseases using weighted gene coexpression network analysis (WGCNA), which allows for the discovery of networks (or modules) of genes with high levels of coexpression (Supplemental Fig. 2A; Zhang and Horvath 2005; Oldham et al. 2008). The top hub gene (or gene with the highest number of connections) in the striatal-associated MsM18 module is Dpp10 (dipeptidyl peptidase) (Fig. 1E). DPP10 is an ASD gene that encodes for a protein that regulates surface expression and properties of the potassium channel Kv4.2 (Mar- shall et al. 2008; Foeger et al. 2012). Of note, the gene encoding Kv4.2, KCND2, has also been implicated in ASD (Lee et al. 2014) and is highlighted within the MsM19 module (Supplemental Fig. 2C). We also observed and confirmed that Dpp10 is increased and that Kcnd2 is decreased in the striatum of *Foxp1*$^{+/-}$ mice (Fig. 1F). Alteration of Kv4.2 function has been previously observed in a mouse model of Fragile X syndrome (FXS) (Gross et al. 2011), and Fragile X mental retardation protein (FMRP)-regulated genes have previously been shown to have significant genomic interactions with ASD-relevant pathways in human brain development (Parikshak et al. 2013). We therefore compared the mouse WGCNA modules with previously identified FMRP targets (Darnell et al. 2011) and found modules containing FMRP targets (MsM1, MsM6, MsM12, MsM14, and MsM23) (Supplemental Fig. 2A). While certainly interesting with regard to potential converging pathways, such enrichments need to be interpreted cautiously, as recent work has uncovered that FMRP targets tend to be highly expressed long genes in

the brain (Ouwenga and Dougherty 2015). Of particular interest, MsM14 correlates with genotype and contains a number of FMRP target genes, including the gene encoding FMRP (*Fmr1*) (Supplemental Fig. 2B), highlighting a potential direct role for coordination of disease-relevant genes in the striatum by Foxp1 and FMRP.

Foxp1 regulates shared targets with Foxp2 in the striatum

As previous work has implicated a role for the related transcription factor FoxP2 in striatal function, including altered MSN electrophysiology and morphology (Enard et al. 2009), and as the striatum is also one of the few brain regions where Foxp1 and Foxp2 have overlapping expression (Ferland et al. 2003), we compared the list of Foxp1 target genes in the striatum with published striatal Foxp2 targets in *Foxp2*$^{+/-}$ mice (Enard et al. 2009). We identified a significant overlap between Foxp1-regulated genes and previously published Foxp2 targets that are changing in the same direction across data sets with reduction of the respective transcription factors, indicating possible coregulation of these targets (Fig. 2A). This overlap represents 12% of the total Foxp1 target genes identified in the striatum. Using independent samples, we confirmed six of these genes changing with Foxp1 expression in the striatum via qRT–PCR (Fig. 2B). Within the in vivo WGCNA analysis, both Foxp1 and Foxp2 are coexpressed within the MsM3 module, which is enriched for striatal DEGs (Fig. 2C). Interestingly, within the MsM3 module, the gene encoding the dopamine receptor Drd1a is coexpressed with both Foxp2 and Foxp1 (Fig. 2C).

MSNs of the striatum are categorized as either D1 (expressing the Drd1a receptor) or D2 (expressing the Drd2 receptor) projection neurons, and these two subpopulations

of neurons are associated with opposing functions in the coordination of motor activity (Gerfen and Surmeier 2011). To investigate whether disrupted Foxp1 signaling in the striatum would be expected to produce differential gene expression changes in D1 versus D2 MSNs, we overlapped our RNA-seq data set with published gene lists obtained from translating ribosome affinity purification of D1 and D2 MSNs (Maze et al. 2014). We found a significant enrichment of both Foxp1 and Foxp2 target genes within D1 MSNs specifically (Fig. 2D). Although we found that the number of Foxp1 target genes is roughly equally distributed between genes enriched in both D1 and D2 MSNs (Fig. 2D), the number of Foxp2 target genes enriched in D1 MSNs is almost twice the number of Foxp2 target genes enriched in D2 MSNs (Heiman et al. 2008; Vernes et al. 2011; Maze et al. 2014). These results are in line with published data showing that Foxp2 is more enriched in D1 MSNs. Moreover, the overlapping targets of Foxp1 and Foxp2 going in the same direction are expressed only in D1 MSNs, supporting coordinated regulation in these specific neurons. Interestingly, Foxp1-specific target genes that are enriched in D2 MSNs include several genes involved in cation transport (e.g., Atp1b1, Kcnk2, Htr7, Kcnip2, and Hrh3) (Supplemental Table 2). Together, these data support a role for Foxp1 and Foxp2 providing coordinated regulation of striatal signaling pathways and that this regulation may be differential between D1 and D2 MSNs in *Foxp1*$^{+/-}$ mice.

Reduction of Foxp1 leads to differential changes in the excitability of striatal MSNs

Together with the coregulation of genes by Foxp1 and Foxp2 (Fig. 2), the gene expression data indicated a role for FoxP1 in regulating genes coding for proteins involved in both ion channel and neuronal activity, in particular within D2 MSNs

(Supplemental Tables 1, 2). We therefore investigated the effect of reduced Foxp1 expression on neuronal activity within either D1 or D2 MSNs. At postnatal day 18 (P18), acute striatal slices were made from progeny of *Foxp1*$^{+/-}$ mice crossed with either *Drd1a-tdTomato*$^{+/-}$ or *Drd2-GFP*$^{+/-}$ reporter mice (Gong et al. 2003; Ade et al. 2011) and whole-cell recordings of MSNs were carried out. D2 (GFP^{+}) MSNs from *Drd2-GFP*$^{+/-}$*;Foxp1*$^{+/-}$ mice (Fig. 3A) exhibited significantly increased excitability, as indicated by the higher number of action potentials evoked for a given current step (Fig. 3B,C), an increase in input resistance (Fig. 3D), and a decrease in current threshold (Fig. 3E). We also observed no differences in resting potential (Fig. 3F), the action potential width (Fig. 3G), or the frequency of the spontaneous excitatory postsynaptic events (sEPSCs) of D2 MSNs (Fig. 3H). We did observe a significant decrease in the amplitude of sEPSCs of these MSNs (Fig. 3I). Together, these data demonstrate that reduction of Foxp1 leads to increased excitability of D2 MSNs in response to reduced Foxp1 expression.

Given the opposing functions traditionally associated with D1 and D2 MSNs (Gerfen and Surmeier 2011) and the possibility for differential regulation of gene expression within D1 and D2 MSNs in the *Foxp1*$^{+/-}$ mouse striatum (Fig. 2D), we asked whether the increased excitability of D2 neurons due to Foxp1 loss was generalizable to all MSNs. Again, at P18, we carried out whole-cell recordings on MSNs from acute striatal slices. Although trending toward a decrease in excitability, D1 (tdTomato^{+}) MSNs from *Drd1a-tdTomato*$^{+/-}$*; Foxp1*$^{+/-}$ mice (Supplemental Fig. 3A) exhibited no significant change in their excitability compared with controls (Supplemental Fig. 3B, C). We also found no significant increase in input resistance (Supplemental Fig. 3D) or current threshold

(Supplemental Fig. 3E) and no significant difference in resting potential (Supplemental Fig. 3F) or action potential width with reduction of Foxp1 in these neurons (Supplemental Fig. 3G). Finally, we observed no changes in the frequency or amplitude (Supplemental Fig. 3H, I) of sEPSCs. These data indicate that haploinsufficiency of Foxp1 causes differential changes in the membrane excitability of D1 and D2 MSNs.

Foxp1 regulates mouse USVs

Huntington's and Parkinson's disease mouse models provide evidence for the involvement of MSNs in directing the production of USVs (Pietropaolo et al. 2011; Grant et al. 2014). Additionally, knockout of the Drd2 receptor reduces the number of USVs produced by mouse pups (Curry et al. 2013). Because we uncovered a significant overlap between *Foxp1*$^{+/-}$ and *Foxp2*$^{+/-}$ striatal target genes as well as altered MSN excitability as a response to loss of Foxp1, we hypothesized that reduction of Foxp1 would lead to an altered USV phenotype similar to that seen in Foxp2 mutant mice (Shu et al. 2005). To test this hypothesis, we examined USVs in a maternal separation paradigm. Paralleling what has previously been seen in *Foxp2*$^{+/-}$ mice (Shu et al. 2005), we observed a significant decrease in both the number of times a *Foxp1*$^{+/-}$ mouse pup called ("bouts") (Fig. 4A) and the total number of calls (Fig. 4B) compared with littermate controls at P4 and P7 (see the Materials and Methods; Supplemental Fig. 4A for analysis details). Additionally, as a trend, the call bouts and total number of calls produced by the *Foxp1*$^{+/-}$ mouse pups are reduced across all days (Fig. 4A, B). We also observed a significant decrease in the mean call frequency, as a trend across all days, in the *Foxp1*$^{+/-}$ mouse pups (Fig. 4C). Other parameters, such as average call duration and the fraction of calls

with jumps, were not altered (Fig. 4D, E). Interestingly, we observed that the average slope of a call was significantly decreased in *Foxp1*$^{+/-}$ mice compared with controls (Fig. 4F). This result is the opposite of the increase in call slope exhibited by humanized Foxp2 mice (Enard et al. 2009).

Differences in weight gain have been proposed to explain some variation seen in the postnatal USVs of transgenic mouse models (Scattoni et al. 2009). However, there were no significant differences in the weight gain of *Foxp1*$^{+/-}$ mice compared with controls (Supplemental Fig. 4B). To assess whether the vocalization deficits observed in the *Foxp1*$^{+/-}$ mice are secondary to a generalized impairment in striatal-mediated behaviors, we assessed locomotion in the open field test as well as rotorod performance, forelimb and hindlimb grip strength, nest building, and grooming behaviors in these animals (Supplemental Fig. 5). We also performed postnatal righting reflexes as part of an abbreviated SHIRPA battery to evaluate overall neurological function in these mice (see the Materials and Methods; Supplemental Figs. 5A, 6). In summary, we found that Foxp1$^{+/-}$ mice display no differences in either the SHIRPA test, righting reflexes, nest building, rotorod performance, or grooming behaviors. Interestingly, *Foxp1*$^{+/-}$ mice do display hyperactivity in the open field test and decreased performance in the forelimb and hindlimb grip test. Together, these data suggest that wild-type levels of Foxp1 expression are important for normal mouse vocal behavior but are not required for most striatal-based behaviors.

FOXP1 gene regulation in human neural cells

In order to identify FoxP1 target genes that are most relevant to human brain development and ASD, we characterized the FOXP1 target genes in hNPs, which demonstrate a higher fidelity with *in vivo* brain transcriptomic data than either human embryonic stem cells or induced pluripotent stem cells (Konopka et al. 2012; Stein et al. 2014) and are genetically tractable using lentiviruses (Konopka et al. 2009). As undifferentiated hNPs do not express FOXP1 endogenously and given the current paucity of chromatin immunoprecipitation (ChIP)-grade antibodies against FoxP1, we ascertained direct FOXP1 targets by transducing hNPs with a lentivirus containing Flag-tagged FOXP1 or a GFP control virus (Fig. 5A). Forced expression of FOXP1 was limited to the nucleus (Fig. 5D).

To identify genome-wide direct targets of FOXP1, we conducted both RNA-seq and ChIP followed by DNA sequencing (ChIP-seq) in hNPs overexpressing FOXP1. Using the Flag tag on FOXP1, we identified >600 genes enriched for FOXP1 binding (Fig. 5B,E; Supplemental Table 1). These directly bound targets are enriched for forkhead motifs (Supplemental Fig. 7; Stroud et al. 2006). Again, using RNA-seq, an FDR of <0.05, and an absolute log fold of ≥0.3, we uncovered >1500 DEGs within this cellular paradigm (Fig. 5E; Supplemental Table 1). These DEGs are significantly enriched for gene ontology (GO) categories such as axon guidance, neuronal development, and neuronal differentiation, and the overlap between both ChIP and RNA-seq data represents directly regulated FOXP1 targets in hNPs (Supplemental Table 3). RNA-seq and ChIP-seq genes significantly overlap (Fig. 5E); however, because this overlap is significant yet small,

these results suggest that the majority of gene regulation by FOXP1 occurs through indirect effects on signaling cascades, as might be expected for a transcription factor.

FOXP1 regulates ASD-relevant genes in hNPs

To further characterize the identified hNP FOXP1 targets with respect to ASD etiology, we again compared the list of FOXP1 DEGs to the current list of annotated ASD genes in the SFARI database. We observed a significant overlap of FOXP1 targets and ASD genes (Fig. 5F). When we over- lapped the list of hNP DEGs with the curated list of ASD genes (i.e., not including genes in categories #5 or #6), we also obtained a significant overlap (48 genes, P = 0.023, hypergeometric test) (data not shown). hNP DEGs that over- lapped with the SFARI gene database were selected and confirmed within an independent hNP cell line using an independent measure of expression: qRT–PCR (Fig. 5G). Previous work suggested that the members of the Foxp subfamily of forkhead transcription factors are primarily transcriptional repressors (Wang et al. 2003). However, we showed that the related transcription factor FOXP2 is also able to activate transcription (Spiteri et al. 2007). In line with those data, we found an almost equal representation of activated and repressed FOXP1 targets that overlap with ChIP-seq and ASD lists (Fig. 5H). Additionally, we also confirmed that FOXP1 directly binds within the first intron of DPP10 and represses its expression in hNPs overexpressing FOXP1 (Fig. 5I,J). Together with the results from the *Foxp1*$^{+/-}$ mice (Fig. 1F), this indicates that Dpp10 is a conserved direct repressed target of FoxP1. Moreover, many genes overlapped with directional consistency between striatum and hNPs (12%) (Supplemental Table 1).

Using WGCNA again, we uncovered nine modules with first principal components correlating to FOXP1 expression (hNPM2, M3, M4, M6, M7, M13, M16, M20, and M21) (Supplemental Fig. 8). We then compared the hNP^{FOXP1} RNA-seq data to recently reported coexpression modules derived from in vivo developing human brains (Parikshak et al. 2013). We found a significant overlap of DEGs in the hNP^{FOXP1} data set with this report's M17 module (Supplemental Table 1). The M17 module is one of three modules previously identified to contain a significant overlap with known ASD genes. We also compared the hNP^{FOXP1} RNA-seq data with two other coexpression modules: asdM12 and asdM16 (derived from human brain tissue samples from ASD cases and controls), which were highly correlated with ASD disease status (Supplemental Table 1; Voineagu et al. 2011). We found that many genes within these two modules were also found within the modules correlating to FOXP1 expression. Interestingly, DPP10 is also present in asdM12, which further emphasizes its relevance to ASD etiology. Thus, the data from manipulation of FOXP1 expression in the in vitro system recapitulate identified genomic relationships from in vivo human brain data.

Conserved regulation of FoxP1 targets within the striatum

To further demonstrate the relevance of the *Foxp1*$^{+/-}$ mouse data with human biology and disease, we performed an analysis of module preservation (Langfelder et al. 2011) between either the *Foxp1*$^{+/-}$ mouse hippocampal or striatal WGCNA data and the hNP WGCNA data. This approach allows one to determine how conserved gene coexpression relationships are between the two species. Interestingly, we found that there was significantly greater preservation of modules between the *Foxp1*$^{+/-}$ mouse

striatal modules and the hNP modules than between the *Foxp1*$^{+/-}$ mouse hippocampal modules and the hNP modules (Fig. 6A). To examine whether any of the preserved human coexpression modules contain specific transcription factor-binding motifs, we used the ChIP enrichment analysis (ChEA) database, which contains experimental ChIP and ENCODE data sets (Lachmann et al. 2010). We found enrichment of FOXP2 motifs as well as other autism-related transcription factors (Fig. 6B). Finally, we used a recently developed tool, Cell-Specific Expression Analysis (CSEA, Xu et al. 2014), to examine within which brain regions and cellular populations the conserved FoxP1 targets are enriched. We found that DEGs down-regulated with loss of Foxp1 and up-regulated with overexpression of FOXP1 are enriched for striatal genes (Fig. 6C). In contrast, genes up-regulated with loss of Foxp1 and down-regulated with overexpression of FOXP1 are enriched for neocortical genes (Fig. 6D). Together, these data suggest that FoxP1 regulates conserved pathways in both humans and mice that are important in preserving MSN identity.

DISCUSSION

Using unbiased genome-wide approaches in a patient-relevant *Foxp1*$^{+/-}$ mouse model and human neural cells, we uncovered a role for FoxP1 regulation of ASD-relevant genes. We observed that Foxp1 regulates gene expression in a region-specific manner within the brain, with the hippocampus and the striatum of *Foxp1*$^{+/-}$ mice containing DEGs enriched for distinct ontological categories. We also uncovered altered neuronal excitability in distinct populations of MSNs as well as gross alterations in the postnatal USVs of *Foxp1*$^{+/-}$ mice. Last, we provide evidence that FoxP1 regulates evolutionarily

conserved neuronal pathways within the striatum, which are important for striatal identity.

The inclusion of FMRP target genes within FoxP1-correlated modules suggests overarching brain mechanisms at risk in ASD pathophysiology. FMRP is an RNA-binding protein that is expressed throughout the brain and is involved in dendritic morphology and plasticity through the translational regulation of numerous genes that function at the synapse (Darnell and Klann 2013). Deletions and mutations of the *FMR1* gene can lead to FXS, which is characterized by autistic traits and intellectual disability (Hernandez et al. 2009). We found an enrichment of genes encoding ion channels altered in both the human and rodent FoxP1 models. For example, DPP10 is an ASD gene that is a conserved FoxP1 target (Figs. 1F, 5I, J). DPP10 functions to traffic surface expression of the KCND2 and KCND3 (or Kv4.2 and Kv4.3, respectively) potassium channels in neurons. We also uncovered activation of Kcnd2 by FoxP1 (Fig. 1F). Moreover, KCND2 is also an FMRP target (Kim et al. 2005); rare variants and genetic association of KCND2 have been reported in autism (Klassen et al. 2011; Lee et al. 2014), and impaired KCND2 function has been implicated in FXS (Gross et al. 2011). This convergence of Foxp1 downstream genes with FMRP-related genes suggests potential converging transcriptional and translational dysregulation in these disorders.

Relative to the entire brain, Foxp1 is among the top 100 enriched genes in the striatum (Heiman et al. 2008). This striatal enrichment of Foxp1 in the brain is greater than the comparative relative striatal expression of Foxp2. We showed significant overlaps between Foxp1 and Foxp2 gene targets in the striatum (in particular, D1 MSN enriched genes) (Fig. 2A, D) and increased D2 MSN excitability in *Foxp1*$^{+/-}$ mice (Fig. 3). Given that Foxp2 is preferentially expressed in D1 MSNs (Vernes et al. 2011), we

hypothesize that Foxp1 and Foxp2 may work in concert to differentially regulate neuronal excitability in these two populations of MSNs and therefore control striatal-based vocalizations. Therefore, the lack of alteration of D1 MSN excitability in *Foxp1*$^{+/-}$ mice might be due to compensation by Foxp2, as supported by the overlapping target genes of Foxp1 and Foxp2 among D1 MSN enriched genes. The identification of Foxp1-specific targets that are known to be involved in neuronal excitability within D2 MSNs also supports the idea that differential gene regulation by Foxp1 in specific MSN subpopulations governs the observed neuronal and organismal phenotypes. For instance, Foxp1 may operate as a master regulator of genes important for overall neuronal function and activity in the striatum, with Foxp2 acting as a limiting factor for shared targets involved in vocalizations. This idea is bolstered by previous findings that Fmr1 and Foxp2 mutant mice exhibit increased striatal GABAergic transmission from and increased long-term depression in MSNs as well as decreased striatal volumes and deficits in postnatal USVs (Shu et al. 2005; Centonze et al. 2008; Enard et al. 2009; Roy et al. 2012; Ellegood et al. 2015). In addition, Foxp2 levels are unchanged in the striatum of *Foxp1*$^{+/-}$mice (Supplemental Table 1) and do not appear to be significantly altered in either MSN population specifically (data not shown), further suggesting that alterations in Foxp2/Foxp1 stoichiometry in D1 MSNs could be driving our findings. Finally, the significant gene coexpression module preservation between the mouse striatal and hNP gene expression data supports the relevance of these mouse data to a human disorder such as ASD. Given the evolutionary distance between these two species and the developmental differences between hNPs and the adult mouse striatum, it is remarkable that these correlations were found. Therefore, such a finding is evidence for the

robustness and relevance of these gene coexpression networks with respect to FoxP1 expression and function.

These data suggest a role for Foxp1 in regulating ASD risk genes in a region-specific manner within the brain. In particular, we demonstrate that Foxp1 plays an important role in regulating genes involved in striatal development and function. In this study, we also provide the first evidence that Foxp1 specifically contributes to vocal communication. It will be important to determine how these changes occur throughout development in further experiments. Since the *Foxp1*$^{+/-}$ mice used in this study were whole-body knockouts and because Foxp1 has been shown to regulate the development of a host of organ systems (Wang et al. 2004; Hu et al. 2006; Shu et al. 2007; Dasen et al. 2008; Rousso et al. 2008), it cannot be entirely ruled out that the behavioral phenotypes displayed by these mice are secondary to the peripheral consequences of the knockout. Additionally, it should be noted that other brain regions besides the striatum, such as the neocortex, are known to both express Foxp1 and contribute to the production of USVs (Hisaoka et al. 2010; Sia et al. 2013). Moreover, while this study focused on a patient-relevant model of FOXP1 function (namely, haploinsufficiency), at least one study has demonstrated increased FOXP1 expression in lymphoblastoid cell lines from ASD patients (Chien et al. 2013). Therefore, the regional contribution and dosage relevance of FoxP1 to the behavioral manifestations presented in this study remain to be determined.

FIGURES

FIGURE 2.1. Regulation of ASD genes by Foxp1 in the mouse brain.

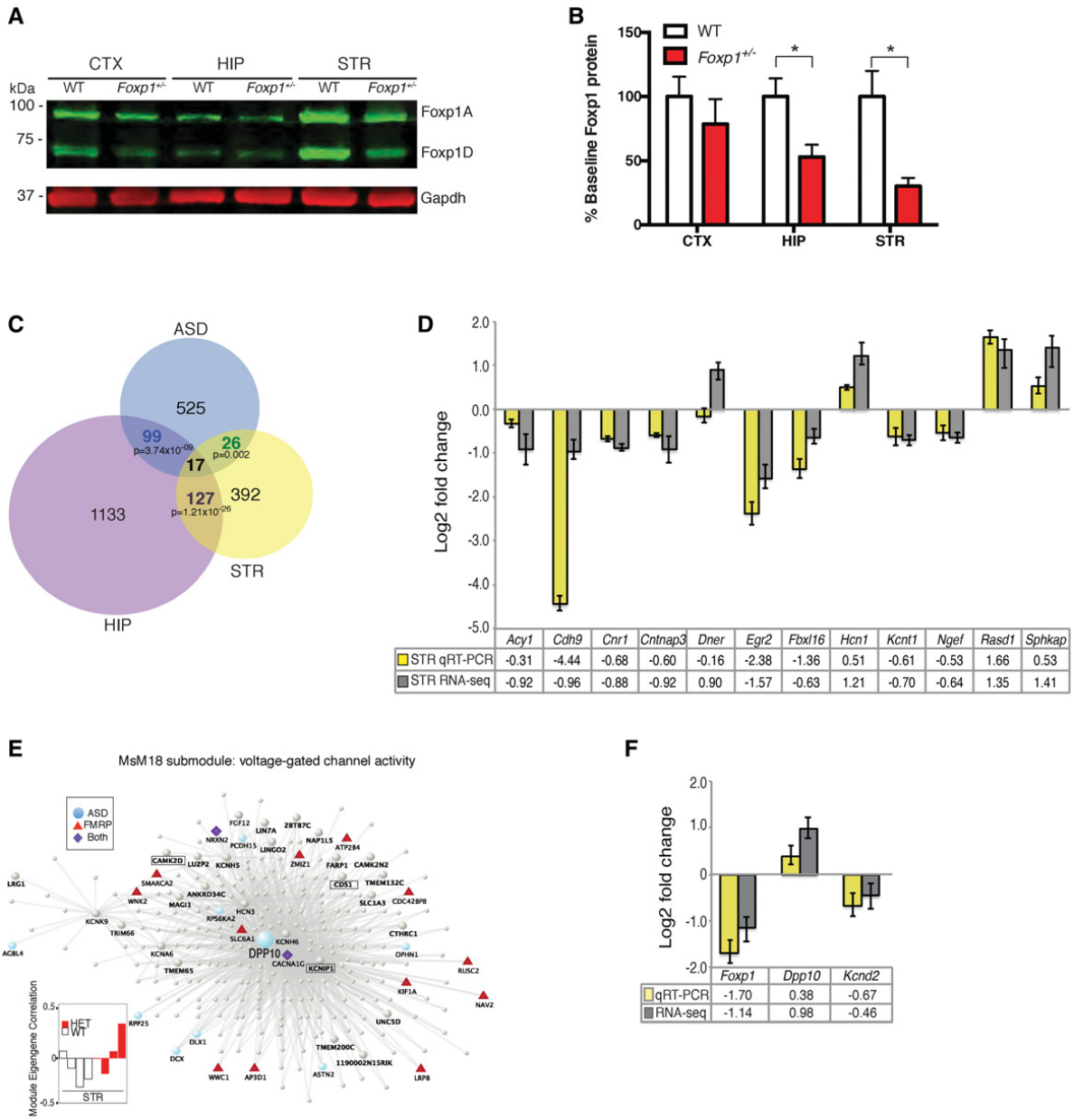

A) Representative immunoblot displaying reduced Foxp1 protein levels in the hippocampus (HIP) and striatum (STR), but not the neocortex (CTX), of *Foxp1*$^{+/-}$ mice. Gapdh was used as a loading control. (B) Quantification of Foxp1 expression in adult Foxp1$^{+/-}$ mouse brains. Data are represented as means ± SEM. n= 4 mice per genotype for each region. (*) P = 0.033 (hippocampus); (*) P = 0.0163 (striatum), Student's t-test,

compared with wild-type levels normalized to Gapdh. (C) Venn diagram showing overlaps between the differentially expressed genes (DEGs) in the mouse and ASD gene lists (144 genes be- tween the hippocampus and striatum [$P = 1.21 \times 10^{-26}$], 116 genes between the hippocampus and ASD [$P = 3.74 \times 10^{-9}$], and 43 genes be- tween the striatum and ASD [P = 0.002], hypergeometric test [P-values were adjusted using Benjamini-Hochberg FDR procedure]). (D) Confirmation of salient ASD-related gene targets in independent striatal samples from *Foxp1*$^{+/-}$ mice using quantitative RT–PCR (qRT–PCR). Data are represented as means ± SEM. n = 4 mice per genotype. With the exception of *Dner*, all qRT–PCR values displayed are significant at $P < 0.05$ (Student's t-test, compared with wild-type levels normalized to actin). (E) Visualization of a striatal-specific submodule (MsM18) that contains Dpp10 (dipeptidyl peptidase) as a major hub gene. (F) qRT–PCR confirmation of Dpp10 and Kcnd2 activation in *Foxp1*$^{+/-}$ mouse striatal samples. Data are represented as means ± SEM. n = 4 mice per genotype. All qRT–PCR values displayed are significant at $P < 0.05$ (Student's t-test, compared with wild-type levels normalized to actin).

FIGURE 2.2. Foxp1 and Foxp2 regulate overlapping targets within the striatum.

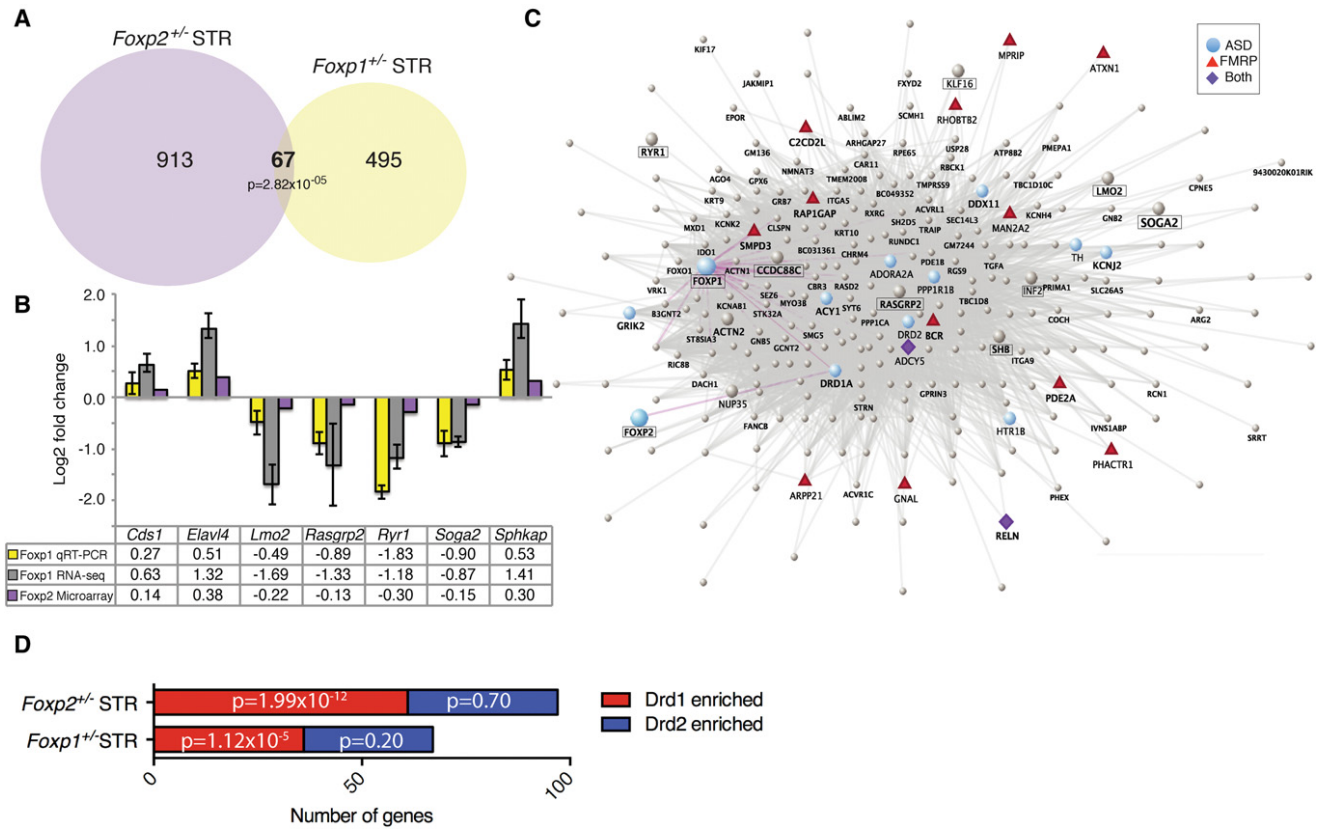

	Cds1	Elavl4	Lmo2	Rasgrp2	Ryr1	Soga2	Sphkap
Foxp1 qRT-PCR	0.27	0.51	-0.49	-0.89	-1.83	-0.90	0.53
Foxp1 RNA-seq	0.63	1.32	-1.69	-1.33	-1.18	-0.87	1.41
Foxp2 Microarray	0.14	0.38	-0.22	-0.13	-0.30	-0.15	0.30

(A) Significant overlap of DEGs in the striatum of *Foxp1*$^{+/-}$ and *Foxp2*$^{+/-}$ mice (67 genes between the *Foxp1*$^{+/-}$ and the *Foxp2*$^{+/-}$ striatal data sets [P = 2.82 × 10^{-5}], hypergeometric test). (B) qRT–PCR confirmation of a subset of these genes in independent *Foxp1*$^{+/-}$ striatal samples. Data are represented as means ± SEM. n = 3 mice per genotype. All qRT–PCR values displayed are significant at P < 0.05 (Student's t-test, compared with wild-type levels normalized to actin). (C) Visualization of the regionally specific striatal module MsM3 showing coexpression of both Foxp1 and Foxp2. Foxp1 and Foxp2 connections are highlighted in magenta. Genes in bold typeface indicate striatal DEGs, and boxed genes indicate Foxp1 and Foxp2 DEGs that overlap. (D) RNA-seq data from *Foxp1*$^{+/-}$ mice and microarray data from *Foxp2*$^{+/-}$ mice were overlapped with the most recently published list of known enriched transcripts within D1 or D2 MSNs (Maze et al. 2014). Genes from both *Foxp1*$^{+/-}$ and *Foxp2*$^{+/-}$ mice significantly

overlapped with D1 MSN-enriched genes (36 genes [$P = 1.12 \times 10^{-5}$] and 61 genes [$P = 1.99 \times 10^{-12}$], respectively, hypergeometric test). P- values for each overlap are shown within bar graphs.

FIGURE 2.3. D2 MSNs of Foxp1$^{+/-}$ mice have increased excitability.

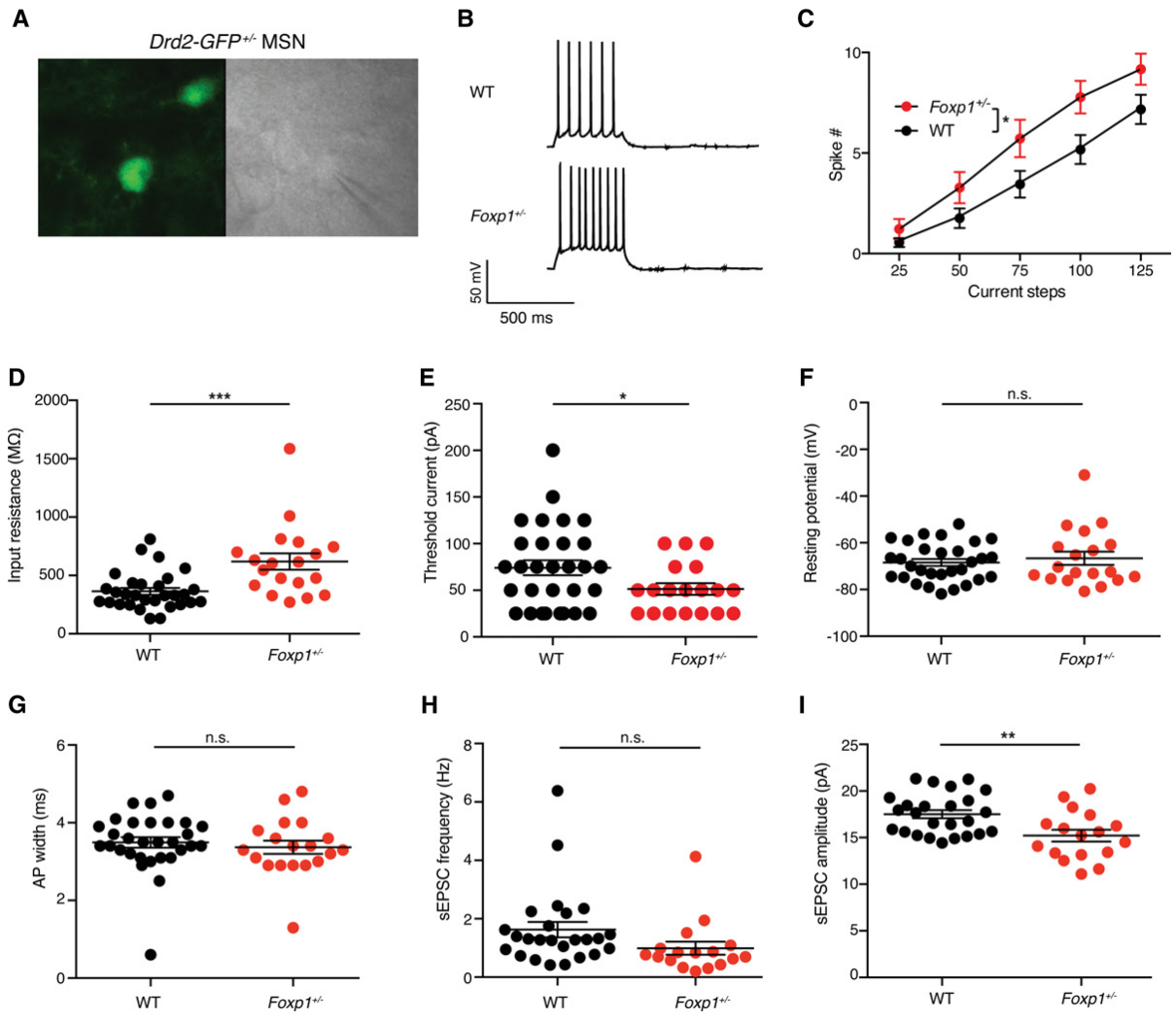

(A) Example image of a recorded GFP^{+} (D2) neuron. (B) Example recordings depicting spiking in response to a 125-pA current step in control and *Foxp1*$^{+/-}$ MSNs. (C) Firing rate versus input curves is significantly increased in *Foxp1*$^{+/-}$ MSNs. Data are represented as means ± SEM. n = 18 wild-type cells and 29 *Foxp1*$^{+/-}$ cells. (*) P = 0.040, two-way ANOVA with repeated measures for current step, compared between genotypes. (D) Input resistance is significantly increased *Foxp1*$^{+/-}$ MSNs. Data are represented as means ± SEM. n = 19 wild-type cells and 30 *Foxp1*$^{+/-}$ cells. (***) P = 0.0004, Student's t-test, compared between genotypes. (E) The minimum, threshold current required for evoking an

action potential is significantly decreased in *Foxp1*$^{+/-}$ MSNs. Data are represented as means ± SEM. n = 19 wild-type cells and 30 *Foxp1*$^{+/-}$ cells. (*) P = 0.049, Student's t-test, compared between genotypes. (F) Resting potential is not significantly changed in *Foxp1*$^{+/-}$ MSNs. Data are represented as means ± SEM. n = 19 wild-type cells and 30 *Foxp1*$^{+/-}$ cells. P = 0.53, Student's t-test, compared between genotypes. (G) Action potential width is not significantly altered in *Foxp1*$^{+/-}$ MSNs. Data are represented as means ± SEM. n = 19 wild-type cells and 30 *Foxp1*$^{+/-}$ cells. P = 0.57, Student's t-test, compared between genotypes. (H) Spontaneous EPSC frequency is not significantly changed in *Foxp1*$^{+/-}$ MSNs. Data are represented as means ± SEM. n = 17 wild-type cells and 25 *Foxp1*$^{+/-}$ cells. P = 0.091, Student's t-test, compared between genotypes. (I) Spontaneous EPSC amplitude is significantly decreased in *Foxp1*$^{+/-}$ MSNs. Data are represented as means ± SEM. n = 17 wild-type cells and 25 *Foxp1*$^{+/-}$ cells. (**) P = 0.004, Student's t-test, compared between genotypes.

FIGURE 2.4. Foxp1 haploinsufficiency results in reduced mouse vocalizations.

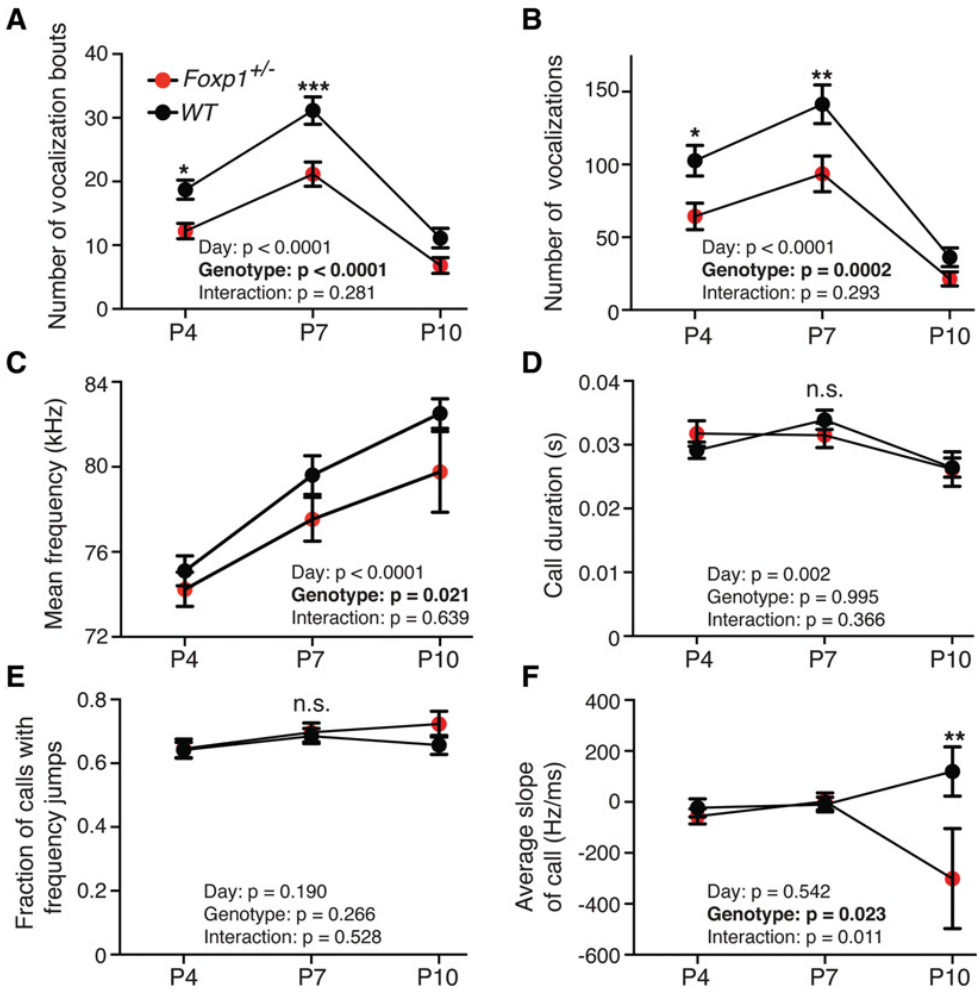

(A) *Foxp1*$^{+/-}$ mouse pups exhibit a significantly reduced number of vocalization bouts. Data are represented as means ± SEM. n = 57 wild-type pups and 34 *Foxp1*$^{+/-}$ pups. (*) P = 0.033 at P4; (***) P = 0.0003 at P7, two-way ANOVA with a Sidak multiple comparison test, compared between genotypes. (B) *Foxp1*$^{+/-}$ mouse pups exhibit fewer total numbers of USVs at P7. Data are represented as means ± SEM. n = 57 wild- type pups and 34 *Foxp1*$^{+/-}$ pups. (*) P = 0.038 at P4; (**) P = 0.006 at P7, two-way ANOVA with a Sidak multiple comparison test, compared between genotypes. (C) As a trend, *Foxp1*$^{+/-}$ mouse pups exhibit a significant reduction in their mean call frequency across all days. Data are represented as means± SEM. n = 57 wild-type pups and 34 *Foxp1*$^{+/-}$

pups. Two-way ANOVA with a Sidak multiple comparison test, compared between genotypes. (D) Foxp1$^{+/-}$ mice show no differences in average call duration. Data are represented as means ± SEM. n = 57 wild-type pups and 34 *Foxp1*$^{+/-}$ pups. P = 0.99, two-way ANOVA with a Sidak multiple comparison test, compared between genotypes. (E) *Foxp1*$^{+/-}$ mice show no difference in the fraction of calls with frequency jumps. Data are represented as means ± SEM. n = 57 wild-type pups and 34 *Foxp1*$^{+/-}$ pups. P = 0.27, two-way ANOVA with a Sidak multiple comparison test, compared between genotypes. (F) *Foxp1*$^{+/-}$ mice display a significant reduction in the average slope of a call at P10. Data are represented as means ± SEM. n = 57 wild-type pups and 34 *Foxp1*$^{+/-}$ pups. (**) P = 0.001, two-way ANOVA with a Sidak multiple comparison test, compared between genotypes. The main effects for genotype and postnatal day and the interactions between these two variables are reported at the bottom of each panel.

FIGURE 2.5. Gene regulation by FOXP1 in human neural cells.

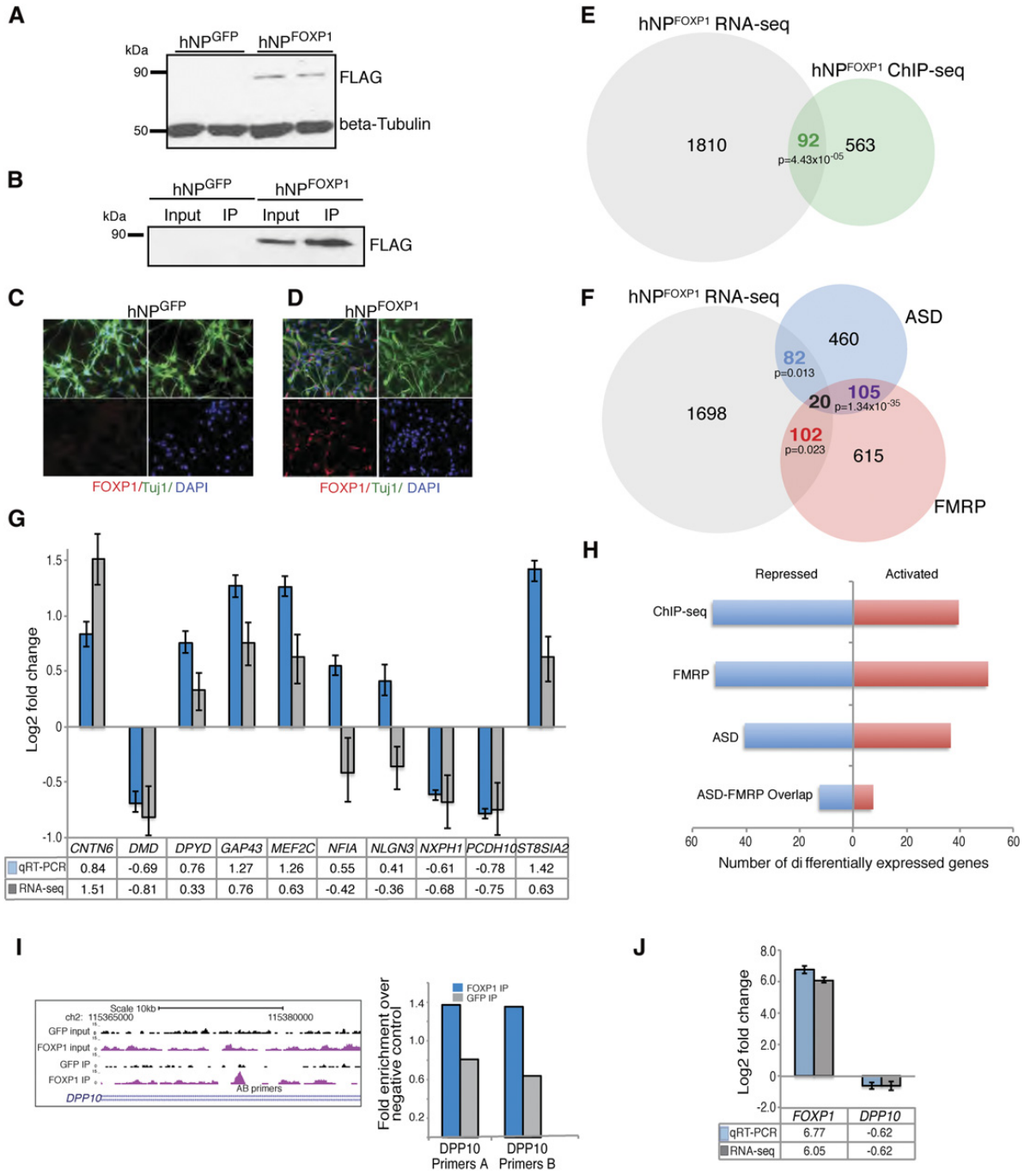

(A) Representative immunoblot depicting overexpression of FOXP-Flag signal in hNPs transduced with a FOXP1-Flag expression construct (hNP^{FOXP1}) but not in hNPs with a GFP expression construct (hNP^{GFP}). β-Tubulin was used as a loading control. (B) Representative immunoblot confirming expression of FOXP1-Flag in input samples and

enrichment of FOXP1-Flag during the immunoprecipitation (IP) portion of ChIP from hNP^{FOXP1} lysates. (C, D) Representative images of hNP^{GFP} and hNP^{FOXP1} demonstrate that FOXP1 expression (red) in hNP^{FOXP1} is restricted to the nucleus (DAPI, blue) and that FOXP1 is not expressed within neurites (Tuj1, green) and is absent in hNP^{GFP}. (E) Significant overlap between gene targets from RNA-seq and ChIP-seq (ChIP followed by DNA sequencing) performed on hNP^{FOXP1} (92 genes between hNP^{FOXP1} RNA-seq and hNP^{FOXP1} ChIP-seq [$P = 4.43 \times 10^{-5}$, hypergeometric test]). (F) Significant overlap among RNA-seq DEGs, ASD genes, and FMRP targets (102 genes between hNP^{FOXP1} RNA-seq and ASD genes [P = 0.013], 122 genes between hNP^{FOXP1} RNA-seq and FMRP genes [P = 0.023], and 125 genes between ASD and FMRP genes [$P = 1.34 \times 10^{-35}$], hypergeometric test [P-values were adjusted using Benjamini-Hochberg FDR procedure]). (G) qRT–PCR confirmation of a subset of these overlapping genes in independent hNP^{FOXP1} samples. Data are represented as means ± SEM. n = 4 samples per treatment. All qRT–PCR values displayed are significant at $P < 0.05$ (Student's t-test, compared with hNP^{GFP} levels normalized to actin). (H) DEGs from these overlaps are equally represented among repressed and activated genes. (I, left panel) Human genome browser view showing the ChIP-seq result of enrichment of FOXP1 binding compared with GFP control. (Right panel) ChIP- PCR confirmation of enriched binding of DPP10 by FOXP1 in hNP^{FOXP1} compared with hNP^{GFP} using two separate primer pairs (DPP10 primers A and B) compared with control primers. Quantified data are represented as means ± SEM, four samples per treatment. All qRT–PCR values displayed are significant at $P < 0.05$ (Student's t-test, compared with hNP^{GFP} levels normalized to actin). (J) DPP10 is repressed with FOXP1 overexpression in hNP^{FOXP1} samples. Quantified data are represented as means ± SEM, four samples per treatment. All qRT–PCR values displayed are significant at $P < 0.05$ (Student's t-test, compared with hNP^{GFP} levels normalized to actin).

FIGURE 2.6. Coexpression network preservation between mouse and human data sets.

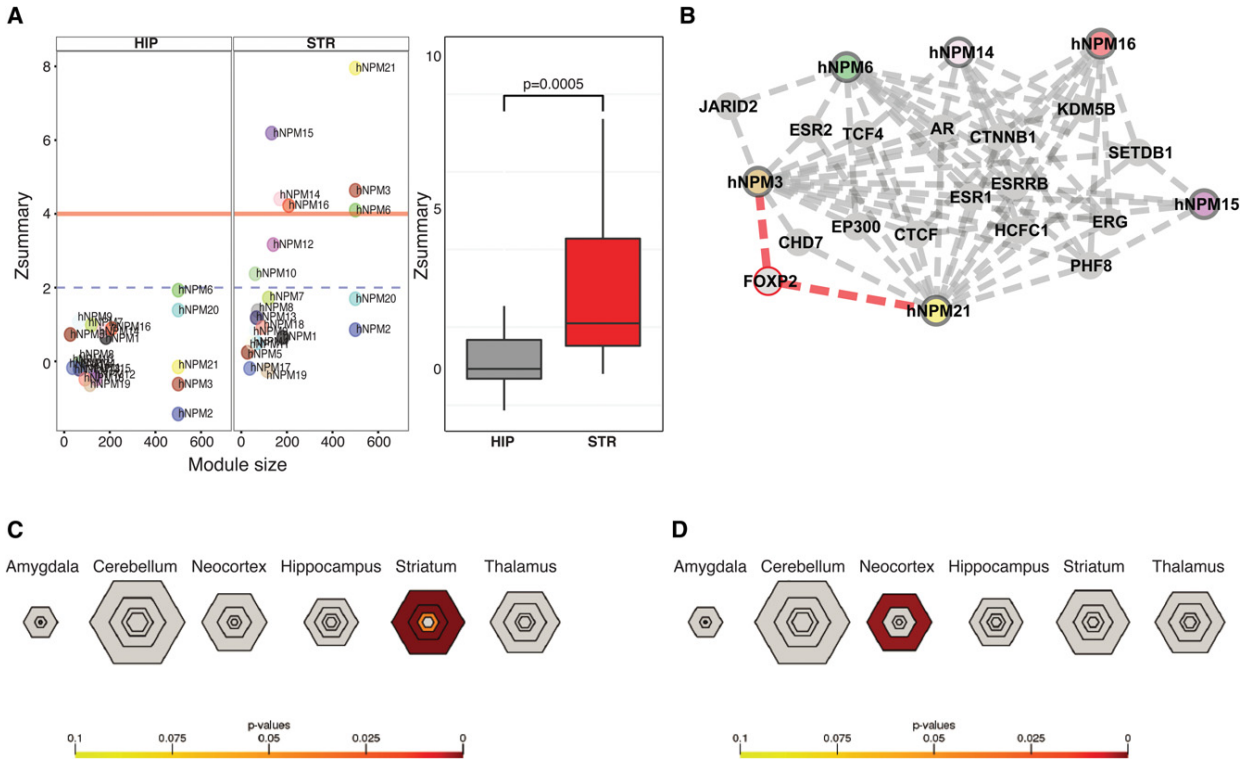

(A) Module preservation analysis revealed that significantly more hNP modules are preserved in the striatum compared with the hippocampus. Zsummary scores >4 are well preserved, and those <2 are poorly preserved. (B) Genes in modules shared between humans and mice contain conserved binding sites for ASD-associated transcription factors, including FoxP2. (C) Genes down-regulated by loss of Foxp1 in mice and up-regulated by overexpression of FOXP1 in hNPs are enriched for striatal-associated genes. (D) Genes up-regulated by loss of Foxp1 in mice and down-regulated by overexpression of FOXP1 in hNPs are enriched for cortical genes. Briefly, hexagons are scaled to the stringency values of the specificity index thresholds (pSI), which ranks the region-specific enriched transcript gene lists from least specific to highly specific transcripts; i.e., outer hexagons represent larger, less specific lists (pSI of 0.05), while inner hexagons represent shorter, highly specific lists (pSI of 0.001). Bonferroni-Hochberg (BH)-corrected P-values are shown.

SUPPLEMENTAL FIGURE 2.1. Immunoblot for Foxp1 demonstrating antibody specificity.

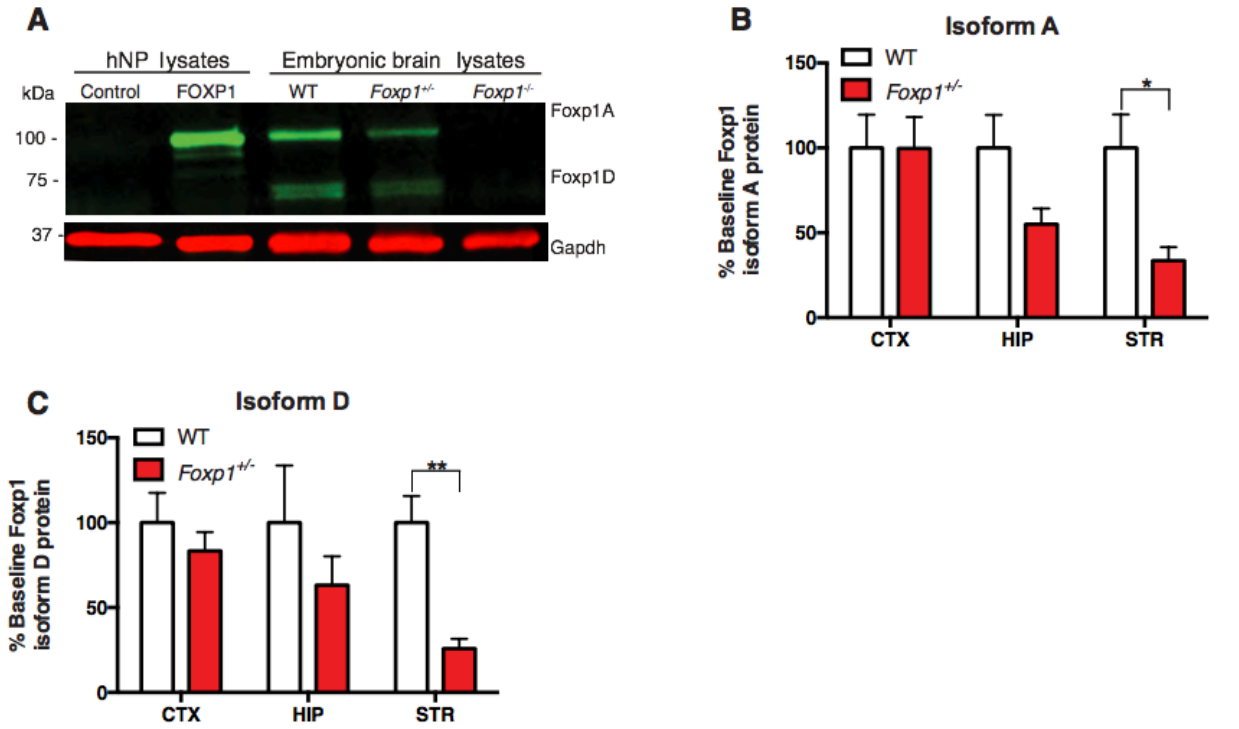

(**A**) hNP samples expressing FOXP1 and E13.5 mouse brain lysates from control and *Foxp1*$^{+/-}$ mice demonstrate expression whereas hNPs with GFP expression and brain lysate from *Foxp1* KO embryos do not demonstrate expression. (**B**) Foxp1A is significantly reduced only in the STR of *Foxp1*$^{+/-}$ mice. Data are represented as means (±SEM). N=4 mice/genotype for each region. *P=0.02 (Student's t-test, compared to wildtype (WT) levels normalized to Gapdh). (**C**) Foxp1D is significantly reduced only in the STR of *Foxp1*$^{+/-}$ mice. Data are represented as means (±SEM). N=4mice/genotype for each region. *P=0.004 (Student's t-test, compared to wildtype (WT) levels normalized to Gapdh).

SUPPLEMENTAL FIGURE 2.2. Foxp1 and Foxp2 regulate overlapping targets within the striatum.

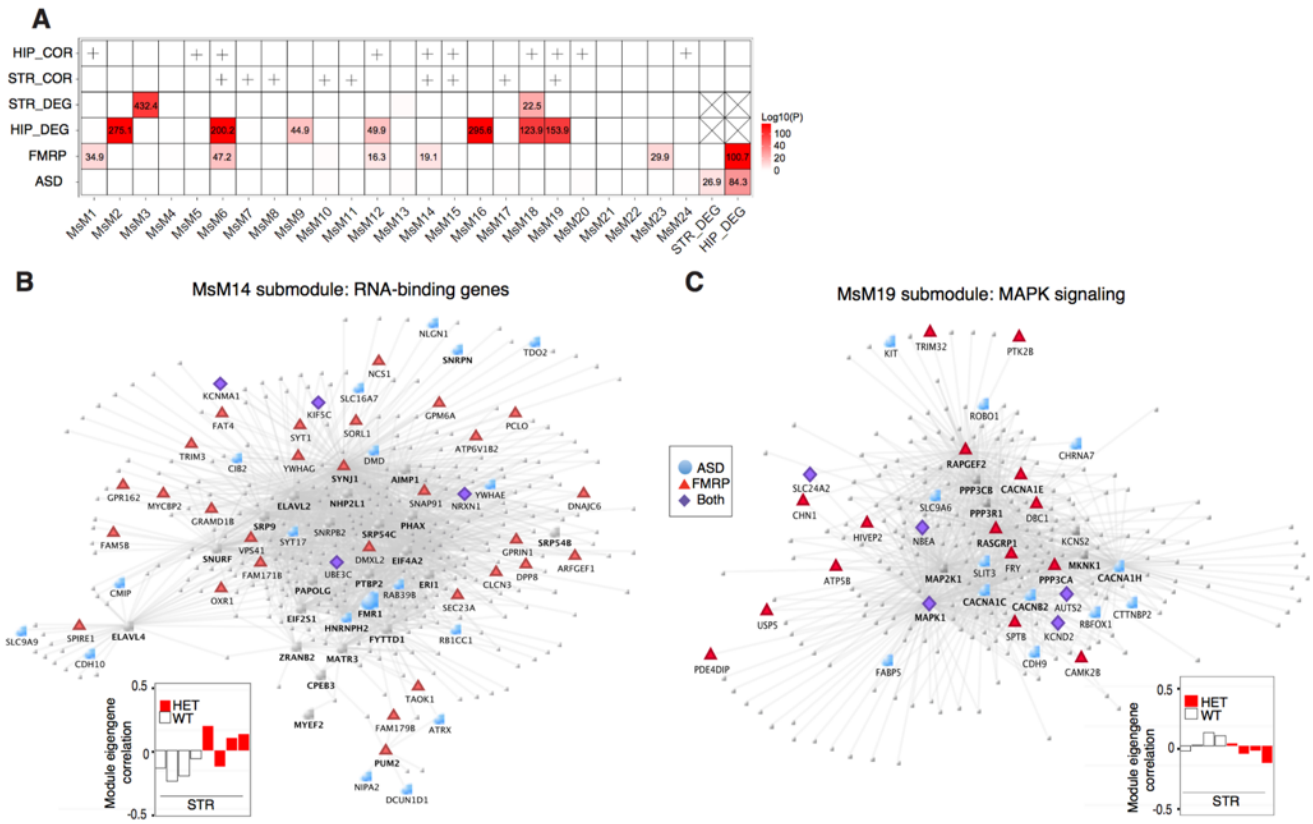

(**A**) Heatmap displaying *Foxp1*$^{+/-}$ mouse RNA-seq WGCNA modules that contain significant enrichments of DEGs, ASD genes and/or FMRP targets. Plus signs indicate a genotype correlation of modules within specific brain regions. Log-transformed adjusted P-values from Benjamini-Hochberg false-discovery test (hypergeometric test). (**B** and **C**) Visualization of MsM19 containing genes significantly enriched in GO categories (using DAVD bioinformatics tool, http://david.abcc.ncifcrf.gov) for MAPK signaling (MsM19). Inserts: eigengene correlation plots show that genotype correlates negatively for MsM19 within the striatum.

SUPPLEMENTAL FIGURE 2.3. D1 positive medium spiny neurons of Foxp1$^{+/-}$ mice have no change in excitability.

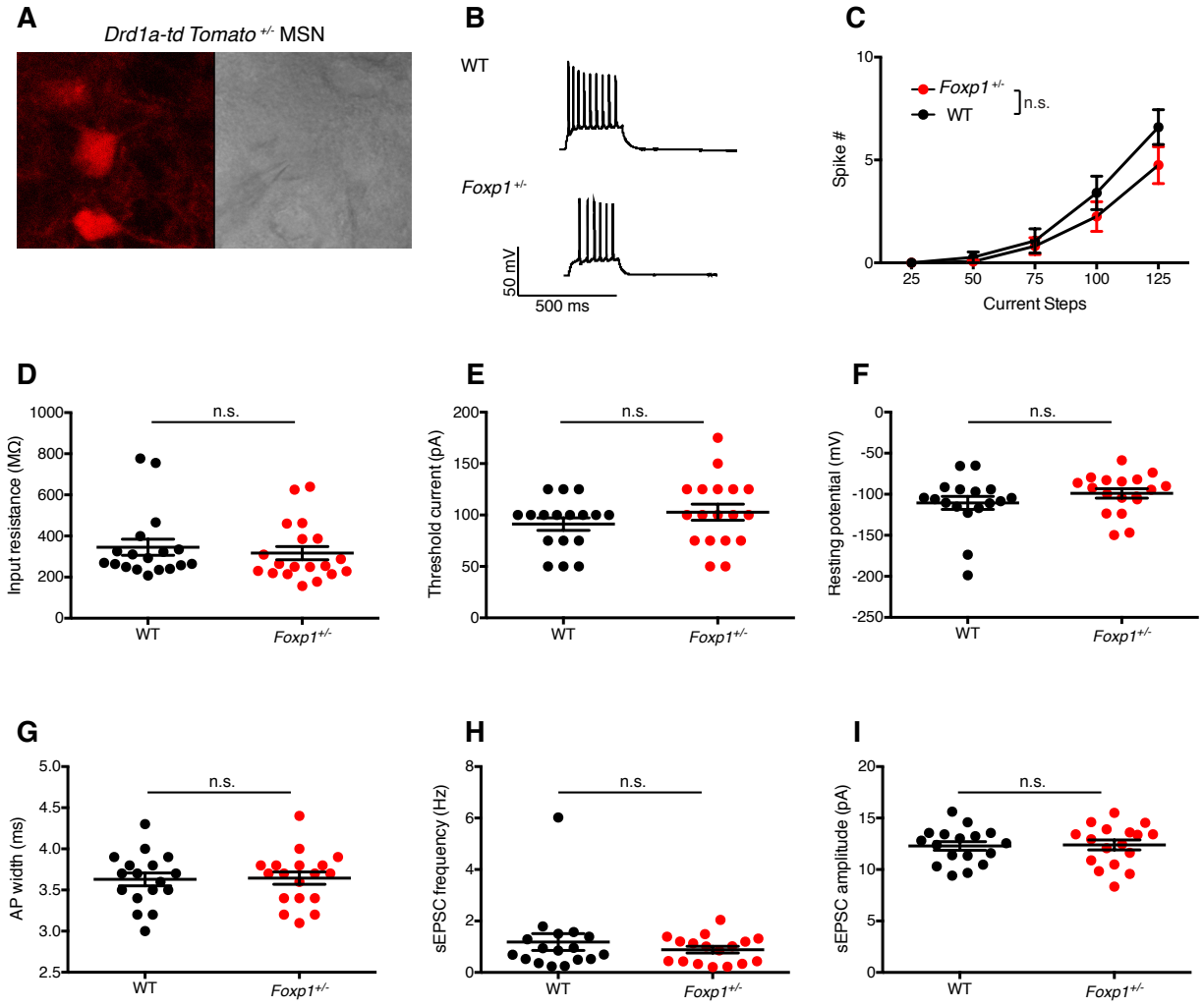

(**A**) Example image of a recorded tdTomato+ (D1) neuron. (**B**) Example recordings depicting spiking in response to a 125 pA current step in control and *Foxp1*$^{+/-}$ MSNs. (**C**) Firing rate versus input curves are not significantly changed in *Foxp1*$^{+/-}$ MSNs. Data are represented as means (±SEM). N=15 WT cells, 16 *Foxp1*$^{+/-}$ cells. P=0.26 (two-way ANOVA with repeated measures for current step, compared between genotypes). (**D**) Input resistance is not significantly different in *Foxp1*$^{+/-}$ MSNs. Data are represented as means (±SEM). N=18 WT cells, 19 *Foxp1*$^{+/-}$ cells. P=0.58 (Student's t-test, compared between genotypes). (**E**) The minimum threshold current required for evoking an action potential is not significantly altered in *Foxp1*$^{+/-}$ MSNs. Data are represented as means (±SEM). N=17 WT cells, 18 *Foxp1*$^{+/-}$ cells. P=0.25 (Student's t-test, compared between

genotypes). (**F**) Resting potential is not significantly changed in *Foxp1*$^{+/-}$ MSNs. Data are represented as means (±SEM). N=17 WT cells, 18 *Foxp1*$^{+/-}$ cells. P=0.24 (Student's t-test, compared between genotypes). (**G**) Action potential width is not significantly altered in *Foxp1*$^{+/-}$ MSNs. Data are represented as means (±SEM). N=17 WT cells, 18 *Foxp1*$^{+/-}$ cells. P=0.89 (Student's t-test, compared between genotypes). (**H**) Spontaneous EPSC frequency is not significantly changed in *Foxp1*$^{+/-}$ MSNs. Data are represented as means (±SEM). N=17 WT cells, 17 *Foxp1*$^{+/-}$ cells. P=0.40 (Student's t-test, compared between genotypes). (**I**) Spontaneous EPSC amplitude is significantly decreased in *Foxp1*$^{+/-}$ MSNs. Data are represented as means (±SEM). N=17 WT cells, 17 *Foxp1*$^{+/-}$ cells. P=0.88 (Student's t-test, compared between genotypes).

SUPPLEMENTAL FIGURE 2.4. USV analysis parameters and weight gain of Foxp1$^{+/-}$ mice.

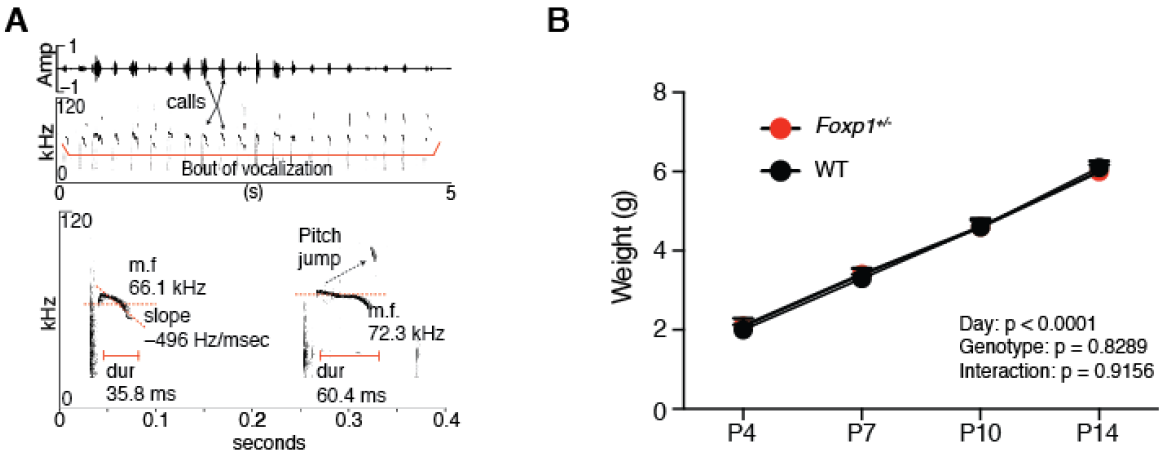

(**A**) Illustration marking all major USV parameters measured including bouts, calls, mean frequency (m.f.), call duration (dur), slope, and jumps. (**B**) *Foxp1*$^{+/-}$ mice do not weigh significantly less than control littermates. Data are represented as means (±SEM). N=38 WT pups, 22 *Foxp1*$^{+/-}$ pups. P=0.83 (two-way ANOVA with a Sidak multiple comparison test, compared between genotypes). The main effects for genotype and postnatal day, and the interactions between these two variables, are reported at the bottom of the panel.

SUPPLEMENTAL FIGURE 2.5. Behavioral characterization of Foxp1$^{+/-}$ mice.

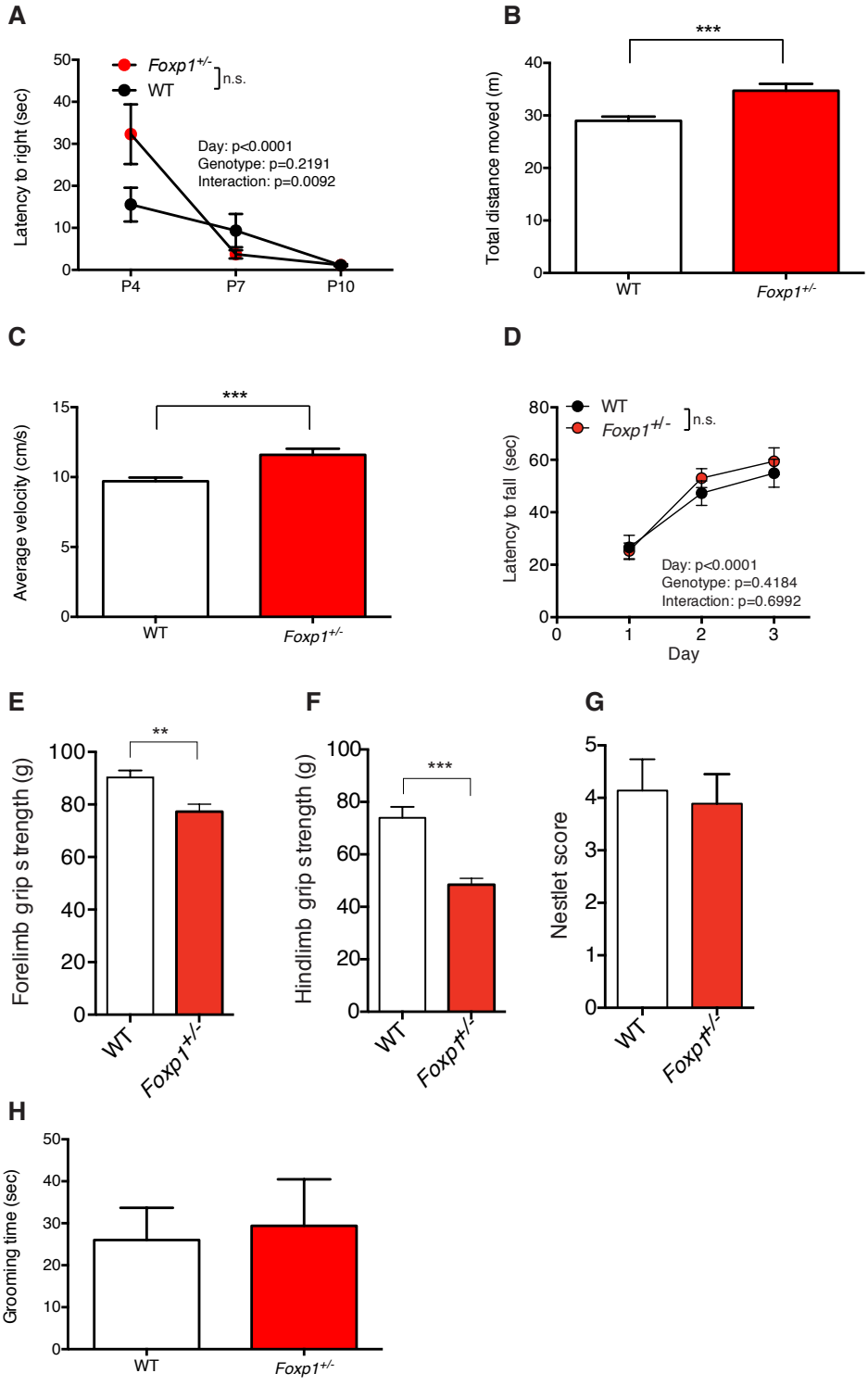

(**A**) Righting reflexes in *Foxp1*$^{+/-}$ pups at P4, P7, and P10. Data are represented as means (±SEM). N=11 *Foxp1*$^{+/-}$ pups, 15 WT pups. P=0.22 (two-way ANOVA with a Sidak multiple

comparison test, compared between genotypes). (**B and C**) *Foxp1*$^{+/-}$ mice display hyperactivity in the open field test. (**B**) *Foxp1*$^{+/-}$ mice display increased total distance moved and (**C**) an increased average velocity in the open field test compared to WT mice. Data are represented as means (±SEM). N= 27 *Foxp1*$^{+/-}$ mice, 39 WT mice. P=0.0006, P=0.0007, respectively (unpaired Student's t-test, compared between genotypes). (**C**) *Foxp1*$^{+/-}$ mice do not exhibit deficits in motor coordination as measured by the latency to fall during the Rotorod behavioral test. Data represented as means (±SEM) of 4 trials per day. N=9 *Foxp1*$^{+/-}$ mice*,* 7 WT mice (two-way ANOVA with a Sidak multiple comparison test, compared between genotypes). **(D**) *Foxp1*$^{+/-}$ mice exhibit deficits in grip strength in both forelimbs and (**E**) hindlimbs. Data represented as means (±SEM). N=9 *Foxp1*$^{+/-}$ adults*,* 7 WT adults. **P=0.0058, ***P<0.0001 (unpaired Student's t-test, compared between genotypes). (**F**) *Foxp1*$^{+/-}$ mice show no difference in nesting behavior. Data represented as means (±SEM). N=9 *Foxp1*$^{+/-}$ mice*,* 7 WT mice. P=0.7667 (unpaired Student's t-test, compared between genotypes). (**G**) *Foxp1*$^{+/-}$ mice show no difference in grooming behavior. Data represented as means (±SEM). N=5 *Foxp1*$^{+/-}$ mice, 5 WT mice. P=0.81 (unpaired Student's t-test, compared between genotypes).

SUPPLEMENTAL FIGURE 2.6. SHIRPA battery results.

Test	*Foxp1*$^{+/-}$	WT	*p-value*
1. Body position	1 (±0)	1 (±0)	NS
2. Tremor	0 (±0)	0 (±0)	NS
3. Palpebal closure	0 (±0)	0 (±0)	NS
4. Coat appearance	0.11 (±0.99)	0 (±0)	NS
5. Skin color	1 (±0)	1 (±0)	NS
6. Whiskers	0 (±0)	0 (±0)	NS
7. Lacrimation	0 (±0)	0 (±0)	NS
8. Defecation	0.22 (±0.44)	0.57 (±0.53)	NS
9. Gait	0 (±0)	0 (±0)	NS
10. Tail elevation	0 (±0)	0 (±0)	NS
11. Touch escape	1.89 (±0.33)	2 (±0)	NS
12. Trunk curl	0.22 (±0.44)	0.14 (±0.38)	NS
13. Limb grasping	0.89 (±0.33)	1 (±0)	NS
14. Pinna reflex	1 (±0)	1 (±0)	NS
15. Corneal reflex	1 (±0)	1 (±0)	NS
16. Contact righting reflex	0 (±0)	0 (±0)	NS
17. Evidence of biting	0 (±0)	0 (±0)	NS
18. Vocalization (audible)	0 (±0)	0.14 (±0.38)	NS
19. Startle response	1 (±0)	1 (±0)	NS
20. Positional passivity	0.78 (±0.83)	0.43 (±0.53)	NS

Foxp1$^{+/-}$ mice underwent a modified SHIRPA behavioral screen and no differences were found between the 20 different categories tested. Individual tests were scored between 0-1, 0-2, or 0-3. Data represented as means (±SEM). N=9 *Foxp1*$^{+/-}$ mice, 7 WT mice.

SUPPLEMENTAL FIGURE 2.7. FOXP1 ChIP-seq characterization.

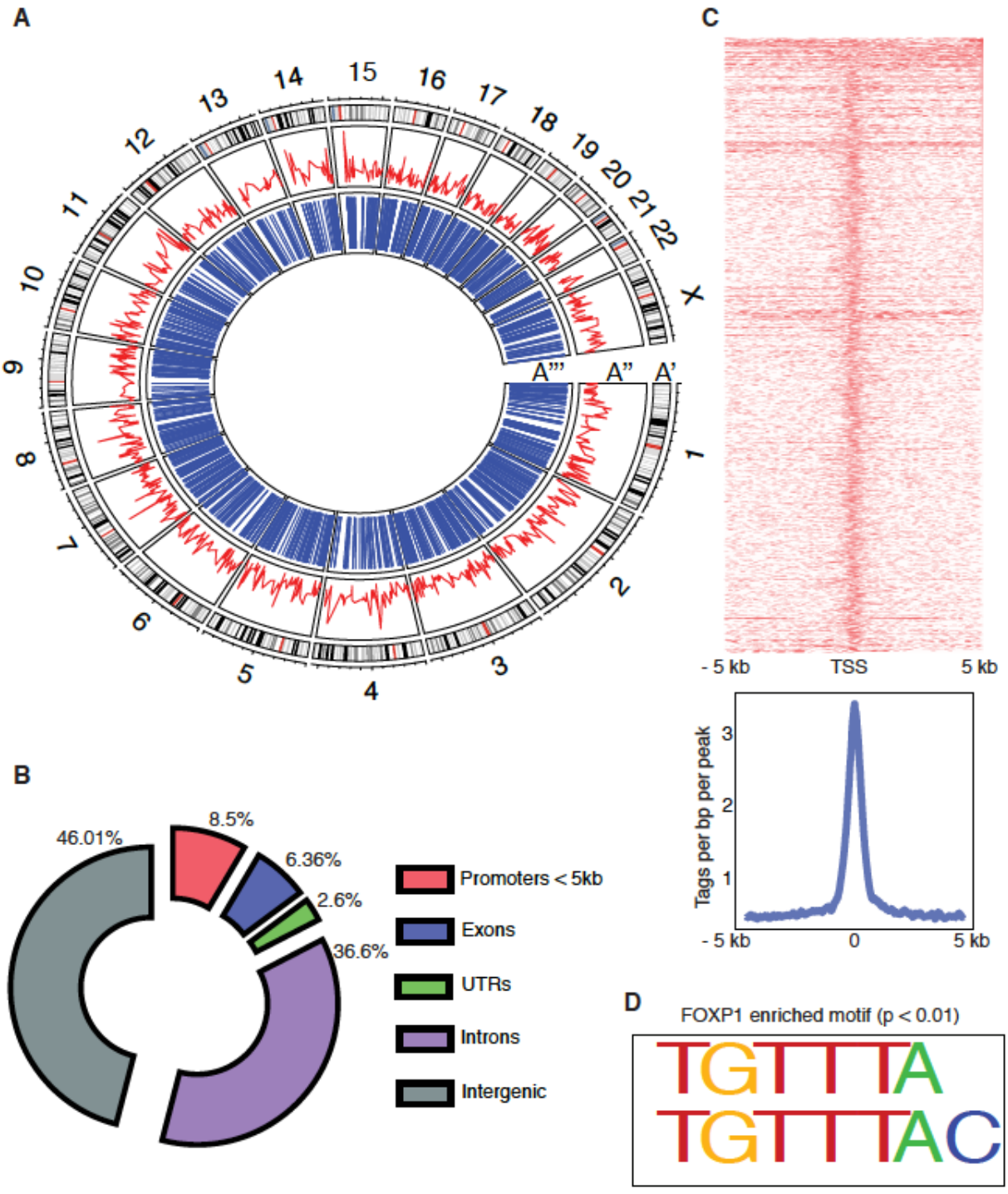

A) Circular visualization of FOXP1 ChIP-seq. A' represents the chromosomal cytoband, A'' represents the FOXP1 peak height, and A''' represents the genomic distribution of FOXP1 binding sites. (**B**) Distribution of all FOXP1 binding site peaks in relation to gene

structure. (**C**) Heat map of FOXP1 ChIP-seq enrichment within gene promoters. Each row represents a 10-kb window extending 5kb upstream and 5kb downstream of the transcriptional start site (TSS). Bottom panel shows the average FOXP1 ChIP-seq enrichment across 5kb upstream and 5kb downstream of the TSS. (**D**) Enriched FOXP1 motifs within the detected peaks compared with GFP control.

SUPPLEMENTAL FIGURE 2.8. Overlaps between hNP WGCNA modules and gene lists.

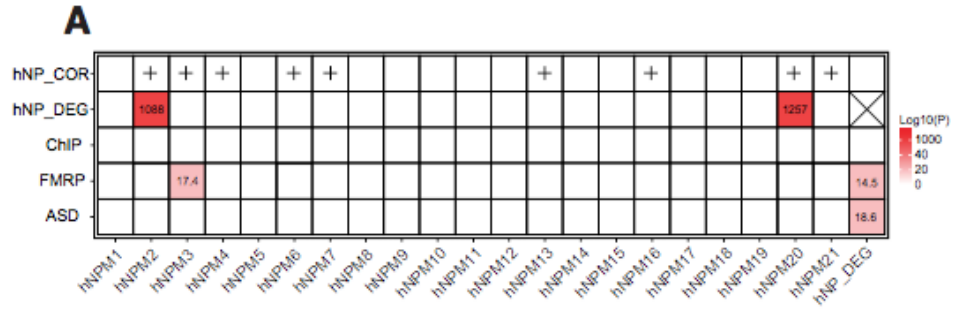

A) Heatmap displaying hNP^{FOXP1} WGCNA modules that contain significant enrichments of DEGs, ASD genes. ASD scored genes, and/or FMRP targets. Log-transformed adjusted P-values from Benjamini-Hochberg false-discovery test (hypergeometric test). hNP_COR positive modules correlate with FOXP1 genotype. hNP_DEG indicates enrichment of FOXP1 differentially expressed genes.

METHODS

Mice

Foxp1 heterozygous knockout (*Foxp1*$^{+/-}$) mice were backcrossed with C57BL/6J mice for at least 10 generations to obtain congenic animals. Drd1a-tdTomato line 6 and Drd2-GFP reporter mice were generously provided by Dr. Craig Powell and maintained on a C57BL/6J background. Mice were kept in the barrier facilities of the University of Texas Southwestern Medical Center un- der a 12 h light–dark cycle and given ad libitum access to water and food. All studies with mice were approved by the University of Texas Southwestern Institutional Animal Care and Use Committee.

hNP cultures

hNP cultures were purchased from Lonza and maintained as previously described (Konopka et al. 2012). hNPs were transduced with lentiviruses containing pLUGIP-FOXP1-3XFlag or pLUGIP- GFP (control) and harvested 3 d after transduction for down-stream applications, including immunoblotting, qRT–PCR, RNA-seq, and ChIP-seq.

RNA harvesting and real-time RT–PCR

RNA was purified from either hNPs or tissues dissected out from P47 male *Foxp1*$^{+/-}$ mice and littermate controls using an mRNeasy minikit (Qiagen) following the manufacturer's recommendations. qRT–PCR was performed as previously described (Spiteri et al. 2007). All primer sequences are available on request.

RNA-seq

mRNA was isolated from total RNA samples using polyA selection. Four independent samples from each brain region or cell type per genotype were included for a total of 24 mouse samples and eight human samples. Samples were randomized, and bar- coded libraries were generated following the manufacturer's instructions (Illumina). RNA-seq was performed by the McDermott Sequencing Core at the University of Texas Southwestern Medical Center on an Illumina HiSeq 2000 sequencer (Illumina). Stranded, single-end 50-base-pair (bp) reads were generated for the hNP data, and stranded, paired-end 100-bp reads were generated for the mouse data.

RNA-seq data analysis

Reads were aligned to either hg19 or mm10 using TopHat (Trap- nell et al. 2009) and Bowtie (Langmead et al. 2009). To obtain the gene counts, we used the HTSeq package (Anders et al. 2014), and the reads were normalized using the RPKM (reads per kilobase per million mapped reads) method (Mortazavi et al. 2008) implemented in the RSeQC package (Wang et al. 2012). For further analysis, we performed a sample-specific RPKM filtering considering genes with RPKM values of 0.5 in treatments or controls. EdgeR (Robinson et al. 2010) was used to detect the DEGs in each species. We applied a filter of FDR of <0.05 and absolute log fold change of >0.3 for both the human and mouse data sets. We then reconstructed the human and mouse coexpression networks using the R package WGCNA (Langfelder and Horvath 2008). Modules were characterized using the biweight midcorrelation followed by signed network topology for both human and mouse data. Modules containing ≥30 genes were included in our analyses. For module

visualization, we used the publicly available VisANT software (Hu et al. 2013). To determine the re- liability of the WGCNA module characterization and the DEGs, we performed a permutation test randomizing 1000 times the expression data associated with each gene, calculated the DEGs, and then applied the same module characterization. None of the permuted data showed similar module detection or different expression profiles compared with the observed data. We then considered the detected modules, the detected DEGs, and the further gene overlaps significantly different from random expectation (permutation test, $P = 0.001$). To infer the significance of the potential overlaps, we adapted a hypergeometric test. The resultant P-values were adjusted using the Benjamini-Hochberg FDR method (Benjamini and Hochberg 1995).

Foxp2 microarray analysis

Data from project GSE13588 (Enard et al. 2009) were downloaded from Gene Expression Omnibus (GEO) (http://www.ncbi.nlm.nih .gov/geo). Only Foxp2 heterozygous and matching control samples were selected for further analysis. Microarrays were analyzed using the R programming language and Bioconductor packages. We determined gene expression levels (robust multichip average [RMA] values) and MAS5 detection P-values from the probes using the “affy” library (Gautier et al. 2004). We considered the probe sets detected in at least one sample for a $P < 0.05$. Differentially expressed probe sets were then determined adapting the f-test function implemented in the “multtest” library (Pollard et al. 2005). The resulting P-values were then adjusted with the Benjamini-Hochberg method. Probe sets were considered differentially expressed for an adjusted $P < 0.05$.

GO analysis

GO analysis was carried out using DAVID (http://david.abcc.ncifcrf.gov). A category containing at least three genes and a corrected P-value of <0.05 (Benjamini-Hochberg method) was considered significant.

Antibodies

The following antibodies were used for immunoblotting (IB), immunoprecipitation (IP), or immunocytochemistry (ICC): anti- β-tubulin (rabbit, 1:10,000; abcam, 6046 [IB]), anti-Flag (mouse, 1:10,000 [IB/ICC], 10 µg [IP]; Sigma, F1804), anti-Foxp1 (rabbit, 1:5000 [IB], 1:1000 [ICC]) (Spiteri et al. 2007), anti-Gapdh (mouse, 1:5000; Millipore [IB]), and anti-Tuj1 (mouse, 1:1000 [ICC]; Covance, MMS-435P).

ChIP-seq

Fifty-million hNPs were used per experimental condition. Cells were fixed in 1% methanol-free formaldehyde for 10 min at room temperature and then quenched with glycine (125 mM final). Cells were washed twice in 1× cold PBS, resuspended in 10 mL of lysis buffer (50 mM HEPES-KOH at pH 7.5, 140 mM NaCl, 1 mM EDTA, 10% glycerol, 0.5% IGEPAL-CA630, 0.25% TritonX-100, 10 µL/mL protease inhibitor [PI] cocktail [Sigma], 7 µL/mL PMSF), and incubated for 10 min on ice. Pelleted cell nuclei were then resuspended in 1 mL of nucleus lysis buffer (200 mM NaCl, 1 mM EDTA, 0.5 mM EGTA, 10 mM Tris-HCl at pH 8.0, 10 µL/mL PI, 7 µL/mL PMSF) and incubated for 10 min on ice. Samples were sonicated in 300 µL of shearing buffer (1 mM EDTA, 0.5 mM EGTA, 10 mM Tris-HCl at pH 8.0, 0.1% SDS, 10 µL/mL PI, 7 µL/mL PMSF) using a Bioruptor (Diagenode) at 3-min

intervals for a total of 12 min. Ten percent of volume from each sample was collected for input controls. One-hundred micrograms of precleared sheared chromatin and 1 µg of msFlag antibody were incubated overnight at 4°C while rotating. Magnetic IgG Dynabeads (Invitrogen) were washed three times with 5 mg/mL BSA solution in PBS and then incubated with sheared chromatin/antibody solution for 2 h at 4°C. Magnets were applied to samples at 4°C, and beads were washed with 500 µL of each of the following solutions supplemented with PI and rotated for 5 min at 4°C followed by magnetic separation: (1) low-salt wash buffer (0.1% SDS, 1% TritonX-100, 2 mM EDTA, 20 mM Tris-HCl at pH 8.0, 150 mM NaCl), (2) high-salt wash buffer (0.1% SDS, 1% TritonX-100, 2 mM EDTA, 20 mM Tris-HCl at pH 8.0, 500 mM NaCl), (3) LiCl wash buffer (0.25 M LiCl, 1% IGEPAL-CA630, 1% deoxycholic acid, 1 mM EDTA, 10 mM Tris-HCl at pH 8.0), and (4) TE buffer. After washes, beads were resuspended in elution buffer (50 mM Tris-HCl, 10 mM EDTA, 1% SDS) and incubated for 15 min at 65°C with vortexing every 2 min. Beads were magnetically separated, supernatant was collected, and cross-linking of all samples and inputs was reversed overnight at 65°C. DNA was purified using Qiagen MinElute columns and quantified using a Qubit Fluorometer. Sequencing was performed by the University of Texas Southwestern Medical Center McDermott Sequencing Core.

ChIP-seq data analysis

Reads were mapped to the human genome (hg19) using TopHat (Trapnell et al. 2009) and Bowtie (Langmead et al. 2009). The aligned reads were subsequently downsampled according to the lowest number of reads detected, whereas the potential duplicated reads were removed using the Picard package (http://broadinstitute.github.io/picard). The

uniquely mapped reads were then analyzed using MACS (Zhang et al. 2008) for the detection of potential peaks. PeakSplitter (Salmon-Divon et al. 2010) was used to subdivide the larger peaks into smaller, more precise peaks using a height filtering of 0.7. The FOXP1 peaks were further compared with the GFP peaks applying a tag density ratio (TDR). For further analysis, we considered FOXP1 peaks with a TDR >2.0. The uncovered peaks were then annotated using the annotatePeaks function implemented in the HOMER package (Heinz et al. 2010).

Immunoblotting

Cellular lysates were obtained using lysis buffer containing 0.5% Nonidet P-40,1 mM PMSF, 0.1 mM Na_3VO_4, 50 mM NaF, 1 uM DTT, 2 µg/mL pepstatin, and 1 µg/mL leupeptin. Tissue samples were lysed in buffer containing 1% Igepal, 1 mM PMSF, 0.1 mM Na_3VO_4, 2 µg/mL pepstatin, and 1 µg/mL leupeptin. Protein concentrations were determined using a Bradford assay (Bio-Rad). A total of 35–45 µg of each sample was run and processed following standard protocols for both HRP-conjugated and fluorescent secondary antibodies.

Immunocytochemistry

hNPs were grown on glass coverslips and fixed with 4% PFA in PBS for 15 min and then washed with TBS at room temperature. Cells were permeabilized with TBS-T (0.4% Triton-X) for 15 min at room temperature and then washed with TBS at room temperature. Cells were treated with a blocking solution made of 3% normal donkey serum in TBS-T (0.2% Triton-X) for 30 min at room temperature. Cells were then incubated with primary

antibodies diluted in blocking solution overnight at 4°C. Afterward, cells were rinsed with TBS, treated with secondary antibodies diluted in blocking solution for 1 h, and then rinsed with TBS, all at room temperature. Slides were imaged using a Zeiss Observer.Z1 inverted microscope and ZEN 2011 software.

Electrophysiology methods

Electrophysiology

Acute brain slices were prepared from *Foxp1*$^{+/-}$ and *Foxp1*$^{+/+}$ mice crossed with either *Drd1a-tdTomato* or *Drd2-GFP* reporter mice (P17–P20) with the following procedure. Mice were anesthetized with 125 mg/kg ketamine and 25 mg/kg xylazine, and the brains were removed. Thalamocortical slices (Agmon and Connors 1991) 300 μm thick were cut at ~4°C in dissection buffer, placed in ACSF for 30 min at 35°C, and slowly cooled over the next 30 min to 21°C. Whole-cell recordings were performed in the dorsal striatum, and cells were targeted with IR-DIC optics in an Olympus FV300 confocal microscope. Recordings were performed at 21°C. Data were collected with a 10-kHz sampling rate and a 3-kHz Bessel filter. Striatal neurons were identified by GFP or tdTomato fluorescence using confocal microscopy.

Electrophysiology solutions

ACSF contained 126 mM NaCl, 3 mM KCl, 1.25 mM NaH_2PO_4, 2 mM $MgSO_4$, 26 mM $NaHCO_3$, 25 mM dextrose, and 2 mM $CaCl_2$. All slices were prepared in the following dissection buffer: 75 mM sucrose, 87 mM NaCl, 3 mM KCl, 1.25 mM NaH_2PO_4, 7 mM $MgSO_4$, 26 mM $NaHCO_3$, 20 mM dextrose, 0.5 mM $CaCl_2$, and 1 mM kynurenate. All

solutions were pH 7.4. ACSF was saturated with 95% O_2/5% CO_2. Unless stated otherwise, the pipette solution consisted of 130 mM K-Gluconate, 6 mM KCl, 3 mM NaCl, 10 mM HEPES, 0.2 mM EGTA, 4 mM ATP-Mg, 0.3 mM GTP-Tris, 14 mM phosphocreatine-Tris, and 10 mM sucrose. This was adjusted to pH 7.25 and 290 mOsm. The junction potential was ~10 mV and was not corrected.

Ultrasonic vocalization recordings

Acquisition and processing

USVs were recorded from pups isolated from their dams at P4, P7, and P10. Pups were placed into clean plastic containers inside soundproof styrofoam boxes and recorded for 3 min. Recordings were acquired using an UltraSoundGate condenser microphone (Avisoft Bioacoustics, CM16) positioned at a fixed height of 20 cm above the pups and were amplified and digitized (~20 dB gain, sampled at 16 bits, 250 kHz) using UltraSoundGate 416H hardware and Avisoft RECORDER software (Avisoft Bioacoustics). Sound spectrograms were prepared in MATLAB (50% overlapping, 512-point Hamming windows), resulting in 1.024-msec temporal resolution and 488.3-Hz spectral resolution. Spectrograms were band-pass filtered to 20–120 kHz and filtered for white noise. Positions of ultrasonic calls were determined automatically using a previously published method (Holy and Guo 2005).

Spectral and temporal measurements

Vocalization behavior occured in spurts of activity ("bouts") separated by longer pauses. To quantify bouts of vocalization, spectrograms were segmented using a pause length of

≥0.25 sec, which was chosen based on the empirical distribution of pause times between calls. All intercall pauses <0.25 sec represent constituents of the same bout of vocalization. The means of the dominant frequency ("mean frequency") as well as the duration time of individual calls were averaged over all calls by animal. The presence of instantaneous pitch jumps in calls was determined by a previously published method (Holy and Guo 2005), and the fraction of all calls containing such jumps was determined for each animal. The trend slope (in hertz per millisecond) of calls lacking instantaneous pitch jumps was determined by linear regression, and slopes were averaged over all calls by animal.

Statistics

Differences between genotypes on all measured features of vocalization were assessed using two-way analysis of variance, testing for main effects of genotype, day, and interaction of genotype by day. Post-hoc multiple comparisons were assessed using Sidak's procedure. Features of vocalization were considered independently.

Postnatal righting reflexes

Righting reflexes were assessed in P4, P7, and P10 *Foxp1*$^{+/-}$ and littermate control pups. In brief, pups were placed in a supine position on a clean, unobstructed surface, and the time taken to right onto all fours was measured using a stopwatch. A pup failed the test if its time to right exceeded 1 min. In such cases, the time was scored as 60 sec. Each pup received one trial at each postnatal time point.

Open field test

The open field assay was performed on adult *Foxp1*$^{+/-}$ and littermate control mice by individually placing each animal in a 16-in × 16-in Plexiglass box and allowing them to explore the arena for 5 min. Videos of each mouse were obtained and scored for average velocity of movement and total distance moved using the EthoVision XT software package (Noldus).

Rotorod test

Adult mice were placed on a textured drum within individual lanes of a Series 8 IITC Life Science rotorod. The drum was programed to accelerate from 4 to 40 rpm within a maximum time frame of 300 sec. Each mouse was positioned forward on the drum, and sensors detected the latency to fall, maximum revolutions per minute at fall, and total distance travelled for each mouse. Sensors were manually activated whenever a mouse made a full rotation holding onto the drum. Mice were tested for three consecutive days with four trials per day, separated by 20-min intervals.

Grip strength test

Forelimb and hindlimb grip strength was measured on adult mice using Chatillon Force Measurement equipment. Forelimbs or hindlimbs of each mouse were placed on a mesh wire meter and pulled away from the wire at constant force. Five consecutive measurements were recorded for both hindlimbs and forelimbs and averaged for a final grip strength measurement for each mouse.

Nesting behavior

Mouse nesting behavior was analyzed using a previously described approach (Deacon 2006). Briefly, adult mice were singly housed overnight with 3 g of intact nestlet material in a clean cage. After 16–18 h, the amount of unused nestlet material was weighed, and the nests formed were assessed to generate a nest quality score of 1–5 for each mouse.

Grooming behavior

Grooming behavior was assessed in adult mice by individually placing each mouse in a clean cage without nesting material and allowing them to habituate for 10 min. Afterward, grooming behaviors were recorded using an HDR-CX535 Handycam video camera (Sony), and videos were then manually scored based on the number of grooming bouts and total time spent grooming for 10 min.

SHIRPA

A modified SHIRPA behavioral screen from Rogers et al. (1997) was performed on adult mice. First, mice were individually placed in a viewing jar for 5 min. During this time, mice were scored for (1) body position (inactive [0], active [1], or excessive activity [2]), (2) tremors (absent [0] or present [1]), (3) palpebral closure (open [0] or closed [1]), (4) coat appearance (tidy and well-groomed coat [0] or irregularities/piloerection [1]), (5) skin color (blanched [0], pink [1], or deep red [2]), (6) whiskers (absent [1] or present [0]), (7) lacrimation (absent [0] or present [1]), (8) defecation (absent [0] or present [1]), (9) gait (fluid with 3-mm pelvic elevation [0] or lack of fluidity [1]), (10) tail elevation (dragging [0], horizontal elevation [1], or elevated tail [2]), and (11) startle response (none [0], Preyer

reflex [1], or reaction in addition to Preyer reflex [2]). Mice were then transferred to a clean cage, and the following behaviors were recorded in or above this arena: (12) touch escape (no response [0], response to touch [1], or flees prior to touch [2]), (13) trunk curl (absent [0] or present [1]), (14) limb grasping (absent [0] or present [1]), (15) pinna reflex (absent [0] or present [1]), (16) corneal reflex (absent [0] or present [1]), (17) contact righting reflex (absent [0] or present [1]), (18) evidence of biting (none [0] or biting in response to handling [1]), (19) vocalizations (nonvocal [0] or audible in response to handling [1]), (20) positional passivity (struggles when held by tail [0], when held by neck [1], or laid supine [2] or no struggle [3]). Both pinna and corneal reflexes were tested with a 0.15-mm-diameter nylon filament from Touch Test Sensory Evaluators (Semmes-Weinstein Monofilaments).

Other statistics

P-values were calculated with Student's *t*-test (two-tailed, type 2). *F*-values were calculated with two-way ANOVA followed by a Tukey post-hoc test for multiway comparison. Data were assumed to be normally distributed. *P*-values for overlaps were calculated with a hypergeometric test using a custom-made R script. We obtained an independent background for population size (for humans, human protein-coding genes [20,389 genes] and BrainSpan-expressed genes [15,585 genes] (Kang et al., 2011), and for mice, Allen brain-expressed genes [13,600 genes] (Lein et al., 2007). We used the protein-coding genes for background in the hypergeometric test used in Figure 5E. We used the BrainSpan-expressed genes for background in the hypergeometric test used in Figure 5F and Supplemental Figure 8. We used the Allen brain-expressed genes for

background in the hypergeometric test used for Figure 1C and 2A, D, and Supplemental Figure 2A. *P*-values were adjusted for multiple comparisons using the Benjamini-Hochberg FDR procedure when required. A two-way permutation test of 1000 was adapted to validate the overlaps. First, we randomized the external gene sets (for example, ASD or FMRP) by randomly selecting the same number of genes from an independent brain-expressed gene list (for humans, BrainSpan-expressed gene list; for mice Allen-expressed gene list) and subsequently calculating the overlap *P*-values. The second approach randomized the internal gene sets (for example, STR_DEG or hNP_DEG) by randomly selecting the same number of genes from RNA-seq-expressed genes and subsequently calculating the overlap *P*-values. Moreover, we adapted a permutation test to evaluate the detected DEGs, randomizing 1000 times the RNA-seq data and recalculating the DEGs. Analysis for RNA-seq, ChIP-seq, and microarrays were performed using custom-made R scripts implementing functions and adapting statistical designs comprised in the libraries used.

TABLE 2.1: Striatal DEGs in *Foxp1*$^{+/-}$ mice

Gene	logFC	FDR	Gene	logFC	FDR
41699	0.649	1.90E-02	Lancl3	1.228	9.86E-03
1190002N15Rik	0.855	6.20E-04	Laptm4B	0.576	2.70E-02
1700001O22Rik	-0.848	3.77E-02	Lhfp	0.823	1.85E-03
1700020I14Rik	0.639	4.82E-02	Lhx9	3.678	6.71E-04
1700024P16Rik	2.154	5.97E-03	Lifr	0.721	2.06E-03
1700040L02Rik	-1.023	2.30E-02	Lin7A	0.816	9.59E-04
1810041L15Rik	0.790	9.16E-03	Lingo2	0.615	3.22E-02
2310067B10Rik	-0.465	4.14E-02	Lingo3	-0.943	3.04E-02
3632451O06Rik	0.815	8.10E-03	Lipa	0.607	2.14E-02
6330409D20Rik	1.177	2.67E-02	Lmo2	-1.693	1.60E-06
9230009I02Rik	-2.606	7.32E-06	Lonrf3	0.654	1.47E-02
9430020K01Rik	-0.624	1.90E-02	Lpl	-0.998	1.92E-02
A830018L16Rik	0.588	4.43E-02	Lrg1	2.408	2.33E-02
A830082K12Rik	0.962	3.87E-02	Lurap1L	1.077	1.30E-02
Abhd14A	-0.502	4.62E-02	Luzp2	0.862	8.43E-05
Abhd3	0.558	4.08E-02	Ly6C1	0.588	2.84E-02
Ablim2	-0.684	1.73E-02	Lypla1	0.516	2.85E-02
Ace	-1.493	4.20E-04	Lzts3	-0.673	1.53E-02
Acot5	1.565	2.30E-02	Mab21L1	2.633	3.84E-03
Acsl3	0.485	4.97E-02	Magi1	0.734	3.80E-03
Acsl4	0.642	2.94E-02	Map3K6	0.848	2.78E-02
Actn1	-0.677	7.40E-03	Map7D2	0.490	3.02E-02
Actn2	-1.412	2.03E-03	Matn2	0.771	4.03E-02
Acvr1	-0.528	2.84E-02	Mctp2	1.671	4.85E-04
Acvr1C	-1.000	1.67E-03	Me1	0.543	4.44E-02
Acvrl1	-1.115	1.36E-03	Megf11	0.680	4.66E-02
Acy1	-0.919	2.55E-02	Melk	-1.023	2.84E-02
Adamtsl5	-0.838	1.99E-02	Mertk	0.615	1.26E-02
Adarb1	0.611	1.14E-02	Mgat4B	-0.460	4.18E-02
Adarb2	0.620	4.49E-02	Mgat5B	-0.543	3.37E-02
Adcy8	0.893	2.78E-02	Mir365-1	-2.271	1.29E-02
Adcyap1	2.177	2.21E-02	Mn1	-0.605	1.79E-02
Ago4	-0.822	2.03E-03	Mpped2	-0.610	3.38E-02
Ai593442	-0.648	3.58E-02	Mreg	1.076	2.05E-02
Ak129341	-0.619	4.43E-02	Mxd1	-0.667	7.01E-03
Akap2	0.584	1.34E-02	Mybpc1	1.972	3.91E-02
Ampd2	-0.492	4.37E-02	Mylk3	2.336	3.04E-02
Amz1	-0.625	8.47E-03	Myo16	0.588	2.44E-02
Angptl4	1.233	2.30E-03	Myo3B	-1.612	5.87E-03

Gene	logFC	FDR	Gene	logFC	FDR
Ank1	0.727	5.43E-03	Myoc	1.382	4.47E-02
Ankrd29	0.641	1.25E-02	Myom3	-0.782	2.14E-02
Ankrd34C	1.275	3.11E-03	Nab2	-0.614	4.13E-03
Ano3	-0.810	3.58E-02	Nap1L5	0.474	3.58E-02
Apln	0.633	4.00E-02	Napepld	0.871	5.56E-03
Arc	-1.082	4.13E-03	Ndst3	1.279	1.99E-03
Arg2	-1.360	2.31E-02	Ndst4	2.761	3.80E-03
Arhgap10	-0.583	1.88E-02	Necab2	-1.018	4.66E-02
Arhgap27	-0.750	3.66E-02	Nefh	1.245	7.20E-05
Arhgap33	-0.632	1.29E-02	Nefl	0.536	2.97E-02
Arhgdib	-1.171	4.59E-03	Nek2	-1.338	8.92E-03
Arhgef15	-0.677	1.92E-02	Nek7	0.496	4.97E-02
Arid3B	-0.781	2.30E-02	Nell1	0.665	1.30E-02
Arid5B	0.533	4.28E-02	Neurod1	1.897	4.86E-02
Arl4D	-0.765	6.04E-03	Ngef	-0.638	3.64E-03
Asap2	0.674	2.58E-02	Ngf	1.313	2.81E-02
Asb11	-0.932	2.14E-02	Nhsl1	0.674	1.14E-02
Asic1	-0.496	2.75E-02	Nkrf	0.672	5.60E-03
Asph	0.523	2.52E-02	Nlk	0.721	2.02E-02
Asphd2	-0.597	6.78E-03	Nmbr	2.291	2.46E-03
Atp10A	0.686	2.84E-02	Nmnat3	-1.198	9.36E-03
Atp1B1	0.537	2.55E-02	Nostrin	0.738	3.77E-02
Atp6Ap2	0.517	3.02E-02	Npas4	-1.450	6.39E-05
Atp8B2	-0.482	3.23E-02	Npy1R	0.746	2.14E-02
B2M	0.488	4.77E-02	Nr1D1	-0.612	6.21E-03
B3Gnt2	-0.920	1.08E-02	Nr4A1	-1.264	3.27E-05
Bbs9	-0.553	2.87E-02	Nrip3	0.912	2.55E-02
Bc031361	-0.899	2.48E-03	Nrp2	1.109	1.90E-02
Bc048546	1.136	2.94E-02	Nrxn1	0.658	1.07E-02
Bc049352	-1.328	3.46E-02	Nt5Dc3	0.603	3.26E-02
Bc055324	-1.113	1.25E-02	Ntng1	1.468	2.78E-04
Bcat1	0.834	3.27E-05	Nucb2	-0.644	5.60E-03
Bcr	-0.768	4.13E-02	Nudt4	0.571	4.77E-02
Bhlhe22	1.673	3.58E-02	Nup93	-0.547	3.36E-02
Bhlhe40	0.800	2.04E-02	Nxph1	0.542	2.21E-02
Btbd11	1.063	7.77E-03	Oacyl	-1.246	9.80E-04
Btbd3	1.064	7.43E-07	Odf4	-1.682	1.12E-02
Bves	-1.141	4.77E-02	Onecut2	-1.386	1.20E-06
C2Cd2L	-0.598	1.45E-02	Oprk1	-0.761	4.92E-02
C530008M17Rik	0.551	9.69E-03	Otof	0.823	9.86E-03
C730002L08Rik	2.504	2.94E-02	Oxr1	0.873	6.56E-03

Gene	logFC	FDR	Gene	logFC	FDR
Cacna1H	-0.650	3.80E-02	Palm2	0.834	4.58E-03
Cadps	0.731	7.24E-03	Palmd	0.726	2.58E-02
Calb2	1.245	4.67E-04	Paqr8	0.652	7.01E-03
Calcoco1	-0.609	5.60E-03	Pard6B	-0.769	2.75E-02
Camk2D	1.233	3.17E-05	Pcdh19	0.665	1.62E-02
Camk2N2	0.837	4.68E-02	Pcdh20	0.654	3.80E-02
Camkv	-0.555	2.87E-02	Pcdh8	0.790	3.02E-02
Car11	-0.699	7.40E-03	Pcsk7	-0.518	2.92E-02
Cartpt	2.088	4.67E-04	Pde1B	-1.281	1.90E-02
Cav2	0.791	4.11E-03	Pde2A	-0.554	3.08E-02
Cbln4	1.308	2.33E-04	Per1	-0.662	2.16E-03
Cbr3	-0.964	4.43E-02	Phactr2	0.964	1.10E-04
Ccdc136	0.807	2.49E-02	Phex	-1.740	3.07E-04
Ccdc141	0.839	2.46E-03	Phyh	0.698	7.27E-04
Ccdc88C	-0.911	1.47E-02	Phyhip	-0.504	4.62E-02
Ccng1	0.712	4.19E-04	Pid1	0.815	2.32E-03
Ccno	-1.583	2.37E-04	Pip5K1B	1.245	5.60E-05
Cd83	0.905	8.02E-03	Pkib	1.312	6.34E-05
Cdh12	1.271	2.65E-03	Pkp2	0.951	5.91E-03
Cdh8	-0.675	2.94E-02	Pla2G7	0.604	2.30E-02
Cdh9	-0.963	1.32E-03	Plcb4	0.851	2.31E-02
Cdk14	1.006	1.60E-02	Plcd4	0.708	2.48E-02
Cdkn1A	0.736	5.87E-03	Plch1	0.993	1.26E-02
Cds1	0.627	4.43E-02	Plcl1	0.565	2.99E-02
Celf3	-0.513	2.95E-02	Plcxd1	-0.744	3.04E-02
Cep128	-0.738	2.10E-02	Plcxd2	1.386	2.37E-04
Cep63	-0.577	2.84E-02	Pld5	-0.857	3.23E-02
Chdh	-1.114	1.14E-02	Pmepa1	-0.661	1.19E-02
Chrm4	-1.185	1.10E-04	Pnoc	1.493	2.13E-02
Cish	-0.834	2.66E-02	Pnp2	-1.374	3.65E-03
Clspn	-2.245	4.15E-06	Pou3F1	-0.984	7.27E-04
Cnr1	-0.879	1.34E-02	Ppargc1A	0.534	2.16E-02
Cnst	-0.657	2.05E-02	Ppargc1B	-0.666	3.13E-02
Cntn3	0.493	4.76E-02	Ppfia2	0.669	9.69E-03
Cntnap3	-0.921	1.12E-02	Ppfibp1	0.718	4.02E-03
Coch	-1.414	2.62E-08	Ppm1E	1.245	8.46E-03
Col11A2	-0.692	3.37E-02	Ppm1L	0.897	6.49E-03
Cpne5	-0.724	1.45E-02	Ppp1Ca	-0.643	1.61E-02
Cpne7	0.892	1.41E-02	Ppp4R4	-0.753	5.75E-03
Crh	1.354	6.22E-04	Prima1	-1.290	2.84E-02
Crocc	-0.897	1.37E-03	Prkar2A	0.484	2.84E-02

Gene	logFC	FDR	Gene	logFC	FDR
Crot	0.511	3.22E-02	Prkg2	0.826	1.85E-03
Crtac1	0.758	2.43E-02	Prr13	0.708	2.94E-02
Csgalnact1	0.894	6.29E-03	Prr16	0.732	3.39E-02
Cthrc1	0.941	3.80E-03	Prrt4	-0.883	4.62E-02
Cux2	1.090	4.65E-02	Ptch2	-1.218	2.99E-03
Cyr61	-1.072	4.82E-02	Ptchd2	0.772	4.37E-02
Dach1	-1.382	4.43E-02	Ptgds	0.897	2.32E-04
Dbp	-0.770	1.56E-03	Ptgs2	1.426	4.14E-02
Dcc	-0.725	3.95E-02	Ptpn3	1.492	1.60E-02
Ddit4L	-0.779	1.14E-02	Ptpn5	-0.961	1.25E-02
Ddx11	-1.286	1.55E-03	Ptprg	0.663	2.73E-03
Dgat2	-0.713	2.39E-02	Pvalb	1.589	2.99E-02
Dio2	0.581	3.03E-02	Pvrl1	1.149	4.67E-04
Disp2	0.641	2.71E-02	Pvrl3	0.829	3.65E-02
Dlgap1	0.865	4.86E-02	Pwwp2B	-0.827	7.01E-03
Dmkn	-1.803	3.27E-05	Qrfpr	2.464	9.50E-06
Dnajc3	0.505	2.16E-02	Ralyl	0.845	1.61E-02
Dner	0.905	2.48E-03	Ramp3	1.245	3.10E-02
Dpp10	0.985	1.22E-03	Rap1Gap	-0.810	1.89E-02
Dtnb	-0.496	1.45E-02	Rarg	-0.698	4.13E-02
Dusp1	-0.718	3.58E-02	Rasd1	1.350	4.51E-03
Dusp4	1.223	6.41E-03	Rasd2	-1.268	4.68E-02
Edil3	0.674	2.14E-02	Rasgef1B	-0.600	5.43E-03
Efr3A	0.948	1.19E-02	Rasgrf2	1.398	1.93E-03
Egr2	-1.572	3.67E-05	Rasgrp2	-1.328	4.43E-02
Egr4	-1.048	1.35E-02	Rbck1	-0.544	2.84E-02
Ehbp1L1	-0.609	1.35E-02	Rbm38	-0.938	2.94E-02
Elavl2	0.800	2.96E-03	Rbms1	-0.709	2.21E-02
Elavl4	1.318	7.27E-04	Rcn1	-0.805	3.06E-02
Elfn1	0.691	2.44E-02	Reln	-0.712	3.35E-03
Elovl4	0.493	3.75E-02	Rem2	-1.522	7.01E-03
Eml5	-0.512	4.40E-02	Ret	1.885	1.83E-03
Enah	0.491	2.84E-02	Rgs11	-0.599	1.37E-02
Endod1	0.536	3.92E-02	Rgs6	0.741	4.78E-02
Epha10	1.048	6.09E-04	Rgs9	-1.451	4.60E-02
Epha5	0.852	2.16E-02	Rhobtb2	-0.577	2.58E-02
Epor	-0.800	3.04E-02	Rhou	0.631	1.77E-02
Eps15	0.520	3.58E-02	Ric8B	-0.826	2.31E-02
Eps8	0.668	8.30E-03	Rin1	-0.475	2.94E-02
Erf	-0.565	7.93E-03	Rnf115	0.528	3.54E-02
Evc2	1.266	2.08E-02	Rpe65	-1.155	5.60E-03

Gene	logFC	FDR	Gene	logFC	FDR
Exph5	1.159	1.97E-03	Rps6Ka4	-0.581	8.46E-03
F730043M19Rik	1.031	3.35E-03	Rreb1	-0.932	1.38E-05
Fam105A	-0.530	2.84E-02	Rundc1	-0.555	3.96E-02
Fam107A	0.640	6.29E-03	Rxfp3	1.891	1.13E-03
Fam132A	-0.695	1.87E-02	Rxrg	-1.392	2.29E-02
Fam150B	2.258	3.24E-02	Ryr1	-1.180	1.71E-06
Fam155A	0.774	3.58E-02	Scmh1	-0.479	2.84E-02
Fam160B2	-0.532	2.74E-02	Sdc4	0.548	3.58E-02
Fam19A1	2.199	2.23E-02	Sdf2L1	0.759	1.99E-02
Fam19A2	1.533	2.73E-04	Sec14L1	-0.574	1.09E-02
Fam222A	-0.981	9.61E-03	Sec14L3	-1.525	6.77E-03
Fam3C	0.478	4.97E-02	Sema3F	-0.847	2.50E-02
Fam78A	-1.059	9.30E-04	Serpinb1B	-1.361	5.86E-03
Fam84B	-0.987	4.66E-03	Serpini1	1.278	4.55E-03
Fancb	-0.975	3.98E-02	Sertm1	1.183	8.54E-03
Farp1	0.676	1.66E-02	Sez6	-0.849	1.97E-02
Fbln5	-1.008	1.90E-02	Sez6L	1.054	2.74E-02
Fbxl16	-0.630	2.17E-02	Sh2D5	-0.720	1.48E-02
Fbxo32	-1.029	2.48E-03	Shb	-1.156	1.49E-02
Fbxo34	0.624	1.07E-02	Shf	-0.527	3.57E-02
Fcho1	-0.566	1.47E-02	Shisa2	-1.704	3.36E-04
Fgf10	1.363	2.57E-02	Sipa1L2	0.704	1.30E-03
Fgf12	0.800	1.18E-03	Slc17A6	2.505	1.96E-04
Fgf9	0.570	3.04E-02	Slc1A3	0.468	3.58E-02
Flna	-0.656	1.49E-02	Slc26A5	-1.773	3.84E-03
Flt3	1.445	9.36E-03	Slc2A1	0.540	4.09E-02
Fmnl2	0.487	2.93E-02	Slc38A5	-1.449	5.27E-04
Foxo1	-1.119	5.13E-03	Slc6A6	-0.603	6.78E-03
Foxp1	-1.136	8.63E-05	Slc8A1	1.019	1.92E-02
Frmpd1	0.861	2.13E-02	Slc9A2	-1.357	2.20E-03
Fxyd2	-0.836	3.24E-02	Slc9A9	0.812	9.10E-03
Gabra1	1.064	3.19E-05	Slit2	0.879	3.75E-02
Gabra3	0.961	4.43E-02	Smg5	-0.540	4.93E-02
Gabrd	-0.619	2.84E-02	Smim3	0.920	1.36E-03
Gabrg1	0.799	9.69E-03	Smpd3	-0.907	2.31E-02
Gabrg2	0.548	3.25E-02	Soga2	-0.867	1.58E-04
Galnt16	0.458	4.29E-02	Sorcs2	-0.779	2.84E-04
Gcnt2	-0.924	3.03E-03	Sorl1	0.593	4.58E-02
Gjb6	1.110	8.43E-05	Sox17	0.732	3.75E-02
Glra3	1.505	3.55E-03	Sox8	-0.546	4.43E-02
Gm136	-1.632	4.02E-03	Spata2L	-0.650	4.51E-03

Gene	logFC	FDR	Gene	logFC	FDR
Gm13629	1.185	3.55E-02	Sphkap	1.411	1.92E-03
Gm20300	0.493	2.90E-02	Spint1	-1.235	3.94E-02
Gm7244	-2.022	9.41E-03	Spp1	1.734	2.81E-03
Gmpr	-0.663	5.18E-03	Spry2	-0.627	6.36E-03
Gnai1	0.635	9.86E-03	Sptssb	1.409	1.88E-02
Gnas	0.659	4.77E-02	Srm	-0.496	4.84E-02
Gnb2	-0.481	4.52E-02	Srrt	-0.511	4.03E-02
Gnb5	-0.606	4.03E-02	St8Sia1	0.662	2.65E-03
Gng4	0.800	2.81E-02	St8Sia2	-1.228	1.50E-03
Gpnmb	1.124	4.21E-02	St8Sia3	-0.689	3.03E-02
Gpr155	-0.998	5.60E-03	Stard10	-0.593	7.77E-03
Gpr22	1.017	9.12E-03	Stard8	1.197	1.14E-02
Gprin3	-1.309	2.16E-02	Steap2	0.932	3.74E-03
Gpx6	-3.783	3.75E-14	Stk32A	-1.394	3.91E-02
Grb7	-1.418	1.34E-02	Strn	-0.852	3.36E-02
Grik2	-0.668	4.78E-02	Stxbp6	0.906	7.99E-06
Gyk	0.490	4.78E-02	Synj2	0.837	1.90E-02
H2-Dma	-0.581	4.38E-02	Syt6	-1.102	2.05E-02
Hapln1	0.595	9.61E-03	Tagln	-0.897	1.40E-02
Hapln4	1.369	6.78E-03	Tanc1	0.721	3.22E-02
Hcn1	1.222	2.33E-04	Tbc1D1	0.798	1.94E-02
Hcrtr2	1.406	4.67E-04	Tbc1D10C	-1.117	3.94E-02
Hdac9	0.894	9.30E-04	Tbc1D8	-1.123	5.62E-03
Hif3A	0.961	3.55E-03	Tcerg1L	0.773	3.66E-02
Homer2	1.065	4.11E-03	Tesc	-0.732	9.61E-03
Hpca	-0.994	1.32E-03	Tgfa	-1.027	3.95E-02
Hrh3	-0.632	1.08E-02	Thbs3	-0.768	1.92E-03
Hs3St1	0.864	1.72E-02	Theg	-1.663	7.27E-04
Hspa12A	0.562	2.17E-02	Tmem108	1.014	9.86E-03
Hspa1A	0.846	4.31E-02	Tmem132C	1.297	5.60E-03
Hspa1B	1.061	1.12E-02	Tmem181A	-0.802	3.27E-05
Hspa2	0.482	4.14E-02	Tmem181B-Ps	-1.287	3.75E-14
Hspa5	0.574	1.74E-02	Tmem181C-Ps	-0.988	4.06E-08
Htr2A	0.891	2.76E-03	Tmem191C	-0.479	4.58E-02
Htr7	1.312	2.65E-03	Tmem200A	1.522	2.20E-02
Id2	0.588	4.97E-02	Tmem200B	-1.371	5.60E-03
Ido1	-1.918	1.63E-02	Tmem200C	1.177	7.74E-03
Igf1	0.994	2.94E-02	Tmem215	1.978	3.02E-02
Igfn1	2.165	3.36E-02	Tmem229A	0.577	4.32E-02
Igsf3	0.733	5.43E-03	Tmem252	-1.589	3.35E-04
Igsf9	-1.087	5.20E-04	Tmem65	0.632	5.69E-03

Gene	logFC	FDR	Gene	logFC	FDR
Il17Rc	-1.131	6.21E-03	Tmprss9	-1.433	2.17E-02
Ildr2	1.046	1.10E-04	Tox2	0.760	2.70E-02
Inf2	-0.927	1.12E-02	Tpd52L1	-0.859	5.27E-04
Isyna1	-0.737	2.65E-02	Tpst1	-0.615	1.34E-02
Itga11	-0.907	4.47E-02	Traip	-1.089	2.48E-03
Itga5	-1.844	8.43E-05	Trim11	-0.635	1.30E-02
Itga9	-0.915	2.43E-02	Trim66	0.748	1.02E-02
Itpk1	0.611	1.12E-02	Tsc22D3	0.807	4.19E-04
Itpr1	-0.558	2.14E-02	Tshz2	0.922	2.37E-04
Ivns1Abp	-0.642	2.73E-02	Ttc34	-1.253	7.01E-03
Jag1	-0.704	4.53E-02	Ttc39B	0.510	3.63E-02
Jakmip1	-0.484	3.22E-02	Ubash3B	0.603	4.43E-02
Jdp2	1.050	5.95E-03	Ube2E1	0.480	2.78E-02
Junb	-1.196	5.31E-04	Ublcp1	0.490	4.27E-02
Kcna4	-0.967	2.31E-02	Unc5D	1.097	1.11E-03
Kcnab1	-1.071	2.21E-02	Upp2	0.671	4.92E-02
Kcnab3	0.961	2.43E-02	Usp28	-0.727	4.67E-04
Kcnc2	1.411	5.05E-03	Usp53	0.591	2.16E-02
Kcnd3	0.775	1.20E-04	Utp14B	0.827	3.04E-02
Kcnh4	-0.909	5.02E-03	Vamp1	1.212	8.47E-04
Kcnh5	0.794	4.93E-02	Vrk1	-0.820	2.00E-02
Kcnip1	1.029	3.90E-04	Vsnl1	1.218	1.72E-02
Kcnip2	-0.754	4.11E-02	Vstm2A	0.534	1.90E-02
Kcnip4	0.641	3.34E-03	Wdr54	-0.644	2.79E-02
Kcnj2	-0.700	3.24E-02	Wnt5A	0.840	2.67E-02
Kcnj3	1.065	4.66E-02	Zbtb16	2.248	1.48E-10
Kcnk2	-0.969	3.53E-03	Zbtb7C	1.089	3.34E-03
Kcnmb2	1.435	2.17E-02	Zbtb8A	-1.295	4.99E-06
Kcnn2	0.592	6.40E-03	Zfhx2	-0.526	4.32E-02
Kcns3	1.032	2.55E-02	Zfp385B	-0.646	3.74E-03
Kcnt1	-0.698	1.73E-03	Zfp467	-0.815	1.37E-02
Kctd17	-0.680	2.92E-02	Zfp536	0.723	2.55E-02
Kif17	-0.622	1.07E-02	Zfyve28	-0.622	6.36E-03
Klf16	-0.640	5.34E-03			
Klhdc7A	0.730	2.31E-02			
Klhdc8A	1.086	1.54E-03			
Klhl1	-1.062	1.26E-02			
Kras	0.602	1.23E-02			
Krt10	-1.246	1.34E-02			
Krt12	1.180	1.83E-03			
Krt9	-1.308	2.48E-03			

REFERENCES

Agmon A, Connors BW. 1991. Thalamocortical responses of mouse somatosensory (barrel) cortex in vitro. Neuroscience 41: 365–379.

Anders S, Pyl PT, Huber W. 2014. HTSeq—a Python framework to work with high-throughput sequencing data. Bioinfor- matics 31: 166–169.

Bacon C, Rappold GA. 2012. The distinct and overlapping pheno- typic spectra of FOXP1 and FOXP2 in cognitive disorders. Hum Genet 131: 1687–1698.

Bacon C, Schneider M, Le Magueresse C, Froehlich H, Sticht C, Gluch C, Monyer H, Rappold GA. 2015. Brain-specific Foxp1 deletion impairs neuronal development and causes au- tistic-like behaviour. Mol Psychiatry 20: 632–639.

Benjamini Y, Hochberg Y. 1995. Controlling the false discovery rate: a practical and powerful approach to multiple testing. J R Stat Soc Ser B 57: 289–300.

Centonze D, Rossi S, Mercaldo V, Napoli I, Ciotti MT, De Chiara V, Musella A, Prosperetti C, Calabresi P, Bernardi G, et al. 2008. Abnormal striatal GABA transmission in the mouse model for the Fragile X syndrome. Biol Psychiatry 63: 963–973.

Chien WH, Gau SS, Chen CH, Tsai WC, Wu YY, Chen PH, Shang CY, Chen CH. 2013. Increased gene expression of FOXP1 in patients with autism spectrum disorders. Mol Autism 4: 23.

Curry T, Egeto P, Wang H, Podnos A, Wasserman D, Yeomans J. 2013. Dopamine receptor D2 deficiency reduces mouse pup ultrasonic vocalizations and maternal responsiveness. Genes Brain Behav 12: 397–404.

Darnell JC, Klann E. 2013. The translation of translational control by FMRP: therapeutic targets for FXS. Nat Neurosci 16: 1530–1536.

Darnell JC, Van Driesche SJ, Zhang C, Hung KY, Mele A, Fraser CE, Stone EF, Chen C, Fak JJ, Chi SW, et al. 2011. FMRP stalls ribosomal translocation on mRNAs linked to synaptic func- tion and autism. Cell 146: 247–261.

Dasen JS, De Camilli A, Wang B, Tucker PW, Jessell TM. 2008. Hox repertoires for motor neuron diversity and connectivity gated by a single accessory factor, FoxP1. Cell 134: 304–316.

Deacon RM. 2006. Assessing nest building in mice. Nat Protoc 1: 1117–1119.

Ellegood J, Anagnostou E, Babineau BA, Crawley JN, Lin L, Gen- estine M, DiCicco-Bloom E, Lai JK, Foster JA, Penagarikano O, et al. 2015. Clustering autism: using

neuroanatomical differ- ences in 26 mouse models to gain insight into the heterogeneity. Mol Psychiatry 20: 118–125.

Enard W, Gehre S, Hammerschmidt K, Holter SM, Blass T, Somel M, Bruckner MK, Schreiweis C, Winter C, Sohr R, et al. 2009. A humanized version of Foxp2 affects cortico–basal ganglia circuits in mice. Cell 137: 961–971.

Ferland RJ, Cherry TJ, Preware PO, Morrisey EE, Walsh CA. 2003. Characterization of Foxp2 and Foxp1 mRNA and protein in the developing and mature brain. J Comp Neurol 460: 266–279.

Fisher SE, Scharff C. 2009. FOXP2 as a molecular window into speech and language. Trends Genet 25: 166–177.

Foeger NC, Norris AJ, Wren LM, Nerbonne JM. 2012. Augmenta- tion of Kv4.2-encoded currents by accessory dipeptidyl pepti- dase 6 and 10 subunits reflects selective cell surface Kv4.2 protein stabilization. J Biol Chem 287: 9640–9650.

French CA, Jin X, Campbell TG, Gerfen E, Groszer M, Fisher SE, Costa RM. 2012. An aetiological Foxp2 mutation causes aber- rant striatal activity and alters plasticity during skill learning. Mol Psychiatry 17: 1077–1085.

Gautier L, Cope L, Bolstad BM, Irizarry RA. 2004. Affy—analysis of Affymetrix GeneChip data at the probe level. Bioinfor- matics 20: 307–315.

Gerfen CR, Surmeier DJ. 2011. Modulation of striatal projection systems by dopamine. Annu Rev Neurosci 34: 441–466.

Geschwind DH, State MW. 2015. Gene hunting in autism spec- trum disorder: on the path to precision medicine. Lancet Neu- rol. doi: 10.1016/S1474-4422(15)00044-7.

Gong S, Zheng C, Doughty ML, Losos K, Didkovsky N, Schambra UB, Nowak NJ, Joyner A, Leblanc G, Hatten ME, et al. 2003. A gene expression atlas of the central nervous system based on bacterial artificial chromosomes. Nature 425: 917–925.

Grant LM, Richter F, Miller JE, White SA, Fox CM, Zhu C, Ches- selet MF, Ciucci MR. 2014. Vocalization deficits in mice over- expressing α-synuclein, a model of pre-manifest Parkinson's disease. Behav Neurosci 128: 110–121.

Gross C, Yao X, Pong DL, Jeromin A, Bassell GJ. 2011. Fragile X mental retardation protein regulates protein expression and mRNA translation of the potassium channel Kv4.2. J Neurosci 31: 5693–5698.

Heiman M, Schaefer A, Gong S, Peterson JD, Day M, Ramsey KE, Suarez-Farinas M, Schwarz C, Stephan DA, Surmeier DJ, et al. 2008. A translational profiling approach for the molecular characterization of CNS cell types. Cell 135: 738–748.

Heinz S, Benner C, Spann N, Bertolino E, Lin YC, Laslo P, Cheng JX, Murre C, Singh H, Glass CK. 2010. Simple combinations of lineage-determining transcription factors prime cis-regulato- ry elements required for macrophage and B cell identities. Mol Cell 38: 576–589.

Hernandez RN, Feinberg RL, Vaurio R, Passanante NM, Thomp- son RE, Kaufmann WE. 2009. Autism spectrum disorder in Fragile X syndrome: a longitudinal evaluation. Am J Med Ge- net A 149A: 1125–1137.

Hisaoka T, Nakamura Y, Senba E, Morikawa Y. 2010. The fork- head transcription factors, Foxp1 and Foxp2, identify different subpopulations of projection neurons in the mouse cerebral cortex. Neuroscience 166: 551–563.

Holy TE, Guo Z. 2005. Ultrasonic songs of male mice. PLoS Biol 3: e386.

Hu H, Wang B, Borde M, Nardone J, Maika S, Allred L, Tucker PW, Rao A. 2006. Foxp1 is an essential transcriptional regula- tor of B cell development. Nat Immunol 7: 819–826.

Hu Z, Chang YC, Wang Y, Huang CL, Liu Y, Tian F, Granger B, Delisi C. 2013. VisANT 4.0: Integrative network platform to connect genes, drugs, diseases and therapies. Nucleic acids re- search 41: W225–W231.

Iossifov I, O'Roak BJ, Sanders SJ, Ronemus M, Krumm N, Levy D, Stessman HA, Witherspoon KT, Vives L, Patterson KE, et al. 2014. The contribution of de novo coding mutations to autism spectrum disorder. Nature 515: 216–221.

Kaestner KH, Knochel W, Martinez DE. 2000. Unified nomencla- ture for the winged helix/forkhead transcription factors. Genes Dev 14: 142–146.

Kang HJ, Kawasawa YI, Cheng F, Zhu Y, Xu X, Li M, Sousa AM, Pletikos M, Meyer KA, Sedmak G, et al. 2011. Spatio-temporal transcriptome of the human brain. Nature 478: 483–489.

Kim J, Wei DS, Hoffman DA. 2005. Kv4 potassium channel sub- units control action potential repolarization and frequency- dependent broadening in rat hippocampal CA1 pyramidal neurones. J Physiol 569: 41–57.

Klassen T, Davis C, Goldman A, Burgess D, Chen T, Wheeler D, McPherson J, Bourquin T, Lewis L, Villasana D, et al. 2011. Exome sequencing of ion channel genes reveals complex pro- files confounding personal risk assessment in epilepsy. Cell 145:1036–1048.

Konopka G, Bomar JM, Winden K, Coppola G, Jonsson ZO, Gao F, Peng S, Preuss TM, Wohlschlegel JA, Geschwind DH. 2009. Human-specific transcriptional regulation of CNS develop- ment genes by FOXP2. Nature 462: 213–217.

Konopka G, Wexler E, Rosen E, Mukamel Z, Osborn GE, Chen L, Lu D, Gao F, Gao K, Lowe JK, et al. 2012. Modeling the func- tional genomics of autism using human neurons. Mol Psychi- atry 17: 202–214.

Lachmann A, Xu H, Krishnan J, Berger SI, Mazloom AR, Ma'ayan A. 2010. ChEA: transcription factor regulation inferred from integrating genome-wide ChIP-X experiments. Bioinfor- matics 26: 2438–2444.

Langfelder P, Horvath S. 2008. WGCNA: an R package for weight- ed correlation network analysis. BMC Bioinformatics 9: 559. Langfelder P, Luo R, Oldham MC, Horvath S. 2011. Is my net- work module preserved and reproducible? PLoS Comput

Biol 7: e1001057.
Langmead B, Trapnell C, Pop M, Salzberg SL. 2009. Ultrafast and

memory-efficient alignment of short DNA sequences to the

human genome. Genome Biol 10: R25.
Lee H, Lin MC, Kornblum HI, Papazian DM, Nelson SF. 2014.

Exome sequencing identifies de novo gain of function mis- sense mutation in KCND2 in identical twins with autism and seizures that slows potassium channel inactivation. Hum Mol Genet 23: 3481–3489.

Lein ES, Hawrylycz MJ, Ao N, Ayres M, Bensinger A, Bernard A, Boe AF, Boguski MS, Brockway KS, Byrnes EJ, et al. 2007. Ge- nome-wide atlas of gene expression in the adult mouse brain. Nature 445: 168–176.

Li S, Weidenfeld J, Morrisey EE. 2004. Transcriptional and DNA binding activity of the Foxp1/2/4 family is modulated by het- erotypic and homotypic protein interactions. Mol Cell Biol 24: 809–822.

Maloney SE, Rieger MA, Dougherty JD. 2013. Identifying essen- tial cell types and circuits in autism spectrum disorders. Int Rev Neurobiol 113: 61–96.

Marshall CR, Noor A, Vincent JB, Lionel AC, Feuk L, Skaug J, Shago M, Moessner R, Pinto D, Ren Y, et al. 2008. Structural variation of chromosomes in autism spectrum disorder. Am J Hum Genet 82: 477–488.

Maze I, Chaudhury D, Dietz DM, Von Schimmelmann M, Kenne- dy PJ, Lobo MK, Sillivan SE, Miller ML, Bagot RC, Sun H, et al. 2014. G9a influences neuronal subtype specification in stria- tum. Nat Neurosci 17: 533–539.

Mortazavi A, Williams BA, McCue K, Schaeffer L, Wold B. 2008. Mapping and quantifying mammalian transcriptomes by RNA-seq. Nat Methods 5: 621–628.

Oldham MC, Konopka G, Iwamoto K, Langfelder P, Kato T, Hor- vath S, Geschwind DH. 2008. Functional organization of the transcriptome in human brain. Nat Neurosci 11: 1271–1282.

Ouwenga RL, Dougherty J. 2015. Fmrp targets or not: long, highly brain-expressed genes tend to be implicated in autism and brain disorders. Mol Autism 6: 16.

Parikshak NN, Luo R, Zhang A, Won H, Lowe JK, Chandran V, Horvath S, Geschwind DH. 2013. Integrative functional geno- mic analyses implicate specific molecular pathways and cir- cuits in autism. Cell 155: 1008–1021.

Parikshak NN, Gandal MJ, Geschwind DH. 2015. Systems biol- ogy and gene networks in neurodevelopmental and neurode- generative disorders. Nat Rev Genet 16: 441–458.

Pietropaolo S, Delage P, Cayzac S, Crusio WE, Cho YH. 2011. Sex- dependent changes in social behaviors in motor pre-sympto- matic R6/1 mice. PLoS One 6: e19965.

Pollard KS, Dudoit S, Laan MJ. 2005. Multiple testing procedures: R multtest package and applications to genomics. In Bioinformatics and computational biology solutions using R and bioconductor (ed. Gentleman R, et al.), pp. 249–271. Springer, New York.

Robinson MD, McCarthy DJ, Smyth GK. 2010. edgeR: a Biocon- ductor package for differential expression analysis of digital gene expression data. Bioinformatics 26: 139–140.

Rogers DC, Fisher EM, Brown SD, Peters J, Hunter AJ, Martin JE. 1997. Behavioral and functional analysis of mouse phenotype: SHIRPA, a proposed protocol for comprehensive phenotype assessment. Mamm Genome 8: 711–713.

Rousso DL, Gaber ZB, Wellik D, Morrisey EE, Novitch BG. 2008. Coordinated actions of the forkhead protein Foxp1 and Hox proteins in the columnar organization of spinal motor neu- rons. Neuron 59: 226–240.

Rousso DL, Pearson CA, Gaber ZB, Miquelajauregui A, Li S, Por- tera-Cailliau C, Morrisey EE, Novitch BG. 2012. Foxp-mediat- ed suppression of N-cadherin regulates neuroepithelial character and progenitor maintenance in the CNS. Neuron 74: 314–330.

Roy S, Watkins N, Heck D. 2012. Comprehensive analysis of ul- trasonic vocalizations in a mouse model of Fragile X syndrome reveals limited, call type specific deficits. PLoS One 7: e44816.

Salmon-Divon M, Dvinge H, Tammoja K, Bertone P. 2010. Peak- Analyzer: genome-wide annotation of chromatin binding and modification loci. BMC Bioinformatics 11: 415.

Scattoni ML, Crawley J, Ricceri L. 2009. Ultrasonic vocalizations: a tool for behavioural phenotyping of mouse models of neuro- developmental disorders. Neurosci Biobehav Rev 33: 508– 515.

Shu W, Cho JY, Jiang Y, Zhang M, Weisz D, Elder GA, Schmeidler J, De Gasperi R, Sosa MA, Rabidou D, et al. 2005. Altered ul- trasonic vocalization in mice with a disruption in the Foxp2 gene. Proc Natl Acad Sci 102: 9643–9648.

Shu W, Lu MM, Zhang Y, Tucker PW, Zhou D, Morrisey EE. 2007. Foxp2 and Foxp1 cooperatively regulate lung and esoph- agus development. Development 134: 1991–2000.

Sia GM, Clem RL, Huganir RL. 2013. The human language-asso- ciated gene SRPX2 regulates synapse formation and vocaliza- tion in mice. Science 342: 987–991.

Spiteri E, Konopka G, Coppola G, Bomar J, Oldham M, Ou J, Vernes SC, Fisher SE, Ren B, Geschwind DH. 2007. Identifica- tion of the transcriptional targets of FOXP2, a gene linked to speech and language, in developing human brain. Am J Hum Genet 81: 1144–1157.

State MW, Sestan N. 2012. Neuroscience. The emerging biology of autism spectrum disorders. Science 337: 1301–1303.

Stein JL, de la Torre-Ubieta L, Tian Y, Parikshak NN, Hernandez IA, Marchetto MC, Baker DK, Lu D, Hinman CR, Lowe JK, et al. 2014. A quantitative framework to evaluate modeling of cortical development by neural stem cells. Neuron 83: 69–86.

Stroud JC, Wu Y, Bates DL, Han A, Nowick K, Paabo S, Tong H, Chen L. 2006. Structure of the forkhead domain of FOXP2 bound to DNA. Structure 14: 159–166.

Tang B, Becanovic K, Desplats PA, Spencer B, Hill AM, Connolly C, Masliah E, Leavitt BR, Thomas EA. 2012. Forkhead box pro- tein p1 is a transcriptional repressor of immune signaling in the CNS: implications for transcriptional dysregulation in Huntington disease. Hum Mol Genet 21: 3097–3111.

Teramitsu I, Kudo LC, London SE, Geschwind DH, White SA. 2004. Parallel FoxP1 and FoxP2 expression in songbird and hu- man brain predicts functional interaction. J Neurosci 24: 3152–3163.

Trapnell C, Pachter L, Salzberg SL. 2009. TopHat: discovering splice junctions with RNA-seq. Bioinformatics 25: 1105– 1111.

Vernes SC, Oliver PL, Spiteri E, Lockstone HE, Puliyadi R, Taylor JM, Ho J, Mombereau C, Brewer A, Lowy E, et al. 2011. Foxp2 regulates gene networks implicated in neurite outgrowth in the developing brain. PLoS Genet 7: e1002145.

Voineagu I, Wang X, Johnston P, Lowe JK, Tian Y, Horvath S, Mill J, Cantor RM, Blencowe BJ, Geschwind DH. 2011. Transcrip- tomic analysis of autistic brain reveals convergent molecular pathology. Nature 474: 380–384.

Wang B, Lin D, Li C, Tucker P. 2003. Multiple domains define the expression and regulatory properties of Foxp1 forkhead tran- scriptional repressors. J Biol Chem 278: 24259–24268.

Wang B, Weidenfeld J, Lu MM, Maika S, Kuziel WA, Morrisey EE, Tucker PW. 2004. Foxp1 regulates cardiac outflow tract, endo- cardial cushion morphogenesis and myocyte proliferation and maturation. Development 131: 4477–4487.

Wang L, Wang S, Li W. 2012. RSeQC: quality control of RNA-seq experiments. Bioinformatics 28: 2184–2185.

Xu X, Wells AB, O'Brien DR, Nehorai A, Dougherty JD. 2014. Cell type-specific expression analysis to identify putative cellular mechanisms for neurogenetic disorders. J Neurosci 34: 1420–1431.

Zhang B, Horvath S. 2005. A general framework for weighted gene co-expression network analysis. Stat Appl Genet Mol Biol doi: 10.2202/1544-6115.1128.

Zhang Y, Liu T, Meyer CA, Eeckhoute J, Johnson DS, Bernstein BE, Nusbaum C, Myers RM, Brown M, Li W, et al. 2008. Mod- el-based analysis of ChIP-seq (MACS). Genome Biol 9: R137.

CHAPTER 3: SINGLE-CELL ANALYSIS OF FOXP1-DRIVEN MECHANISMS ESSENTIAL FOR STRIATAL DEVELOPMENT

Adapted from: **Anderson, A.G.**, Kulkarni, A., Harper, M., and Konopka, G. (2019). Single-cell analysis of Foxp1-driven mechanisms essential for striatal development. bioRxiv *10*, 611780. **Submitted for peer-review.**

ABSTRACT

The striatum is a critical forebrain structure for integrating cognitive, sensory, and motor information from diverse brain regions into meaningful behavioral output. However, the transcriptional mechanisms that underlie striatal development and organization at single-cell resolution remain unknown. Here, we show that Foxp1, a transcription factor strongly linked to autism and intellectual disability, regulates organizational features of striatal circuitry in a cell-type-dependent fashion. Using single-cell RNA-sequencing, we examine the cellular diversity of the early postnatal striatum and find that cell-type-specific deletion of *Foxp1* in striatal projection neurons alters the cellular composition and neurochemical architecture of the striatum. Importantly, using this approach, we identify the non-cell autonomous effects produced by disrupting one cell-type and the molecular compensation that occurs in other populations. Finally, we identify Foxp1-regulated target genes within distinct cell-types and connect these molecular changes to functional and behavioral deficits relevant to phenotypes described in patients with *FOXP1* loss-of-function mutations. These data reveal cell-type-specific transcriptional mechanisms underlying distinct features of striatal circuitry and identify Foxp1 as a key regulator of striatal development.

INTRODUCTION

The striatum is the major input nucleus of the basal ganglia and receives dense glutamatergic inputs from the cortex and thalamus, as well as dopaminergic innervations from the substantia nigra and other neuromodulatory circuits. The principal neurons that receive and integrate this information within the striatum are GABAergic spiny projection neurons (SPNs)(Gerfen and Surmeier, 2011). Proper function of striatal circuitry is essential for coordinated motor control, action selection, and reward-based behaviors(Cui et al., 2013; Tecuapetla et al., 2016). Dysfunction of this system is implicated across many neurological disorders, including Huntington's disease, Parkinson's disease, autism spectrum disorder (ASD), and obsessive-compulsive disorder(Crittenden and Graybiel, 2011; Fuccillo, 2016).

Striatal organization has two prominent features: the division of the striatum into distinct neurochemical zones, the striosome and matrix compartments, and the division of SPNs into the direct or indirect projection pathways. Striosome and matrix compartments are enriched for distinct neuropeptides and contribute differentially to striatal connectivity and behavior(Crittenden and Graybiel, 2011; Crittenden et al., 2016; Friedman et al., 2015; Smith et al., 2016). Recent evidence suggests that striosome-matrix compartmentalization is the initial organizational plan during striatal development with distinct intermediate progenitor pools in the lateral ganglionic eminence (LGE) giving rise first to striosome SPNs then matrix SPNs(Kelly et al., 2018). These progenitor pools then generate either direct and indirect pathway SPNs, which populate both compartments(Kelly et al., 2018). Direct pathway SPNs express dopamine receptor 1 (D1, dSPNs) and project to the globus pallidus internal (GPi) and substantia nigra (SN).

Indirect pathway SPNs express dopamine receptor 2 (D2, iSPNs) and project to the globus pallidus external(Gerfen and Surmeier, 2011). Ultimately, these pathways work to bidirectionally modulate excitatory inputs back onto the cortex(Gerfen and Surmeier, 2011).

Mature dSPNs and iSPNs have distinct molecular profiles based on expression profiling studies(Gokce et al., 2016; Heiman et al., 2008; Lobo et al., 2006a; Saunders et al., 2018), and several transcription factors and chromatin regulators have been identified for both pan-SPN and d/iSPN sub-specification (see **Chapter 1, Part II**) (Anderson et al., 1997; Arlotta et al., 2008; Corbin et al., 2000; Ehrman et al., 2013; Garel et al., 1999; Kim et al., 2008b; Lobo et al., 2008; Long et al., 2009; Lu et al., 2014; Martín-Ibáñez et al., 2017; Maze et al., 2014; Waclaw et al., 2017; Xu et al., 2018). However, a limitation of these previous studies was that non-cell autonomous changes in gene expression were unable to be detected. Moreover, the cellular diversity of the early postnatal striatum, in general, has not been characterized at single-cell resolution. This time point is an important and understudied period of striatal development before excitatory synaptic density onto SPNs markedly increases and where perturbations of cortical-striatal activity can have long lasting effects on SPN spine density and circuit activity(Kozorovitskiy et al., 2012; Peixoto et al., 2016).

Forkhead-box protein 1 (Foxp1) is a transcription factor with enriched expression in the striatum compared to the rest of the brain(Heiman et al., 2008). Foxp1 is highly expressed within both SPN populations and loss-of-function *FOXP1* variants are strongly linked to ASD and intellectual disability in humans(Fong et al., 2018; Meerschaut et al., 2017; Siper et al., 2017). Expression of Foxp1 begins in the LGE at E12.5 with enrichment

in the marginal zone and is maintained throughout striatal development(Ferland et al., 2003b; Xu et al., 2018). While previous studies have suggested a role for Foxp1 in striatal development(Precious et al., 2016),(Bacon et al., 2015b),(Araujo et al., 2015), no study has examined the contribution of Foxp1 to striatal circuit organization in a cell-specific manner.

To ascertain the cell-type specific role of Foxp1, we generated mice with deletion of *Foxp1* from dSPNs, iSPNs, or both populations, and used a combination of single-cell RNA-sequencing (scRNA-seq), whole brain 3D-imaging, and behavioral assays to delineate the contribution of Foxp1 to striatal development and function. We show that Foxp1 is crucial for maintaining the cellular composition of the striatum, especially iSPN specification, and proper formation of the striosome-matrix compartments. We uncover downstream targets regulated by Foxp1 within iSPNs and dSPNs and connect these molecular findings to cell-type-specific deficits in motor and limbic system-associated behaviors, including motor-learning, ultrasonic vocalizations, and fear conditioning. Moreover, we identify the non-cell autonomous effects produced by disruption of one SPN subpopulation and the molecular compensation that occurs. These findings provide an important molecular window into postnatal striatal development and further our understanding of striatal circuits mediating ASD-relevant behavioral phenotypes.

RESULTS

Early postnatal scRNA-seq of striatal cells across *Foxp1 cKO* mice

To examine the contribution of Foxp1 to striatal development in a cell-type-specific manner, we generated *Foxp1* conditional knockout (cKO) mice using BAC-transgenic

mice driving Cre expression under the D1- or D2-receptor promoters(Gong et al., 2007) crossed to *Foxp1*$^{flox/flox}$ mice(Araujo et al., 2017; Feng et al., 2010b; Usui et al., 2017a) (**Figure 3.1A**). Four genotypes were used for downstream analyses: *Drd1-Cre*$^{tg/+}$; *Foxp1*$^{flox/flox}$ (***Foxp1***^{D1}, deletion of *Foxp1* in dSPNs), *Drd2-Cre* $^{tg/+}$; *Foxp1*$^{flox/flox}$ (***Foxp1***^{D2}, deletion of *Foxp1* in iSPNs), *Drd1-Cre* $^{tg/+}$; *Drd2-Cre* $^{tg/+}$; *Foxp1*$^{flox/flox}$ (***Foxp1***^{DD}, deletion of *Foxp1* in both d/iSPNs), and *Foxp1*$^{flox/flox}$ (***Foxp1***^{CTL}). We confirmed that Foxp1 was reduced at both the transcript and protein levels within the striatum (**Figure 3.1B-D**). Foxp1 is also reduced in lower-layer cortical neurons expressing *Drd1* (**Figure 3.S1A**).

Using 10X Genomics Chromium technology(Zheng et al., 2017), we profiled the transcriptome of 62,778 striatal cells across control and the three *Foxp1 cKO* mouse lines at postnatal day 9 (N=4/genotype; 16 samples total) (**Figure 3.1A**). We detected 5,587 UMIs (median= 3,837) and 1,794 genes (median=1,532) per cell (**Figure 3.1E**). All cells were combined across genotype and filtered for downstream clustering, resulting in 43 clusters driven by cell-type (**Figure 3.1F**; **Table S1**). For unbiased characterization of striatal cell-types, we used a previously annotated adult striatal single-cell dataset(Saunders et al., 2018) to assign cell-types to each cluster using two separate methods, a previously published expression weighted cell-type enrichment (EWCE) analysis(Skene and Grant, 2016) and an in-house correlation analysis (see methods) (**Figure 3.S1B**). We confirmed the cell-type annotation of our dataset by examining the expression of known marker genes for each major cell-type (**Figure 3.S1C-F**; **Table S1**). The principal cell-types found within the early postnatal striatum were neurogenic progenitor cells, spiny projection neurons (SPNs), astrocytes, and oligodendrocyte precursor cells (OPCs) (**Figure 3.1F-G**; **Table S2**). Endothelial, microglia, ependymal,

interneurons, and mural cells made up a smaller percentage of total cells within the postnatal striatum (**Figure 3.1F-G**). Unexpectedly, at postnatal day 9, we found a large neurogenic progenitor population (~30% of total cells within control samples) with clusters expressing proliferation markers (*Mki67*, **Figure 3.S1E**), progenitor markers (*Ascl1*, *Dlx2,* **Figure 3.S1E**), and SPN-specification markers (*Sp9, Ppp1r1b, Drd1, Drd2*, **Figure 3.S1F**). These data suggest ongoing striatal neuronal differentiation and neurogenesis into early postnatal development.

The cell-type with the largest number of unique subclusters were SPNs with 13 unique clusters (**Figure 3.1F**). SPNs and neurogenic progenitors made up 52% of the total cell population (**Figure 3.1G**) in line with previously published adult scRNA-seq datasets(Gokce et al., 2016; Saunders et al., 2018). Genotype-specific variations were observed primarily within SPN clusters, where Foxp1 is selectively deleted (**Figure 3.1G-J**; **Table S2).** To more directly compare the composition of striatal cell-types across genotypes and better control for variations in total cells sequenced between genotypes, we down-sampled the dataset to yield equal cell numbers across genotypes and reclustered the resultant cells separately. We found analogous results in the percentage of cell-types from down-sampling experiments compared to the full dataset (**Figure 3.S1G**). Variations within the SPN and progenitor populations in *Foxp1 cKO* samples compared to control were consistent across down-sampling, with more neurons (SPNs) and fewer progenitor cells within all *Foxp1 cKO* samples (**Figure 3.1G-J** and **3.S1G**; **Table S2**). Our data reveal at the single-cell level that deletion of *Foxp1* reduces the population of striatal neurogenic cells, while increasing the percentage of mature SPNs. These data highlight the diversity of the cellular composition of the early-postnatal

striatum and demonstrate that Foxp1 plays an important role in striatal neurogenesis and development.

Diversity of early post-natal striatal projection neurons

To further characterize early postnatal SPN subtypes and the effects of *Foxp1* deletion, we next isolated all clusters identified as neuronal from the annotation analyses (see Figure 1 and methods) and reclustered them separately (18,073 cells total and 24 clusters) (**Figure 3.2A-E**). Three interneuron clusters (Clusters-14, 15, 20) were identified by the interneuron marker *Nkx2-1* (**Figure 3.2A** and **S2A**; **Table S1**). We could clearly distinguish dSPN clusters (Clusters-0, 1, 3, 4, 5, 9) and iSPN clusters (Clusters-2, 8, 10, 16) using canonical markers (*Drd1* and *Tac1* for dSPNs, *Drd2* and *Penk* for iSPNs) (**Figure 3.2F** and **Figure 3.S2B**; **Table S1**). Pairwise comparisons between the major dSPN and iSPN clusters confirmed enrichment of known genes within each population (**Figure 3.2C**). One small cluster (Cluster-19) co-expressed both *Drd1* and *Drd2* receptors, termed “ddSPNs” (**Figure3. 2F**). SPNs expressing both *Drd1* and *Drd2* receptors were also scattered throughout other clusters and comprised ~1% of the total SPN population (**Figure 3.S2D**; **Table S2**). We identified a recently described SPN subpopulation termed “eccentric” SPNs (eSPNs)(Saunders et al., 2018) within Cluster-7 that uniquely expressed markers such as *Casz1* and *Otof* (**Figure 3.2F** and **S2E**; **Table S1**). We also found two clusters (Cluster-6, 23) that were enriched for the neurogenic transcription factors *Sox4* (**Figure 3.2F** and **S2F**) and *Sox11* (**Table S1**). *Sox4* and *Sox11* function during the terminal steps of neurogenesis to promote neuronal maturation(Bergsland et al., 2006; Chen et al., 2015a); therefore, we termed these

clusters “immature SPNs” (imSPNs). We confirmed the presence of $Sox4^{+}$ cells within and near the subventricular zone of the lateral ventricle and populating zones in P7 ventral striatum (**Figure 3.S2G**). Additionally, several clusters enriched for d/iSPN markers also have high expression of *Sox4* (dSPN Clusters-9,11, 13, 17 and iSPN Clusters-16), indicating these may be less mature SPNs (**Figure 3.2G** and **S2F**). Two clusters (Cluster-12, 18) were composed primarily of cells from $Foxp1^{D1}$ and $Foxp1^{D2}$ and could not be classified into distinct SPN subclusters (**Figure 3.2A-F)**. *Foxp2*, another Foxp transcription factor with high amino acid sequence similarity to *Foxp1*(Shu et al., 2001), is an SPN marker with enriched expression in dSPNs (**Figure 3.S2C**)(Fong et al., 2018; Vernes et al., 2011). Within our dataset, *Foxp2* is highly expressed within all dSPN clusters and one iSPN cluster (Cluster-8). Surprisingly, the highest expression of *Foxp2* is found within eSPN Cluster-7 and imSPN Cluster-6, where notably *Foxp1* is not highly expressed (**Figure 3.2F** and **S2H**). *Foxp2* expression is also maintained within adult eSPNs(Saunders et al., 2018). We confirmed that Foxp2 is expressed in cells other than mature dSPNs and iSPNs at postnatal day 9 using $D1\text{-}tdTomato^{tg/-}$ and $D2\text{-}eGFP^{tg/-}$ reporter mice (**Figure 3.S2I**).

Foxp1 regulates SPN subtype composition and iSPN specification

We next asked whether Foxp1 regulates the development of specific SPN populations by examining the percentages of SPN subtypes across genotypes (**Figure 3.2G**). Control samples have nearly double the number of dSPN relative to iSPNs (61% dSPNs, 31% iSPNs), with imSPNs contributing ~4% of the total SPN population and both eSPNs and ddSPNs contributing ~2% (**Figure 3.2G**). This percentage of dSPNs to iSPNs

at P9 is similar to those seen at P14 using reporter mice (Thibault et al., 2013). The percentage of SPN subtypes varied across *Foxp1 cKO* samples (**Figure 3.2G**). Notably, the number of eSPNs increased 2-4-fold across *Foxp1 cKO* samples. Strikingly, within *Foxp1*^{D2} and *Foxp1*^{DD} samples, the number of iSPNs was reduced by two-thirds compared to control levels (**Figure 3.2G**). Cells with deletion of *Foxp1* were transcriptionally distinct and clustered largely separately from control cells (**Figure 3.2H**).

To independently confirm the reduction of iSPNs in *Foxp1*^{D2} and *Foxp1*^{DD} samples, we crossed all *Foxp1 cKO* mice to *D2-eGFP* reporter animals (*D2-eGFP*$^{tg/-}$*; Foxp1*$^{flox/flox}$) to label iSPNs (**Figure 3.2I**). Within *Foxp1*^{D2} mice, we again found a significant two-thirds reduction of iSPNs (D2-eGFP^{+} cells) as seen in the scRNA-seq data (**Figure 3.2I-J**). Compared to *Foxp1*^{CTL}*, Foxp1*^{DD} mice also showed significantly reduced iSPNs, but they also showed increased iSPNs compared to *Foxp1*^{D2} (**Figure 3.2I- J**). The remaining iSPNs in the *Foxp1*^{D2} mice were not the product of *D2-Cre* inefficiency, as these cells did not express Foxp1 (**Figure 3.S2J**). Only 7 iSPNs within the single-cell *Foxp1*^{CTL} data did not express Foxp1 (0.2% of total iSPNs) (**Figure 3.S2D**), therefore, we would not expect the remaining iSPNs in *Foxp1*^{D2} mice to be a naturally occurring Foxp1 negative population. Taken together, these results indicate that Foxp1 is required for the specification of distinct iSPN subpopulations and may function to repress the generation of eSPNs.

Deletion of *Foxp1* disrupts striosomal area and iSPN localization

We identified distinct subclusters within dSPNs and iSPNs in our scRNA-seq data (**Figure 3.3A**). Using a pairwise differential gene expression analysis between clusters,

we found that two *Foxp1*^{CTL} dSPN clusters (Cluster-0, 5) corresponded to either matrix or striosome compartments, respectively, based on the enrichment of known striosome (*Oprm1*, *Isl1*, *Pdyn*, *Lypd1*, *Tac1*, and *Nnat*) or matrix markers (*Ebf1*, *Epha4*, *Mef2c*) (**Figure 3.3B**; **Table S3**). Within iSPNs, Cluster-8 was enriched for striosomal markers (*Nnat*, *Lypd1*, *Foxp2*) and Cluster-2 for matrix markers (*Penk*, *Chrm3*, *Epha4*) (**Figure 3.3C**; **Table S3**).

We next wanted to determine whether the remaining subpopulation of iSPNs within *Foxp1*^{D2} or *Foxp1*^{DD} mice localized within either the striosome or matrix compartment. To do this, we stained for the canonical striosome marker MOR (*Oprm1*) in *Foxp1 cKO* mice crossed to *D2-eGFP* reporter mice (**Figure 3.3D-F**). We found that few remaining iSPNs within *Foxp1*^{D2} and *Foxp1*^{DD} mice localized within the striosome compartment. They clustered primarily around the border of the striosome compartments and were scattered throughout the matrix (**Figure 3.3D-F**). Taken together, these data show that Foxp1 specifies iSPNs of both striosome and matrix compartments but may not be necessary for specification of a subpopulation of iSPNs near the striosomal border. We also found that striosomal area was significantly reduced across all *Foxp1 cKO* animals at P7 (**Figure 3.3G**) and that fewer striosome "patches" were observed specifically within *Foxp1*^{DD} mice (**Figure 3.3H**). These data indicate that Foxp1 plays a critical role within both dSPNs and iSPNs to maintain proper striosome-matrix architecture.

Cell-type-specific Foxp1 regulated targets

To better understand the molecular mechanisms regulated by Foxp1, we performed a cell-type-specific "pseudobulk" differential gene expression analysis (see

methods) of the scRNA-seq data across genotypes. We identified differentially expressed genes (DEGs) regulated by *Foxp1* within dSPNs or iSPNs, both cell-autonomously and non-cell-autonomously (**Figure 3.4A-B**; **Table S4**). Cell-autonomous DEGs are found in Cre active cells (dSPNs in *Foxp1*^{D1} samples or iSPNs in *Foxp1*^{D2} samples) and non-cell-autonomous DEGs are found in Cre inactive cells (iSPNs in *Foxp1*^{D1} samples or dSPNs in *Foxp1*^{D2} samples). We observed more total iSPN-DEGs (647) compared to dSPNs-DEGs (285) across genotypes (**Figure 3.4A-B**). There were more cell-autonomous changes than non-cell-autonomous within both dSPNs and iSPNs of *Foxp1*^{D1} and *Foxp1*^{D2} samples and no differences in the ratio of cell-autonomous to non-cell autonomous DEGs within dSPNs or iSPNs were observed (**Figure 3.4C**). However, significantly more iSPN-DEGs were shared between *Foxp1*^{D2} and *Foxp1*^{DD} samples (211 DEGs) compared to dSPN-DEGs shared between *Foxp1*^{D1} and *Foxp1*^{DD} samples (47 DEGs) (**Figure 3.4D**). The DEGs unique to *Foxp1*^{DD} samples were termed “interaction-DEGs”. We found significantly more interaction-DEGs in dSPNs suggesting that iSPN dysfunction exerts more transcriptional changes upon dSPNs than vice versa (**Figure 3.4D**).

The striking difference in total number of DEGs between iSPNs and dSPNs could be due to transcriptional compensation by Foxp2 in dSPNs. Foxp2 is enriched in dSPNs relative to iSPNs (**Figure 3.S2C**) and we previously found that Foxp1 and Foxp2 have shared striatal targets(Araujo et al., 2015). Interestingly, *Foxp2* is increased in iSPNs with loss of Foxp1, suggesting that Foxp1 may function to repress Foxp2 within distinct iSPN subtypes (**Figure 3.4A**; **Table S4**). *Six3* (Six homeobox 3), a transcription factor crucial for iSPN specification(Xu et al., 2018), is also upregulated within the remaining iSPNs of

Foxp1^{D2} and *Foxp1*^{DD} mice (**Table S4**). We previously found that *SIX3* was a direct target of FOXP1 in human neural progenitors(Araujo et al., 2015). Therefore, upregulation of both *Foxp2* and *Six3* in iSPNs may play a role in the specification of the remaining iSPNs within *Foxp1*^{D2} and *Foxp1*^{DD} mice.

Gene ontology (GO) analysis of the shared iSPN-DEGs within *Foxp1*^{D2} and *Foxp1*^{DD} supports a role for Foxp1 in axon guidance, neurogenesis, and neuronal differentiation of iSPNs (**Table S5**). Shared upregulated dSPN-DEGs within *Foxp1*^{D1} and *Foxp1*^{DD} suggest altered synaptic and voltage-gated mechanisms (**Table S5**). We confirmed changes in cell-type-specific gene expression via immunohistochemistry for a subset of top DEGs (*Pde1a*, *Calb1*, and *Darpp32*) using dual-reporter mice labelling dSPNs with tdTomato (*Drd1-tdTomato*$^{tg/+}$*; Foxp1*$^{flox/flox}$) and iSPNs with eGFP (*Drd2-eGFP*$^{tg/+}$*; Foxp1*$^{flox/flox}$) crossed to *Foxp1 cKO* strains (**Figure 3.S3A-E**). *Pde1a*, a gene encoding a calmodulin/Ca^{2+} activated phosphodiesterase, was upregulated in both SPN subtypes within all *Foxp1 cKO* samples in a cell autonomous and non-cell-autonomous manner (**Figure 3.4A-B**; **Figure 3.S3A, D-E**). Previous *in vitro* work found that loss of Foxp1 reduced the expression of DARPP-32 (*Ppp1r1b*), a critical phosphatase in the dopamine signaling cascade(Precious et al., 2016). We show this decrease in DARPP-32 is specific to iSPNs *in vivo* (**Figure 3.S3B, D-E**). We also confirmed the increase of calbindin 1 (*Calb1*) selectively in dSPNs with deletion of *Foxp1* (**Figure 3.S3C-E**).

Given our previous finding that striatal targets of Foxp1 overlapped significantly with ASD-associated genes(Araujo et al., 2015), we examined the cell-type-specificity of this overlap (**Figure 3.S3F**). Using the SFARI ASD gene list, we found a significant overlap with high-confidence ASD-risk genes (SFARI gene score 1-4) with iSPNs-DEGs

with cell-autonomous deletion of *Foxp1*. These genes included three members of the contactin-family of axon-associated cell adhesion molecules: *Cntn4*, *Cntn5*, *Cntn6* (**Figure 3.4A** and **3.S3F**). There was no significant overlap with ASD-risk genes and cell-autonomous DEGs in dSPNs (**Figure 3.S3F**). Surprisingly, we found a significant overlap with upregulated, non-cell autonomous iSPN-DEGs within *Foxp1*^{D1} samples (*Kirrel3*, *Nlgn1*) (**Figure 3.S3F**). Both iSPN- and dSPN-DEGs within *Foxp1*^{DD} samples overlapped with ASD-risk genes (**Figure 3.S3F**). These data demonstrate that cell-type-specific deletion of *Foxp1* specifically within iSPNs modulates ASD-associated molecular pathways both cell-autonomously and non-cell-autonomously.

Two ASD-risk genes that were upregulated with deletion of *Foxp1* in dSPNs were *Cntnap2* (contactin-associated protein like 2) and *Dpp10* (dipeptidyl peptidase like 10) (**Figure 3.4B**; **Table S4**). *Cntnap2* is a known repressed downstream target of both Foxp1 and Foxp2(O'Roak et al., 2011b; Vernes et al., 2008) and we previously found upregulation of *Dpp10* within *Foxp1*$^{+/-}$ striatal tissue using bulk RNA-sequencing (Araujo et al., 2015). Here, using scRNA-seq, we show this regulation is specific to dSPNs.

Upregulation of eSPN molecular markers with deletion of *Foxp1*

To determine whether deletion of *Foxp1* within SPNs altered cell identity, we overlapped the top 50 enriched gene markers of distinct SPN subpopulations (eSPNs, imSPNs, and matrix and striosome dSPNs and iSPNs) (**Table S1**) with upregulated or downregulated iSPN-DEGs (**Figure 3.4E**) or dSPN-DEGs (**Figure 3.4F**) found within each *Foxp1 cKO* group. The upregulated DEGs in both iSPNs and dSPNs with cell-autonomous deletion of *Foxp1* were significantly enriched for molecular markers of

eSPNs. Upregulated iSPN-DEGs were specifically enriched for the top four enriched eSPNs markers: *Adarb2*, *Ntng1, Asic2*, and *Foxp2* (**Figure 3.4A**, **E-F**). iSPN and dSPN subtype enriched genes significantly overlapped with downregulated DEGs in both *Foxp1^{D1}* and *Foxp1^{D2}* samples (**Figure 3.4A, E-F**). Taken together, these results indicate that Foxp1 is important for maintaining the molecular identity of dSPNs and iSPNs within both matrix and striosome compartments and repressing eSPN molecular identity within these cell-types.

Altered direct and indirect pathway projections in *Foxp1^{D2}* mice

Many DEGs regulated by Foxp1 within SPNs are involved in axonogenesis and neuron projection (**Tables S4** and **S5**). We therefore examined SPN projection patterns impacted by cell-type-specific deletion of *Foxp1* in adult mice using serial two-photon tomography combined with a machine-learning-based quantification algorithm(Ragan et al., 2012; Sommer et al., 2011). We crossed *Foxp1^{D1} and Foxp1^{D2}* mice to D1-tdTomato and/or D2eGFP reporter mice (described above) to visualize projection patterns of both the direct (dSPN) and indirect (iSPN) pathway, respectively. We first quantified total striatal area across genotypes and found a significant decrease in striatal area in *Foxp1^{D2}* mice, while no changes were found in *Foxp1^{D1}* animals (**Figure 3.5A**). We next found a significant reduction of iSPN terminals onto the GPe in *Foxp1^{D2}* mice, which was not unexpected given the significant decrease in iSPNs (**Figure 3.5B, D-E**). iSPN terminals onto the GPe were unaltered in *Foxp1^{D1}* mice (**Figure 3.5B-C, E**). Moreover, there were no changes in dSPN projection patterns in *Foxp1^{D1}* mice; however, *Foxp1^{D2}* mice had significant deficits in dSPN projections onto the GPi, supporting a non-cell-autonomous

role for Foxp1 in iSPNs (**Figure 5B-D, F**). These findings indicate that Foxp1 regulates both iSPN and dSPN projection patterns through its role in iSPNs (**Figure 3.5G**). Within our scRNA-seq data, non-cell-autonomous dSPN-DEGs in *Foxp1*^{D2} samples were enriched for GO categories such as neuron projection (**Table 3.S5**). Since projections onto the GPi were not altered in *Foxp1*^{D1} mice, dSPN-DEGs unique to *Foxp1*^{D2} samples are most likely responsible for the altered dSPN projection patterns found within *Foxp1*^{D2} animals. We therefore examined the overlap of dSPN-DEGs within *Foxp1*^{D1} (cell-autonomous) and *Foxp1*^{D2} samples (non-cell-autonomous) (**Figure 3.5H**). dSPN-DEGs unique to *Foxp1*^{D2} samples involved in neuron projection include *Akap5*, *Asic2*, *Kirrel3*, *Cdh8*, and *Cntn4* (**Figure 3.5H**). Interestingly, *Kirrel3*, *Cdh8*, and *Cntn4* are also ASD-risk genes (**Figure 3.5H**). These findings suggest deletion of *Foxp1* within iSPNs alters the gene expression profiles within both iSPNs and dSPNs important for proper striatal projection patterning.

Distinct behavioral deficits with cell-type-specific deletion of *Foxp1*

We hypothesized that severe reduction of iSPNs and altered projection patterns with deletion of *Foxp1* from iSPNs would result in altered motor behaviors. We therefore first tested behaviors classically characterized as being governed by striatal circuits, such as motor learning and activity levels. To test motor learning, we used the accelerating rotarod assay and found that *Foxp1*^{D2} and *Foxp1*^{DD} mice had significant deficits at remaining on the accelerating beam compared to control and *Foxp1*^{D1} mice (**Figure3. 6A**). This phenotype was not due to differences in grip strength (**Figure 3.S4A-B**) or gait abnormalities (**Figure 3.S4C-F**). *Foxp1*^{D2} and *Foxp1*^{DD} mice were also hyperactive in the

open field behavioral paradigm compared to control mice **(Figure 3.6B**); however, no difference was observed in novel cage activity between genotypes (**Figure 3.S4G**). There was no difference in time spent in the periphery versus the center of the open field between genotypes (**Figure 3.6C**), suggesting no changes in anxiety-like behavior.

Since genetic variants in *FOXP1* are strongly associated with ASD, we next examined ASD-relevant social communication behaviors. Using a maternal separation paradigm, we recorded pup ultrasonic vocalizations (USVs) at three postnatal time points (P4, P7, and P10). We found that *Foxp1*^{D1} mice produced significantly fewer calls with altered call slope compared to control pups (**Figure 3.6D-E**). In addition, *Foxp1*^{D1} pups had significantly lower pitch at P4, while *Foxp1*^{DD} mice exhibited deficits in pitch across all developmental time points (**Figure 3.6F**). No significant USV changes were measured solely in *Foxp1*^{D2} pups. We also tested nest building behavior, an important communal behavior in rodents(Deacon, 2006; Silverman et al., 2010), and found that *Foxp1*^{D1} and *Foxp1*^{DD} mice produced low-quality nests compared to control and *Foxp2*^{D2} nests (**Figure 3.6G-H**).

Because individuals with *FOXP1* mutations are frequently comorbid for intellectual disability(Meerschaut et al., 2017; Siper et al., 2017), we next assessed whether learning and memory circuits were altered using the cued and contextual fear conditioning (FC) paradigm (**Figure 3.6I-J**). All *Foxp1 cKO* mice had significantly reduced freezing behavior during cued-evoked fear memory recall (**Figure 3.6I**); however, only *Foxp1*^{D1} and *Foxp1*^{DD} mice showed significant deficits in context-evoked fear memory (**Figure 3.6J**). While hippocampal and amygdala circuits are classically associated with fear conditioning, striatal D1 receptors are also important for mediating proper contextual FC

in mice(Ikegami et al., 2014a). We also found that striosome-matrix architecture was more severely disrupted over postnatal development in *Foxp1*^{D1} and *Foxp1*^{DD} adult animals compared to control and *Foxp1*^{D2} mice (**Figure 3.S4H**).

DISCUSSION

In this study, we use single-cell transcriptomics to examine the molecular mechanisms underlying striatal neuronal specification by sequencing thousands of striatal cells across control and cell-type-specific *Foxp1* conditional mouse models. We show that Foxp1 influences striatal development through cell-type-specific molecular pathways and describe the molecular, functional, and behavioral consequences of *Foxp1* deletion within distinct striatal circuits (**Figure 3.7**).

The first weeks of postnatal striatal development is an important period of excitatory synaptogenesis onto SPNs (Kozorovitskiy et al., 2012; Peixoto et al., 2016; Tepper et al., 1998) and the cellular composition of the striatum during this time has been understudied. We surprisingly found that neurogenic progenitors make up a large component of the early postnatal striatum and that deletion of *Foxp1* decreases the ratio of these neurogenic progenitors to mature SPNs. These findings suggest that Foxp1 regulates intermediate progenitor pools and the differentiation of SPNs within the developing striatum. Furthermore, we found that Foxp1 is required for the specification of iSPNs that localize to the matrix and striosome compartments. iSPNs that remain with deletion of *Foxp1* localize to the striosome-matrix border and significantly upregulate top marker genes of a recently identified eSPN population, including *Foxp2*(Saunders et al., 2018). Future work will help resolve the functional contribution of eSPNs to striatal development.

Deletion of *Foxp1* specifically within iSPNs leads to both cell-autonomous and non-cell-autonomous changes in SPN projection patterns. Fewer iSPN terminals onto the globus pallidus external and fewer dSPN terminals onto the globus pallidus internal were observed. dSPNs and iSPNs are known to form inhibitory axon collaterals onto neighboring SPNs and modulate their excitability (Tunstall et al., 2002),(Taverna et al., 2008; Tecuapetla et al., 2009). iSPNs and dSPNs also cooperate together to intermix within the striosome and matrix compartments(Tinterri et al., 2018). We not only found that manipulation of iSPNs led to functional changes of dSPNs, but we captured a molecular snapshot of this inter-SPN communication, including differentially expressed ASD-risk genes involved in neuron projection such as *Cntn4*, *Cdh8*, and *Kirrel3.*

FOXP1 is among a subset of genes repeatedly and significantly linked to ASD (Iossifov et al., 2016; Stessman et al., 2017). Thus, connecting our molecular findings to behavioral deficits is particularly relevant to a behaviorally diagnosed disorder that hinges upon two key behavioral phenotypes, impairments in language and social interactions and restrictive or repetitive behaviors. The majority of individuals with *FOXP1* mutations are diagnosed with ASD and all reported cases are comorbid with intellectual disability, gross motor delays, and/or selective language impairments (Meerschaut et al., 2017; Siper et al., 2017). We found that mice with iSPN-deletion of *Foxp1* caused significant motor disruptions, as measured by increased hyperactivity and motor-learning deficits on the rotarod. Concordant with our data, mice with ablated iSPNs or mice with *Darpp32* deletion from iSPNs were also hyperactive in the open field (Bateup et al., 2010; Durieux et al., 2009). Adult mice with induced ablation of D2-receptors displayed severe motor learning impairments on the accelerating rotarod(Bello et al., 2016). These data indicate

that loss of iSPNs with deletion of *Foxp1* lead to significant motor-learning and activity deficits.

Pup USVs are an important measure of affective state and social behavior in mice (Boulanger-Bertolus et al., 2017; Silverman et al., 2010) and peak between postnatal days 4 and 10(Araujo et al., 2015). Disruption of neonatal call number and structure with deletion of *Foxp1* within dSPNs is particularly interesting given the high co-expression of both Foxp1 and Foxp2 within this cell-type and the ability of Foxp1 and Foxp2 to heterodimerize to regulate gene expression (Li et al., 2004a). Foxp2 plays a critical role in the vocal behavior across many species, including humans, mice and songbirds (Konopka and Roberts, 2016). We show that *Cntnap2*, a known shared target of Foxp1 and Foxp2 (O'Roak et al., 2011b; Vernes et al., 2008), is significantly upregulated within dSPNs. Variants in *CNTNAP2* are also associated with ASD and *Cntnap2* KO mice have altered pup USVs (O'Roak et al., 2011b). We previously found that *Foxp1* heterozygous mice display altered USV phenotypes, including deficits in call number, call structure, and pitch (Araujo et al., 2015). Additionally, mice with cortical and hippocampal deletion of *Foxp1* also produced fewer USVs, though no changes were observed in call structure or pitch (Usui et al., 2017a). Here, we observed changes in all three parameters within $Foxp1^{D1}$ and $Foxp1^{DD}$ mice suggesting that Foxp1 regulates distinct aspects of mouse vocal behavior largely through cortical-striatonigral circuitry.

Striosome compartments are smaller and architecturally disorganized with deletion of *Foxp1* in iSPNs and/or dSPNs in the early postnatal striatum. Loss of striosome-matrix compartmentalization is particularly striking in adulthood with dSPN-specific deletion of *Foxp1*. These findings indicate that dSPN-targets regulated by Foxp1 exert a stronger

influence over maintaining striatal neurochemical organization. Behaviors specific to *Foxp1*^{D1} mice include deficits in contextual fear memory recall, a known limbic-circuitry associated behavior. Striosomes receive preferential inputs from limbic subcortical regions, including the amygdala and bed nucleus of the stria terminalis(Smith et al., 2016); thus, inputs from these limbic regions targeting striosomes may be disrupted and contribute to the limbic-associated behavioral deficits seen in *Foxp1*^{D1} and *Foxp1*^{DD} mice. Additionally, mice with cortical and hippocampal deletion of *Foxp1* did not show deficits in cued or contextual fear conditioning (Araujo et al., 2017). Therefore, Foxp1 is likely mediating fear conditioned behaviors via disruption of striatal circuits.

While ASD is a genetically complex disorder, several studies have shown that striatal SPNs may be particularly vulnerable to ASD-linked mutations (Chang et al., 2014; Coe et al., 2019; Takata et al., 2018; Turner et al., 2017a; Xu et al., 2014). Our study uncovers the molecular targets of Foxp1 in SPN subtypes and finds that Foxp1 regulates ASD-relevant behaviors via distinct striatal circuits. We show that iSPNs are particularly vulnerable with loss of Foxp1 and that Foxp1 regulated iSPN-targets are enriched for high-confidence ASD risk-genes, suggesting that striatopallidal circuitry might be particularly at risk with loss-of-function *FOXP1* mutations. Our data provide important molecular insights for the development of future therapies targeting striatal circuits.

FIGURES

FIGURE 3.1. Early postnatal scRNA-seq of striatal cells across Foxp1 cKOs.

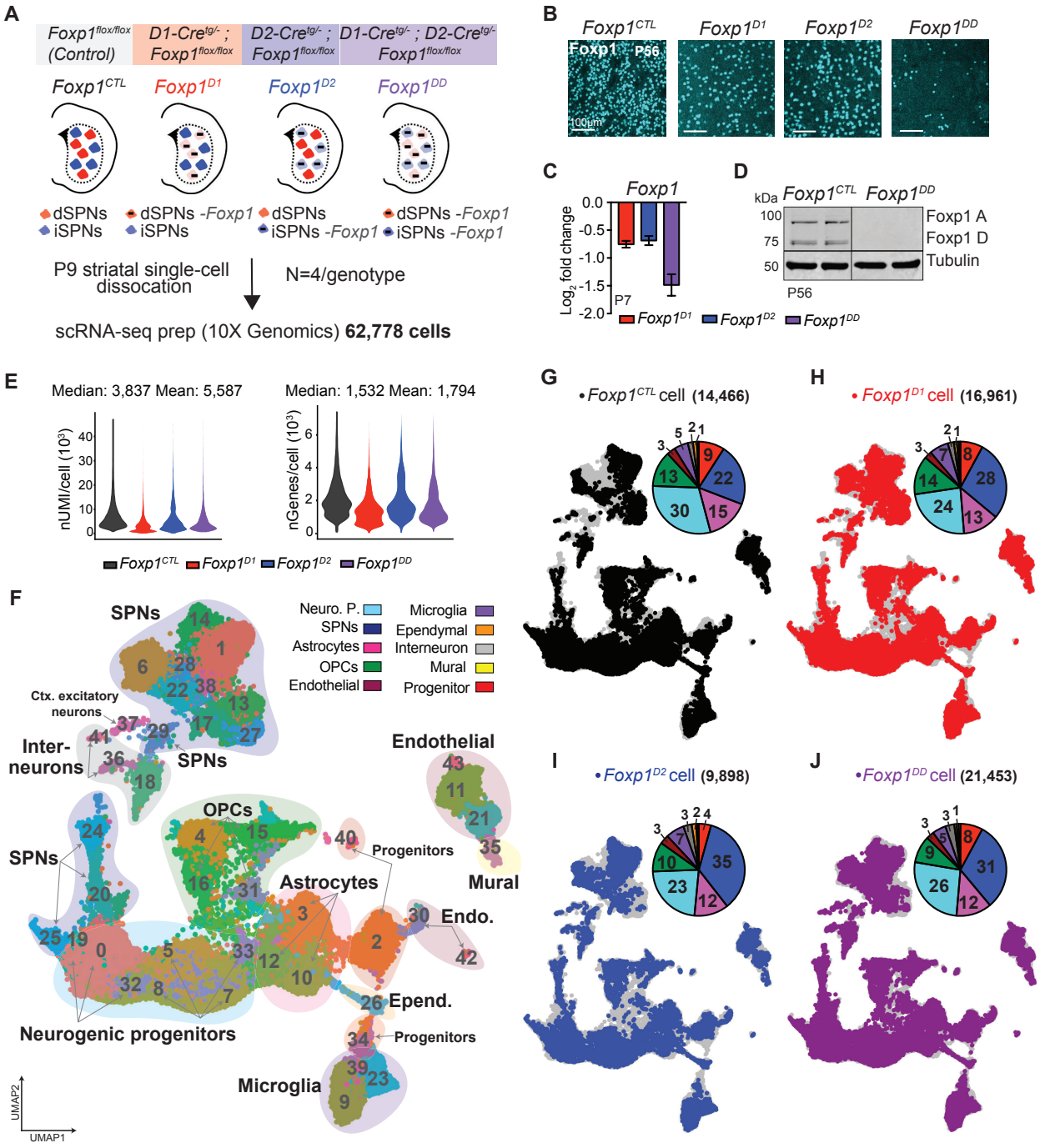

A) Schematic of the scRNA-seq experiment using striatal tissue from P9 mice (N=4/genotype) with cell-type-specific conditional deletion of *Foxp1* within the dopamine receptor-1 (*Foxp1*^{D1}), dopamine receptor-2 (*Foxp1*^{D2}), or both (*Foxp1*^{DD}) cell-types. **B-D**)

Foxp1 is reduced in the striatum via immunohistochemistry (P56) (**B**) and quantitative RT-PCR (P7) (**C**) within each cKO line, with near complete reduction in *Foxp1*^{DD} striatal tissue via immunoblot (P56) (**D**) (100μm scale bar). **E**) Violin plots of median and mean number of UMIs or genes per cell across all genotypes. **F**) Non-linear dimensionality reduction with UMAP of all 62,778 post-filtered cells combined across genotype and used for downstream analyses. Cell-type annotation is overlaid to identify the major cell-type represented by each cluster (43 total clusters). **G**-**J**) UMAP plot of cells from (**F**) color-coded to identify each cell by genotype. Pie charts using colors from (**F**) show the striatal cell-type composition as a percentage of total cells within each genotype.

FIGURE 3.2. Foxp1 specifies distinct SPN subpopulations.

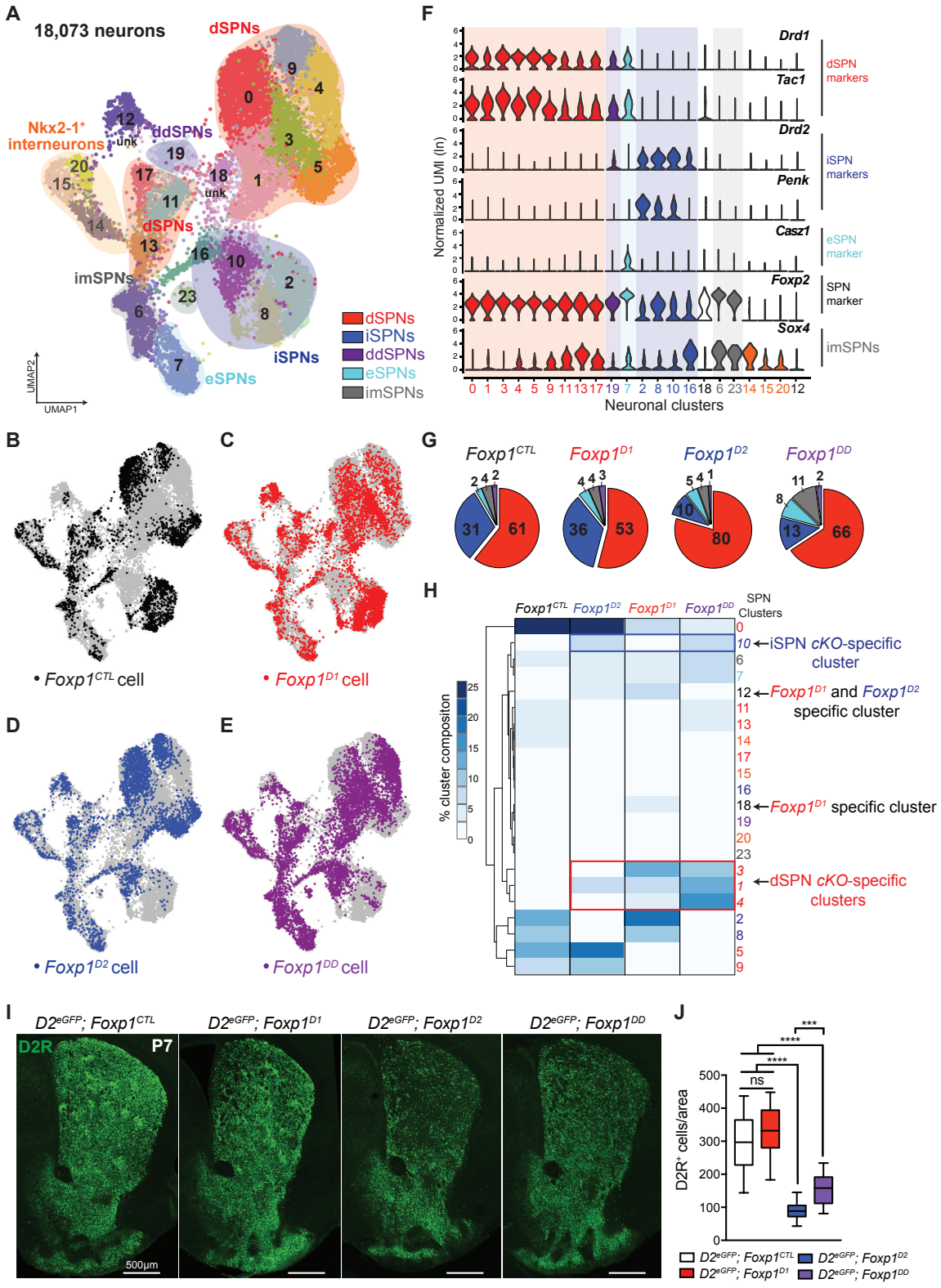

A) UMAP plot showing each neuronal subcluster by color with overlay colors showing neuronal subpopulation identity. **B**-**E**) UMAP plots of cells from (**A**) color-coded to identify each cell by genotype. **F**) Violin plots of the normalized UMI expression of markers of SPN subpopulations: dSPNs (*Drd1*, *Tac1, Foxp2*), iSPNs (*Drd2*, *Penk*), ddSPNs (*Drd2*, *Drd1*, *Tac1*), eSPNs (*Casz1*), and imSPNs (*Sox4*). **G**) Pie charts showing altered composition of SPN subtypes within *Foxp1 cKO* mice (using colors from **A**). **H**) Heatmap showing the percentage of cells contributing to each cluster across genotype (using colors from **A**). **I**-**J**) *Foxp1 cKO* mice were crossed to $D2^{eGFP}$ reporter lines to label dopamine receptor-2 (D2R) iSPNs in green (coronal section, 500μm scale bar). $Foxp1^{D2}$ *and* $Foxp1^{DD}$ mice had significantly fewer iSPNs compared to $Foxp1^{CTL}$ mice at P7, while $Foxp1^{DD}$ mice had significantly more iSPNs compared to $Foxp1^{D2}$ animals. Data are represented as a box plot, n=3-6 mice/genotype. ****p<0.0001, ***p<0.005, one-way ANOVA with Tukey's multiple comparisons test.

FIGURE 3.3. Foxp1 regulates striosome-matrix organization.

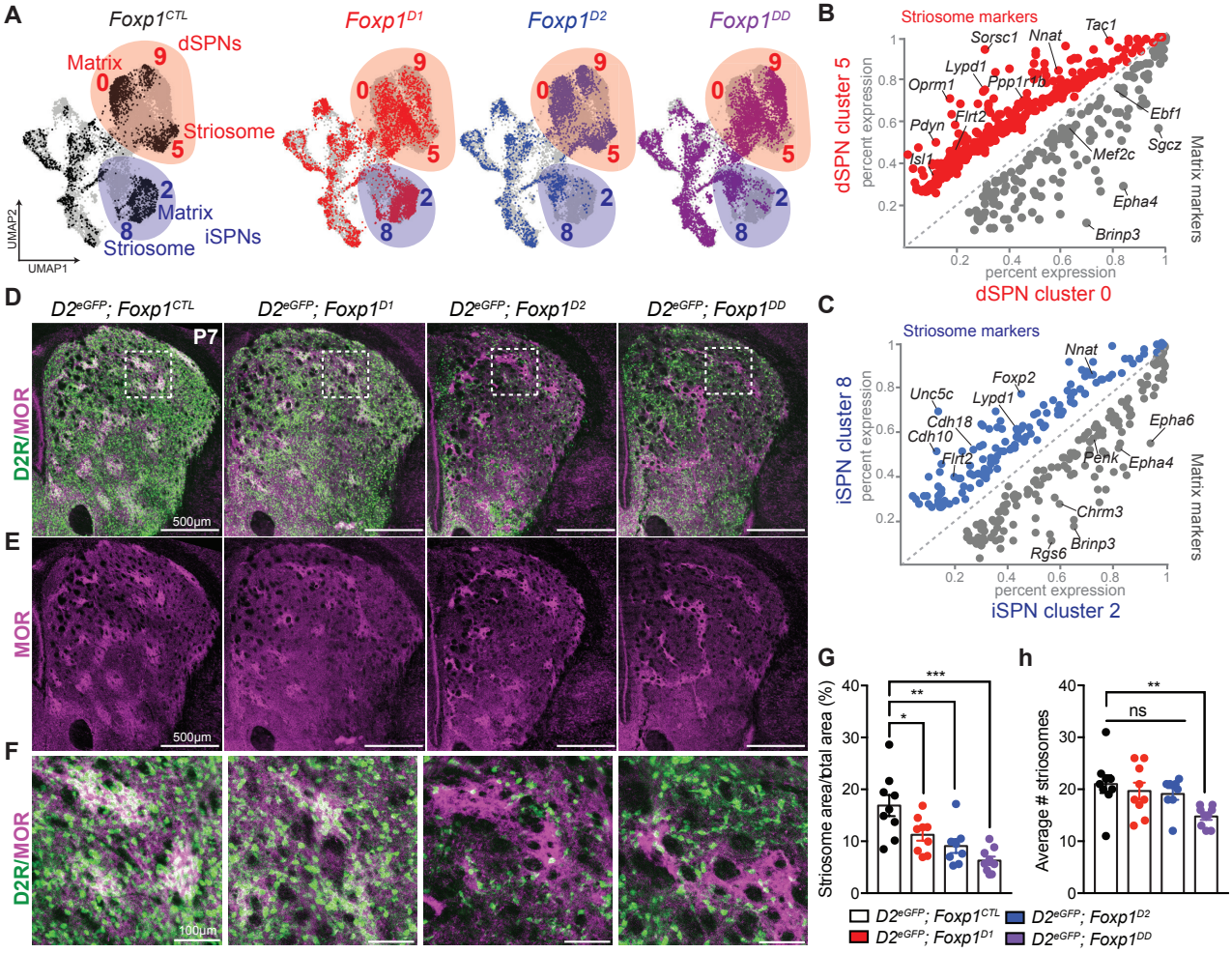

A) Within *Foxp1*^{CTL} samples, dSPN and iSPNs have large sub-clusters (Clusters-0 and -5 for dSPNs and Clusters-2 and -8 for iSPNs). Cells with deletion of *Foxp1* cluster largely separately from control cells and subclusters within iSPNs and dSPNs are more intermixed (*Foxp1*^{D1} dSPNs) or lost completely (*Foxp1*^{D2} iSPNs). **B-C**) Scatter plots showing the percent expression of enriched transcripts between Clusters-0 and-5 (**B**) or Clusters-2 and-8 (**C**). Striosome markers are enriched in dSPN Cluster-5 and iSPN Cluster-8, while matrix markers are enriched in dSPN Cluster-0 and iSPN Cluster-2 (p.adj<0.05). **D-F**) iSPNs within *Foxp1*^{D2} and *Foxp1*^{DD} mice localized primarily along the striosomal border marked by IHC for Mu-Opiod Receptor (MOR) in P7 animals crossed to D2-eGFP reporter mice (500µm scale bar in D-E, 100µm scale bar in **F**). **G-H**) The

striosome compartment was significantly reduced across all *Foxp1 cKO* mice as a percent of total striatal area (measuring only dorsal striosomes) and the number of striosome "patches" was significantly reduced in *Foxp1*^{DD} animals. Data are represented as mean ± SEM, n=4 mice/genotype. *p<0.05, p**<0.005, ***p<0.0001, one-way ANOVA with Tukey's multiple comparisons test.

FIGURE 3.4. Foxp1 regulates cell-type-specific molecular pathways.

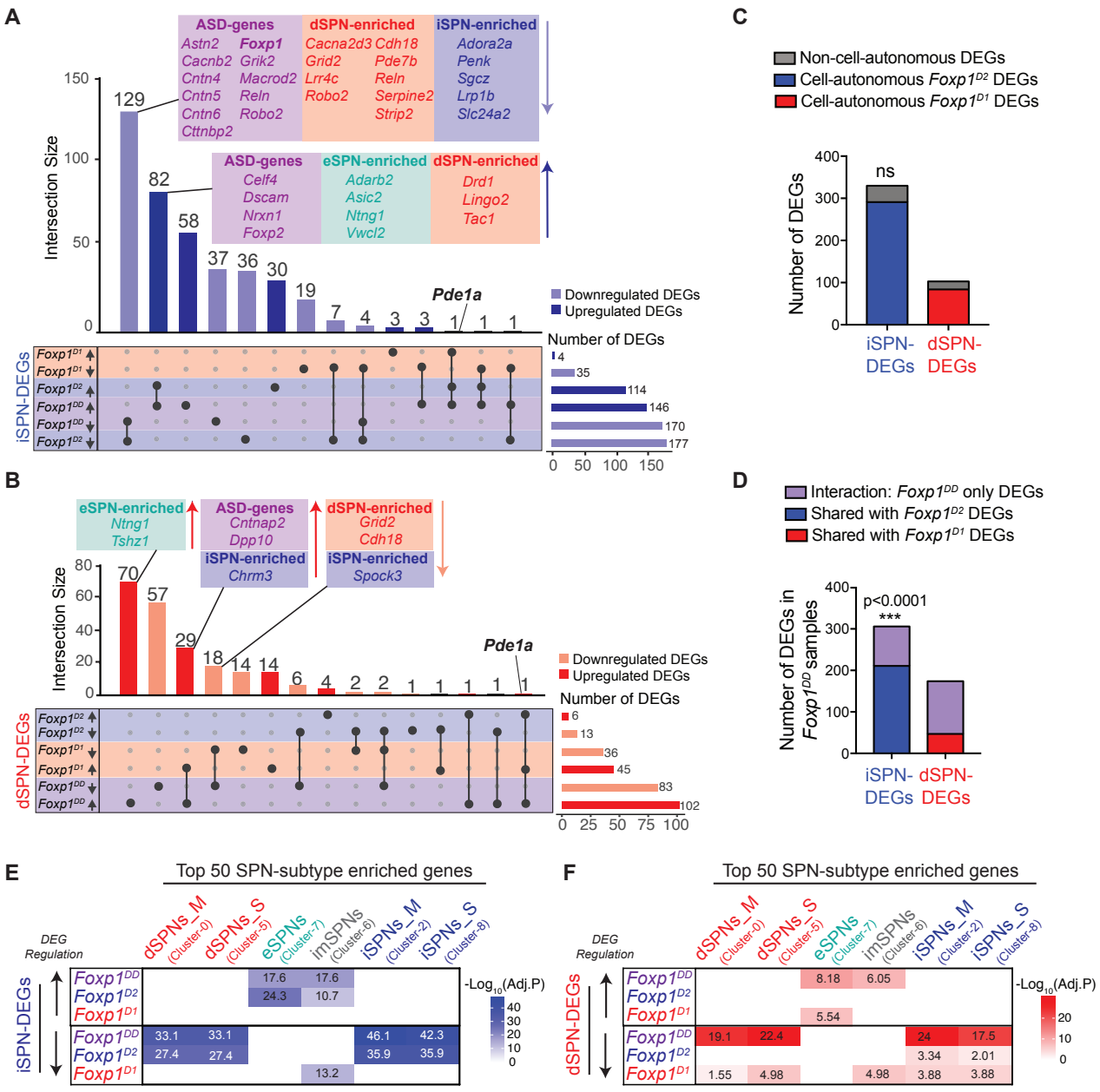

A-B) SPN cell-type-specific differential gene expression between genotypes. Upset plot showing the overlap of upregulated or downregulated DEGs across genotypes within iSPNs (**A**) or dSPNs (**B**). Genes shown within boxes are color-coded by categories indicated. **C**) No significant difference between the number of DEGs within iSPNs and dSPNs that are cell-autonomous vs non-cell-autonomous (p=0.0975, two-sided Fisher's

exact test). **D**) There is a significant difference in the number of DEGs within *Foxp1*^{DD} mice that overlap with *Foxp1*^{D2} or *Foxp1*^{D1} DEGs to unique *Foxp1*^{DD} DEGs (interaction DEGs) ($p<0.0001$, two-sided Fisher's exact test). **E**-**F**) Enrichment of upregulated or downregulated iSPN-DEGs (**E**) or dSPN-DEGs (**F**) across *Foxp1 cKO* samples in distinct SPN subtypes (top 50 most enriched genes/cluster) using a hypergeometric overlap test (8,000 genes used as background).

FIGURE 3.5. Deletion of *Foxp1* in iSPNs alters projection patterns to the GPe and dSPN projections to the GPi.

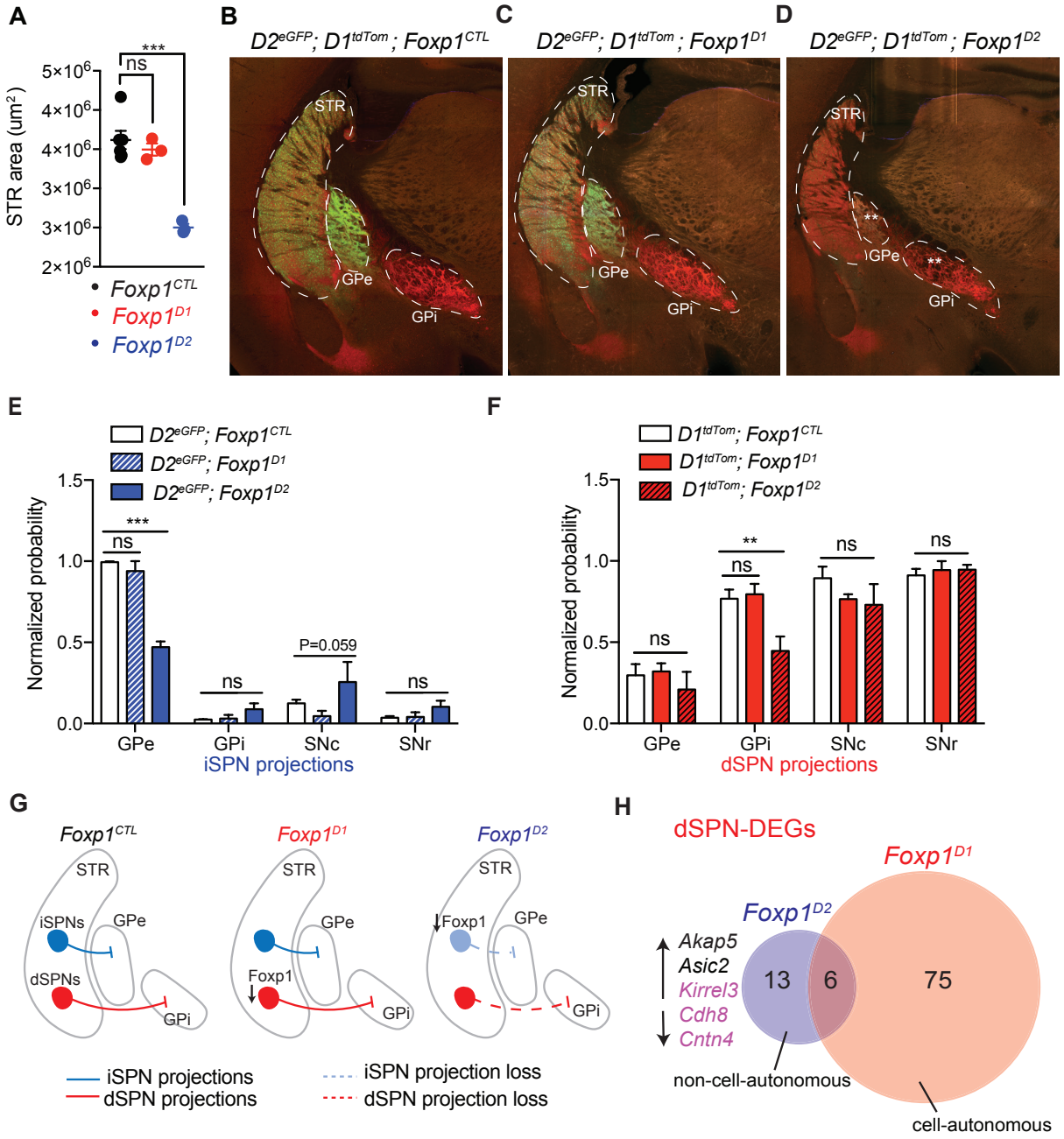

A) Striatal area quantification of four serial slices from anterior to posterior at 400um increments within *Foxp1*^{CTL}, *Foxp1*^{D1}, and *Foxp1*^{D2} adult mice. Data are represented as mean ± SEM, n=3-4 mice/genotype. ***p<0.001, one-way ANOVA with Tukey's multiple comparisons test. **B-D**) Representative Tissuecyte 1000 coronal section showing the

projections of dSPNs and iSPNs using *D1*^{tdTom} and *D2*^{eGFP} reporter mice, respectively, crossed to *Foxp1*^{CTL} (**B**), *Foxp1*^{D1} (**C**), or *Foxp1*^{D2}(**D**). **E**) Quantification of the normalized probability maps of iSPN (eGFP) projections within *Foxp1*^{CTL}, *Foxp1*^{D1}, and *Foxp1*^{D2} mice showing reduced GPe projections from iSPNs within *Foxp1*^{D2} mice. No significant changes were seen in projection patterns onto the SNc or SNr. Data are represented as mean ± SEM, n=3-4 mice/genotype. ***p<0.0001, two-way ANOVA with Dunnett's multiple comparisons test. **F**) Quantification of the normalized probability maps of dSPN (tdTomato) projections within *Foxp1*^{CTL}, *Foxp1*^{D1}, and *Foxp1*^{D2} mice showing reduced GPi projections from dSPNs within *Foxp1*^{D2} mice. Data are represented as mean ± SEM, n=2-4 mice/genotype. **p<0.01, two-way ANOVA with Dunnett's multiple comparisons test. **G**) Schematic of cell-autonomous and non-cell-autonomous projection deficits found in the *Foxp1*^{D2} animals. **H**) Overlap of dSPN-DEGs within *Foxp1*^{D1} or *Foxp1*^{D2} cells. Unique *Foxp1*^{D2} dSPN-DEGs that are involved in neuron projection are shown, with ASD-risk genes highlighted in purple. GPi= globus pallidus internal, GPe= globus pallidus external, STR= striatum, SNr=substantia nigra pars reticulata, SNc= substantia nigra pars compacta.

FIGURE 3.6. Foxp1 regulates behaviors via distinct striatal circuits.

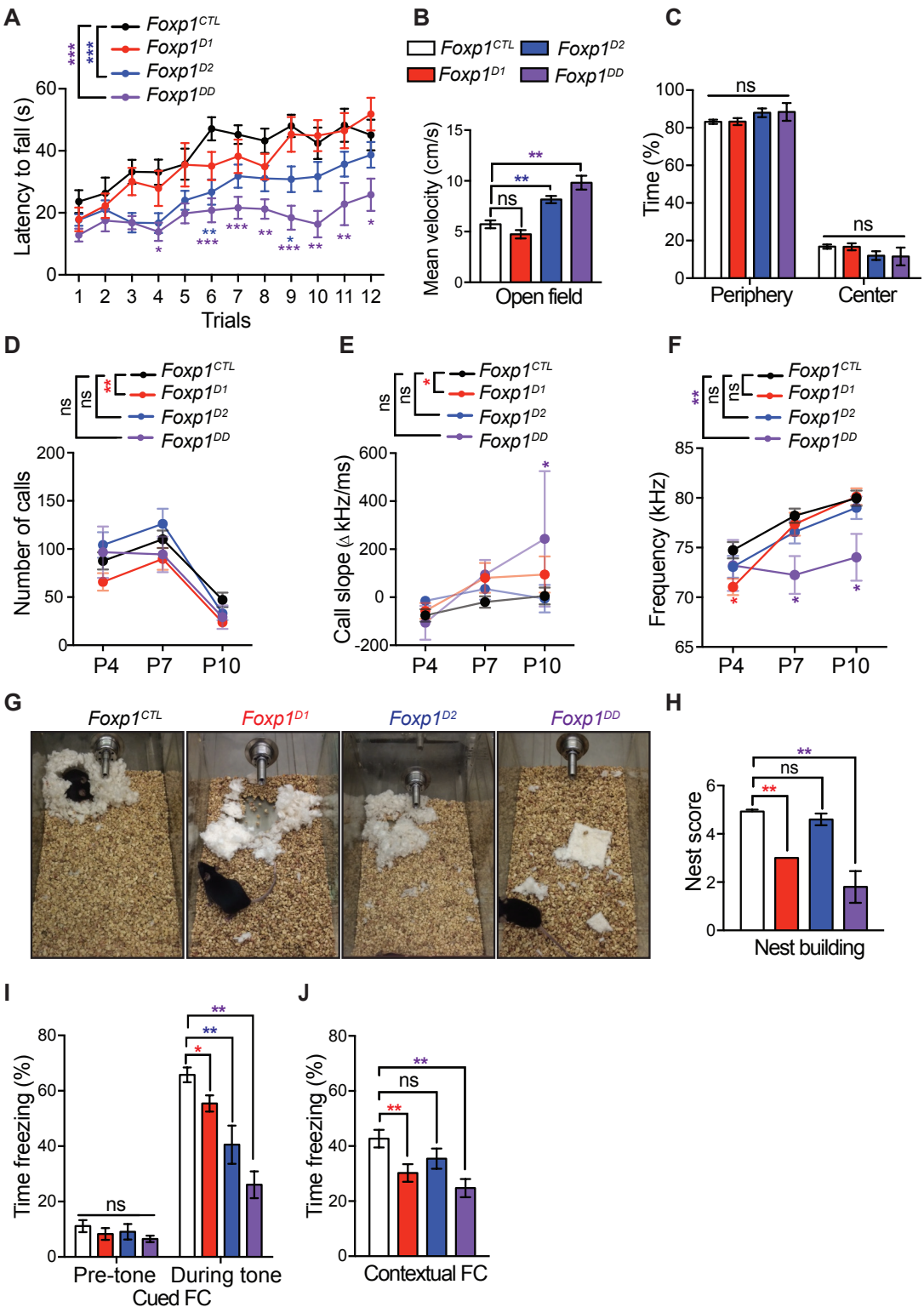

A) Latency to fall was measured on the accelerating rotarod. *Foxp1^{D2}* and *Foxp1^{DD}* mice exhibit significant deficits. Data are represented as mean ± SEM, n=11 *Foxp1^{CTL}*; n=17 *Foxp1^{D1}*; n= 18 *Foxp1^{D2}*; n=12 *Foxp1^{DD}*. *p<0.05, **p<0.005, ***p<0.0001, two-way ANOVA with Sidak's multiple comparisons test. **B**-**C**) Mice were tested within the open field paradigm with velocity (**B**) and percent time spent in the periphery vs center (**C**) plotted. *Foxp1^{D2}* and *Foxp1^{DD}* mice had significant increase in activity with no difference in percent time spent in the periphery and center. Data are represented as mean ± SEM. n=4 *Foxp1^{DD}*; n=14 *Foxp1^{D1}*; n=17 *Foxp1^{D2}*; n=22 *Foxp1^{CTL}*. ***p<0.0001, one-way ANOVA with Sidak's multiple comparisons test. **D**-**F**) Neonatal isolation vocalizations were measured at P4, P7, and P10. (**D**) The number of isolation calls were significantly reduced in *Foxp1^{D1}* mice. (**E**) Mean frequency (kHz) of the isolation calls was significantly altered in *Foxp1^{DD}* mice and at P4 within *Foxp1^{D1}* animals. (**F**) The call slope or "structure" of the call was significantly altered over postnatal development in *Foxp1^{D1}* pups and specifically at P10 within *Foxp1^{DD}* pups. Data are represented as mean ± SEM. n=11 *Foxp1^{DD}*; n=47 *Foxp1^{D1}*; n=36 *Foxp1^{D2}*; n=71 *Foxp1^{CTL}*. *p<0.05, **p<0.005, ***p<0.0001, two-way ANOVA with Sidak's multiple comparisons test. **G**) Representative images of nests. **H**) *Foxp1^{D1}* and *Foxp1^{DD}* mice produced nests with significantly lower quality scores compared to *Foxp1^{D2}* and *Foxp1^{DD}* mice. Data are represented as mean ± SEM. n=5 *Foxp1^{DD}*; n=4 *Foxp1^{D1}*; n=5 *Foxp1^{D2}*; n=7 *Foxp1^{CTL}*. **p<0.005, one-way ANOVA with Sidak's multiple comparisons test. **I**-**J**) Associative fear memory was assessed using the fear conditioning (FC) paradigm. All *Foxp1 cKO* mice displays deficits in cued FC (**H**) shown as the percent of time spent freezing. Only *Foxp1^{D1}* and *Foxp1^{DD}* mice displayed deficits in contextual FC (**I**). Data are represented as mean ± SEM. n=15 *Foxp1^{DD}*; n=22 *Foxp1^{D1}*; n=11 *Foxp1^{D2}*; n=23 *Foxp1^{CTL}*. *p<0.05, **p<0.005, ***p<0.0001, two-way ANOVA with Dunnett's multiple comparisons test.

FIGURE 3.7. Summary of cellular, structural, functional, and behavioral findings within cell-type-specific *Foxp1 cKO* mice.

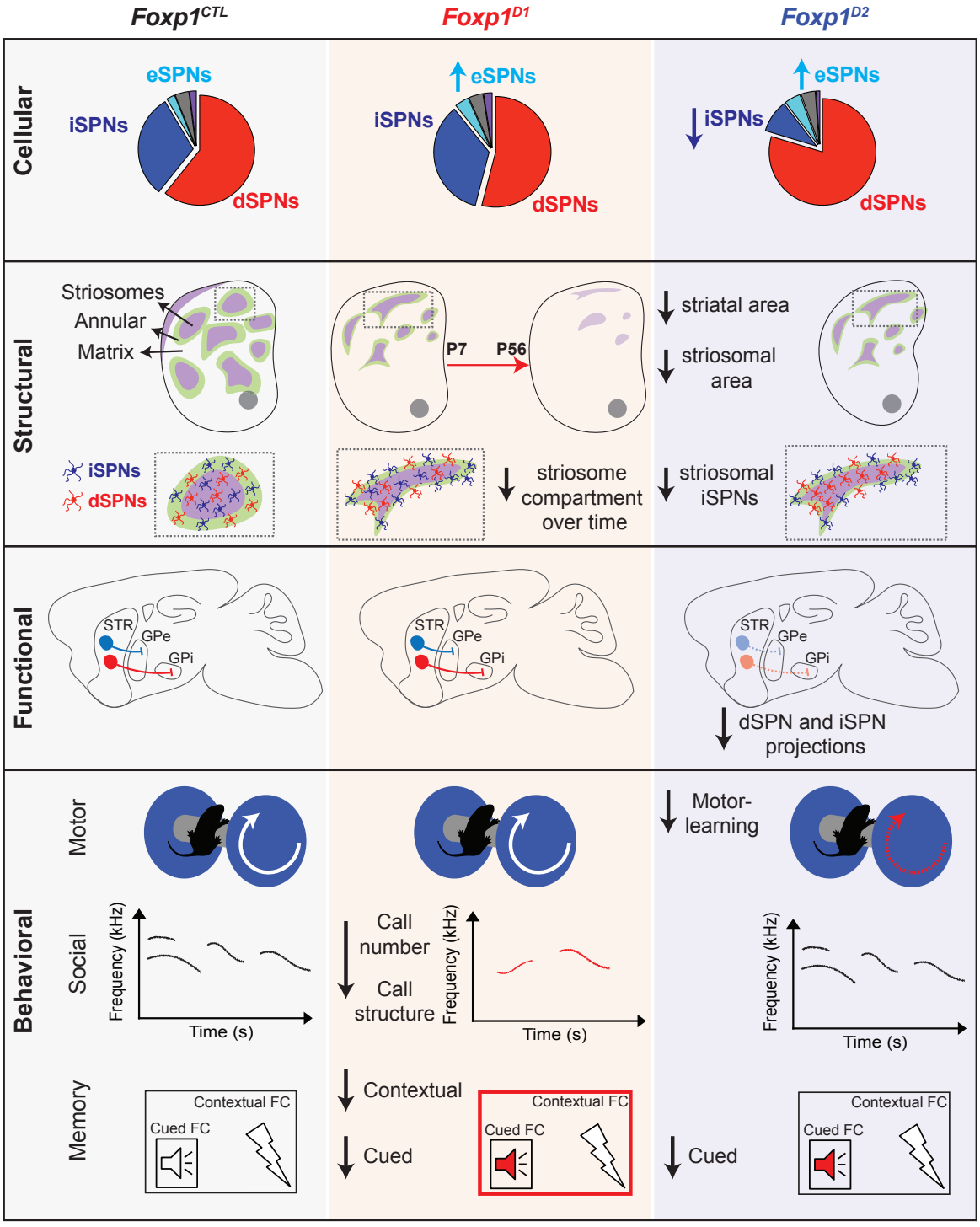

Foxp1^{D1} mice have an increase in eSPN subpopulations, reduced striosomal area, no gross SPN projection deficits, and distinct behavioral deficits relevant to social

communication behavior and contextual fear conditioning. *Foxp1*^{D2} mice have a marked decrease in iSPN and increase in eSPN subpopulations, reduced striosomal area with few striosomal iSPNs, dSPN and iSPN projection deficits, and distinct behavioral deficits relevant to motor learning and cued fear conditioning.

SUPPLEMENTAL FIGURE 3.1. Cell-type annotation of early postnatal striatal scRNA-seq.

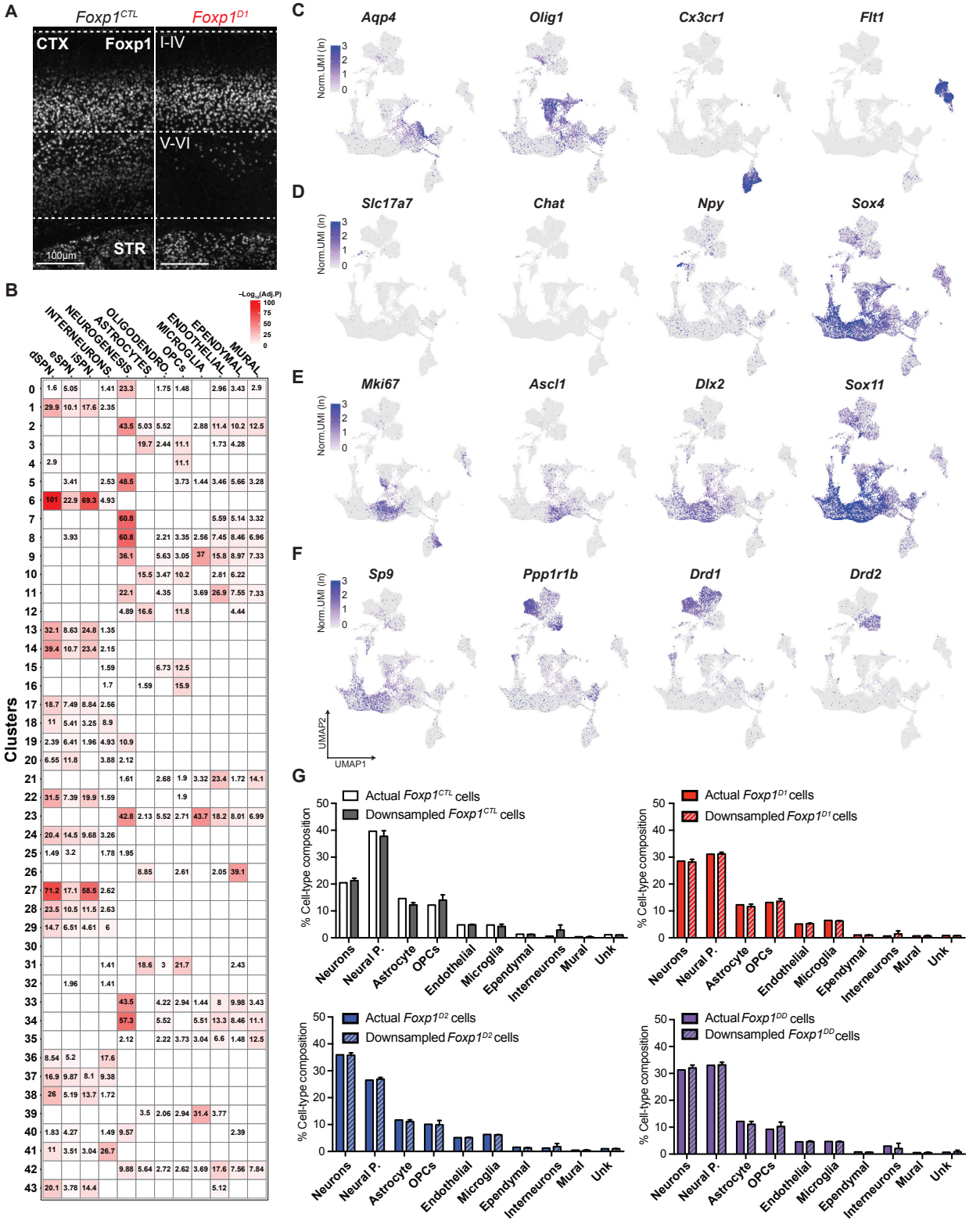

A) Confocal imaging of the somatosensory cortex of *Foxp1*^{CTL} or *Foxp1*^{D1} adult mice showing reduction of Foxp1 expression within cortical layers V-VI (scale bar is 100um, CTX= cortex, STR=striatum). **B**) Heatmap showing the enrichment of genes within each cluster that correlate to a previously annotated dataset (Saunders et al., 2018) using the hypergeometric overlap test. **C**-**D**) Expression plots showing the normalized UMI (ln) for known marker genes of distinct cell-types: (**C**) *Aqp4* for astrocytes, *Olig1* for OPCs, *Cx3cr1* for microglia, *Flt2* for endothelial, (**D**) *Slc17a7* for glutamatergic cortical neurons, interneuron populations (*Chat*, *Npy*), neurogenic and neural differentiation marker (Sox4). (**E**) Expression plots of markers identifying neurogenic populations: proliferating cells (*Mki67*), neural progenitors (*Ascl1*), neural progenitors derived from the lateral ganglionic eminence (*Dlx2*), neurogenic and neural differentiation marker (*Sox11*). **F**) Expression plots of genes important for iSPN specification (*Sp9*), mature SPN marker (*Ppp1r1b*), and major SPN subtypes (*Drd1*, *Drd2*). **G**) No changes in cell-type composition were observed between the average down-sampled datasets (10 iterations with 9,898 cells within each genotype) compared to the actual dataset.

SUPPLEMENTAL FIGURE 3.2. Neuronal subclusters and the intersection of Foxp1 and Foxp2 expressing striatal neurons.

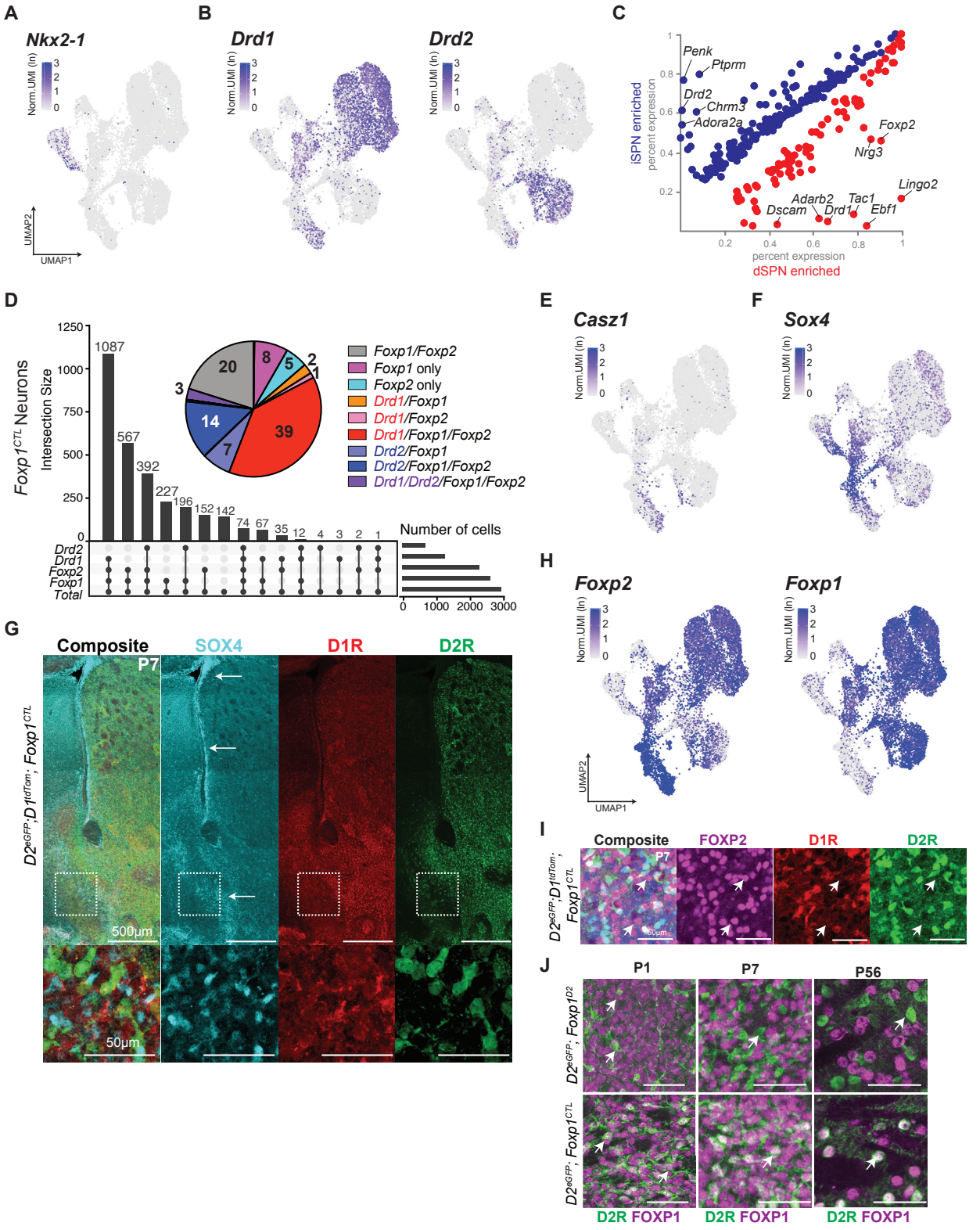

A-**B**) Expression plots with the normalized UMI counts for interneuron marker *Nkx2-1* (**A**) or SPN markers *Drd1* (dSPNs) or *Drd2* (iSPNs) (**B**). **C**) Scatter plots showing the percent expression of enriched transcripts between the largest iSPN (Cluster-2) and dSPN (Cluster-0) clusters. **D**) Upset plot showing the number of cells that overlap in expression of *Drd1*, *Drd2*, *Foxp1*, or *Foxp2* transcripts within neurons of control samples. Pie chart inlet shows the percent composition of this overlap (percentages <1% not visualized). **E**-**F**) Expression plots with the normalized UMI counts for eSPN marker *Casz1* (**E**) and imSPN marker *Sox4* (**F**). **G**) Coronal striatal image of control animals crossed to both *Drd1-tdTomato* and *Drd2-eGFP* reporter mice to label dSPNs or iSPNs, respectively, and stained for Sox4 at P7 (500μm scale bar). White arrows indicate the location of Sox4+ neurons, with inlet showing 63X confocal image (50μm scale bar). **H**) Expression plots with the normalized UMI counts for *Foxp2* and *Foxp1*. **I**) The same mice from (**G**) stained for Foxp2. White arrows indicate example cells where Foxp2 does not co-localized with either dSPNs or iSPNs (50μm scale bar). **J**) Foxp1 is not expressed within remaining iSPNs within *Foxp1*^{D2} mice crossed to Drd2-eGFP reporter mice at P1, P7, or P56 (adult) timepoints (50μm scale bar).

SUPPLEMENTAL FIGURE 3.3. Confirmation of cell-type-specific targets regulated by Foxp1 and overlap with ASD-associated genes.

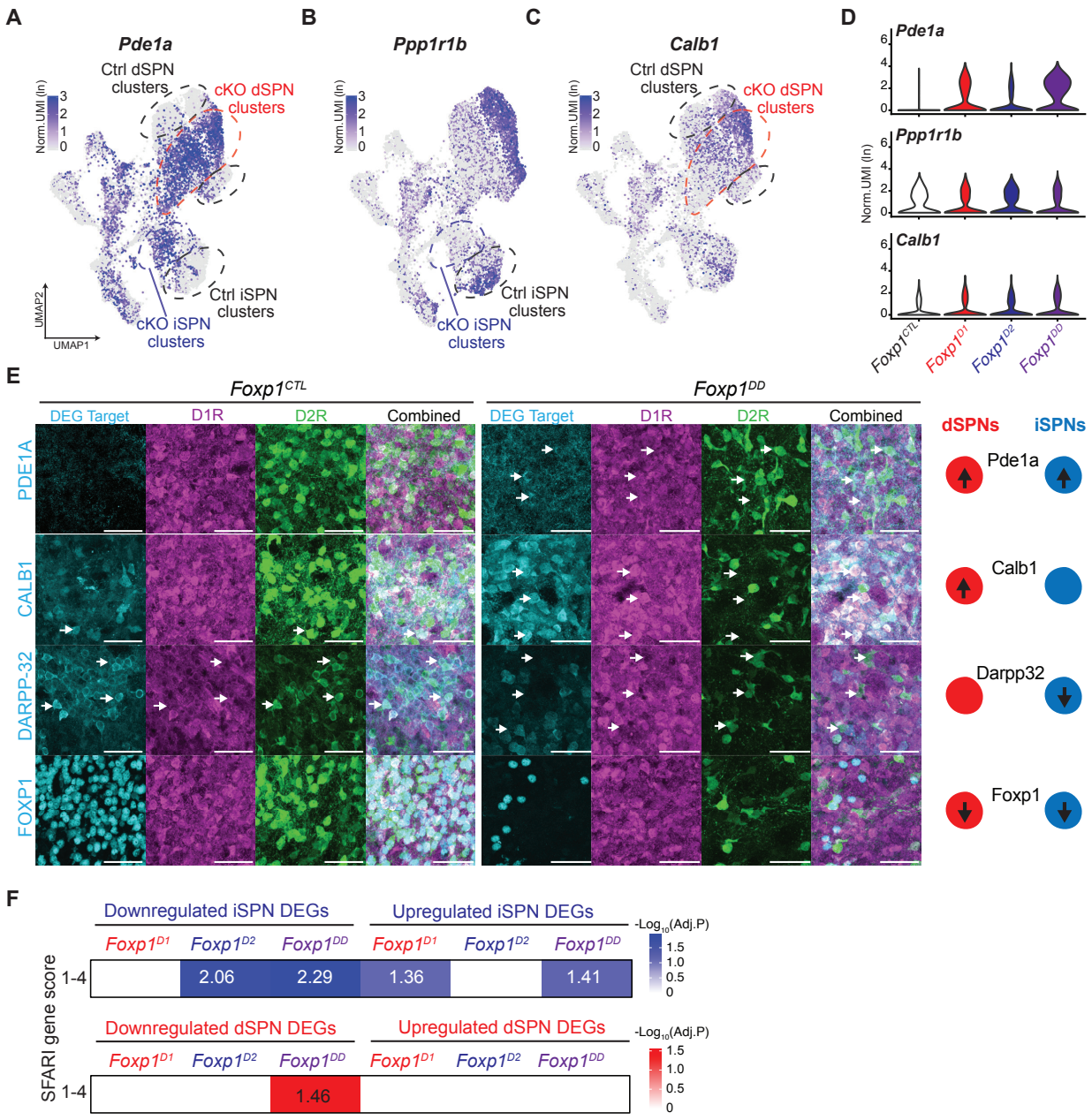

A-**C**) Expression plots of significant DEGs regulated by Foxp1 in both iSPNs and dSPNs (*Pde1a*), iSPNs (*Ppp1r1b*), or dSPNs (*Calb1*). **D**) Violin plots showing the average normalized UMI (ln) of significant DEGs across genotype within all neuronal clusters of *Pde1a Ppp1r1b*, and *Calb1*. **E**) 63X confocal images of coronal, striatal sections stained for Pde1a, Calb1, and Darpp32 in *Foxp1*^{CTL} and *Foxp1*^{DD} mice crossed to reporter mice

labelling dSPNs with tdTomato and iSPNs with eGFP (50μm scale bars). White arrows indicate specific cells where Foxp1 is either 1) upregulating a target (Pde1a) in both dSPNs and iSPNs, 2) upregulating a target (Calb1) in dSPNs only, or 3) downregulating a target (Darpp32) in iSPNs only. **F**) Enrichment of ASD-risk genes SFARI score 1-4 with upregulated or downregulated iSPN-DEGs (blue) or dSPN-DEGs (red) across *Foxp1 cKO* samples using a hypergeometric overlap test (8,000 genes used as background).

SUPPLEMENTAL FIGURE 3.4. Supplemental behavioral testing of *Foxp1 cKO* mice.

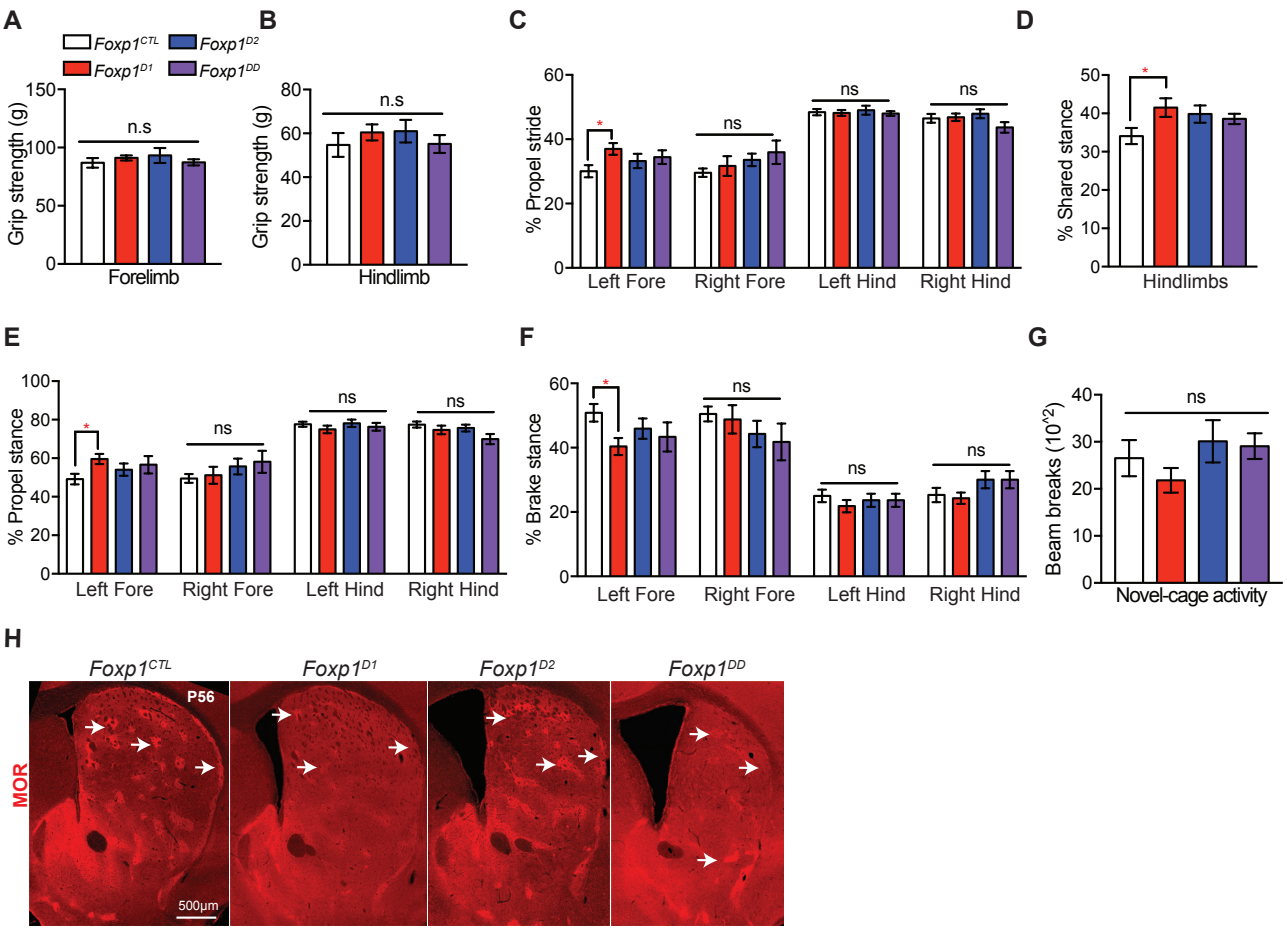

A-**B**) No change in forelimb (**A**) or hindlimb (**B**) grip strength was detected across *Foxp1 cKO* mice. Data are represented as mean ± SEM. n=12 *Foxp1*^{DD}; n=17 *Foxp1*^{D1}; n=16 *Foxp1*^{D2}; n=11 *Foxp1*^{CTL}. Forelimb: p=0.8520 (*Foxp1*^{D1}), p=0.6477 (*Foxp1*^{D2}), p=0.999 (*Foxp1*^{DD}); Hindlimb: p=0.7225 (*Foxp1*^{D1}), p=0.6786 (*Foxp1*^{D2}), p=0.999 (*Foxp1*^{DD}), one-way ANOVA with Dunnett's multiple comparisons test. **C**-**F**) Digigait analysis examining propel stance (**C**), shared stance (**D**), propel stride (**E**), or brake stance (**F**) across *Foxp1 cKO* mice. Only *Foxp1*^{D1} mice exhibited a significant increase in left forelimb propel stance, propel stride, shared stance, and decrease in left forelimb break stance compared to control animals. Data are represented as mean ± SEM. n=7 *Foxp1*^{DD}; n=9 *Foxp1*^{D1}; n=10 *Foxp1*^{D2}; n=10 *Foxp1*^{CTL}. *p<0.05, two-way ANOVA with Dunnett's multiple comparisons test. **G**) Activity levels within a novel-cage environment were unaltered in

Foxp1 cKO mice. Data are represented as mean ± SEM. n=7 *Foxp1*^{DD}; n=9 *Foxp1*^{D1}; n=10 *Foxp1*^{D2}; n=10 *Foxp1*^{CTL}. p=0.6834 (*Foxp1*^{D1}), p=0.8145 (*Foxp1*^{D2}), p=0.9374 (*Foxp1*^{DD}), one-way ANOVA with Dunnett's multiple comparisons test. **H**) Confocal images of striatal sections stained for Mu-Opiod Receptor (MOR) across adult *Foxp1 cKO* mice. White arrows show example striosomes (500μm scale bar).

SUPPLEMENTAL FIGURE 3.5. Serial two-photon tomography of dSPN and iSPN projection patterns across all striatal *Foxp1 cKO* strains

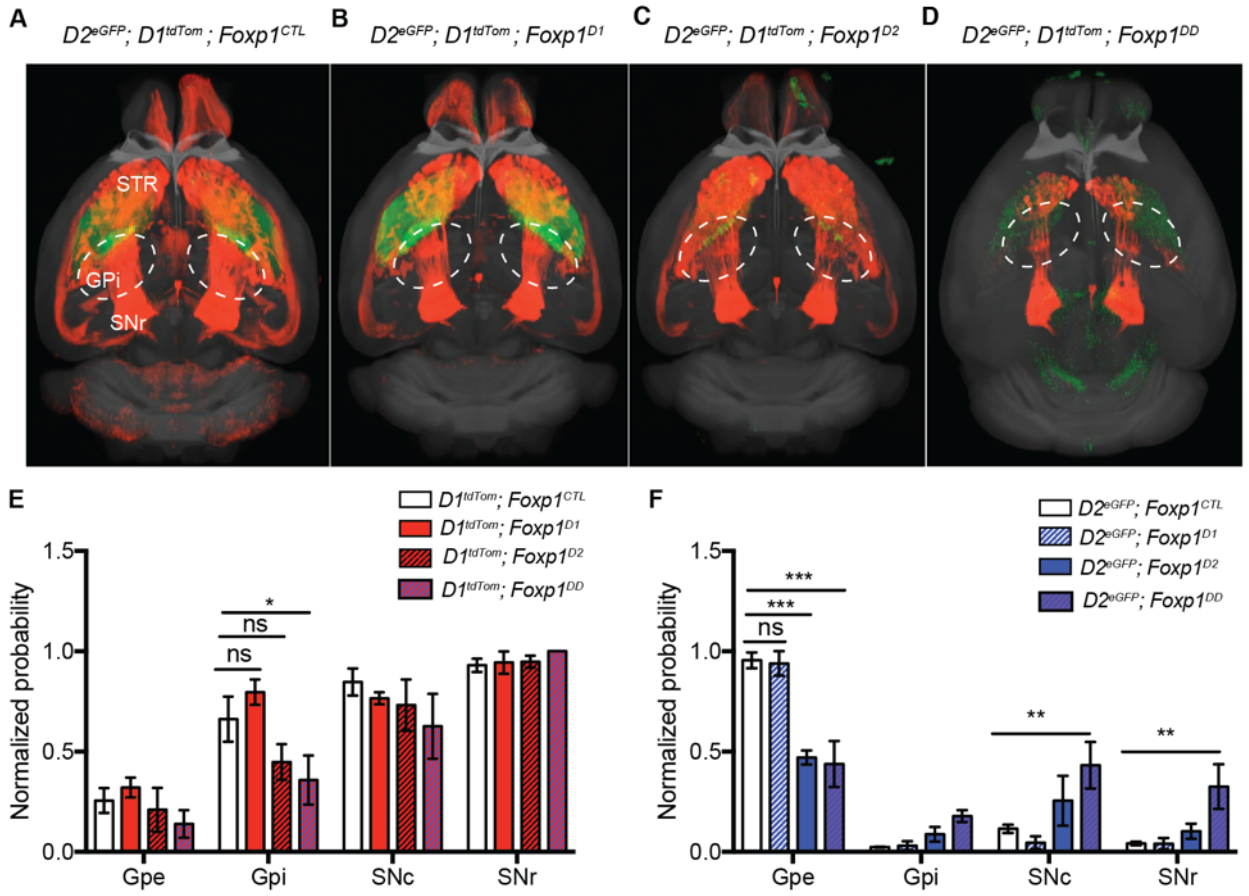

Representative TissueCyte 1000, 3-D images of probability maps from raw fluorescent images from dual reporter labelled *Foxp1 cKO* brains mapped onto the Allen Brain Institute reference brain image (grey) using the Image J Clear Brain plugi. Images show the projections of dSPNs and iSPNs using $D1^{tdTom}$ and $D2^{eGFP}$ reporter mice crossed into Cre lines: $Foxp1^{CTL}$ (**A**), $Foxp1^{D1}$ (**B**), $Foxp1^{D2}$ (**C**), and $Foxp1^{DD}$ (**D**) strains. **E**) Quantification of the normalized probability maps of dSPN (tdTom) projections within $Foxp1^{CTL}$, $Foxp1^{D1}$, $Foxp1^{D2}$, and $Foxp1^{DD}$ mice. Data are represented as mean ± SEM, n=2-5 mice/genotype. *p<0.05, **p<0.01, ***p<0.0001, two-way ANOVA with Dunnett's multiple comparisons test. **F**) Quantification of the normalized probability maps of iSPN (eGFP) projections within $Foxp1^{CTL}$, $Foxp1^{D1}$, and $Foxp1^{D2}$, and $Foxp1^{DD}$ mice. Data are represented as mean ± SEM, n=3-5 mice/genotype. **p<0.01, two-way ANOVA with

Dunnett's multiple comparisons test. GPi= globus pallidus internal, STR= striatum, SNr=substantia nigra pars reticulata.

METHODS

Mice

All experiments were performed according to procedures approved by the UT Southwestern Institutional Animal Care and Use Committee. *Foxp1*$^{flox/flox}$ mice(Zhang et al., 2010) were provided by Dr. Haley Tucker and backcrossed to C57BL/6J for at least 10 generations to obtain congenic animals as previously described (Araujo et al., 2017; Usui et al., 2017a). *Drd1a-Cre* (262Gsat, 030989-UCD) and *Drd2-Cre* (ER44Gsat, 032108-UCD) mice were obtained from MMRC. *Drd2-eGFP* (Gong et al., 2007) and *Drd1-tdTomato*(Ade et al., 2011) mice were provided by Dr. Craig Powell. We bred individual *Cre* or reporter lines to *Foxp1*$^{flox/flox}$ mice to obtain all *Foxp1 cKO* mice in one litter that were heterozygous for *Cre* or reporter transgene. Mice used for single-cell RNA-sequencing and behavior experiments were not crossed with *Drd1-* or *Drd2*-reporter mice. Reporter mice were crossed with *Foxp1 cKO* lines for immunohistochemistry experiments and neuronal projection quantification. Mice were maintained on a 12-hr light on/off schedule.

Protein isolation and immunoblotting

Striatal tissue was dissected, flash frozen, and stored at -80C before protein extraction. Protein was extracted from tissue using 1X RIPA Buffer (750mM NaCl, 250mM Tris-HCl pH7.4, 0.5% SDS, 5% Igepal, 2.5% Sodium deoxycholate, 5mM EDTA, 5mM NaVO4) with fresh protease inhibitor cocktail (10ul/ml), 10ul/ml of 100mM PMSF, and 25ul/ml of 200mM sodium orthovanadate. Tissue was homogenized in RIPA buffer using the TissueLyser LT (Qiagen) with a sterile, stainless-steel bead for 1min at 50 Hz. Samples

were agitated for 1hr at 4C, spun down at 12,000rpm for 15 min, and supernatant was transfer to a fresh tube. Protein was quantified using a standard Bradford assay (Bio-Rad) and 20ug of protein per sample were run on 10% SDS-Page gels. PVDF membranes (Bio-Rad, 162-0177) were incubated in blocking solution (1% Skim milk in TBS with 0.1% Tween-20) for 30 min at room temperature (RT) and probed with primary antibodies overnight at 4C. Membranes were washed with TBS-T (TBS with 0.1% Tween-20) and incubated with appropriate, species-specific fluorescent secondary antibodies in blocking solution for 1hr at RT, and washed in TBS-T. Images were collected using the Odyssey infrared imaging system (LI-COR Biosciences).

RNA isolation and quantitative real-time PCR

RNA from fresh or flash frozen tissue was harvested using miRNAeasy kit guidelines. RNA was converted to cDNA using recommended guidelines from SSIII Superscript Kit (Invitrogen) and qRT-PCR was performed using the CFX384 Real-Time System (Bio-Rad).

Immunohistochemistry

For P7 or P9 mice, rapid decapitation was performed. Brains were extracted and dropped into ice-cold PBS for 1min before transfer into 4% PFA overnight. Brains were then transferred to 30% sucrose for 48 hours. 35um coronal slices were made using a SM2000 R sliding microtome (Leica) and free-floating sections were stored in PBS with 0.01% sodium azide. Slices were washed with TBS and incubated for 30min in 3% hydrogen peroxide in PBS, washed, then incubated in 30min in 3M glycine in 0.4% Triton-X, TBS.

Slices were incubated in primary antibodies overnight at 4C, washed, and incubated in secondary antibodies for 1hr at room temperature. Slices were washed then mounted onto slides and allowed to dry overnight. Sections were incubated in DAPI solution (600nM in PBS) on the slide for 5 minutes and washed 3X with PBS. Sections were allowed to dry before mounting coverslips using Prolong Diamond Antifade Mountant.

Imaging and Analysis

Images were collected using a Zeiss Confocal laser scanning microscope (LSM880) and all image quantification was performed using Fiji image processing package. For iSPN quantification, 20X z-stack images of dorsolateral, dorsomedial, and ventral striatum were taken within one hemisphere of four separate striatal sections from anterior to posterior per animal (3 images/section, 4 sections/animal, at least 3 animals/genotype). All images were taken within approximately similar sections across samples. Maximum projection images were quantified within a 1024x1024 pixel field of view across all images and averaged per section. For striosome quantification, 10X z-stack images were taken from one hemisphere of four separate striatal section from anterior to posterior per animal (4 sections/animals, at least 3 animals/genotype). Individual MOR+ patches were numbered, and area measurements summed for the total striosomal area measurement per section. Total striatal area was also measured per section to calculate the percentage of striosome area to total area per section. Differences between genotypes were assessed using a one-way ANOVA with multiple comparisons.

Antibodies

The following primary antibodies were used for either immunoblots (IB) or immunohistochemistry (IHC) experiments: chicken anti-GFP (1:1,000, Aves Labs, GFP-1010), rabbit polyclonal anti-MOR (1:350, Millipore, AB5511), rabbit polyclonal anti-PDE1A (1:500, Proteintech, 12442-2-AP), rabbit polyclonal anti-DARPP32 (1:1,000, Millipore, AB1778), goat anti-tdTomato (1:500, LifeSpan Biosciences, LS-C340696), mouse monoclonal anti-FOXP1 (1:500, Abcam, ab32010), rabbit polyclonal anti-FOXP1 (IHC:1:1,000, IB: 1:5,000 (Spiteri et al., 2007), rabbit polyclonal anti-Calbindin (1:500, Millipore AB1778), goat anti-FOXP2 (N-terminal) (1:500, Santa Cruz 21069), rabbit polyclonal anti-β-Tubulin (IB: 1:10,000, Abcam, ab243041), and mouse monoclonal anti-SOX4 (1:500, Abcam, ab243041). All IHC following secondary antibodies were used at a 1:1,000 dilutions Alexa Fluor 488 Donkey Anti-Chicken IgG (Thermo Fisher, 703-545-155), Alexa Fluor 555 Donkey Anti-Goat IgG (Thermo Fisher, A-21432), Alexa Fluor 647 Donkey Anti-Rabbit IgG (Thermo Fisher, 711-605-152), Alexa Fluor 647 Donkey Anti-Mouse IgG (Thermo Fisher, A-31571). For IB, the following secondary antibodies were used at a 1:10,000 dilution: IRDye 800CW Donkey anti-Rabbit IgG (Licor, 925-32213) and IRDye 680RD Donkey anti-Rabbit IgG (Licor, 925-68071).

Tissue processing for single-cell RNA-sequencing (scRNA-seq)

Mice (P9) were sacrificed by rapid decapitation and brains were quickly removed and placed in ACSF (126mM NaCl, 20mM $NaHCO_3$, 20mM D-Glucose, 3mM KCl, 1.25mM NaH_2PO_4, 2mM of $CaCl_2$ and $MgCL_2$ freshly added) bubbled with 95%O_2 and 5%CO_2. Coronal slices at 500um were made using a VF-200 Compresstome in ACSF and

transferred to a recovery chamber at room temperature in ACSF with 50uM AP5, 20uM DNQX, and 100nM TTX (ACSF+cb)(Tasic et al., 2016). Striatal punches were taken from these slices and incubated in 1mg/ml of pronase in ACSF+cb for 5min. Punches were washed with ACSF+ 0.04% BSA twice and gently dissociated into single-cell suspension using polished Pasteur pipettes with 600um, 300um, and 150um opening diameters, sequentially. Cells were centrifuged and washed twice, filtered through Flowmi Tip 40uM strainers, and resuspended with ACSF+ 0.04% BSA. Cell viability was quantified using the trypan blue exclusion method and cell concentration was adjusted for targeted sequencing of 10,000 cells/sample using the 10X Genomics Single Cell 3' Reagent Kits v2 protocol to prepare libraries(Zheng et al., 2017). A total of 16 mice (4 mice/genotype, 2 males and 2 females per genotype) were processed for single-cell sequencing. Libraries were sequenced using the McDermott Sequencing Core at UT Southwestern.

Pre-processing of Sequencing Data

Raw sequencing data was acquired from the McDermott Sequencing Core at UT Southwestern in the form of binary base call (BCL) files. BCL files were then de-multiplexed with the 10X Genomics i7 index (used during library preparation) using Illumina's bcl2fastq v2.17.1.14(Andrews, 2010) and *mkfastq* command from 10X Genomics CellRanger v2.1.1 tools(Zheng et al., 2017). Extracted paired-end fastq files (26 bp long R1 - cell barcode and UMI sequence information, 124 bp long R2 - transcript sequence information) were checked for read quality using FASTQC v0.11.5(Andrews, 2010). R1 reads were then used to estimate and identify real cells using *whitelist* command from UMI-tools v0.5.4(Smith et al., 2017a) program. A whitelist of cell-barcodes

(putative real cells) and R2 fastq files were later used to extract reads corresponding to real cells only (excluding sequence information representing empty beads, doublets, low quality/degrading cells, etc.) using *extract* command from UMI-tools v0.5.4(Smith et al., 2017a). This step also appends the cell-barcode and UMI sequence information from R1 to read names in R2 fastq file. Extracted R2 reads were then aligned to reference mouse genome (MM10/GRCm38p6) from UCSC genome browser(Kent et al., 2002) and reference mouse annotation (Gencode vM17) using STAR aligner v2.5.2b(Dobin et al., 2013) allowing up to 5 mismatches. Uniquely mapped reads were then assigned to exons using *featureCounts* program from Subread package (v1.6.2)(Liao et al., 2014). Assigned reads sorted and indexed using Samtools v1.6(Li et al., 2009) were then used to generate raw expression UMI count tables using *count* command from UMI-tools v0.5.4(Smith et al., 2017a; 2017b) program. This raw expression matrix contains cells as rows and genes as columns and can be further used for downstream analysis such as normalization, clustering, differentially expressed genes, etc.

Clustering Analysis

Raw single-cell RNA-seq UMI count data was used for clustering analysis using Seurat R analysis pipeline(Butler et al., 2018). First, cells with more than 50,000 molecules (nUMI per cell) and cells with more than 10% mitochondrial content were filtered out to discard potential doublets and degrading cells. Also, genes from mitochondrial chromosome and chromosomes X and Y were removed as samples were from mixed genders. This dataset is referred to as *primary filtered dataset*. Post filtering, the raw UMI counts from primary filtered dataset were used for log-normalization and scaled using a factor of 10,000 and

regressed to covariates such as number of UMI per cells and percent mitochondrial content per cell as described in Seurat analysis pipeline(Butler et al., 2018). To further identify the top variable genes, the data were used to calculate principal components (PCs). Using Jackstraw analysis, statistically significant PCs were used to identify clusters within the data using original Louvain algorithm as described in Seurat analysis pipeline followed by visualizing the clusters with uniform manifold approximation and projection (UMAP) in two dimensions(Becht et al., 2018). Genes enriched in each cluster compared to the remainder of the cells (adj. p-value <= 0.05 and log fold change >= 0.3) were identified as described in Seurat analysis pipeline. Genes corresponding to each cluster were used to identify the cell-type by correlating to genes expressed in previously published adult mouse striatal single cell data(Saunders et al., 2018). Cell-types were assigned to clusters based on (i) statistically significant enrichment of gene sets using the hypergeometric test (with a background of 7,500 genes, the number of expressed genes within our dataset) and (ii) expression weighted cell-type enrichment (EWCE) analysis (Skene and Grant, 2016) (https://github.com/NathanSkene/EWCE). Clusters that overlapped significantly with multiple cell-types were called for the most significant overlap (smallest Adj. P-value) and analyzed for expression of top marker genes of known cell-types. Cells from clusters that fell into neuronal categories (referred to as *secondary neuronal dataset*) were used to re-cluster the cells to define specific spiny projection neuronal sub-types using a similar approach as described above. Note that two small clusters (Clusters-21, 22) that corresponded to excitatory cortical neurons and a cluster with less than 30 cells total (Cluster-24) were excluded from the secondary neuronal dataset UMAP plots to focus on striatal cell-types.

Differential Gene Expression (DEG) Analyses

Pairwise DEG analysis SPNs

For the spiny projection neuronal sub-type clusters identified using secondary neuronal dataset, pairwise differential gene expression analysis tests were performed within each cluster-pair using a Poisson likelihood ratio test from the Seurat R analysis pipeline(Butler et al., 2018) to identify genes enriched (adj. p-value <= 0.05, log_2FC>|0.25|) in SPN sub-types.

Pseudobulk DEG analysis

Within the secondary neuronal dataset, neurons identified as either dSPNs (*Drd1*+) or iSPNs (*Drd2*+) were combined into pools of cells segregated by genotypes. Differential expression within pools of dSPN or iSPNs of Foxp1 cKO samples were then compared to control samples using Poisson likelihood ratio test from the Seurat R analysis pipeline accounting for averaged expression differences in either dSPNs or iSPNs across genotypes irrespective of the identified clusters. Significant expression changes (adj. p-value <=0.05, log_2FC>|0.3|) reflected the differences in expression of genes in one specific cell population (dSPNs or iSPNs) across genotypes instead of detected clusters.

Down-sampled Dataset Analysis

Cells from the primary filtered dataset were used to randomly select the cells from each genotype matching the number of cells present in each genotype with the lowest representation of the cells ($Foxp1^{CTL}$ = 14466 cells, $Foxp1^{D1}$= 16,961 cells, $Foxp1^{D2}$ = 9,898 cells, $Foxp1^{DD}$= 21,453 cells, using random sampling, the same number of cells

from *Foxp1*^{CTL}, *Foxp1*^{D1}and *Foxp1*^{DD} were matched to *Foxp1*^{D2}). This is referred to as the *primary down-sampled dataset*. This dataset was further used to separate the cells into clusters and identify cell-types as described in the clustering analysis section above. Clusters corresponding to SPNs from the primary down-sampled dataset (referred to as the *secondary down-sampled neuronal dataset*) were re-clustered to identify SPN subtypes in a similar manner as described in the clustering section above.

Availability of Data and Code

The sequencing data reported in this paper can be access at NCBI GEO with accession number GSE125290. Code that was used to perform data pre-processing, clustering and differential gene expression analysis is available at GitHub repository (https://github.com/konopkalab/early-postnatal-striatal-single-cell-rna-seq).

TissueCyte Imaging and Quantification

STPT and image acquisition

Serial two-photon tomography (STPT)(Ragan et al., 2012), in which automated block face imaging of the brain is repetitively alternated with vibratome sectioning, was conducted on the TissueCyte 1000 platform using the manufacturer's custom software for operation (Orchestrator). Mouse brains were perfusion-fixed in 4% paraformaldehyde and embedded in low-melting point oxidized agarose (4.5% w/v; Sigma #A0169). Vibratome sections were prepared at 75 μm thickness using a frequency of 70 Hz and a speed of 0.5 mm/sec. 185-190 total sections were collected of each brain. A 9 by 13 mosaic of tile images was collected at each level using lateral resolution of 0.875 μm/pixel. Optical

sectioning was used to collect three z-planes within each 75 μm physical section to obtain 25 μm axial resolution. The two-photon excitation laser (Spectra Physics MaiTai DeepSee) was tuned to 920 nm to excite both eGFP and tdTomato. The emission fluorescence from the red, green and blue channels was independently collected using photomultiplier tube detectors. The tile images were saved to network attached servers and automatically processed to perform flat field correction and then stitched into single-channel 2D coronal sections in 16-bit .tif format using the manufacturer's custom software (AutoStitcher).

Sample preparation and details

Mice (8 weeks) were perfused with PBS followed by 4% PFA. Brains were removed and post-fixed overnight in 4% PFA at 4C. Samples were transferred to PBS + 0.1% sodium azide and stored at 4C until imaging. A total of 24 whole mouse brain images were collected in three cohorts for machine learning analysis according to their patterns of fluorophore expression. The first cohort consisted of 8 samples expressing tdTomato (detected predominantly in the red channel), the second cohort had 8 samples that expressed eGFP (detected predominantly in the green channel) and the third cohort consisted of 6 dual-labeled (eGFP + tdTomato) samples.

TissueCyte image processing and registration

STPT image processing was performed via BioHPC, an advanced computing cluster at UT Southwestern. All channels of the coronal sections were downsampled to 10 μm lateral resolution, intensity adjusted to fill the 16-bit range, and combined to form 3D image stacks using custom MATLAB software. The image stacks were then processed through a 3D median filter to remove high-contrast noise. The 3D image stacks were

registered to Allen Institute for Brain Science Common Coordinate Framework (version 3, CCFv3) at 10 μm x 10 μm x 100 μm resolution using NiftyReg software(Modat et al., 2014). Briefly, registration involved three steps: (i) Affine transformation (reg-aladin) for global registration (ii) Cubic B-spline transformation (reg-f3d) to achieve local transformation and (iii) Resampling the transformed brains to Atlas coordinates (reg-resample). Registration transformations were established based on the red channel, then applied equally to all other data channels, including the probability maps (described below).

Interactive Image training for classifying signals of interest

The three raw channels of the 2D stitched coronal sections were downsampled to 1.5 μm lateral resolution. A maximum intensity projection of the three optical sections was produced for each physical section across all 3 color channels, creating an RGB image stack with the same number of 2D frames as physical sections (e.g. 185 or 190). Ilastik (Interactive learning and segmentation toolkit)(Sommer et al., 2011) software was deployed on BioHPC and used to train a pixel-wise random forest classifier to identify features of interest (e.g. fluorescent neuronal cell bodies and axonal projections). Three or four representative sections were chosen from the 185-190 image stack for model training. A supervised random forest model was trained by users to classify fluorescent features of interest (e.g. eGFP and/or tdTomato), and to distinguish them from other image features (e.g., bright microbubbles, empty space, autofluorescence) using the interactive features in Ilastik. An independent random forest model was trained for each of the image batches described above. The random forest classifiers were used to detect features of interest in all image sections, creating a “probability map” for each voxel in

each 3D whole brain image. In these probability map images, the value of each voxel in each virtual channel (corresponding to each image feature, e.g. eGFP) represents the probability that the voxel includes information for the desired feature. These exported probability maps were registered to the CCFv3.0 using the transformation parameters using NiftyReg (reg-aladin).

Quantification and visualization

The features of interest in the registered probability maps were quantified by automatically segmenting brain regions of interest based upon CCFv3.0 volumetric annotations. Custom MATLAB software aggregated brain regions of interest (e.i., nucleus accumbens, caudate putamen, globus pallidus external and internal, substantia nigra pars compacta and pars reticulata), calculated the cumulative probabilities of all voxels in each region, and normalized these values by the volume of each structure. This exported data matrix thus included normalized probability intensity values for each machine learning feature, each brain region of interest, and each brain. For visualization, the combined probability map stacks were rendered in 3D using the ClearVolume plugin for Fiji/ImageJ (Royer et al., 2015).

Behavior tests

All behavior was performed on both male and female mice using littermate controls at the age described below behavior methods.

Open Field

Mice age 8-12 weeks were allowed to acclimate to the testing room for 1hr before being placed in a 55cm x55cm x 36cm matrix (Phenome Technologies) and recorded for 30min.

Total distance and velocity measurements were analyzed using Actimetrics LimeLight software.

Novel-cage activity

As previously described(Araujo et al., 2017), mice were moved into individual cages (18x28cm) with minimal bedding. Cage was placed into a dark Plexiglas box and the movements were measured using a Photobeam Activity System-Home Cage software for two hours. The number of beam breaks was recorded every 5 min and averaged over two hours for statistical analyses.

Rotarod

Following previously published methods(Araujo et al., 2015), mice (8-12 weeks) were acclimated to the testing room for 30min before placed in one lane of a 5-lane accelerating rotarod (Series 8 ITCC Life Science rotarod). The textured drum within the individual lanes was programed to accelerate from acceleration from 4-40 rpm within a maximum time frame of 300 sec. Each mouse was positioned facing away from the experimenter. Latency to fall was recorded once the trial was initiated. Manual activation of the sensors occurred when an animal made a full rotation holding onto the drum. Animals received four trials per day (20min intervals) with lanes cleaned between animals with NPD over the course of three consecutive days.

Grip strength test

Grip strength was tested following previously published methods(Araujo et al., 2015). Briefly, following rotorad experiments, the forelimb and hindlimb grip strength mice were measured using Chatillon Force Measurement equipment. The forelimbs, followed by the hindlimbs, for each animal were tested first by placing forelimb paws on a mesh wire

meter and pulling them away from the wire at constant force. Five consecutive measurements were recorded for both hindlimbs and forelimbs and averaged for a final grip strength measurement.

Nestlet behavior

Nesting behavior was analyzed using a previously published approach(Araujo et al., 2017; Deacon, 2006). Mice (8-12 weeks) were isolated into clean cages overnight with 3 g of intact nestlet. After 16-18 hrs, the amount of unused nestlet was measured and images of the nests were taken to assess the quality and given a score.

Neonatal ultrasonic vocalization measurements

USVs were recorded as described previously(Araujo et al., 2015; 2017). Briefly, pups were isolated from dams at P4, P7, and P10 and placed into a soundproof container. USVs were recorded for 3min with an UltraSoundGate condenser microphone using Avisoft Bioacoustic software. Analysis of sound spectrograms was automatically performed using MATLAB codes(Rieger and Dougherty, 2016).

Digigait

Mice (8-12 weeks) were placed onto the transparent treadmill using the DigiGait Imaging System (Mouse Specifics, Inc) at 10 cm/sec. The speed was quickly increased to 20 cm/sec with a high-speed video camera mounted under the clear treadmill to capture images of all four paws at the 20 cm/sec speed. A section of video with at least 6-10 steps is analyzed and the paw placement is automatically detected and quantified by the software system. Right and left forelimb and hindlimb paw measurements were analyzed separately.

Fear Conditioning

Fear conditioning was measured using boxes with metal grid floors connected to a scrambled shock generator (Med Associates Inc., St. Albans). Mice were trained by placing them individually in the chamber for 2min before they received 3 tone-shock pairings (30sec white noise, 80dB tone, co-terminated with a 2 sec, 0.5mA footshock, 1min intertrial interval). Twenty-four hours later, contextual memory was measured by placing the mice into the same chamber and measuring freezing behavior using the Med Associates software. Forty-eight hours post training, memory of the white noise cue was measured by placing mice in new environment, with altered floors, walls, different lighting, and a vanilla smell. Freezing was measured for 3 min and then noise cue was turned on for an additional 3 min and freezing was measured.

Statistics and reproducibility

Statistical methods and code used for scRNA-seq and analysis are provided in the above methods sections. All statistical test used (and p-values obtained) for SPN projection analysis, behavior, and immunohistochemistry are described in figure legends. No statistical methods were used to estimate sample size, but behavior cohorts were based on previously published papers (Araujo et al., 2015; 2017; Usui et al., 2017a). Sample size for each experiment is indicated in figure legends.

Key Resource Table

REAGENT or RESOURCE	SOURCE	IDENTIFIER
Antibodies		
Chicken anti-GFP	Aves Labs	Cat#: GFP-1010 Lot#: GFP879484
Rabbit polyclonal anti-MOR	Millipore	Cat#: AB5511 Lot#: 3131193
Rabbit polyclonal anti-PDE1A	Proteintech	Cat#:12442-2-AP
Rabbit polyclonal anti-DARPP32	Millipore	Cat#: AB10518
Mouse monoclonal anti-FOXP1 [JC12]	Abcam	Cat#: ab32010
Rabbit polyclonal anti-FOXP1	(Spiteri et al., 2007)	
Rabbit polyclonal anti-Calbindin	Millipore	Cat#: AB1778
Goat anti-FOXP2 (N-terminal)	Santa Cruz	Cat#: 21069
Rabbit polyclonal anti-B-Tubulin	Abcam	Cat#: AB6046
Mouse monoclonal anti-SOX4	Abcam	Cat#: 243041
Alexa Fluor 488 Donkey Anti-Chicken IgG	Thermo Fisher	Cat#: 703-545-155
Alexa Fluor 555 Donkey Anti-Goat IgG	Thermo Fisher	Cat#: A-21432
Alexa Fluor 647 Donkey Anti-Rabbit IgG	Thermo Fisher	Cat#: 711-605-152
Alexa Fluor 647 Donkey Anti-Mouse IgG	Thermo Fisher	Cat#: A-31571
IRDye 800CW Donkey anti-Rabbit IgG	Licor	Cat#: 925-32213
IRDye 680RD Donkey anti-Rabbit IgG	Licor	Cat#: 925-68071
Chemicals, Peptides, and Recombinant Proteins		
TTX	Tocris	Cat#: 1078
DNQX	Sigma-Aldrich	Cat#: D0540
APV	Tocris	Cat#: 3693
5X RIPA Buffer	In house	
ProLong Diamond Antifade Mountant	Thermo Fisher	Cat#: P36970
Critical Commercial Assays		
Chromium Single Cell 3' Reagent Kits v2	10X Genomics, Inc	Cat#: 120237
miRNeasy mini kit	Qiagen	Cat#:217004
SSIII First-strand super mix	Life Technologies	Cat#: 18080400
iTaq Universal SYBR Green Supermix	Bio-Rad	Cat#: 172-5124
Deposited Data		
Raw and analyzed data	This paper	GEO: GSE125290 Token: **stavqcosvnylxqj**
Adult striatal single-cell RNA-seq dataset	Saunders et al. 2018	GEO: GSE116470
Software and Algorithms		
Bcl2fastq v2.17.1.14	Illumina Inc	https://support.illumina.com/sequencing/sequencing_software/bcl2fastq-conversion-software.html
CellRanger v2.1.1	10X Genomics	https://www.10xgenomics.com/solutions/single-cell/
FASTQC v0.11.5	Babraham Bioinformatics	https://www.bioinformatics.babraham.ac.uk/projects/fastqc/
UMI Tools v0.5.4	(Smith et al., 2017)	https://github.com/CGATOxford/UMI-tools
STAR v2.5.2b	(Dobin et al., 2013)	https://github.com/alexdobin/STAR

Subread v1.6.2 (featureCounts)	WEHI	http://bioinf.wehi.edu.au/featureCounts/
Samtools v1.6	(Li et al., 2009)	https://github.com/samtools/samtools
Seurat v2.3.4	(Butler et al., 2018)	https://satijalab.org/seurat/, https://github.com/satijalab/seurat
EWCE	(Skene and Grant, 2015)	https://github.com/NathanSkene/EWCE
Toppgene	(Chen et al., 2009)	https://toppgene.cchmc.org
Ilastik version 1.2.2	(Sommer et al., 2011)	http://ilastik.org/
NiftyReg	(Modat et al., 2014)	https://github.com/KCL-BMEIS/niftyreg/wiki
Experimental Models: Organisms/Strains		
Mouse: B6.FVB(Cg)-Tg(Drd1-cre)EY262Gsat	MMRRC	030989-UCD
Mouse: B6.FVB(Cg)-Tg(Drd2-cre)ER44Gsat	MMRRC	032108-UCD
Mouse: Drd1-tdTomato BAC Transgenic	(Ade et al. 2011)	
Mouse: Drd2-eGFP BAC Transgenic	(Gong et al. 2007)	
Oligonucleotides		
Mus-Foxp1 F: CTACCGCTTCCATGGGAAAT Mus-Foxp1 R: ACTGTGGTTGGCTGTTGTCA	This paper	
Mus-Actin F: CCATCACAATGCCTGTGGTA Mus-Actin R: CTAAGGCCAACCGTGAAAAG	This paper	
Drd1-Cre genotyping primers: F: GCTATGGAGATGCTCCTGATGGAA R: CGGCAAACGGACAGAAGCATT		
Drd2-Cre genotyping primers: F: GTGCGTCAGCATTTGGAGCAA R: CGGCAAACGGACAGAAGCATT		
Drd1-tdTomato genotyping primers: F: CTTCTGAGGCGGAAAGAACC R: TTTCTGATTGAGAGCATTCG		
Drd2-eGFP genotyping primers: F: CCCGAAGCTTCTCGAGGCGCGCCCTGTGC GTCA GCATTTGGAGCAAC R: TCAGGGTCAGCTTGCCGTAGG		
Foxp1-flox genotyping primers: F: CCAGGGATCAGAGATTACTGTAGC R: CACCCTCTCCAAGTCTGCCTCAG		

TABLE 3.1: Cell-type annotation of clusters identified in striatal scRNA-seq data

Cluster	Control	D1; Foxp1 cKO	D2; Foxp1 cKO	DD; Foxp1 cKO	Cell-type Annotation
3	903	1141	581	1203	Astrocytes
10	627	539	356	775	Astrocytes
12	580	400	221	625	Astrocytes
37	37	78	43	156	Ctx excitatory neurons
11	445	597	301	558	Endothelial
21	246	258	176	345	Endothelial
42	2	6	13	50	Endothelial
43	6	12	18	30	Endothelial
30	166	145	99	147	Endothelial
26	195	180	155	174	Ependymal
36	48	82	79	141	Interneurons
41	9	19	15	35	Interneurons
18	196	247	186	476	Interneurons
9	286	842	451	723	Microglia
23	382	214	139	198	Microglia
39	23	42	34	82	Microglia
35	60	124	46	125	Mural
32	29	13	31	460	Neurogenic progenitor
0	1358	1537	670	2385	Neurogenic progenitor
19	408	181	103	396	Neurogenic progenitor
5	840	779	495	844	Neurogenic progenitor
7	642	709	455	618	Neurogenic progenitor
8	764	540	385	670	Neurogenic progenitor
33	129	153	58	126	Neurogenic progenitor
4	800	1232	437	974	OPCs
15	375	436	260	429	OPCs
16	447	402	218	427	OPCs
31	142	159	87	152	OPCs
2	1019	1209	377	1495	Progenitor
34	168	67	26	122	Progenitor
40	87	18	10	29	Progenitor
25	319	86	47	397	SPN
1	789	1196	1099	1527	SPN
6	284	353	666	1159	SPN
13	575	978	34	60	SPN
14	324	309	520	350	SPN
17	108	173	296	779	SPN
20	128	189	148	574	SPN
22	176	197	163	405	SPN
24	68	189	158	510	SPN
27	206	371	8	48	SPN
28	2	157	54	419	SPN
29	18	312	145	139	SPN
38	50	90	35	116	SPN
Total/Genotype	**14466**	**16961**	**9898**	**21453**	**62778**

TABLE 3.2: DEGs from iSPNs or dSPNs pseudobulk analysis in *Foxp1 cKO* mice

Gene	Avg_logFC	pct.1_CTL	pct.2_cKO	P_val_adj	Regulation	Cell-type	Sample
2510009E07Rik	0.335	0.486	0.257	1.1E-30	DOWN	iSPNs	D2cKO
Ablim1	-0.401	0.157	0.332	8.0E-19	UP	iSPNs	DDcKO
Ablim1	-0.301	0.157	0.28	4.3E-03	UP	iSPNs	D2cKO
AC103635.1	-0.386	0.489	0.59	3.5E-04	UP	iSPNs	DDcKO
AC114005.5	0.385	0.958	0.867	0.0E+00	DOWN	dSPN	D1cKO
AC114005.5	0.477	0.958	0.872	0.0E+00	DOWN	dSPNs	DDcKO
AC114005.5	0.386	0.963	0.856	0.0E+00	DOWN	iSPNs	D1cKO
AC166332.1	-0.373	0.238	0.353	2.5E-04	UP	iSPNs	DDcKO
Actb	0.355	0.826	0.733	0.0E+00	DOWN	dSPN	D1cKO
Actb	0.498	0.894	0.746	0.0E+00	DOWN	iSPNs	D1cKO
Actn2	0.401	0.628	0.412	8.9E-192	DOWN	dSPNs	DDcKO
Actn2	0.572	0.564	0.223	4.0E-112	DOWN	iSPNs	DDcKO
Actn2	0.441	0.564	0.237	9.7E-45	DOWN	iSPNs	D2cKO
Acvr1	0.358	0.461	0.287	1.1E-111	DOWN	dSPNs	DDcKO
Acvr1	0.348	0.438	0.23	6.5E-54	DOWN	iSPNs	DDcKO
Acvr1	0.326	0.438	0.249	7.6E-26	DOWN	iSPNs	D2cKO
Acvr1c	0.452	0.352	0.1	3.5E-126	DOWN	dSPN	D1cKO
Acvr1c	0.499	0.352	0.102	2.5E-220	DOWN	dSPNs	DDcKO
Acvr1c	0.565	0.358	0.072	1.9E-98	DOWN	iSPNs	DDcKO
Acvr1c	0.537	0.358	0.091	5.2E-41	DOWN	iSPNs	D2cKO
Adamts6	-0.570	0.182	0.325	4.5E-15	UP	iSPNs	D2cKO
Adarb2	-1.228	0.247	0.478	1.3E-292	UP	iSPNs	DDcKO
Adarb2	-1.388	0.247	0.421	3.8E-164	UP	iSPNs	D2cKO
Adcy1	0.450	0.787	0.532	1.3E-181	DOWN	iSPNs	DDcKO
Adcy1	0.528	0.787	0.489	1.9E-99	DOWN	iSPNs	D2cKO
Adcy2	-0.309	0.063	0.17	7.7E-21	UP	iSPNs	DDcKO
Adcy5	0.648	0.781	0.443	4.7E-198	DOWN	iSPNs	DDcKO
Adcy5	0.621	0.781	0.416	2.2E-87	DOWN	iSPNs	D2cKO
Adgrb3	0.325	0.991	0.965	0.0E+00	DOWN	iSPNs	DDcKO
Adora2a	0.459	0.568	0.198	2.1E-111	DOWN	iSPNs	DDcKO
Adora2a	0.446	0.568	0.222	3.7E-44	DOWN	iSPNs	D2cKO
Adra1a	-0.415	0.073	0.204	1.9E-18	UP	iSPNs	D2cKO
Adrbk2	-0.320	0.066	0.195	2.7E-16	UP	iSPNs	DDcKO
Adrbk2	-0.345	0.066	0.199	1.9E-07	UP	iSPNs	D2cKO
Aff3	0.428	0.802	0.524	9.9E-131	DOWN	iSPNs	DDcKO
Aff3	0.370	0.802	0.526	2.3E-68	DOWN	iSPNs	D2cKO

Gene	Avg_logFC	pct.1_CTL	pct.2_cKO	P_val_adj	Regulation	Cell-type	Sample
Agap2	0.309	0.377	0.185	5.7E-44	DOWN	iSPNs	DDcKO
Agbl4	-0.741	0.286	0.524	2.1E-45	UP	iSPNs	DDcKO
Agbl4	-0.825	0.286	0.564	4.2E-45	UP	iSPNs	D2cKO
Agpat4	-0.482	0.164	0.315	1.4E-02	UP	iSPNs	D2cKO
Akap5	-0.434	0.327	0.5	1.6E-52	UP	dSPNs	DDcKO
Akap5	-0.316	0.327	0.464	2.1E-49	UP	dSPNs	D2cKO
Alcam	0.498	0.949	0.712	0.0E+00	DOWN	iSPNs	DDcKO
Alcam	0.470	0.949	0.73	5.3E-219	DOWN	iSPNs	D2cKO
Alk	-0.489	0.261	0.421	1.3E-14	UP	iSPNs	D2cKO
Ankfn1	-0.354	0.047	0.136	4.4E-07	UP	iSPNs	D2cKO
Ano3	0.319	0.858	0.712	0.0E+00	DOWN	dSPNs	DDcKO
Ano3	0.653	0.827	0.448	1.7E-301	DOWN	iSPNs	DDcKO
Ano3	0.651	0.827	0.426	1.5E-151	DOWN	iSPNs	D2cKO
Ano4	-0.411	0.302	0.423	8.4E-05	UP	iSPNs	D2cKO
Arpc5	-0.303	0.45	0.577	3.6E-18	UP	dSPNs	DDcKO
Arpp21	0.375	0.991	0.931	0.0E+00	DOWN	iSPNs	DDcKO
Arpp21	0.327	0.991	0.957	0.0E+00	DOWN	iSPNs	D2cKO
Asic2	-0.552	0.7	0.71	2.3E-58	UP	iSPNs	DDcKO
Asic2	-0.816	0.7	0.753	3.9E-108	UP	iSPNs	D2cKO
Asic2	-0.346	0.6	0.727	9.2E-73	UP	dSPNs	D2cKO
Aste1	0.363	0.229	0.073	1.9E-99	DOWN	dSPNs	DDcKO
Astn2	0.474	0.804	0.635	0.0E+00	DOWN	dSPNs	DDcKO
Astn2	0.592	0.838	0.596	0.0E+00	DOWN	iSPNs	DDcKO
Astn2	0.487	0.838	0.574	3.3E-152	DOWN	iSPNs	D2cKO
Astn2	0.397	0.804	0.638	1.1E-127	DOWN	dSPNs	D2cKO
Atp2a2	0.347	0.83	0.639	1.1E-127	DOWN	iSPNs	DDcKO
Atp2a2	0.353	0.83	0.617	1.4E-75	DOWN	iSPNs	D2cKO
Atp2b1	0.538	0.974	0.836	0.0E+00	DOWN	iSPNs	DDcKO
Atp2b1	0.341	0.974	0.884	2.1E-227	DOWN	iSPNs	D2cKO
Atp2b4	-0.344	0.231	0.337	1.0E-10	UP	iSPNs	DDcKO
Atp2b4	-0.394	0.231	0.353	5.5E-04	UP	iSPNs	D2cKO
Atp2c1	0.316	0.755	0.538	5.9E-161	DOWN	dSPN	D1cKO
Atp2c1	0.485	0.755	0.539	7.8E-262	DOWN	dSPNs	DDcKO
Atp6v1a	-0.343	0.486	0.622	6.5E-52	UP	dSPNs	DDcKO
Atxn7l3b	-0.377	0.502	0.671	1.1E-50	UP	dSPNs	DDcKO
B3galt1	0.349	0.938	0.737	1.5E-186	DOWN	iSPNs	DDcKO
B3galt1	0.377	0.938	0.708	1.4E-147	DOWN	iSPNs	D2cKO
Baiap2	0.421	0.637	0.386	3.2E-68	DOWN	iSPNs	DDcKO

Gene	Avg_logFC	pct.1_CTL	pct.2_cKO	P_val_adj	Regulation	Cell-type	Sample
Baiap2	0.425	0.637	0.375	5.3E-38	DOWN	iSPNs	D2cKO
Basp1	-0.365	0.728	0.756	2.6E-10	UP	iSPNs	DDcKO
Brinp1	0.409	0.917	0.812	0.0E+00	DOWN	dSPNs	DDcKO
Brinp1	0.613	0.897	0.678	0.0E+00	DOWN	iSPNs	DDcKO
Brinp1	0.444	0.897	0.69	8.9E-143	DOWN	iSPNs	D2cKO
C2cd2	0.345	0.608	0.399	2.2E-139	DOWN	dSPN	D1cKO
C2cd2	0.510	0.608	0.361	1.4E-303	DOWN	dSPNs	DDcKO
C2cd2	0.448	0.59	0.337	5.7E-126	DOWN	iSPNs	DDcKO
Cachd1	-0.303	0.134	0.227	5.4E-05	UP	dSPN	D1cKO
Cacna2d2	-0.395	0.392	0.494	4.8E-06	UP	iSPNs	D2cKO
Cacna2d3	0.488	0.965	0.83	0.0E+00	DOWN	iSPNs	DDcKO
Cacna2d3	0.615	0.965	0.741	0.0E+00	DOWN	iSPNs	D2cKO
Cacnb2	0.342	0.875	0.682	1.1E-214	DOWN	iSPNs	DDcKO
Cacnb2	0.385	0.875	0.647	2.1E-116	DOWN	iSPNs	D2cKO
Cadm1	-0.463	0.839	0.888	4.1E-06	UP	dSPN	D1cKO
Cadm1	-0.656	0.768	0.894	1.7E-75	UP	iSPNs	DDcKO
Cadm1	-0.537	0.768	0.861	1.2E-06	UP	iSPNs	D2cKO
Cadm2	0.353	0.999	0.986	0.0E+00	DOWN	dSPNs	DDcKO
Cadm2	0.519	0.996	0.933	0.0E+00	DOWN	iSPNs	DDcKO
Cadm2	0.395	0.996	0.952	0.0E+00	DOWN	iSPNs	D2cKO
Calb1	-0.427	0.364	0.441	3.3E-20	UP	dSPN	D1cKO
Calb1	-0.648	0.364	0.546	5.4E-157	UP	dSPNs	DDcKO
Calm1	-0.504	0.743	0.822	5.4E-180	UP	dSPNs	DDcKO
Calm3	-0.344	0.556	0.688	1.3E-42	UP	dSPNs	DDcKO
Caln1	0.337	0.966	0.871	4.6E-296	DOWN	iSPNs	DDcKO
Caln1	0.336	0.966	0.849	3.4E-168	DOWN	iSPNs	D2cKO
Camk2b	0.346	0.746	0.494	7.3E-47	DOWN	iSPNs	D2cKO
Camk2d	-0.630	0.185	0.414	1.6E-57	UP	iSPNs	DDcKO
Camk2d	-0.700	0.185	0.411	1.0E-28	UP	iSPNs	D2cKO
Camk2n1	0.395	0.52	0.335	3.3E-40	DOWN	iSPNs	D2cKO
Camk2n2	-0.341	0.142	0.285	5.6E-25	UP	iSPNs	DDcKO
Camk4	0.332	0.775	0.532	1.6E-228	DOWN	dSPN	D1cKO
Camk4	0.387	0.775	0.592	3.5E-301	DOWN	dSPNs	DDcKO
Camk4	0.689	0.767	0.422	1.6E-259	DOWN	iSPNs	DDcKO
Camk4	0.706	0.767	0.418	3.2E-123	DOWN	iSPNs	D2cKO
Car10	-0.382	0.038	0.118	1.3E-29	UP	iSPNs	DDcKO
Car10	-0.591	0.038	0.141	1.1E-35	UP	iSPNs	D2cKO
Casz1	-0.386	0.05	0.176	9.8E-20	UP	iSPNs	D2cKO

Gene	Avg_logFC	pct.1_CTL	pct.2_cKO	P_val_adj	Regulation	Cell-type	Sample
Ccnd2	0.348	0.419	0.303	7.0E-202	DOWN	iSPNs	D1cKO
Cd47	0.303	0.867	0.776	2.6E-198	DOWN	dSPNs	DDcKO
Cd47	0.492	0.869	0.622	7.8E-199	DOWN	iSPNs	DDcKO
Cd47	0.365	0.869	0.657	3.9E-72	DOWN	iSPNs	D2cKO
Cdh11	0.350	0.771	0.571	6.1E-113	DOWN	iSPNs	DDcKO
Cdh11	0.325	0.771	0.542	9.8E-54	DOWN	iSPNs	D2cKO
Cdh12	0.583	0.725	0.439	0.0E+00	DOWN	dSPNs	DDcKO
Cdh12	0.465	0.617	0.362	3.5E-137	DOWN	iSPNs	DDcKO
Cdh12	0.342	0.725	0.577	6.0E-112	DOWN	dSPNs	D2cKO
Cdh13	0.353	0.9	0.701	8.2E-286	DOWN	dSPN	D1cKO
Cdh13	0.329	0.9	0.744	1.3E-228	DOWN	dSPNs	DDcKO
Cdh18	0.545	0.722	0.436	0.0E+00	DOWN	dSPN	D1cKO
Cdh18	0.544	0.722	0.524	0.0E+00	DOWN	dSPNs	DDcKO
Cdh18	0.639	0.508	0.266	3.5E-172	DOWN	iSPNs	DDcKO
Cdh18	0.371	0.508	0.237	3.9E-71	DOWN	iSPNs	D2cKO
Cdh2	-0.569	0.391	0.568	1.5E-23	UP	iSPNs	DDcKO
Cdh2	-0.574	0.391	0.547	2.5E-06	UP	iSPNs	D2cKO
Cdh4	-0.307	0.213	0.361	1.7E-31	UP	dSPNs	DDcKO
Cdh4	-0.492	0.195	0.393	1.4E-31	UP	iSPNs	DDcKO
Cdh4	-0.520	0.195	0.302	1.1E-06	UP	iSPNs	D2cKO
Cdh8	0.696	0.948	0.81	0.0E+00	DOWN	dSPNs	DDcKO
Cdh8	0.651	0.947	0.708	0.0E+00	DOWN	iSPNs	DDcKO
Cdh8	0.483	0.947	0.688	1.5E-285	DOWN	iSPNs	D2cKO
Cdh8	0.463	0.948	0.895	0.0E+00	DOWN	dSPNs	D2cKO
Cdh9	0.305	0.494	0.318	2.2E-102	DOWN	dSPN	D1cKO
Cdh9	0.428	0.53	0.273	3.8E-94	DOWN	iSPNs	DDcKO
Celf1	0.362	0.868	0.652	3.3E-88	DOWN	iSPNs	D2cKO
Celf2	0.328	1	0.997	0.0E+00	DOWN	iSPNs	DDcKO
Celf2	0.332	1	1	0.0E+00	DOWN	iSPNs	D2cKO
Celf4	-0.460	0.785	0.887	9.9E-155	UP	dSPNs	DDcKO
Celf4	-0.475	0.846	0.918	2.4E-59	UP	iSPNs	DDcKO
Celf4	-0.516	0.846	0.914	1.2E-08	UP	iSPNs	D2cKO
Cep126	0.398	0.446	0.211	2.0E-55	DOWN	iSPNs	DDcKO
Cep126	0.324	0.446	0.262	3.3E-21	DOWN	iSPNs	D2cKO
Chd3os	-0.311	0.389	0.558	1.8E-31	UP	dSPNs	DDcKO
Chn2	-0.315	0.152	0.296	3.0E-46	UP	dSPNs	DDcKO
Chn2	-0.529	0.233	0.431	2.3E-36	UP	iSPNs	DDcKO
Chn2	-0.470	0.233	0.388	5.2E-11	UP	iSPNs	D2cKO

Gene	Avg_logFC	pct.1_CTL	pct.2_cKO	P_val_adj	Regulation	Cell-type	Sample
Chrm2	-0.388	0.04	0.134	2.8E-11	UP	iSPNs	D2cKO
Chrm3	-0.555	0.092	0.24	2.5E-36	UP	dSPN	D1cKO
Chrm3	-0.652	0.092	0.314	1.3E-101	UP	dSPNs	DDcKO
Clmp	-0.353	0.27	0.387	2.0E-04	UP	iSPNs	DDcKO
Clmp	-0.437	0.27	0.37	2.5E-03	UP	iSPNs	D2cKO
Clstn2	-0.677	0.163	0.409	5.0E-52	UP	iSPNs	DDcKO
Clstn2	-0.813	0.163	0.428	5.4E-56	UP	iSPNs	D2cKO
Clvs1	0.310	0.763	0.653	1.6E-221	DOWN	dSPNs	DDcKO
Clvs1	0.552	0.822	0.542	2.4E-211	DOWN	iSPNs	DDcKO
Clvs1	0.612	0.822	0.494	1.3E-134	DOWN	iSPNs	D2cKO
Cnrip1	-0.387	0.248	0.403	3.1E-11	UP	iSPNs	DDcKO
Cnrip1	-0.457	0.248	0.385	1.4E-07	UP	iSPNs	D2cKO
Cntn3	-0.622	0.526	0.615	1.0E-73	UP	dSPN	D1cKO
Cntn3	-0.539	0.526	0.682	3.8E-100	UP	dSPNs	DDcKO
Cntn3	-0.448	0.624	0.667	2.9E-06	UP	iSPNs	DDcKO
Cntn4	0.843	0.876	0.565	0.0E+00	DOWN	dSPNs	DDcKO
Cntn4	1.246	0.918	0.495	0.0E+00	DOWN	iSPNs	DDcKO
Cntn4	1.125	0.918	0.481	0.0E+00	DOWN	iSPNs	D2cKO
Cntn4	0.309	0.876	0.773	2.8E-98	DOWN	dSPNs	D2cKO
Cntn5	0.728	0.978	0.863	0.0E+00	DOWN	dSPNs	DDcKO
Cntn5	0.508	0.963	0.828	0.0E+00	DOWN	iSPNs	DDcKO
Cntn5	0.315	0.963	0.834	6.7E-291	DOWN	iSPNs	D2cKO
Cntn6	0.400	0.437	0.224	1.7E-147	DOWN	dSPNs	DDcKO
Cntn6	0.528	0.435	0.183	1.4E-99	DOWN	iSPNs	DDcKO
Cntn6	0.307	0.435	0.262	6.0E-25	DOWN	iSPNs	D2cKO
Cntnap2	-0.393	0.972	0.974	1.9E-20	UP	dSPN	D1cKO
Cntnap2	-0.527	0.972	0.984	0.0E+00	UP	dSPNs	DDcKO
Cntnap2	-0.424	0.975	0.975	5.3E-03	UP	iSPNs	DDcKO
Cntnap5b	0.437	0.818	0.65	0.0E+00	DOWN	dSPNs	DDcKO
Cntnap5b	0.594	0.887	0.537	0.0E+00	DOWN	iSPNs	DDcKO
Cntnap5b	0.551	0.887	0.534	2.8E-203	DOWN	iSPNs	D2cKO
Cntnap5c	-0.404	0.148	0.268	1.1E-12	UP	iSPNs	DDcKO
Cplx2	-0.381	0.632	0.709	7.5E-53	UP	dSPNs	DDcKO
Cpne4	-0.387	0.113	0.21	1.9E-12	UP	iSPNs	DDcKO
Cpne4	-0.427	0.113	0.169	6.7E-08	UP	iSPNs	D2cKO
Crmp1	-0.333	0.399	0.539	1.0E-41	UP	dSPNs	DDcKO
Crmp1	-0.327	0.438	0.499	2.0E-13	UP	iSPNs	DDcKO
Csgalnact1	-0.360	0.161	0.256	1.3E-10	UP	dSPN	D1cKO

Gene	Avg_logFC	pct.1_CTL	pct.2_cKO	P_val_adj	Regulation	Cell-type	Sample
Csgalnact1	-0.494	0.161	0.385	2.3E-63	UP	dSPNs	DDcKO
Ctnna3	0.480	0.692	0.458	0.0E+00	DOWN	dSPNs	DDcKO
Ctnna3	0.506	0.59	0.35	5.0E-115	DOWN	iSPNs	DDcKO
Ctnnbip1	-0.313	0.256	0.392	1.3E-05	UP	iSPNs	DDcKO
Cttnbp2	0.394	0.885	0.699	5.7E-168	DOWN	iSPNs	DDcKO
Cttnbp2	0.364	0.885	0.69	4.8E-96	DOWN	iSPNs	D2cKO
Cx3cl1	0.348	0.612	0.4	4.4E-67	DOWN	iSPNs	DDcKO
Cx3cl1	0.408	0.612	0.368	3.5E-39	DOWN	iSPNs	D2cKO
Cxcl14	0.507	0.681	0.49	0.0E+00	DOWN	dSPNs	DDcKO
Cxcl14	0.503	0.662	0.431	3.1E-154	DOWN	iSPNs	DDcKO
Dab1	0.303	0.951	0.865	0.0E+00	DOWN	dSPNs	DDcKO
Dach1	0.336	0.931	0.793	0.0E+00	DOWN	dSPN	D1cKO
Dach1	0.598	0.931	0.756	0.0E+00	DOWN	dSPNs	DDcKO
Dach1	0.917	0.952	0.532	0.0E+00	DOWN	iSPNs	DDcKO
Dach1	0.859	0.952	0.554	0.0E+00	DOWN	iSPNs	D2cKO
Ddn	0.300	0.336	0.179	2.2E-23	DOWN	iSPNs	D2cKO
Dennd5b	0.384	0.58	0.456	0.0E+00	DOWN	dSPN	D1cKO
Dennd5b	0.742	0.64	0.458	4.3E-214	DOWN	iSPNs	D2cKO
Dennd5b	0.389	0.58	0.581	2.8E-303	DOWN	dSPNs	D2cKO
Dennd5b	0.704	0.64	0.421	0.0E+00	DOWN	iSPNs	D1cKO
Dgkb	0.587	0.935	0.762	0.0E+00	DOWN	iSPNs	DDcKO
Dgkb	0.880	0.935	0.645	0.0E+00	DOWN	iSPNs	D2cKO
Dgki	0.399	0.896	0.686	1.0E-215	DOWN	iSPNs	DDcKO
Dgki	0.351	0.896	0.703	2.1E-108	DOWN	iSPNs	D2cKO
Dmkn	0.418	0.197	0.046	2.6E-158	DOWN	dSPNs	DDcKO
Dmkn	0.402	0.211	0.032	8.7E-49	DOWN	iSPNs	DDcKO
Dmkn	0.351	0.211	0.043	1.8E-18	DOWN	iSPNs	D2cKO
Dner	-0.617	0.239	0.44	8.4E-50	UP	iSPNs	DDcKO
Dner	-0.629	0.239	0.451	1.3E-16	UP	iSPNs	D2cKO
Dock10	-0.354	0.468	0.519	8.0E-03	UP	dSPN	D1cKO
Dock10	-0.319	0.468	0.598	5.4E-13	UP	dSPNs	DDcKO
Dpp10	-0.565	0.433	0.541	2.2E-28	UP	dSPN	D1cKO
Dpp10	-0.411	0.433	0.575	1.5E-48	UP	dSPNs	DDcKO
Dpyd	-0.386	0.244	0.375	1.3E-33	UP	dSPNs	DDcKO
Dpyd	-0.561	0.238	0.393	5.5E-26	UP	iSPNs	DDcKO
Dpyd	-0.462	0.238	0.353	2.4E-04	UP	iSPNs	D2cKO
Dpysl2	-0.312	0.731	0.735	1.2E-09	UP	iSPNs	DDcKO
Drd1	-0.546	0.128	0.351	1.5E-43	UP	iSPNs	DDcKO

Gene	Avg_logFC	pct.1_CTL	pct.2_cKO	P_val_adj	Regulation	Cell-type	Sample
Drd1	-0.387	0.128	0.264	1.4E-10	UP	iSPNs	D2cKO
Drg1	0.310	0.61	0.38	6.9E-114	DOWN	dSPN	D1cKO
Drg1	0.374	0.61	0.407	2.7E-172	DOWN	dSPNs	DDcKO
Dscam	-0.586	0.188	0.42	5.4E-25	UP	iSPNs	DDcKO
Dscam	-0.575	0.188	0.433	1.7E-04	UP	iSPNs	D2cKO
Dtnb	0.370	0.833	0.639	3.1E-140	DOWN	iSPNs	DDcKO
Dynll1	-0.326	0.661	0.732	9.0E-20	UP	dSPNs	DDcKO
Dynll2	-0.307	0.435	0.583	7.8E-29	UP	dSPNs	DDcKO
Ebf1	0.303	0.783	0.645	1.9E-255	DOWN	dSPNs	DDcKO
Edil3	-0.356	0.399	0.539	3.2E-27	UP	dSPNs	DDcKO
Eef1a1	-0.371	0.88	0.892	2.8E-28	UP	dSPNs	DDcKO
Eef1a1	-0.307	0.902	0.895	8.8E-14	UP	iSPNs	D1cKO
Efna5	-0.421	0.328	0.441	6.3E-19	UP	dSPN	D1cKO
Efna5	-0.994	0.338	0.639	3.5E-128	UP	iSPNs	DDcKO
Efna5	-1.070	0.338	0.617	1.4E-129	UP	iSPNs	D2cKO
Egfem1	-0.537	0.834	0.865	4.4E-62	UP	dSPN	D1cKO
Egfem1	0.434	0.834	0.656	0.0E+00	DOWN	dSPNs	D2cKO
Egfem1	0.355	0.812	0.639	0.0E+00	DOWN	iSPNs	D1cKO
Eid1	-0.376	0.32	0.49	1.1E-55	UP	dSPNs	DDcKO
Elavl2	-0.394	0.191	0.323	2.1E-20	UP	iSPNs	DDcKO
Elavl4	-0.490	0.14	0.326	2.2E-30	UP	iSPNs	DDcKO
Elavl4	-0.655	0.14	0.35	1.7E-29	UP	iSPNs	D2cKO
Ell2	0.323	0.228	0.068	2.5E-16	DOWN	iSPNs	D2cKO
Eml5	0.459	0.769	0.504	4.9E-140	DOWN	iSPNs	DDcKO
Eml5	0.463	0.769	0.496	2.6E-71	DOWN	iSPNs	D2cKO
Epha3	-0.516	0.107	0.275	5.2E-30	UP	iSPNs	DDcKO
Epha3	-0.433	0.107	0.212	3.3E-05	UP	iSPNs	D2cKO
Epha5	-0.594	0.537	0.626	2.5E-10	UP	iSPNs	DDcKO
Epha5	-0.688	0.537	0.655	4.8E-14	UP	iSPNs	D2cKO
Epha7	0.431	0.731	0.524	4.4E-151	DOWN	iSPNs	DDcKO
Epha7	0.316	0.731	0.521	1.1E-65	DOWN	iSPNs	D2cKO
Epo	0.346	0.386	0.162	3.7E-54	DOWN	iSPNs	D1cKO
Erbb4	-0.477	0.53	0.689	1.0E-203	UP	dSPNs	DDcKO
Erbb4	-0.864	0.256	0.488	4.1E-204	UP	iSPNs	DDcKO
Erbb4	-0.577	0.256	0.39	1.0E-09	UP	iSPNs	D2cKO
Fam126a	-0.331	0.267	0.441	1.5E-24	UP	dSPNs	DDcKO
Fam155a	-0.456	0.502	0.585	5.3E-17	UP	dSPN	D1cKO
Fam155a	-0.403	0.502	0.646	9.6E-68	UP	dSPNs	DDcKO

Gene	Avg_logFC	pct.1_CTL	pct.2_cKO	P_val_adj	Regulation	Cell-type	Sample
Fam155a	-0.455	0.725	0.841	3.4E-13	UP	iSPNs	D2cKO
Fam19a2	-0.344	0.316	0.42	1.1E-23	UP	dSPNs	DDcKO
Fam19a2	-0.678	0.542	0.677	5.8E-54	UP	iSPNs	DDcKO
Fam19a2	-0.750	0.542	0.685	5.8E-56	UP	iSPNs	D2cKO
Fam81a	-0.315	0.28	0.375	4.2E-07	UP	iSPNs	DDcKO
Farp1	-0.450	0.385	0.516	4.4E-20	UP	iSPNs	DDcKO
Farp1	-0.659	0.385	0.605	1.2E-15	UP	iSPNs	D2cKO
Fat3	0.347	0.915	0.729	6.8E-205	DOWN	iSPNs	DDcKO
Fat3	0.392	0.915	0.69	1.6E-146	DOWN	iSPNs	D2cKO
Fgf12	-0.412	0.594	0.655	2.2E-07	UP	dSPN	D1cKO
Fgf12	-0.396	0.594	0.722	1.5E-38	UP	dSPNs	DDcKO
Fgf14	0.380	0.997	0.973	0.0E+00	DOWN	iSPNs	DDcKO
Fgf14	0.388	0.997	0.982	0.0E+00	DOWN	iSPNs	D2cKO
Fkbp1a	-0.379	0.591	0.694	2.1E-34	UP	dSPNs	DDcKO
Flrt2	-1.172	0.354	0.731	0.0E+00	UP	dSPN	D1cKO
Flrt2	-0.781	0.354	0.657	6.7E-200	UP	dSPNs	DDcKO
Foxn3	-0.342	0.436	0.517	2.5E-05	UP	iSPNs	DDcKO
Foxo1	0.335	0.539	0.383	3.9E-138	DOWN	dSPNs	DDcKO
Foxo1	0.392	0.51	0.284	1.7E-79	DOWN	iSPNs	DDcKO
Foxo1	0.388	0.51	0.267	4.5E-39	DOWN	iSPNs	D2cKO
Foxp1	0.316	0.97	0.9	0.0E+00	DOWN	dSPNs	DDcKO
Foxp1	0.413	0.99	0.861	0.0E+00	DOWN	iSPNs	DDcKO
Foxp1	0.356	0.99	0.849	0.0E+00	DOWN	iSPNs	D2cKO
Foxp2	-0.718	0.689	0.687	3.6E-170	UP	iSPNs	DDcKO
Foxp2	-0.717	0.689	0.637	1.8E-63	UP	iSPNs	D2cKO
Fras1	-0.398	0.557	0.615	2.0E-10	UP	dSPN	D1cKO
Frem2	0.472	0.297	0.097	1.9E-70	DOWN	iSPNs	DDcKO
Frem2	0.412	0.297	0.126	4.4E-24	DOWN	iSPNs	D2cKO
Frmd4b	0.339	0.586	0.351	6.1E-129	DOWN	dSPN	D1cKO
Frmd4b	0.485	0.586	0.343	1.1E-221	DOWN	dSPNs	DDcKO
Frmd4b	0.515	0.562	0.261	1.7E-86	DOWN	iSPNs	DDcKO
Frmd4b	0.499	0.562	0.234	2.6E-53	DOWN	iSPNs	D2cKO
Frrs1l	0.334	0.627	0.385	1.4E-29	DOWN	iSPNs	D2cKO
Ftl1	0.323	0.941	0.859	0.0E+00	DOWN	dSPN	D1cKO
Ftl1	0.358	0.94	0.857	0.0E+00	DOWN	iSPNs	D1cKO
Fxyd6	-0.688	0.517	0.683	1.1E-15	UP	iSPNs	D2cKO
Gabra4	0.393	0.579	0.364	6.4E-80	DOWN	iSPNs	DDcKO
Gabra4	0.430	0.579	0.31	4.6E-46	DOWN	iSPNs	D2cKO

Gene	Avg_logFC	pct.1_CTL	pct.2_cKO	P_val_adj	Regulation	Cell-type	Sample
Gabrg3	0.306	0.985	0.929	0.0E+00	DOWN	iSPNs	DDcKO
Gad1	-0.331	0.445	0.5	1.5E-06	UP	iSPNs	DDcKO
Galnt13	0.682	0.972	0.772	0.0E+00	DOWN	iSPNs	DDcKO
Galnt13	0.555	0.972	0.811	0.0E+00	DOWN	iSPNs	D2cKO
Galnt14	0.311	0.294	0.15	8.8E-28	DOWN	iSPNs	DDcKO
Galnt14	0.377	0.294	0.121	6.1E-19	DOWN	iSPNs	D2cKO
Galntl6	0.472	0.985	0.91	0.0E+00	DOWN	dSPN	D1cKO
Galntl6	0.702	0.985	0.879	0.0E+00	DOWN	dSPNs	DDcKO
Galntl6	0.890	0.971	0.724	0.0E+00	DOWN	iSPNs	DDcKO
Galntl6	0.590	0.971	0.756	0.0E+00	DOWN	iSPNs	D2cKO
Garem1	0.323	0.449	0.268	1.8E-45	DOWN	iSPNs	DDcKO
Gcnt2	0.309	0.267	0.12	2.4E-31	DOWN	iSPNs	DDcKO
Gda	-0.360	0.486	0.548	1.3E-11	UP	dSPN	D1cKO
Gda	-0.591	0.486	0.682	5.5E-175	UP	dSPNs	DDcKO
Gda	-0.383	0.505	0.57	7.8E-22	UP	iSPNs	DDcKO
Glce	0.310	0.48	0.285	7.1E-26	DOWN	iSPNs	D2cKO
Glp2r	0.332	0.903	0.735	3.8E-147	DOWN	iSPNs	DDcKO
Glp2r	0.300	0.903	0.728	1.8E-80	DOWN	iSPNs	D2cKO
Glra3	-0.450	0.031	0.145	4.6E-20	UP	iSPNs	DDcKO
Glra3	-0.406	0.031	0.134	3.7E-16	UP	iSPNs	D2cKO
Gnai1	-0.319	0.375	0.517	6.4E-30	UP	dSPNs	DDcKO
Gnal	0.334	0.949	0.815	1.3E-262	DOWN	iSPNs	DDcKO
Gnas	-0.301	0.547	0.651	3.0E-25	UP	dSPNs	DDcKO
Gng2	-0.438	0.191	0.358	1.8E-93	UP	dSPNs	DDcKO
Gng2	-0.707	0.236	0.477	4.5E-68	UP	iSPNs	DDcKO
Gng2	-0.645	0.236	0.458	5.7E-10	UP	iSPNs	D2cKO
Gng7	0.395	0.83	0.613	1.3E-127	DOWN	iSPNs	DDcKO
Gng7	0.450	0.83	0.554	8.2E-82	DOWN	iSPNs	D2cKO
Gpc5	-0.303	0.252	0.306	1.6E-14	UP	dSPNs	DDcKO
Gpc5	-0.594	0.258	0.361	1.2E-52	UP	iSPNs	DDcKO
Gpc6	0.437	0.799	0.695	0.0E+00	DOWN	dSPNs	DDcKO
Gpr158	0.467	0.762	0.522	6.7E-163	DOWN	iSPNs	DDcKO
Gpr158	0.483	0.762	0.504	6.2E-82	DOWN	iSPNs	D2cKO
Gpr6	0.337	0.231	0.066	8.2E-42	DOWN	iSPNs	DDcKO
Gpr88	0.309	0.889	0.776	0.0E+00	DOWN	dSPNs	DDcKO
Gpr88	0.642	0.91	0.641	0.0E+00	DOWN	iSPNs	DDcKO
Gpr88	0.563	0.91	0.673	8.7E-190	DOWN	iSPNs	D2cKO
Gprin3	0.306	0.471	0.295	2.1E-116	DOWN	dSPNs	DDcKO

Gene	Avg_logFC	pct.1_CTL	pct.2_cKO	P_val_adj	Regulation	Cell-type	Sample
Gprin3	0.470	0.574	0.284	2.6E-96	DOWN	iSPNs	DDcKO
Gprin3	0.410	0.574	0.282	6.7E-40	DOWN	iSPNs	D2cKO
Grb14	-0.359	0.054	0.164	2.6E-08	UP	iSPNs	D2cKO
Greb1l	-0.320	0.052	0.192	2.0E-44	UP	dSPNs	DDcKO
Greb1l	-0.549	0.079	0.282	2.0E-27	UP	iSPNs	DDcKO
Greb1l	-0.560	0.079	0.277	7.3E-22	UP	iSPNs	D2cKO
Grid2	0.340	0.988	0.947	0.0E+00	DOWN	dSPN	D1cKO
Grid2	0.494	0.988	0.939	0.0E+00	DOWN	dSPNs	DDcKO
Grid2	0.600	0.962	0.841	0.0E+00	DOWN	iSPNs	DDcKO
Grid2	0.455	0.962	0.851	0.0E+00	DOWN	iSPNs	D2cKO
Grik1	-0.395	0.12	0.177	3.5E-14	UP	dSPN	D1cKO
Grik1	-0.403	0.12	0.222	4.0E-54	UP	dSPNs	DDcKO
Grik1	-0.703	0.188	0.355	5.2E-45	UP	iSPNs	DDcKO
Grik1	-0.607	0.188	0.307	8.9E-08	UP	iSPNs	D2cKO
Grik2	0.435	0.987	0.951	0.0E+00	DOWN	dSPNs	DDcKO
Grik2	0.546	0.987	0.82	0.0E+00	DOWN	iSPNs	DDcKO
Grik2	0.523	0.987	0.809	0.0E+00	DOWN	iSPNs	D2cKO
Grik4	-0.386	0.223	0.37	1.4E-11	UP	iSPNs	DDcKO
Grik4	-0.532	0.223	0.428	4.1E-14	UP	iSPNs	D2cKO
Grin3a	-0.355	0.098	0.226	1.4E-35	UP	dSPNs	DDcKO
Grin3a	-0.400	0.095	0.222	5.2E-14	UP	iSPNs	DDcKO
Grm1	0.405	0.562	0.32	3.9E-48	DOWN	iSPNs	D2cKO
Grm3	0.340	0.903	0.655	5.6E-168	DOWN	iSPNs	DDcKO
Grm3	0.392	0.903	0.645	1.9E-141	DOWN	iSPNs	D2cKO
Grm5	0.395	0.997	0.975	0.0E+00	DOWN	iSPNs	DDcKO
Grm5	0.432	0.997	0.975	0.0E+00	DOWN	iSPNs	D2cKO
Grm8	-0.300	0.165	0.255	1.4E-30	UP	dSPNs	DDcKO
Grm8	-0.860	0.122	0.315	7.5E-67	UP	iSPNs	DDcKO
Grm8	-0.931	0.122	0.305	3.4E-48	UP	iSPNs	D2cKO
Gucy1b3	0.327	0.761	0.561	3.2E-116	DOWN	iSPNs	DDcKO
Gucy1b3	0.308	0.761	0.542	1.3E-57	DOWN	iSPNs	D2cKO
Gulp1	-0.306	0.416	0.474	2.7E-02	UP	dSPN	D1cKO
Hbb-bs	-0.580	0.174	0.155	9.9E-139	UP	dSPNs	DDcKO
Hbb-bs	0.592	0.141	0.262	9.4E-74	DOWN	iSPNs	D2cKO
Hbb-bs	0.600	0.141	0.236	3.4E-111	DOWN	iSPNs	D1cKO
Hcn1	-0.383	0.358	0.533	4.6E-37	UP	dSPNs	DDcKO
Hdac9	-0.385	0.332	0.428	6.4E-11	UP	iSPNs	DDcKO
Homer1	0.314	0.673	0.448	2.7E-46	DOWN	iSPNs	D2cKO

Gene	Avg_logFC	pct.1_CTL	pct.2_cKO	P_val_adj	Regulation	Cell-type	Sample
Hpcal4	-0.342	0.195	0.363	8.5E-43	UP	dSPNs	DDcKO
Hras	0.308	0.436	0.297	3.3E-17	DOWN	iSPNs	D2cKO
Hs3st5	0.736	0.814	0.468	0.0E+00	DOWN	iSPNs	DDcKO
Hs3st5	0.765	0.814	0.474	1.2E-186	DOWN	iSPNs	D2cKO
Hs3st5	0.387	0.814	0.613	7.6E-260	DOWN	iSPNs	D1cKO
Hs6st3	0.432	0.958	0.835	0.0E+00	DOWN	dSPNs	DDcKO
Hs6st3	0.625	0.93	0.628	0.0E+00	DOWN	iSPNs	DDcKO
Hs6st3	0.518	0.93	0.678	7.3E-259	DOWN	iSPNs	D2cKO
Hsbp1	-0.341	0.568	0.705	3.5E-32	UP	dSPNs	DDcKO
Hsp90ab1	-0.391	0.695	0.778	1.8E-48	UP	dSPNs	DDcKO
Hsp90ab1	-0.355	0.755	0.757	2.5E-06	UP	iSPNs	DDcKO
Ikzf2	-0.372	0.291	0.35	8.1E-03	UP	iSPNs	D2cKO
Ildr2	-0.341	0.119	0.233	2.1E-12	UP	dSPN	D1cKO
Inf2	0.380	0.424	0.203	2.5E-47	DOWN	iSPNs	DDcKO
Inhba	0.348	0.292	0.09	4.5E-86	DOWN	dSPN	D1cKO
Inhba	0.451	0.292	0.075	4.6E-201	DOWN	dSPNs	DDcKO
Inhba	0.497	0.269	0.035	2.6E-64	DOWN	iSPNs	DDcKO
Inhba	0.435	0.269	0.065	1.2E-23	DOWN	iSPNs	D2cKO
Inpp4b	-0.336	0.153	0.233	5.2E-07	UP	dSPN	D1cKO
Inpp4b	-0.365	0.153	0.295	8.8E-34	UP	dSPNs	DDcKO
Inpp4b	-0.477	0.135	0.287	3.3E-16	UP	iSPNs	DDcKO
Iqgap2	0.491	0.517	0.226	9.6E-75	DOWN	iSPNs	DDcKO
Iqgap2	0.534	0.517	0.184	5.9E-45	DOWN	iSPNs	D2cKO
Itga5	0.313	0.282	0.148	3.6E-100	DOWN	dSPNs	DDcKO
Itga5	0.383	0.28	0.104	2.4E-49	DOWN	iSPNs	DDcKO
Itpr1	0.422	0.551	0.272	2.3E-77	DOWN	iSPNs	DDcKO
Itpr1	0.457	0.551	0.259	3.0E-44	DOWN	iSPNs	D2cKO
Ivns1abp	0.362	0.511	0.297	1.6E-27	DOWN	iSPNs	D2cKO
Jcad	0.324	0.289	0.118	5.2E-18	DOWN	iSPNs	D2cKO
Kcna4	0.373	0.451	0.234	1.3E-66	DOWN	iSPNs	DDcKO
Kcnab1	0.351	0.937	0.82	0.0E+00	DOWN	dSPNs	DDcKO
Kcnab1	0.681	0.896	0.635	0.0E+00	DOWN	iSPNs	DDcKO
Kcnab1	0.729	0.896	0.569	2.0E-248	DOWN	iSPNs	D2cKO
Kcnc2	-0.422	0.043	0.158	2.1E-30	UP	iSPNs	DDcKO
Kcnc2	-0.459	0.043	0.131	4.7E-09	UP	iSPNs	D2cKO
Kcnd2	0.333	0.981	0.927	0.0E+00	DOWN	iSPNs	D2cKO
Kcnd3	-0.365	0.2	0.38	7.1E-32	UP	dSPNs	DDcKO
Kcnd3	-0.377	0.279	0.415	2.3E-09	UP	iSPNs	DDcKO

Gene	Avg_logFC	pct.1_CTL	pct.2_cKO	P_val_adj	Regulation	Cell-type	Sample
Kcnip1	-0.458	0.191	0.404	1.8E-81	UP	dSPNs	DDcKO
Kcnip1	-0.628	0.289	0.505	3.2E-49	UP	iSPNs	DDcKO
Kcnip1	-0.756	0.289	0.537	5.2E-29	UP	iSPNs	D2cKO
Kcnip2	0.312	0.611	0.469	9.7E-147	DOWN	dSPNs	DDcKO
Kcnip2	0.604	0.63	0.297	1.1E-120	DOWN	iSPNs	DDcKO
Kcnip2	0.776	0.63	0.237	1.6E-77	DOWN	iSPNs	D2cKO
Kcnip4	-0.501	0.891	0.933	3.9E-276	UP	dSPNs	DDcKO
Kcnj3	-0.343	0.12	0.207	1.4E-11	UP	iSPNs	DDcKO
Kcnj3	-0.431	0.12	0.199	2.7E-07	UP	iSPNs	D2cKO
Kcnk2	0.492	0.838	0.584	3.5E-168	DOWN	iSPNs	DDcKO
Kcnk2	0.543	0.838	0.524	1.1E-101	DOWN	iSPNs	D2cKO
Kcnmb2	-0.396	0.044	0.143	9.9E-20	UP	iSPNs	DDcKO
Kcnmb2	-0.417	0.044	0.166	1.8E-14	UP	iSPNs	D2cKO
Kctd8	0.749	0.812	0.433	0.0E+00	DOWN	iSPNs	DDcKO
Kctd8	0.722	0.812	0.431	1.3E-170	DOWN	iSPNs	D2cKO
Kirrel3	-0.454	0.884	0.907	7.8E-08	UP	iSPNs	DDcKO
Kirrel3	-0.313	0.88	0.938	2.8E-156	UP	dSPNs	D2cKO
Kirrel3	-0.389	0.884	0.927	1.4E-02	UP	iSPNs	D1cKO
Klhl1	0.324	0.332	0.16	1.4E-110	DOWN	dSPNs	DDcKO
Klhl2	0.488	0.749	0.486	1.6E-143	DOWN	iSPNs	DDcKO
Klhl2	0.566	0.749	0.436	1.4E-88	DOWN	iSPNs	D2cKO
Lamp5	0.330	0.233	0.076	2.3E-15	DOWN	iSPNs	D2cKO
Ldb2	0.348	0.692	0.426	6.9E-51	DOWN	iSPNs	D2cKO
Ldlrad4	0.405	0.67	0.43	6.9E-122	DOWN	iSPNs	DDcKO
Lingo2	-0.906	0.238	0.452	1.3E-158	UP	iSPNs	DDcKO
Lingo2	-0.837	0.238	0.411	6.0E-37	UP	iSPNs	D2cKO
Lmo3	0.610	0.825	0.533	3.1E-227	DOWN	iSPNs	DDcKO
Lmo3	0.512	0.825	0.537	8.0E-94	DOWN	iSPNs	D2cKO
Lmo7	0.312	0.526	0.307	1.7E-18	DOWN	iSPNs	D2cKO
Lpl	0.482	0.404	0.151	2.4E-75	DOWN	iSPNs	DDcKO
Lpl	0.525	0.404	0.136	1.8E-37	DOWN	iSPNs	D2cKO
Lrfn2	-0.507	0.147	0.324	9.5E-20	UP	iSPNs	DDcKO
Lrfn2	-0.440	0.147	0.275	4.2E-11	UP	iSPNs	D2cKO
Lrfn5	0.391	0.866	0.561	4.3E-147	DOWN	iSPNs	DDcKO
Lrfn5	0.356	0.866	0.521	3.5E-112	DOWN	iSPNs	D2cKO
Lrp1b	0.373	0.946	0.801	0.0E+00	DOWN	iSPNs	DDcKO
Lrrc4c	0.533	0.995	0.971	0.0E+00	DOWN	dSPNs	DDcKO
Lrrc4c	0.468	0.99	0.906	0.0E+00	DOWN	iSPNs	DDcKO

Gene	Avg_logFC	pct.1_CTL	pct.2_cKO	P_val_adj	Regulation	Cell-type	Sample
Lrrc4c	0.451	0.99	0.924	0.0E+00	DOWN	iSPNs	D2cKO
Lrrc7	0.320	0.994	0.965	0.0E+00	DOWN	iSPNs	DDcKO
Lrrc7	0.309	0.994	0.965	6.5E-303	DOWN	iSPNs	D2cKO
Lrrn3	-0.379	0.325	0.413	7.1E-07	UP	iSPNs	DDcKO
Lrrtm3	0.353	0.759	0.498	4.4E-85	DOWN	iSPNs	DDcKO
Lrtm1	0.497	0.592	0.276	1.1E-283	DOWN	dSPNs	DDcKO
Lrtm1	0.376	0.464	0.226	1.2E-85	DOWN	iSPNs	DDcKO
Luzp2	-0.510	0.302	0.439	1.1E-27	UP	iSPNs	DDcKO
Lypd1	0.334	0.661	0.553	3.7E-210	DOWN	dSPNs	DDcKO
Lypd1	0.350	0.683	0.538	4.8E-121	DOWN	iSPNs	DDcKO
Macrod2	0.302	0.996	0.978	0.0E+00	DOWN	iSPNs	DDcKO
Macrod2	0.303	0.996	0.97	0.0E+00	DOWN	iSPNs	D2cKO
Maml2	-0.343	0.182	0.324	2.6E-02	UP	iSPNs	DDcKO
Man1a	0.442	0.761	0.504	3.2E-168	DOWN	iSPNs	DDcKO
Man1a	0.505	0.761	0.433	5.4E-119	DOWN	iSPNs	D2cKO
Map1b	-0.325	0.843	0.854	4.2E-03	UP	iSPNs	DDcKO
March1	-0.615	0.451	0.561	2.4E-19	UP	dSPN	D1cKO
March1	-0.533	0.451	0.591	2.3E-93	UP	dSPNs	DDcKO
March1	-0.789	0.684	0.776	5.7E-101	UP	iSPNs	DDcKO
March1	-0.688	0.684	0.733	6.8E-15	UP	iSPNs	D2cKO
Marcks	-0.348	0.614	0.722	2.2E-67	UP	dSPNs	DDcKO
Marcks	-0.303	0.661	0.704	2.0E-10	UP	iSPNs	DDcKO
Marcksl1	-0.337	0.649	0.681	3.7E-04	UP	iSPNs	DDcKO
Mast4	-0.330	0.082	0.196	8.2E-15	UP	iSPNs	DDcKO
Matk	0.302	0.648	0.453	1.0E-92	DOWN	dSPN	D1cKO
Matk	0.308	0.648	0.521	2.7E-110	DOWN	dSPNs	DDcKO
Matk	0.338	0.568	0.362	2.2E-61	DOWN	iSPNs	DDcKO
Matk	0.324	0.568	0.368	3.4E-25	DOWN	iSPNs	D2cKO
Mbnl2	0.471	0.749	0.491	6.6E-75	DOWN	iSPNs	D2cKO
Mctp1	-0.402	0.652	0.687	4.5E-15	UP	dSPN	D1cKO
Mctp1	-0.352	0.652	0.73	9.6E-31	UP	dSPNs	DDcKO
Mctp1	-0.431	0.495	0.576	6.3E-11	UP	iSPNs	DDcKO
Mdk	0.382	0.337	0.125	1.8E-90	DOWN	dSPN	D1cKO
Mdk	0.429	0.337	0.128	4.4E-153	DOWN	dSPNs	DDcKO
Mei4	0.318	0.345	0.197	4.0E-51	DOWN	iSPNs	DDcKO
Meis1	0.323	0.311	0.154	1.9E-28	DOWN	iSPNs	D2cKO
Mettl23	0.303	0.62	0.411	1.1E-118	DOWN	dSPN	D1cKO
Mettl23	0.314	0.62	0.491	8.0E-135	DOWN	dSPNs	DDcKO

Gene	Avg_logFC	pct.1_CTL	pct.2_cKO	P_val_adj	Regulation	Cell-type	Sample
Mllt11	-0.371	0.654	0.756	1.2E-47	UP	dSPNs	DDcKO
Mmd	0.300	0.645	0.461	4.8E-38	DOWN	iSPNs	D2cKO
Mme	0.431	0.339	0.11	1.1E-103	DOWN	dSPN	D1cKO
Mme	0.465	0.339	0.112	4.9E-167	DOWN	dSPNs	DDcKO
Mme	0.487	0.295	0.075	1.2E-64	DOWN	iSPNs	DDcKO
Mme	0.420	0.295	0.096	6.5E-20	DOWN	iSPNs	D2cKO
Msi2	-0.439	0.3	0.432	3.1E-22	UP	iSPNs	DDcKO
Mt1	0.330	0.493	0.302	1.2E-45	DOWN	iSPNs	D2cKO
Mt3	0.358	0.565	0.39	1.1E-223	DOWN	dSPN	D1cKO
Mt3	0.464	0.643	0.395	4.7E-78	DOWN	iSPNs	D2cKO
Mt3	0.383	0.643	0.471	5.9E-186	DOWN	iSPNs	D1cKO
Mtcl1	0.350	0.367	0.173	1.1E-42	DOWN	iSPNs	DDcKO
Mtcl1	0.309	0.367	0.194	1.8E-20	DOWN	iSPNs	D2cKO
Mtpn	-0.312	0.421	0.565	1.4E-30	UP	dSPNs	DDcKO
Myo16	-0.400	0.335	0.489	1.8E-14	UP	iSPNs	DDcKO
Myo16	-0.440	0.335	0.451	5.2E-03	UP	iSPNs	D2cKO
Myo1b	0.398	0.557	0.333	1.0E-72	DOWN	iSPNs	DDcKO
Myo1b	0.476	0.557	0.254	1.0E-50	DOWN	iSPNs	D2cKO
Myo1d	-0.457	0.181	0.343	4.1E-13	UP	iSPNs	D2cKO
Nap1l5	-0.492	0.226	0.459	2.1E-114	UP	dSPNs	DDcKO
Nap1l5	-0.517	0.272	0.439	2.1E-52	UP	iSPNs	DDcKO
Nap1l5	-0.454	0.272	0.343	1.9E-10	UP	iSPNs	D2cKO
Napb	-0.402	0.321	0.525	5.6E-55	UP	dSPNs	DDcKO
Ncald	-0.404	0.189	0.336	3.3E-20	UP	iSPNs	DDcKO
Ncald	-0.419	0.189	0.315	3.3E-05	UP	iSPNs	D2cKO
Nckap5	-0.329	0.31	0.395	7.1E-03	UP	iSPNs	DDcKO
Ndrg4	-0.341	0.651	0.752	2.9E-51	UP	dSPNs	DDcKO
Ndst3	-0.404	0.232	0.317	3.6E-04	UP	iSPNs	DDcKO
Ndst3	-0.403	0.232	0.345	9.9E-05	UP	iSPNs	D2cKO
Nebl	0.326	0.89	0.714	4.9E-205	DOWN	iSPNs	DDcKO
Nebl	0.374	0.89	0.675	1.1E-93	DOWN	iSPNs	D2cKO
Nedd9	-0.356	0.116	0.217	1.6E-05	UP	iSPNs	D2cKO
Negr1	-0.308	0.984	0.977	7.5E-03	UP	iSPNs	DDcKO
Negr1	-0.348	0.984	0.972	2.6E-04	UP	iSPNs	D2cKO
Nell1	-0.314	0.108	0.151	1.7E-05	UP	dSPN	D1cKO
Nell1	-0.350	0.108	0.205	1.0E-44	UP	dSPNs	DDcKO
Neto1	0.626	0.952	0.725	0.0E+00	DOWN	iSPNs	DDcKO
Neto1	0.614	0.952	0.723	2.2E-245	DOWN	iSPNs	D2cKO

Gene	Avg_logFC	pct.1_CTL	pct.2_cKO	P_val_adj	Regulation	Cell-type	Sample
Nexn	0.341	0.391	0.168	8.6E-59	DOWN	iSPNs	DDcKO
Nexn	0.466	0.391	0.144	5.9E-32	DOWN	iSPNs	D2cKO
Nfib	-0.310	0.289	0.364	1.3E-12	UP	iSPNs	DDcKO
Nfib	0.412	0.289	0.181	0.0E+00	DOWN	iSPNs	D1cKO
Ngef	0.343	0.681	0.427	1.4E-86	DOWN	iSPNs	DDcKO
Nlgn1	-0.312	0.877	0.897	7.3E-48	UP	iSPNs	D1cKO
Nlrp1b	-0.492	0.134	0.336	3.4E-63	UP	dSPNs	DDcKO
Nlrp1b	-0.382	0.148	0.23	4.9E-09	UP	iSPNs	DDcKO
Nnat	-0.334	0.763	0.785	1.8E-112	UP	dSPNs	DDcKO
Nnat	-0.664	0.855	0.879	1.6E-121	UP	iSPNs	DDcKO
Nnat	-0.646	0.855	0.894	6.6E-08	UP	iSPNs	D2cKO
Npas3	-0.354	0.2	0.257	2.4E-18	UP	iSPNs	DDcKO
Nptn	0.448	0.931	0.715	5.7E-224	DOWN	iSPNs	DDcKO
Nptn	0.495	0.931	0.703	3.8E-128	DOWN	iSPNs	D2cKO
Npy	-0.351	0.113	0.194	4.4E-08	UP	iSPNs	DDcKO
Npy	-0.613	0.113	0.217	2.6E-22	UP	iSPNs	D2cKO
Nrep	0.326	0.407	0.282	1.6E-143	DOWN	iSPNs	D1cKO
Nrg1	0.557	0.987	0.884	0.0E+00	DOWN	iSPNs	DDcKO
Nrg1	0.584	0.987	0.902	0.0E+00	DOWN	iSPNs	D2cKO
Nrgn	0.424	0.67	0.412	1.5E-113	DOWN	iSPNs	DDcKO
Nrgn	0.532	0.67	0.383	4.6E-76	DOWN	iSPNs	D2cKO
Nrp1	-0.499	0.077	0.219	6.9E-45	UP	dSPN	D1cKO
Nrp1	-0.359	0.077	0.234	4.8E-48	UP	dSPNs	DDcKO
Nrp1	-0.445	0.112	0.272	2.0E-19	UP	iSPNs	DDcKO
Nrp1	-0.457	0.112	0.234	4.7E-11	UP	iSPNs	D2cKO
Nrp2	-0.485	0.015	0.128	1.8E-18	UP	iSPNs	D2cKO
Nrxn1	-0.673	0.944	0.962	1.6E-141	UP	iSPNs	DDcKO
Nrxn1	-0.670	0.944	0.957	1.5E-30	UP	iSPNs	D2cKO
Ntm	0.564	0.975	0.838	0.0E+00	DOWN	dSPN	D1cKO
Ntm	1.070	0.975	0.771	0.0E+00	DOWN	dSPNs	DDcKO
Ntm	0.864	0.969	0.704	0.0E+00	DOWN	iSPNs	DDcKO
Ntm	0.672	0.969	0.71	0.0E+00	DOWN	iSPNs	D2cKO
Ntm	0.362	0.975	0.932	1.2E-274	DOWN	dSPNs	D2cKO
Ntng1	-0.359	0.099	0.214	5.9E-48	UP	dSPNs	DDcKO
Ntng1	-0.992	0.148	0.408	2.3E-101	UP	iSPNs	DDcKO
Ntng1	-1.252	0.148	0.403	1.9E-117	UP	iSPNs	D2cKO
Nxph1	-0.487	0.104	0.145	5.9E-118	UP	dSPNs	DDcKO
Nxph1	-0.380	0.137	0.187	4.1E-16	UP	iSPNs	DDcKO

Gene	Avg_logFC	pct.1_CTL	pct.2_cKO	P_val_adj	Regulation	Cell-type	Sample
Olfm1	-0.324	0.22	0.357	4.5E-43	UP	dSPNs	DDcKO
Olfm1	-0.540	0.207	0.404	2.3E-43	UP	iSPNs	DDcKO
Olfm1	-0.498	0.207	0.385	3.2E-10	UP	iSPNs	D2cKO
Olfm3	-0.596	0.295	0.435	1.3E-48	UP	dSPN	D1cKO
Olfm3	-0.544	0.295	0.479	5.7E-119	UP	dSPNs	DDcKO
Olfm3	-0.614	0.408	0.573	8.7E-57	UP	iSPNs	DDcKO
Olfm3	-0.640	0.408	0.542	4.0E-35	UP	iSPNs	D2cKO
Opcml	-0.301	0.793	0.844	4.1E-09	UP	dSPN	D1cKO
Opcml	-0.624	0.856	0.897	4.7E-53	UP	iSPNs	D2cKO
Oxr1	-0.309	0.298	0.378	7.3E-10	UP	iSPNs	DDcKO
Oxr1	-0.386	0.298	0.378	4.0E-04	UP	iSPNs	D2cKO
P2ry14	0.326	0.421	0.226	3.4E-122	DOWN	dSPNs	DDcKO
P4ha1	0.311	0.47	0.325	2.3E-87	DOWN	dSPNs	DDcKO
P4ha1	0.336	0.435	0.233	4.2E-54	DOWN	iSPNs	DDcKO
P4ha1	0.318	0.435	0.217	2.4E-23	DOWN	iSPNs	D2cKO
Pam	0.389	0.786	0.576	2.0E-138	DOWN	iSPNs	DDcKO
Pam	0.354	0.786	0.557	3.6E-92	DOWN	iSPNs	D2cKO
Parm1	0.346	0.371	0.223	7.3E-94	DOWN	dSPNs	DDcKO
Parm1	0.447	0.401	0.177	5.5E-63	DOWN	iSPNs	DDcKO
Parm1	0.418	0.401	0.169	4.3E-31	DOWN	iSPNs	D2cKO
Pbx1	-0.440	0.875	0.862	1.3E-40	UP	iSPNs	DDcKO
Pcdh15	-0.376	0.591	0.61	3.1E-04	UP	dSPN	D1cKO
Pcdh17	0.413	0.841	0.823	0.0E+00	DOWN	dSPNs	DDcKO
Pcdh17	0.470	0.883	0.785	0.0E+00	DOWN	iSPNs	DDcKO
Pcdh17	0.450	0.883	0.748	1.8E-184	DOWN	iSPNs	D2cKO
Pcdh17	0.429	0.841	0.732	1.0E-253	DOWN	dSPNs	D2cKO
Pcdh17	0.323	0.883	0.763	0.0E+00	DOWN	iSPNs	D1cKO
Pcdh8	-0.328	0.063	0.171	5.5E-06	UP	iSPNs	D2cKO
Pcdh9	-0.364	0.811	0.898	2.1E-90	UP	dSPNs	DDcKO
Pcp4l1	0.565	0.546	0.297	4.1E-72	DOWN	iSPNs	D2cKO
Pcsk2	0.675	0.968	0.634	0.0E+00	DOWN	iSPNs	DDcKO
Pcsk2	0.640	0.968	0.579	2.9E-221	DOWN	iSPNs	D2cKO
Pde10a	0.330	0.981	0.931	0.0E+00	DOWN	dSPNs	DDcKO
Pde10a	0.720	0.975	0.824	0.0E+00	DOWN	iSPNs	DDcKO
Pde10a	0.626	0.975	0.816	0.0E+00	DOWN	iSPNs	D2cKO
Pde1a	-1.940	0.134	0.683	0.0E+00	UP	dSPN	D1cKO
Pde1a	-1.923	0.134	0.79	0.0E+00	UP	dSPNs	DDcKO
Pde1a	-1.410	0.229	0.699	0.0E+00	UP	iSPNs	DDcKO

Gene	Avg_logFC	pct.1_CTL	pct.2_cKO	P_val_adj	Regulation	Cell-type	Sample
Pde1a	-1.327	0.229	0.617	7.6E-204	UP	iSPNs	D2cKO
Pde1a	-0.542	0.134	0.232	8.1E-66	UP	dSPNs	D2cKO
Pde1a	-0.383	0.229	0.232	2.8E-08	UP	iSPNs	D1cKO
Pde1b	0.492	0.52	0.238	4.9E-89	DOWN	iSPNs	DDcKO
Pde1b	0.591	0.52	0.179	6.4E-50	DOWN	iSPNs	D2cKO
Pde4d	-0.515	0.435	0.634	4.1E-93	UP	dSPNs	DDcKO
Pde4d	-0.692	0.545	0.773	9.9E-69	UP	iSPNs	DDcKO
Pde4d	-0.744	0.545	0.751	6.7E-09	UP	iSPNs	D2cKO
Pde7b	0.457	0.928	0.787	0.0E+00	DOWN	dSPNs	DDcKO
Pde7b	0.717	0.949	0.684	0.0E+00	DOWN	iSPNs	DDcKO
Pde7b	0.592	0.949	0.673	2.7E-293	DOWN	iSPNs	D2cKO
Pdia3	-0.324	0.385	0.359	2.2E-160	UP	dSPNs	DDcKO
Pdia3	-0.692	0.372	0.465	1.6E-155	UP	iSPNs	DDcKO
Pdzd2	0.370	0.643	0.388	8.5E-89	DOWN	iSPNs	DDcKO
Pdzd2	0.377	0.643	0.353	3.8E-50	DOWN	iSPNs	D2cKO
Pdzrn4	-1.101	0.12	0.346	3.3E-92	UP	iSPNs	DDcKO
Pdzrn4	-0.839	0.12	0.254	2.6E-29	UP	iSPNs	D2cKO
Penk	0.591	0.615	0.317	1.1E-242	DOWN	iSPNs	DDcKO
Penk	0.348	0.615	0.335	1.1E-91	DOWN	iSPNs	D2cKO
Pfn2	-0.303	0.582	0.688	1.3E-18	UP	dSPNs	DDcKO
Pid1	-0.420	0.332	0.524	2.3E-40	UP	dSPNs	DDcKO
Pja2	0.307	0.737	0.531	6.5E-41	DOWN	iSPNs	D2cKO
Pla2g3	0.310	0.294	0.167	1.6E-93	DOWN	dSPNs	DDcKO
Plekhh2	-0.448	0.112	0.238	2.8E-15	UP	iSPNs	DDcKO
Plekhh2	-0.387	0.112	0.199	2.2E-08	UP	iSPNs	D2cKO
Plppr1	0.301	0.746	0.577	2.2E-95	DOWN	iSPNs	DDcKO
Plppr1	0.338	0.746	0.544	9.9E-58	DOWN	iSPNs	D2cKO
Plppr4	0.370	0.799	0.577	6.9E-114	DOWN	iSPNs	DDcKO
Plppr4	0.359	0.799	0.557	1.2E-63	DOWN	iSPNs	D2cKO
Plxdc2	-0.374	0.156	0.301	3.1E-36	UP	dSPNs	DDcKO
Plxdc2	-0.680	0.2	0.433	1.7E-41	UP	iSPNs	DDcKO
Plxdc2	-0.641	0.2	0.335	2.8E-13	UP	iSPNs	D2cKO
Plxnc1	-0.334	0.185	0.281	4.6E-11	UP	iSPNs	DDcKO
Pou6f2	0.400	0.399	0.201	2.3E-53	DOWN	iSPNs	DDcKO
Pou6f2	0.327	0.399	0.181	1.8E-26	DOWN	iSPNs	D2cKO
Pphln1	-0.434	0.233	0.343	6.4E-11	UP	iSPNs	D2cKO
Pphln1	-0.349	0.218	0.386	1.5E-79	UP	dSPNs	D2cKO
Ppm1e	-0.641	0.125	0.341	1.1E-56	UP	iSPNs	DDcKO

Gene	Avg_logFC	pct.1_CTL	pct.2_cKO	P_val_adj	Regulation	Cell-type	Sample
Ppm1e	-0.814	0.125	0.368	1.5E-28	UP	iSPNs	D2cKO
Ppp1r1b	0.474	0.69	0.452	1.4E-165	DOWN	iSPNs	DDcKO
Ppp1r1b	0.751	0.69	0.353	7.7E-127	DOWN	iSPNs	D2cKO
Ppp1r2	-0.425	0.324	0.511	2.4E-56	UP	dSPNs	DDcKO
Ppp3ca	0.300	0.994	0.923	0.0E+00	DOWN	iSPNs	DDcKO
Ppp3ca	0.359	0.994	0.929	0.0E+00	DOWN	iSPNs	D2cKO
Prkcb	-0.381	0.833	0.912	1.0E-199	UP	dSPNs	D2cKO
Prr16	-0.390	0.178	0.308	2.8E-10	UP	iSPNs	DDcKO
Prr16	-0.506	0.178	0.297	5.9E-14	UP	iSPNs	D2cKO
Ptn	-0.341	0.628	0.68	1.0E-07	UP	iSPNs	DDcKO
Ptpn5	0.424	0.667	0.389	4.0E-97	DOWN	iSPNs	DDcKO
Ptpn5	0.386	0.667	0.401	2.8E-56	DOWN	iSPNs	D2cKO
Ptprg	-0.440	0.336	0.435	7.9E-09	UP	dSPN	D1cKO
Ptprg	-0.556	0.336	0.559	1.3E-107	UP	dSPNs	DDcKO
Ptprg	-0.815	0.282	0.557	3.9E-87	UP	iSPNs	DDcKO
Ptprg	-0.818	0.282	0.524	8.1E-29	UP	iSPNs	D2cKO
Ptprk	-0.516	0.087	0.22	2.3E-21	UP	iSPNs	DDcKO
Ptprk	-0.594	0.087	0.214	6.2E-16	UP	iSPNs	D2cKO
Ptprt	-0.377	0.58	0.649	7.7E-05	UP	iSPNs	DDcKO
Ptprt	-0.516	0.58	0.637	2.8E-09	UP	iSPNs	D2cKO
Ptprz1	-0.334	0.482	0.475	1.2E-08	UP	iSPNs	DDcKO
Purb	-0.328	0.456	0.633	3.5E-22	UP	dSPNs	DDcKO
Rab6a	-0.316	0.444	0.591	1.5E-36	UP	dSPNs	DDcKO
Rabgap1l	0.474	0.89	0.696	1.4E-232	DOWN	iSPNs	DDcKO
Rabgap1l	0.392	0.89	0.71	4.7E-126	DOWN	iSPNs	D2cKO
Ralyl	-0.469	0.477	0.557	4.2E-20	UP	dSPN	D1cKO
Ralyl	-0.503	0.477	0.639	4.6E-92	UP	dSPNs	DDcKO
Ralyl	-0.649	0.49	0.654	1.3E-61	UP	iSPNs	DDcKO
Ralyl	-0.928	0.49	0.693	7.7E-112	UP	iSPNs	D2cKO
Rap1gap	0.465	0.681	0.425	2.8E-107	DOWN	iSPNs	DDcKO
Rap1gap	0.459	0.681	0.416	2.0E-49	DOWN	iSPNs	D2cKO
Rasd2	0.306	0.264	0.098	1.7E-20	DOWN	iSPNs	D2cKO
Rasgef1b	0.314	0.908	0.8	0.0E+00	DOWN	dSPNs	DDcKO
Rasgrf1	-0.415	0.472	0.585	5.1E-20	UP	dSPN	D1cKO
Rasgrf1	-0.348	0.472	0.627	2.0E-35	UP	dSPNs	DDcKO
Rassf8	0.336	0.451	0.283	1.7E-134	DOWN	dSPNs	DDcKO
Rbm4b	0.368	0.626	0.446	6.1E-192	DOWN	dSPNs	DDcKO
Rbms1	0.382	0.644	0.472	9.6E-190	DOWN	dSPNs	DDcKO

Gene	Avg_logFC	pct.1_CTL	pct.2_cKO	P_val_adj	Regulation	Cell-type	Sample
Rbms1	0.425	0.67	0.427	5.2E-95	DOWN	iSPNs	DDcKO
Rbms1	0.363	0.67	0.406	2.1E-47	DOWN	iSPNs	D2cKO
Reln	0.431	0.87	0.685	0.0E+00	DOWN	dSPNs	DDcKO
Reln	0.470	0.649	0.337	1.1E-143	DOWN	iSPNs	DDcKO
Reln	0.468	0.649	0.33	2.4E-70	DOWN	iSPNs	D2cKO
Rgs2	0.312	0.495	0.285	7.3E-34	DOWN	iSPNs	D2cKO
Rgs4	-0.385	0.319	0.432	1.7E-39	UP	dSPNs	DDcKO
Rgs9	0.501	0.693	0.425	4.5E-250	DOWN	dSPN	D1cKO
Rgs9	0.454	0.693	0.508	1.7E-291	DOWN	dSPNs	DDcKO
Rgs9	0.670	0.675	0.339	1.9E-191	DOWN	iSPNs	DDcKO
Rgs9	0.694	0.675	0.282	1.1E-73	DOWN	iSPNs	D2cKO
Robo2	0.403	0.984	0.808	0.0E+00	DOWN	iSPNs	DDcKO
Robo2	0.392	0.984	0.786	0.0E+00	DOWN	iSPNs	D2cKO
Rora	0.305	0.894	0.816	0.0E+00	DOWN	dSPNs	DDcKO
Rora	0.509	0.884	0.68	1.9E-296	DOWN	iSPNs	DDcKO
Rora	0.473	0.884	0.64	4.2E-148	DOWN	iSPNs	D2cKO
RP23-35N23.2	0.350	0.648	0.442	4.2E-75	DOWN	iSPNs	DDcKO
RP23-35N23.2	0.348	0.648	0.421	5.4E-33	DOWN	iSPNs	D2cKO
RP24-134N2.1	0.370	0.228	0.043	2.0E-52	DOWN	iSPNs	DDcKO
RP24-134N2.1	0.300	0.228	0.073	9.0E-17	DOWN	iSPNs	D2cKO
RP24-175N4.1	-0.361	0.248	0.321	1.3E-16	UP	dSPN	D1cKO
RP24-175N4.1	-0.559	0.248	0.487	2.7E-100	UP	dSPNs	DDcKO
RP24-175N4.1	-0.453	0.325	0.464	1.7E-22	UP	iSPNs	DDcKO
Rpl34	0.320	0.765	0.614	6.5E-256	DOWN	iSPNs	D1cKO
Rpl35	0.384	0.618	0.432	1.1E-276	DOWN	dSPN	D1cKO
Rpl35	0.324	0.692	0.504	1.1E-65	DOWN	iSPNs	D2cKO
Rpl35	0.462	0.692	0.462	2.4E-261	DOWN	iSPNs	D1cKO
Rpl35a	0.342	0.764	0.587	5.7E-266	DOWN	iSPNs	D1cKO
Rpl36	0.321	0.768	0.588	9.5E-230	DOWN	iSPNs	D1cKO
Rpl37	0.414	0.745	0.57	0.0E+00	DOWN	dSPN	D1cKO
Rpl37	0.545	0.821	0.62	0.0E+00	DOWN	iSPNs	D1cKO
Rpl37a	0.332	0.782	0.624	0.0E+00	DOWN	dSPN	D1cKO
Rpl37a	0.513	0.84	0.675	0.0E+00	DOWN	iSPNs	D1cKO
Rpl38	0.399	0.69	0.47	0.0E+00	DOWN	dSPN	D1cKO
Rpl38	0.357	0.747	0.584	2.6E-98	DOWN	iSPNs	D2cKO
Rpl38	0.520	0.747	0.518	0.0E+00	DOWN	iSPNs	D1cKO
Rpl41	0.469	0.945	0.864	0.0E+00	DOWN	dSPN	D1cKO
Rpl41	0.613	0.974	0.878	0.0E+00	DOWN	iSPNs	D1cKO

Gene	Avg_logFC	pct.1_CTL	pct.2_cKO	P_val_adj	Regulation	Cell-type	Sample
Rplp0	0.307	0.918	0.767	0.0E+00	DOWN	iSPNs	D1cKO
Rprml	0.408	0.493	0.251	9.6E-72	DOWN	iSPNs	DDcKO
Rprml	0.440	0.493	0.247	4.1E-40	DOWN	iSPNs	D2cKO
Rps26	0.376	0.747	0.582	3.5E-264	DOWN	iSPNs	D1cKO
Rps27	0.479	0.873	0.698	0.0E+00	DOWN	dSPN	D1cKO
Rps27	0.601	0.885	0.724	0.0E+00	DOWN	iSPNs	D1cKO
Rps28	0.311	0.522	0.334	2.9E-176	DOWN	dSPN	D1cKO
Rps28	0.319	0.59	0.401	5.6E-140	DOWN	iSPNs	D1cKO
Rps29	0.314	0.678	0.532	0.0E+00	DOWN	dSPN	D1cKO
Rps29	0.442	0.78	0.573	3.0E-302	DOWN	iSPNs	D1cKO
Rps6	0.326	0.258	0.108	1.9E-142	DOWN	dSPN	D1cKO
Rps6	0.509	0.336	0.171	9.9E-60	DOWN	iSPNs	D2cKO
Rps6	0.322	0.258	0.179	1.8E-126	DOWN	dSPNs	D2cKO
Rps6	0.556	0.336	0.121	2.0E-144	DOWN	iSPNs	D1cKO
Rps6ka5	0.318	0.642	0.511	5.4E-135	DOWN	dSPNs	DDcKO
Rps6ka5	0.304	0.54	0.327	7.1E-23	DOWN	iSPNs	D2cKO
Rxrg	0.329	0.744	0.505	2.5E-86	DOWN	iSPNs	DDcKO
Ryr3	0.359	0.961	0.881	0.0E+00	DOWN	dSPNs	DDcKO
Ryr3	0.838	0.941	0.656	0.0E+00	DOWN	iSPNs	DDcKO
Ryr3	0.791	0.941	0.688	0.0E+00	DOWN	iSPNs	D2cKO
Scg2	-0.328	0.295	0.391	1.5E-03	UP	dSPN	D1cKO
Scmh1	0.322	0.91	0.791	4.7E-186	DOWN	iSPNs	DDcKO
Scmh1	0.301	0.91	0.78	1.7E-243	DOWN	iSPNs	D1cKO
Scml4	-0.361	0.047	0.161	1.3E-06	UP	iSPNs	D2cKO
Scn4b	0.350	0.26	0.093	1.3E-43	DOWN	iSPNs	DDcKO
Scn4b	0.395	0.26	0.073	5.1E-20	DOWN	iSPNs	D2cKO
Scn8a	0.338	0.721	0.475	2.5E-67	DOWN	iSPNs	DDcKO
Scn9a	0.380	0.583	0.388	4.9E-185	DOWN	dSPN	D1cKO
Scn9a	0.694	0.583	0.326	0.0E+00	DOWN	dSPNs	DDcKO
Scn9a	0.373	0.583	0.462	1.5E-94	DOWN	dSPNs	D2cKO
Sema3a	0.376	0.439	0.258	1.9E-138	DOWN	dSPNs	DDcKO
Sema3e	0.542	0.502	0.217	5.5E-94	DOWN	iSPNs	DDcKO
Sema3e	0.305	0.502	0.282	1.2E-26	DOWN	iSPNs	D2cKO
Sema5b	-0.379	0.178	0.179	6.1E-09	UP	iSPNs	D2cKO
Sepw1	-0.300	0.787	0.823	1.3E-38	UP	dSPNs	DDcKO
Sepw1	0.492	0.853	0.673	3.6E-165	DOWN	iSPNs	D2cKO
Sepw1	0.326	0.853	0.712	0.0E+00	DOWN	iSPNs	D1cKO
Serf1	-0.335	0.316	0.405	3.6E-04	UP	iSPNs	DDcKO

Gene	Avg_logFC	pct.1_CTL	pct.2_cKO	P_val_adj	Regulation	Cell-type	Sample
Serpine2	0.397	0.623	0.372	1.2E-55	DOWN	iSPNs	DDcKO
Serpine2	0.506	0.623	0.34	8.6E-64	DOWN	iSPNs	D2cKO
Serpini1	-0.467	0.224	0.336	1.8E-32	UP	dSPN	D1cKO
Serpini1	-0.329	0.224	0.371	6.2E-44	UP	dSPNs	DDcKO
Sez6l	-0.475	0.078	0.268	3.2E-29	UP	iSPNs	DDcKO
Sez6l	-0.550	0.078	0.275	2.6E-20	UP	iSPNs	D2cKO
Sfxn1	-0.334	0.364	0.41	2.2E-11	UP	dSPN	D1cKO
Sfxn1	-1.815	0.364	0.751	0.0E+00	UP	dSPNs	DDcKO
Sfxn1	-1.388	0.217	0.594	2.2E-247	UP	iSPNs	DDcKO
Sgcd	-0.527	0.772	0.814	1.3E-03	UP	iSPNs	D2cKO
Sgcz	0.680	0.969	0.866	0.0E+00	DOWN	iSPNs	DDcKO
Sgcz	0.728	0.969	0.844	0.0E+00	DOWN	iSPNs	D2cKO
Sik2	0.389	0.642	0.412	1.9E-100	DOWN	iSPNs	DDcKO
Sil1	0.306	0.426	0.219	4.3E-27	DOWN	iSPNs	D2cKO
Six3	-0.438	0.304	0.387	1.9E-25	UP	iSPNs	DDcKO
Six3	-0.429	0.304	0.355	9.4E-07	UP	iSPNs	D2cKO
Skap1	-0.303	0.159	0.231	2.8E-07	UP	dSPN	D1cKO
Skil	0.300	0.432	0.267	2.2E-23	DOWN	iSPNs	D2cKO
Slc1a3	-0.410	0.254	0.289	2.0E-33	UP	iSPNs	DDcKO
Slc24a2	0.438	0.691	0.514	0.0E+00	DOWN	dSPNs	DDcKO
Slc24a2	0.505	0.724	0.52	4.2E-188	DOWN	iSPNs	DDcKO
Slc25a4	-0.382	0.512	0.66	7.7E-43	UP	dSPNs	DDcKO
Slc26a8	-0.512	0.384	0.586	3.7E-100	UP	dSPNs	DDcKO
Slc26a8	-0.441	0.508	0.582	1.2E-21	UP	iSPNs	DDcKO
Slc26a8	0.481	0.508	0.257	1.5E-77	DOWN	iSPNs	D2cKO
Slc26a8	0.359	0.384	0.294	1.7E-133	DOWN	dSPNs	D2cKO
Slc26a8	0.373	0.508	0.36	7.1E-127	DOWN	iSPNs	D1cKO
Slc35f1	-0.625	0.692	0.821	3.9E-62	UP	dSPN	D1cKO
Slc35f1	-0.487	0.692	0.836	3.9E-108	UP	dSPNs	DDcKO
Slc35f1	-0.603	0.731	0.847	5.8E-44	UP	iSPNs	DDcKO
Slc35f1	-0.710	0.731	0.849	8.7E-26	UP	iSPNs	D2cKO
Slc35f4	-0.393	0.314	0.412	1.5E-28	UP	dSPN	D1cKO
Slc35f4	-0.515	0.314	0.531	1.1E-87	UP	dSPNs	DDcKO
Slc35f4	-0.435	0.226	0.392	1.8E-19	UP	iSPNs	DDcKO
Slc35f4	-0.429	0.226	0.401	2.4E-05	UP	iSPNs	D2cKO
Slc4a4	0.395	0.774	0.6	1.2E-250	DOWN	dSPNs	DDcKO
Slc4a4	0.590	0.752	0.409	2.3E-149	DOWN	iSPNs	DDcKO
Slc4a4	0.758	0.752	0.32	6.4E-108	DOWN	iSPNs	D2cKO

Gene	Avg_logFC	pct.1_CTL	pct.2_cKO	P_val_adj	Regulation	Cell-type	Sample
Slc8a1	-0.443	0.588	0.685	2.2E-08	UP	dSPN	D1cKO
Slc8a1	-0.549	0.577	0.761	1.8E-27	UP	iSPNs	DDcKO
Slc8a1	-0.617	0.577	0.746	4.6E-09	UP	iSPNs	D2cKO
Slc9a9	-0.314	0.116	0.208	3.2E-09	UP	iSPNs	DDcKO
Smarca2	-0.347	0.402	0.567	1.3E-35	UP	dSPNs	DDcKO
Smarca2	-0.460	0.489	0.611	8.2E-16	UP	iSPNs	DDcKO
Smpd3	0.438	0.899	0.699	1.7E-192	DOWN	iSPNs	DDcKO
Smyd3	0.311	0.63	0.406	7.5E-37	DOWN	iSPNs	D2cKO
Snap91	-0.303	0.536	0.672	2.3E-23	UP	dSPNs	DDcKO
Snap91	-0.356	0.52	0.608	3.9E-10	UP	iSPNs	DDcKO
Snca	0.318	0.868	0.682	4.9E-162	DOWN	iSPNs	DDcKO
Snca	0.312	0.868	0.71	5.3E-107	DOWN	iSPNs	D2cKO
Sntb2	0.319	0.292	0.123	1.9E-32	DOWN	iSPNs	DDcKO
Sobp	-0.361	0.382	0.513	1.1E-10	UP	iSPNs	DDcKO
Sox11	-0.421	0.583	0.621	1.2E-18	UP	iSPNs	DDcKO
Sox11	-0.414	0.583	0.582	3.0E-08	UP	iSPNs	D2cKO
Sox11	0.480	0.583	0.418	0.0E+00	DOWN	iSPNs	D1cKO
Sox2	-0.326	0.179	0.284	2.7E-13	UP	iSPNs	DDcKO
Sox4	-0.348	0.464	0.537	3.7E-10	UP	iSPNs	DDcKO
Sox4	0.325	0.464	0.348	8.9E-174	DOWN	iSPNs	D1cKO
Sphkap	-0.328	0.106	0.218	1.0E-13	UP	iSPNs	DDcKO
Sphkap	-0.486	0.106	0.247	6.3E-18	UP	iSPNs	D2cKO
Spock3	0.349	0.914	0.785	0.0E+00	DOWN	dSPN	D1cKO
Spock3	0.485	0.914	0.796	0.0E+00	DOWN	dSPNs	DDcKO
Spock3	0.888	0.919	0.615	0.0E+00	DOWN	iSPNs	DDcKO
Spock3	0.879	0.919	0.612	0.0E+00	DOWN	iSPNs	D2cKO
Srgap1	0.305	0.827	0.71	7.0E-203	DOWN	dSPNs	DDcKO
Srpk1	0.384	0.786	0.603	2.7E-244	DOWN	dSPNs	DDcKO
Srpk1	0.424	0.811	0.57	5.5E-150	DOWN	iSPNs	DDcKO
Srpk1	0.705	0.811	0.481	8.7E-218	DOWN	iSPNs	D2cKO
Srpk1	0.719	0.786	0.538	0.0E+00	DOWN	dSPNs	D2cKO
Srpk1	0.347	0.811	0.644	2.2E-296	DOWN	iSPNs	D1cKO
Stk32a	0.519	0.396	0.117	6.3E-85	DOWN	iSPNs	DDcKO
Stk32a	0.471	0.396	0.113	6.6E-37	DOWN	iSPNs	D2cKO
Stmn1	-0.426	0.443	0.575	3.3E-03	UP	iSPNs	DDcKO
Stmn1	-0.801	0.443	0.655	3.0E-22	UP	iSPNs	D2cKO
Stmn2	-0.370	0.628	0.731	1.5E-08	UP	iSPNs	DDcKO
Stmn2	-0.649	0.628	0.761	7.0E-19	UP	iSPNs	D2cKO

Gene	Avg_logFC	pct.1_CTL	pct.2_cKO	P_val_adj	Regulation	Cell-type	Sample
Stmn3	-0.525	0.843	0.861	5.3E-05	UP	iSPNs	D2cKO
Stmn4	-0.642	0.554	0.655	6.6E-17	UP	iSPNs	D2cKO
Strip2	0.326	0.609	0.409	3.3E-63	DOWN	iSPNs	DDcKO
Strip2	0.498	0.609	0.327	9.0E-57	DOWN	iSPNs	D2cKO
Strn	0.326	0.566	0.425	6.5E-130	DOWN	dSPNs	DDcKO
Strn	0.495	0.518	0.281	1.3E-92	DOWN	iSPNs	DDcKO
Strn	0.376	0.518	0.29	5.9E-30	DOWN	iSPNs	D2cKO
Stxbp6	-0.307	0.271	0.432	7.5E-17	UP	dSPNs	DDcKO
Sv2c	0.391	0.604	0.349	1.6E-90	DOWN	iSPNs	DDcKO
Sv2c	0.458	0.604	0.295	3.2E-46	DOWN	iSPNs	D2cKO
Svbp	-0.312	0.301	0.399	3.6E-06	UP	iSPNs	DDcKO
Sybu	0.444	0.814	0.619	2.3E-170	DOWN	iSPNs	DDcKO
Sybu	0.361	0.814	0.612	2.0E-77	DOWN	iSPNs	D2cKO
Synpr	0.316	0.629	0.519	6.6E-189	DOWN	dSPNs	DDcKO
Synpr	0.564	0.656	0.44	9.3E-207	DOWN	iSPNs	DDcKO
Synpr	0.529	0.656	0.408	1.1E-122	DOWN	iSPNs	D2cKO
Syt1	-0.381	0.977	0.985	4.0E-07	UP	dSPN	D1cKO
Syt1	-0.362	0.977	0.985	4.4E-137	UP	dSPNs	DDcKO
Syt1	-0.326	0.987	0.965	2.9E-05	UP	iSPNs	DDcKO
Syt4	0.334	0.63	0.416	4.0E-34	DOWN	iSPNs	D2cKO
Tac1	-0.349	0.822	0.827	2.7E-02	UP	dSPN	D1cKO
Tac1	-0.699	0.175	0.324	1.3E-81	UP	iSPNs	DDcKO
Tac1	-0.787	0.175	0.252	1.4E-33	UP	iSPNs	D2cKO
Tcerg1l	-0.347	0.059	0.154	2.3E-28	UP	dSPN	D1cKO
Tcerg1l	-0.335	0.059	0.199	1.8E-54	UP	dSPNs	DDcKO
Tcerg1l	-0.562	0.079	0.264	5.3E-45	UP	iSPNs	DDcKO
Tcerg1l	-0.473	0.079	0.224	6.4E-26	UP	iSPNs	D2cKO
Tenm2	0.516	0.98	0.906	0.0E+00	DOWN	dSPNs	DDcKO
Tgfa	0.460	0.797	0.529	1.4E-161	DOWN	iSPNs	DDcKO
Tgfa	0.400	0.797	0.504	1.1E-67	DOWN	iSPNs	D2cKO
Thrb	0.318	0.802	0.585	1.2E-106	DOWN	iSPNs	DDcKO
Thsd7a	0.338	0.791	0.558	1.5E-151	DOWN	iSPNs	DDcKO
Thsd7a	0.504	0.791	0.491	6.8E-119	DOWN	iSPNs	D2cKO
Thsd7b	-1.414	0.099	0.56	0.0E+00	UP	dSPNs	DDcKO
Thsd7b	-0.831	0.162	0.455	1.6E-102	UP	iSPNs	DDcKO
Thsd7b	-0.705	0.162	0.365	1.1E-23	UP	iSPNs	D2cKO
Timp2	-0.452	0.463	0.531	9.6E-10	UP	iSPNs	D2cKO
Tmem108	-0.529	0.116	0.237	3.2E-22	UP	iSPNs	DDcKO

Gene	Avg_logFC	pct.1_CTL	pct.2_cKO	P_val_adj	Regulation	Cell-type	Sample
Tmem108	-0.758	0.116	0.234	9.7E-14	UP	iSPNs	D2cKO
Tmem132d	-0.313	0.119	0.206	5.5E-05	UP	iSPNs	DDcKO
Tmem158	0.349	0.891	0.801	0.0E+00	DOWN	dSPNs	DDcKO
Tmem158	0.436	0.815	0.581	4.4E-167	DOWN	iSPNs	DDcKO
Tmem178	-0.317	0.122	0.204	7.7E-03	UP	iSPNs	D2cKO
Tmsb10	0.402	0.856	0.765	0.0E+00	DOWN	dSPN	D1cKO
Tmsb10	-0.317	0.912	0.858	1.1E-04	UP	iSPNs	DDcKO
Tmsb10	0.508	0.912	0.778	0.0E+00	DOWN	iSPNs	D1cKO
Tox	-0.453	0.126	0.242	6.1E-24	UP	iSPNs	DDcKO
Tox	-0.563	0.126	0.229	1.1E-07	UP	iSPNs	D2cKO
Tpm1	0.375	0.502	0.285	2.0E-36	DOWN	iSPNs	D2cKO
Trpc3	-0.318	0.035	0.101	1.6E-05	UP	iSPNs	D2cKO
Trpc4	-0.336	0.119	0.176	3.1E-02	UP	iSPNs	D2cKO
Trpm3	0.378	0.825	0.626	3.6E-176	DOWN	iSPNs	DDcKO
Trps1	0.387	0.621	0.418	5.4E-49	DOWN	iSPNs	D2cKO
Tshz1	-0.341	0.237	0.297	6.2E-47	UP	dSPNs	DDcKO
Tshz1	-0.466	0.276	0.324	6.8E-36	UP	iSPNs	DDcKO
Tshz2	-0.334	0.183	0.232	2.7E-03	UP	dSPN	D1cKO
Tshz2	-0.447	0.183	0.328	9.0E-63	UP	dSPNs	DDcKO
Tshz2	-0.609	0.231	0.388	2.6E-33	UP	iSPNs	DDcKO
Tubb5	-0.354	0.656	0.704	1.9E-06	UP	iSPNs	DDcKO
Unc5d	-0.668	0.088	0.197	2.2E-40	UP	dSPN	D1cKO
Unc5d	-0.817	0.088	0.276	1.2E-186	UP	dSPNs	DDcKO
Unc5d	-1.314	0.504	0.757	0.0E+00	UP	iSPNs	DDcKO
Unc5d	-1.507	0.504	0.766	0.0E+00	UP	iSPNs	D2cKO
Utrn	0.351	0.648	0.429	2.7E-90	DOWN	iSPNs	DDcKO
Utrn	0.420	0.648	0.38	2.5E-46	DOWN	iSPNs	D2cKO
Vamp2	-0.357	0.425	0.585	2.3E-42	UP	dSPNs	DDcKO
Vcan	0.421	0.441	0.26	1.1E-154	DOWN	dSPNs	DDcKO
Vcan	0.352	0.465	0.289	3.6E-52	DOWN	iSPNs	DDcKO
Vcan	0.340	0.465	0.285	4.1E-35	DOWN	iSPNs	D2cKO
Vcan	0.340	0.441	0.307	1.0E-50	DOWN	dSPNs	D2cKO
Vcan	0.340	0.465	0.259	1.4E-116	DOWN	iSPNs	D1cKO
Vsnl1	-0.378	0.291	0.401	5.7E-05	UP	iSPNs	D2cKO
Vstm2a	-0.438	0.339	0.489	1.5E-24	UP	iSPNs	DDcKO
Vstm2a	-0.485	0.339	0.499	1.0E-10	UP	iSPNs	D2cKO
Vwc2l	-0.486	0.057	0.2	1.3E-26	UP	iSPNs	DDcKO
Vwc2l	-0.501	0.057	0.207	3.9E-28	UP	iSPNs	D2cKO

Gene	Avg_logFC	pct.1_CTL	pct.2_cKO	P_val_adj	Regulation	Cell-type	Sample
Wbscr17	0.448	0.572	0.402	1.2E-291	DOWN	dSPNs	DDcKO
Wbscr17	0.652	0.824	0.529	0.0E+00	DOWN	iSPNs	DDcKO
Wbscr17	0.585	0.824	0.537	2.3E-145	DOWN	iSPNs	D2cKO
Ywhag	-0.415	0.479	0.657	1.9E-77	UP	dSPNs	DDcKO
Ywhag	-0.304	0.559	0.618	1.1E-10	UP	iSPNs	DDcKO
Ywhaz	-0.460	0.456	0.657	6.4E-84	UP	dSPNs	DDcKO
Zbtb20	-0.311	0.898	0.919	2.2E-38	UP	dSPN	D1cKO
Zc3h12c	0.318	0.435	0.303	5.0E-85	DOWN	dSPNs	DDcKO
Zc3h12c	0.339	0.495	0.264	2.7E-51	DOWN	iSPNs	DDcKO
Zc3h12c	0.307	0.495	0.27	2.4E-31	DOWN	iSPNs	D2cKO
Zdbf2	-0.471	0.313	0.484	1.2E-60	UP	dSPNs	DDcKO
Zdbf2	-0.866	0.364	0.565	1.1E-81	UP	iSPNs	DDcKO
Zdbf2	-0.547	0.364	0.484	1.9E-11	UP	iSPNs	D2cKO
Zeb1	0.301	0.775	0.539	3.4E-74	DOWN	iSPNs	D2cKO
Zfp385b	0.314	0.829	0.701	1.7E-255	DOWN	dSPNs	DDcKO
Zfp385b	0.313	0.815	0.649	3.1E-141	DOWN	iSPNs	DDcKO
Zfp462	0.344	0.499	0.262	8.5E-37	DOWN	iSPNs	D2cKO
Zfp804b	-0.608	0.076	0.233	3.0E-63	UP	iSPNs	DDcKO
Zfp804b	-0.629	0.076	0.202	3.1E-44	UP	iSPNs	D2cKO
Zfyve28	0.321	0.399	0.21	9.0E-38	DOWN	iSPNs	DDcKO
Zwint	-0.332	0.392	0.546	6.9E-40	UP	dSPNs	DDcKO

CHAPTER 4: FURTHER CHARACTERIZATION OF STRIATAL *FOXP1 cKO* MICE AND RESCUE EXPERIMENTS

SUMMARY

In order to fully characterize the impact of *Foxp1* deletion in dSPNs and/or iSPNs in adult animals, I performed molecular experiments to examine the cellular composition of the striatum in *Foxp1^{D1}, Foxp1^{D2}, Foxp1^{DD},* and control animals. Since individuals with *FOXP1* mutations have mild to moderate intellectual disability and ASD features, I also performed clinically-relevant behaviors to test spatial-learning, social interaction, and grooming behaviors across *Foxp1 cKO* strains. Moreover, we tested striatal-dependent behavior, locomotor and sensitization response to cocaine. Given our findings that indirect pathway spiny projection neurons (iSPNs) are particularly vulnerable with deletion of *Foxp1*, I attempted to pharmacologically rescue one of the most striking behavioral deficits specific to *Foxp1^{D2}* cKO mice, the motor learning deficit on the accelerating rotarod, using drugs targeting the dopamine-2 receptor (D2R) system or pathways commonly associated with autism (e.g. mTOR signaling). However, no drugs tested in acute or chronic conditions rescued rotarod deficits in *Foxp1^{D2}* cKO mice. In tandem with pharmacological rescues, I also developed tools to eventually perform a genetic rescue in *Foxp1 cKO* mice by making a Cre-dependent, AAV construct overexpressing mouse Foxp1 tagged with V5. This construct could be used in future experiments to reintroduce Foxp1 into distinct cell-types in the brain.

INTRODUCTION

While the principal neurons of the adult rodent striatum are spiny projection neurons (SPNs), there are important interneuron subtypes that contribute significantly to

striatal circuitry. Interneurons of the striatum are aspiny and can be distinguished from SPNs under light microscopy by nuclear envelope indentations that are absent from SPNs. A study quantifying striatal SPNs and interneurons based on this morphological feature found that aspiny neurons composed 4-5% of the total cellular population in the rodent striatum, compared to 23% in the primate striatum (Graveland et al.). The major interneuron subtypes express unique molecular markers, including choline acetyl-transferase ($ChAT^+$), parvalbumin (PV^+), calretinin (CR^+), somatostatin (SST^+), neuropeptide Y (NPY^+), and nitric-oxide synthase (NOS^+) (Tepper et al., 2018). However, the diversity of striatal interneurons is still being elucidated and even major interneuron populations have not been thoroughly characterized. For example, the electrophysiological properties of striatal calretinin interneurons still remain unknown (Tepper et al., 2018). Striatal interneurons contribute significant GABAergic tone onto SPNs exerting powerful inhibitory control of the SPN activity. While far fewer in number, one PV^+ fast-spiking interneuron likely innervates over one hundred SPNs (Koós and Tepper, 1999). Disruption of local inhibitory regulation provided by interneurons is disrupted in neurodevelopment disorders such as Tourette's and ASD (Rapanelli et al., 2017).

Currently, there are two FDA-approved drugs for the treatment of ASD, aripiprazole and risperidone. Both atypical antipsychotic medications interact with the dopaminergic system primarily via D2 receptors. Given the reduction of iSPN with loss of Foxp1, we hypothesized that targeting D2R signaling pathways pharmacologically might rescue behaviors specific to *Foxp1*^{D2} mice. Data gathered from *Foxp1*^{D2} mice in collaboration with Jay Gibson's lab has shown these iSPNs to be hyperexcitable, similar

to the phenotype seen in Foxp1 heterozygous mice (**Figure 2.3**). With the possibility of either over (hyperexcitability of remaining iSPNs) or under-activation (loss of iSPNs) of the D2Rs, we tested both agonists (cabergoline, aripiprazole) and antagonists (haloperidol) in rescue paradigms. We also hypothesized that overactivation of the D1R pathway might occur with the loss of iSPNs and therefore tested whether a D1R antagonist (SCH23390) could rescue behaviors in *Foxp1*^{D2} mice. Additionally, we found that components of the mTOR pathway, such as *Rasd2*, were downregulated by loss of Foxp1 specifically in iSPNs within our scRNA-seq data (**Table 3.2**). Rasd2, also known as Rhes, represses the mTOR signaling pathway. This suggests that loss of *Foxp1* might over-activate the mTOR pathway in D2R neurons. Therefore, we tested whether rapamycin, an mTOR pathway inhibitor drug, might also rescue motor-learning behaviors in *Foxp1*^{D2} mice. The purpose of this chapter is to further examine the molecular and behavioral contribution of Foxp1 to striatal function in adult animals and test pharmaceutical interventions.

RESULTS

Loss of Darpp32^{+} SPNs in *Foxp1*^{D2} adult mice

A previous study examining embryonic Foxp1 KO and HET striatal cells in culture found a reduction in Darpp32^{+} cells, a marker of mature SPNs. There was no evidence of cell-death as these cells still expressed beta-tubulin, an immature neuronal marker, and no change in total cell number was observed *in vitro* (Precious et al., 2016). Therefore, to begin characterizing striatal *Foxp1 cKO* mice, I analyzed striatal SPN expression of Darpp32 and pan-neuronal marker, NeuN (*Rbfox3*). Using

immunohistochemistry, I quantified the number of Darpp32^{+} and NeuN^{+} cells within the dorsomedial, dorsolateral, and ventral striatum over a given area. There was a selective decrease in Darpp32^{+} neurons within the striatum of *Foxp1^{D2}* and *Foxp1^{DD}* mice, compared to *Foxp1^{D1}* animals. I also found that NeuN^{+} neurons were selectively reduced in *Foxp1^{D2}* mice. These findings are in line with my postnatal scRNA-seq results that show a selective decrease of Darpp32 expression in iSPNs (not dSPNs) and the significant reduction of the iSPN population with deletion of *Foxp1* (**Figure 3.2** and **Supplemental Figure 3.3**). The decrease in NeuN^{+} cells suggests there are fewer neurons in general within *Foxp1^{D2}* mice and the smaller striatal area of *Foxp1^{D2}* animals indicates that neurodegeneration might occur in *Foxp1^{D2}* mice (**Figure 3.5**). While I did not detect an increase in the apoptotic marker cleaved-caspase 3 (**Figure 4.2A**), I have not yet characterized embryonic timepoints when Cre turns on and could be missing the precise timing of apoptosis. In addition, there are other caspase-independent mechanisms of cell death, such as passive necrosis, where accumulation of reactive oxygen species and calcium in the cytoplasm causes whole-cell swelling and loss of plasma membrane integrity leading to eventual dissolution of the cell. In whole striatal RNA samples from *Foxp1 cKO* mice, there is a significant reduction of glutathione peroxidase 6 (*Gpx6*) at adult timepoints across genotypes (**Figure 4.2B)**. Glutathione peroxidases are important for neutralizing reactive oxygen species in the cell. A decrease in *Gpx6* levels has been reported in the striatum of Huntington mouse models and knockdown of *Gpx6* within the mouse striatum neurons results in cell death (Shema et al., 2015). Additionally, soma size is significantly larger with loss of *Foxp1* in iSPNs (**Figure 4.2C**). Taken together, these

observations indicate that molecular mechanisms of cell death might be occurring with deletion of Foxp1 specifically within iSPNs.

Changes in striatal neuronal composition driven by iSPN-specific loss of Foxp1

Next, I examined whether deletion of *Foxp1* in SPNs produced non-cell autonomous changes in striatal interneuron populations. By immunostaining for markers of the major interneuron subtypes (ChAT, PV, CR, SST, NPY, and NOS) (**Figure 4.3A-G**). The most striking finding was the increase in the number of CR^+ interneurons in the striatum of both $Foxp1^{D2}$ and $Foxp1^{DD}$ animals (**Figure 4.3A-B**). There was also a significant decrease in PV^+ neurons in animals (**Figure 4.3C**). I also found increases in NOS^+ in $Foxp1^{D2}$ sections (**Figure 4.3D**) and NPY^+ (**Figure 4.3E**) interneurons in $Foxp1^{DD}$ samples. Within the postnatal scRNA-seq data set, there is an increase (~1%) in total interneuron populations $Foxp1^{D2}$ and $Foxp1^{DD}$ samples compared to control and $Foxp1^{D1}$ samples (**Figure 3.1G-J**). However, calretinin and parvalbumin are not highly enriched in any cluster, likely because these interneuron populations express mature markers later in development. No changes were found in somatostatin or cholinergic interneuron populations (**Figure 4.3F-G**). To examine whether these changes in interneuron populations could be due to an increase in neurogenesis, which is known to occur along the lateral ventricles throughout development, I stained for the proliferation marker Ki67. There was an increase in $Ki67^+$ cells along the ventricles of $Foxp1^{DD}$ samples selectively (**Figure 4.3 H-I**), with no change in $Foxp1^{D2}$ mice. These results suggest that while there is an increase in proliferating neurons in $Foxp1^{DD}$ mice, this mechanism might not explain the increase of CR+ interneurons in both $Foxp1^{D2}$ and $Foxp1^{DD}$ samples.

Further behavioral characterization of striatal *Foxp1 cKO* mice

Foxp1 cKO mice also underwent a battery of additional behavior tests not discussed in Chapter 3. There was no difference in weight across adult *Foxp1 cKO* mice, either male or female, and no display of clasping behavior, a sign of neurodegeneration (**Figure 4.4**) (Araujo et al., 2017). In collaboration with Dr. Takahashi's lab, I examined the locomotor response to cocaine administration in all *Foxp1 cKO* mice, which is a heavily striatal-dependent behavioral response (**Figure 4.5A**). As additional controls, I also tested *D1-Cre* and *D2-Cre* heterozygous and wild-type animals in this paradigm (**Figure 4.5C-D**). *Foxp1*^{D2} mice had a significantly reduced locomotor response to cocaine compared to the controls. The decrease in locomotor response to cocaine was also observed 7-days later when the sensitization response to cocaine was measure (**Figure 4.5B**). All mice had a sensitization response, even *Foxp1*^{D2} mice, but the response was still significantly reduced compared to control animals.

To test spatial-learning, I performed the Morris water maze task on the *Foxp1 cKO* mice (**Figure 4.6**). While none of the strains exhibited a significant deficit in spatial memory on probe day evaluation, *Foxp1*^{DD} mice did show significant deficits in learning where the hidden platform was located over a 10-day training period. A caveat is that while control animals did learn above chance levels, they did not perform as well as other control animals tested from our lab in the same conditions (Araujo et al., 2017). Therefore, testing conditions might not have been optimal and further evaluation of spatial-memory might be necessary.

Foxp1 cKO mice were also tested for classical behaviors associated with ASD phenotypes, repetitive behaviors and social interaction. Foxp1 cKO mice did not exhibit

an increase in grooming behavior measured by time spent grooming **(Figure 4.7A**) or grooming bouts (**Figure 4.7B**). Additionally, no social interaction deficits were observed in *Foxp1 cKO* mice, as all groups preferred to spend time with the unfamiliar mouse (**Figure 4.7C**).

Rescue experiments performed in *Foxp1^{D2}* mice

Given the vulnerability of the indirect pathway to Foxp1 deletion, I tested whether two D2-agonists, aripiprazole and cabergoline, could rescue the motor-learning phenotypes seen in *Foxp1^{D2}* mice. For aripiprazole, I tried both an acute (30min before testing) and chronic administration (every day injections for 7-days prior to testing) of the drug before testing the mice on rotarod (**Figure 4.8**). No rescue effect was seen in either acute or chronic drug administration protocols by comparing *Foxp1^{D2}* mice that received the drug vs *Foxp1^{D2}* mice that received a vehicle injection. There was a significant difference between genotypes across all conditions. For cabergoline, I tested only acute conditions and found no change between drug and vehicle injected mice within either *Foxp1^{D2}* or control mice (**Figure 4.9A**). Additionally, I performed a chronic injection of D2-antagonist, haloperidol, over a 2-week period only for *Foxp1^{D2}* mice and found no difference between drug and vehicle administered groups (**Figure 4.9D**). Control animals were not used in this experiment. I also tested the D1-antagonist, SCH23390, in *Foxp1^{D2}* and control mice and still found a significant difference between genotypes; however, a vehicle control experiment was not performed (**Figure 4.9C**).

From our scRNA-seq data, I found that *Rasd2*, a repressor of the mTOR pathway, was significantly reduced in iSPNs with deletion of Foxp1. Rasd2 was also reduced in Foxp1$^{+/-}$ mice (**Chapter 2**, **Table 2.1**) and increased in human neural progenitors with

overexpression of Foxp1 (**Chapter 2**). Therefore, I tested a chronic administration of rapamycin over 7-weeks following a previous published protocol (Tsai et al., 2012) (**Figure 4.9D**). There was no rescue effect with rapamycin and vehicle groups in *Foxp1*^{D2} mice, but there was a significant difference between rapamycin and vehicle groups in control animals. A significant difference was also observed between genotypes in vehicle groups.

Other than pharmacological experiments, I wanted to know if reintroducing Foxp1 back into SPNs postnatally might rescue some behavioral phenotypes. Therefore, I cloned an AAV-Foxp1 overexpression constructs for *in vivo* viral injections into the striatum (**Figure 4.10A**). The construct is Cre-dependent to target either dSPNs or iSPNs within a given *Foxp1 cKO* strain. The Foxp1 overexpression vector is also tagged with V5 to discern Foxp1-construct expression vs endogenous Foxp1 expression. The Cre-dependency and tag of the construct are fully functional in 293T cells (**Figure 4.10B**); however, whether this construct can be successfully packaged and delivered in viral form still needs to be tested.

DISCUSSION

Changes in the cellular composition via iSPN-specific *Foxp1* deletion

Foxp1 is not expressed in interneuron populations (Precious et al., 2016). Therefore, the changes measured in interneuron populations is a non-cell autonomous effect of *Foxp1* deletion in iSPNs. The increase in the calretinin^{+} (CR+) interneurons is a particularly striking result. CR+ neurons do not co-localize with other interneuron subtypes and the properties of CR+ neurons have not been well characterized (Petryszyn et al., 2014). Morphologically, CR+ interneurons can be further categorized by cell-body

size and divided into small, medium, and large (measurements) subgroups. All subgroups have been identified across multiple species. Small CR+ neurons are more populous and exhibit a distinct expression pattern within the striatum concentrated near the subventricular zone (SVZ) and near the striatum-corpus callosal border (Petryszyn et al., 2014). Reports in mice have found that small CR+ neurons are generated postnatally between post-natal day 7-20 (Revishchin et al., 2010).

An increase in these interneurons could mean that Foxp1 indirectly enhances the neurogenesis of this subtype. Neurogenesis in the striatum has been reported in humans, primates, rabbits, and rodents. The most recent study using carbon-14 dating to examine striatal neurogenesis in humans showed that newly generated neurons from the SVZ are interneurons, some of which are CR+, and these cells can integrate into the striatum under normal conditions. These postnatally generated striatal interneurons also appeared selectively depleted in Huntington's disease (Ernst et al., 2014). However, an increase in CR+ interneurons has also been observed in other models of neurological disorders, including Huntington's and post-stroke brains, and are thought to be newborn neurons derived from the subventricular zone (SVZ) (Chapman et al., 2015; Yang et al., 2008). Another study found that administration of methylphenidate (MPD), used to treat children suffering from attention deficit disorder (ADHD), seems to specifically affect CR+ neurons within the medial septum (García-Avilés et al., 2015). Taken together, altered regulation of CR+ interneurons is a common finding across diverse neurological disorders.

Another interneuron population was increased with loss of Foxp1 in both SPN populations, neuropeptide-Y+ interneurons (NPY+). NPY+ interneurons have high input resistance and display low-threshold spiking and plateau potentials (PLTS) in response

to intracellular depolarization (Tepper et al., 2018). These interneurons also function in a neuromodulatory role via release of neuropeptides (Tepper et al., 2018). Additionally, a study of Foxp1 in the lung development found that loss of Foxp1 in lung epithelium induced ectopic expression of NPY.

Changes in the number of other interneuron subtypes were also observed with deletion of *Foxp1* in iSPNs. In particular, the decrease in parvalbumin (PV+) neurons could have an important effect on striatal circuitry and function. PV interneurons are GABAergic fast-spiking interneurons (FSI) and localize largely within the dorsal lateral striatum (DLS) (Berke, 2011). The DLS receives dense projections from the motor and sensorimotor cortex that input onto PV interneurons as well as SPNs. PV interneurons make hundreds of synapses onto surrounding SPNs, primarily onto the somatic region, where they can exert strong influence over SPN physiology. PV neurons also receive direct projections from a subpopulation of GPe neurons (Berke, 2011). Clinically, post-mortem studies of individuals with ASD found a significant decrease in PV neurons in the frontal cortex (Hashemi et al., 2017). In summary, the non-cell autonomous effects on interneuron populations with deletion of *Foxp1* in iSPNs could be an important mechanism underlying the behavioral deficits observed in these mice.

Discussion of behavior data

The locomotor response to cocaine behavior results for *Foxp1*^{D2} mice are similar to phenotypes seen in mice when D2R striatal neurons are ablated. Mice with D2R ablation have an increase in spontaneous activity, but reduced activity in response to DA stimulation (Sano et al., 2003). Ablation of D2R in another study again caused

hyperactivity, but enhanced amphetamine response to the conditioned place preference test (Durieux et al., 2009). Another study found that deletion of *Darpp32* from iSPNs, essentially disrupting downstream dopamine signaling for D2R activation, lead to an increase in hyperactivity and an increase locomotor response (Bateup et al., 2010). Deletion of *Darpp32* in dSPNs caused the opposite behaviors: a decrease in spontaneous activity and locomotor response to cocaine (Bateup et al., 2010). An interesting finding in my results is that loss of Foxp1 in both dSPNs and iSPNs (*Foxp1*^{DD} mice) did not change the locomotion response to cocaine, but mice were spontaneously hyperactive. In **Chapter 3**, I found that *Foxp1*^{DD} mice had a subtle rescue of the iSPN reduction, whereby there was a significant increase in the number of iSPNs compared to *Foxp1*^{D2} mice (**Figure 3.2I-J**). Moreover, we found that disruption of iSPNs with deletion of Foxp1 exerted a strong influence over gene expression changes in dSPNs with loss of Foxp1, termed an "interaction effect". This "interaction effect" is reflected in the increase in number DEGs in dSPNs of *Foxp1*^{DD} mice compared to DEGs in dSPNs of *Foxp1*^{D1} mice (81 vs 185, respectively). This suggests that in certain behaviors where *Foxp1*^{DD} mice do not exhibit similar deficits observed in single *Foxp1 cKO* strains (e.g., USV call production and locomotion response to cocaine) an interaction effect within dSPNs might elicit a compensatory response.

FIGURES

FIGURE 4.1. Decrease in Darpp32^{+} and NeuN^{+} cells in adult *Foxp1^{D2}* mice.

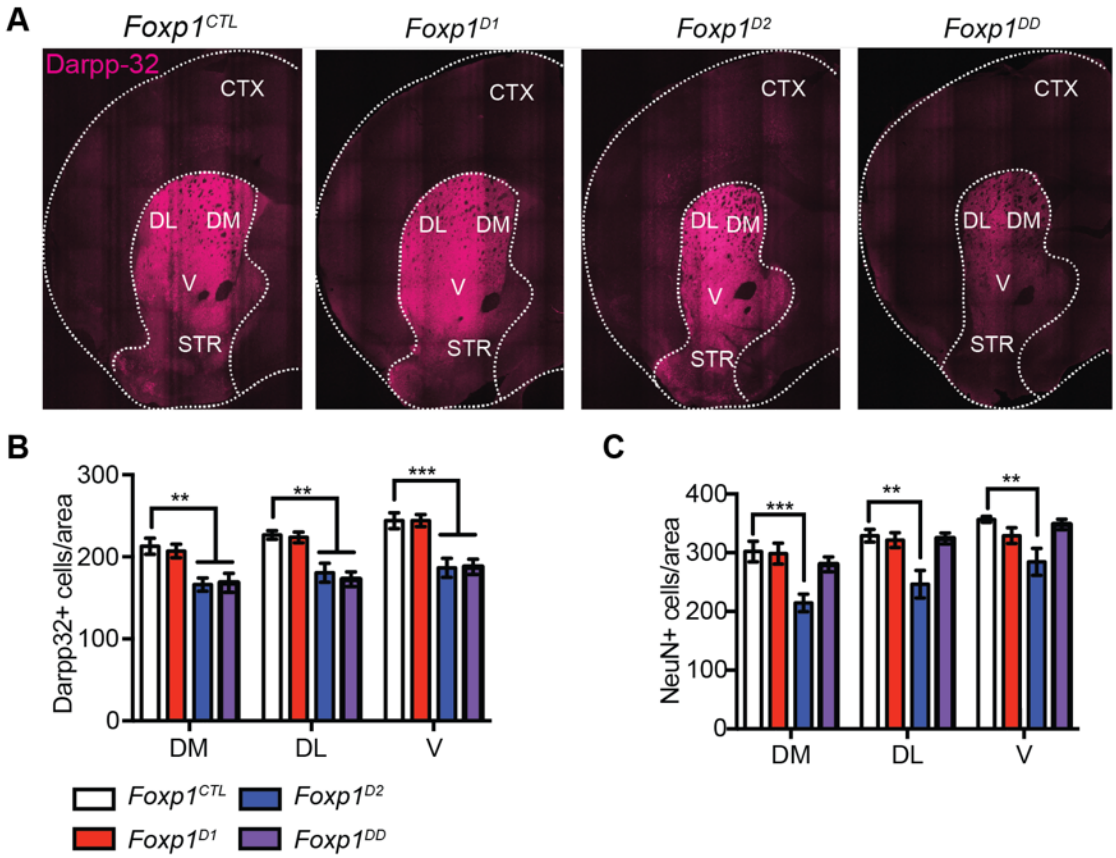

A) Immunohistochemistry for Darpp32 in the cortex and striatum of *Foxp1^{CTL}*, *Foxp1^{D1}* *Foxp1^{D2}*, and *Foxp1^{DD}* and quantification of the number of Darpp32 (B) or NeuN (C) expressing neurons in the dorsolateral (DL), dorsomedial (DM), and ventral (V) regions of the striatum. Data are represented as mean ± SEM with n=3-4 mice/genotype. **p<0.005, ***p<0.0001, two-way ANOVA with Tukey's multiple comparisons test.

FIGURE 4.2. Indirect evidence of cell death in *Foxp1^{D2} cKO* mice.

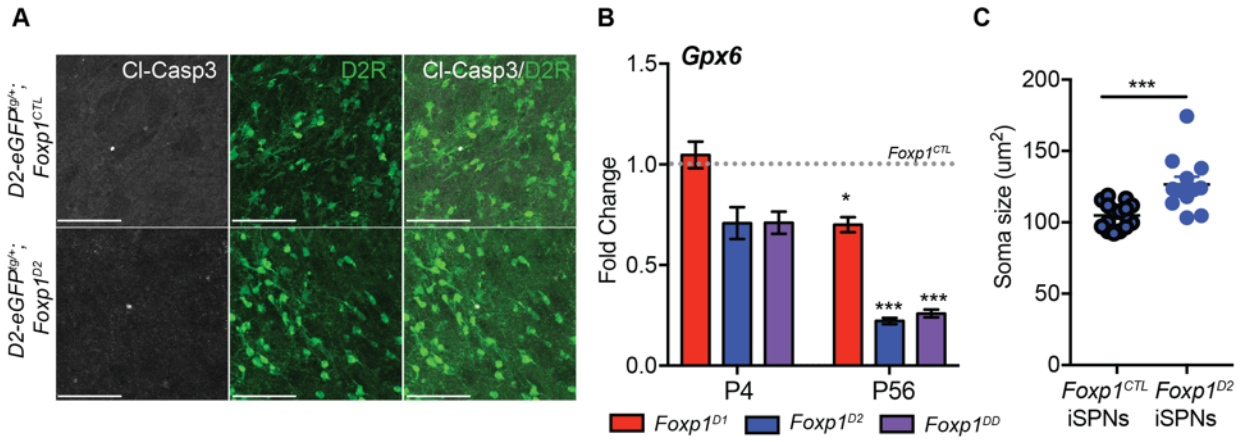

A) Postnatal day 7 staining for canonical apoptosis marker cleaved caspase-3 (Cl-Casp3, gray) in the striatum of *Foxp1^{CTL}* (upper panels) and *Foxp1^{D2}* (lower panels) mice crossed to *D2-eGFP$^{tg/+}$* mice to label iSPNs (green). 100um scale bar. **B**) Quantification of glutathione peroxidase 6 (*Gpx6*) transcript via qRT-PCR across *Foxp1 cKO* lines normalized to control levels at postnatal day 4 and 56. Data are represented as mean ± SEM with (N=3/genotype, 4 replicates/sample). *p<0.05, ***p<0.0001, Student's t-test, compared to control levels normalized to actin). **C**) Soma size area measurements in P7 D2-eGFP reporter mice crossed into *Foxp1^{CTL}* and *Foxp1^{D2}* mice. Data are represented as mean ± SEM (N_{cells}=10-12 cells/animal, N=3/genotype). ***p<0.0001, Student's t-test.

FIGURE 4.3. Changes in interneuron populations and proliferation driven by loss of *Foxp1* in iSPNs.

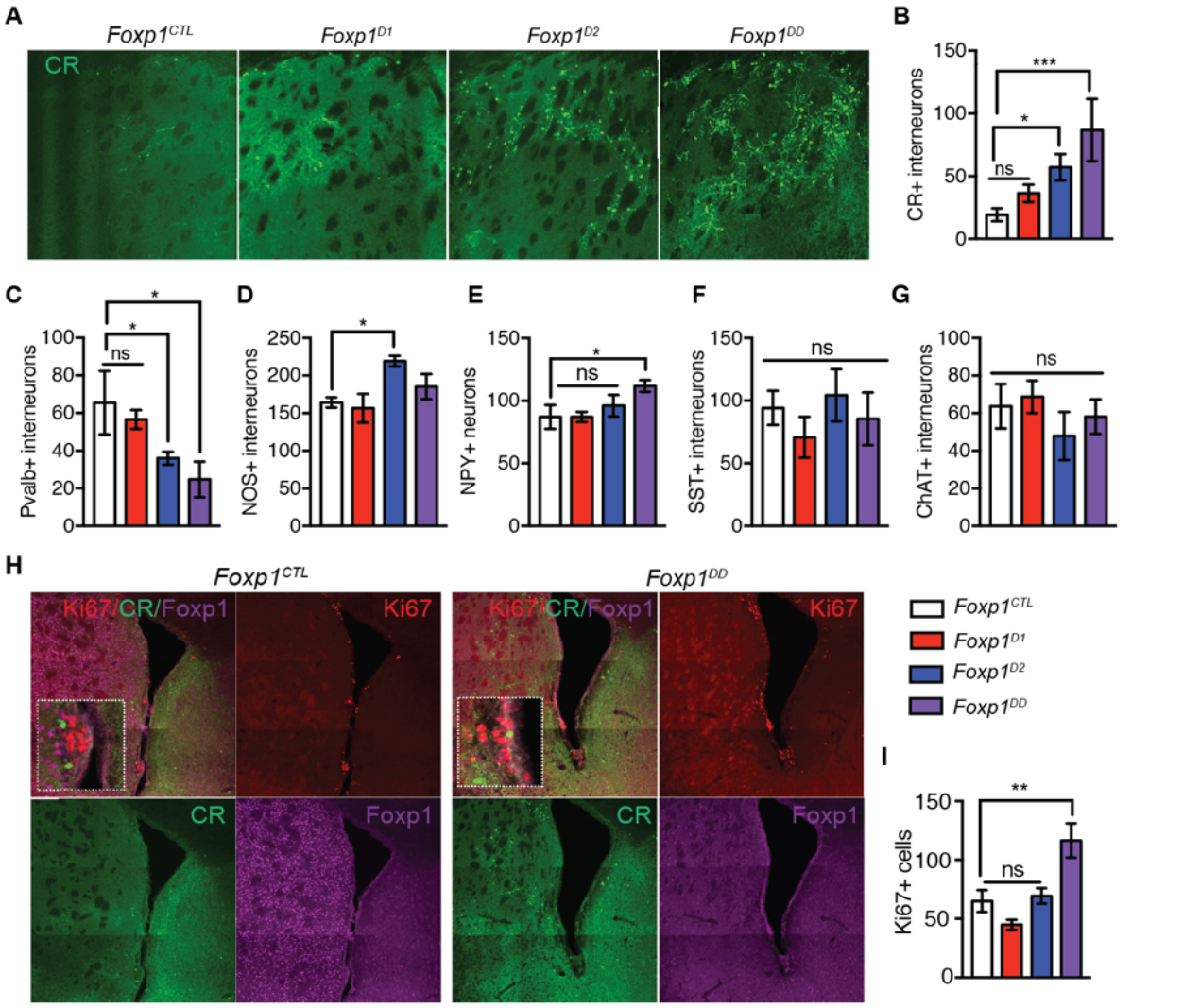

A) Immunohistochemistry (IHC) images for calretinin (CR) interneurons in the adult striatum of *Foxp1*^{CTL}, *Foxp1*^{D1} *Foxp1*^{D2}, and *Foxp1*^{DD} mice and quantification (**B**) of total number of calretinin^{+} cells in each genotype. Quantification of major interneuron populations across genotypes: (**C**) parvalbumin (Pvalb), (**D**) nitric oxide synthase (nNOS), (**E**) somatostatin (SST), (**F**) Choline-O-Acetyltransferase (ChAT) interneurons, and (**G**) neuropeptide y (NPY). **H**) IHC of proliferation marker Ki67 in the adult striatum of *Foxp1*^{CTL}, *Foxp1*^{D1} *Foxp1*^{D2}, and *Foxp1*^{DD} mice and (**I**) quantification. Data are represented as mean ± SEM with n=3-4 mice/genotype. *p<0.05, **p<0.005, ***p<0.0001, one-way ANOVA with Dunnette's multiple comparisons test.

FIGURE 4.4. No change in adult weight or clasping behavior across *Foxp1 cKO* strains

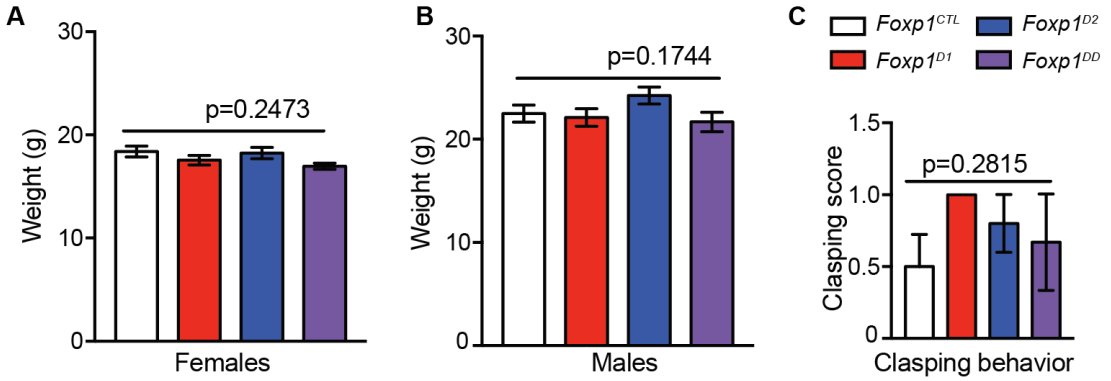

(**A-B**) Weight measurements of adult male and female *Foxp1 cKO* animals. N=7 for *Foxp1*^{CTL}, N=10 for *Foxp1*^{D1}, N= 11 for *Foxp1*^{D2}, and N=7 for *Foxp1*^{DD}. **C**) Analysis of clasping behavior across genotypes. Data are represented as mean ± SEM with. N=6 for *Foxp1*^{CTL}, N=6 for *Foxp1*^{D1}, N= 5 for *Foxp1*^{D2}, and N=3 for *Foxp1*^{DD}. P-values determined using a one-way ANOVA with Dunnett's multiple comparisons test.

FIGURE 4.5. Locomotor and sensitization response to cocaine

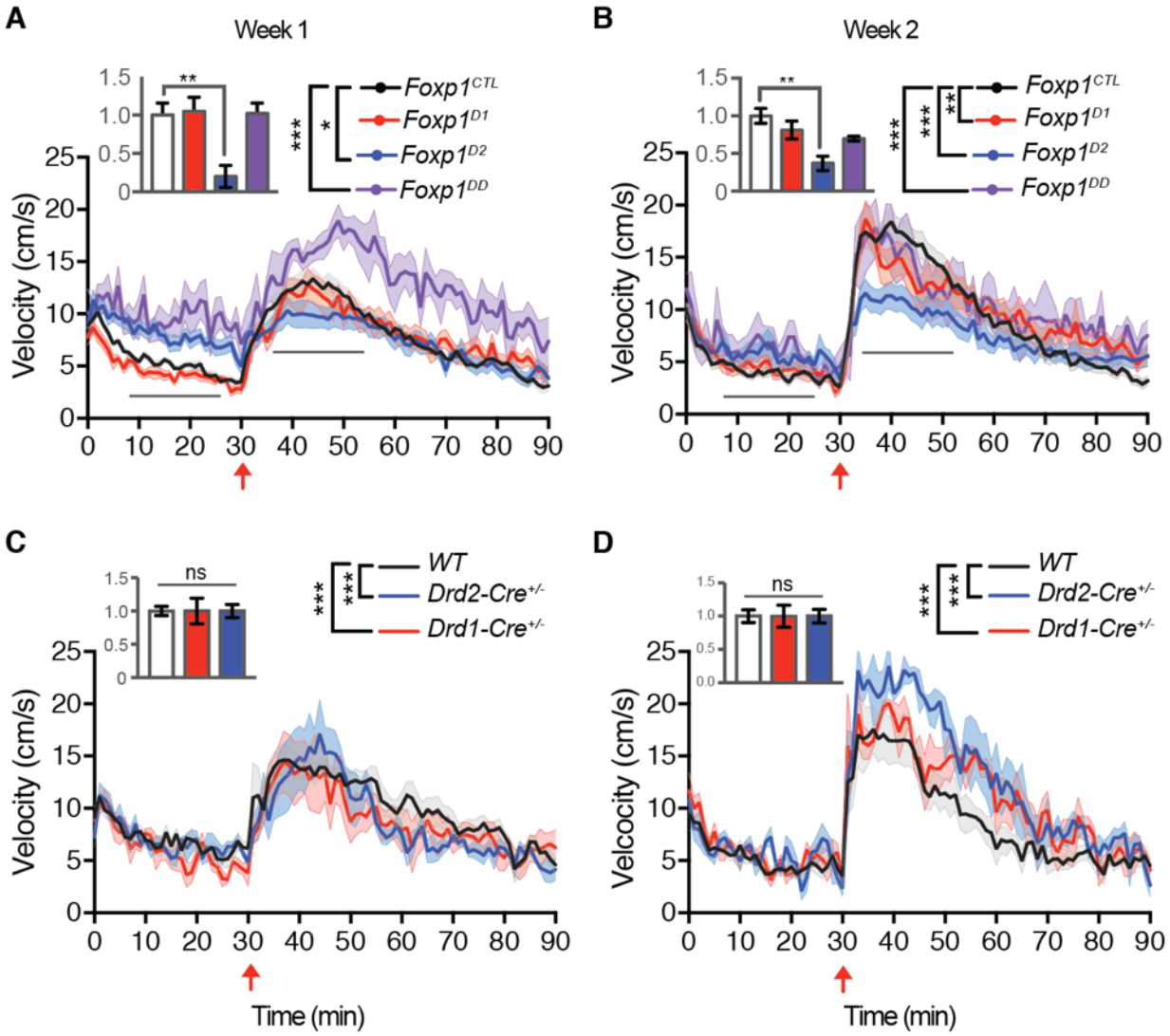

A) Initial (week 1) and (**B**) sensitized (week 2) locomotion response to cocaine (1mg/kg) injection across *Foxp1 cKO* stains (red arrow indicates cocaine was administered after 30min acclimation period) and (**C-D**) for heterozygous Cre-control animals. The inlet graph shows the relative magnitude of the cocaine response between the baseline (0-30min) and cocaine response (30-60min) represented by grey lines. Data are represented

as mean ± SEM with n=23 for *Foxp1*^{CTL}, 20 for *Foxp1*^{D2}, 14 for *Foxp1*^{D1}, and 4 for *Foxp1*^{DD}. N=8 for WT, 5 for D1-Cre, 5 for D2-Cre (week 1) and 3 for D2-Cre (week 2) *p<0.05, **p<0.005, ***p<0.0001, two-way ANOVA with Sidak's multiple comparisons test.

FIGURE 4.6. Morris water maze (MWM) task

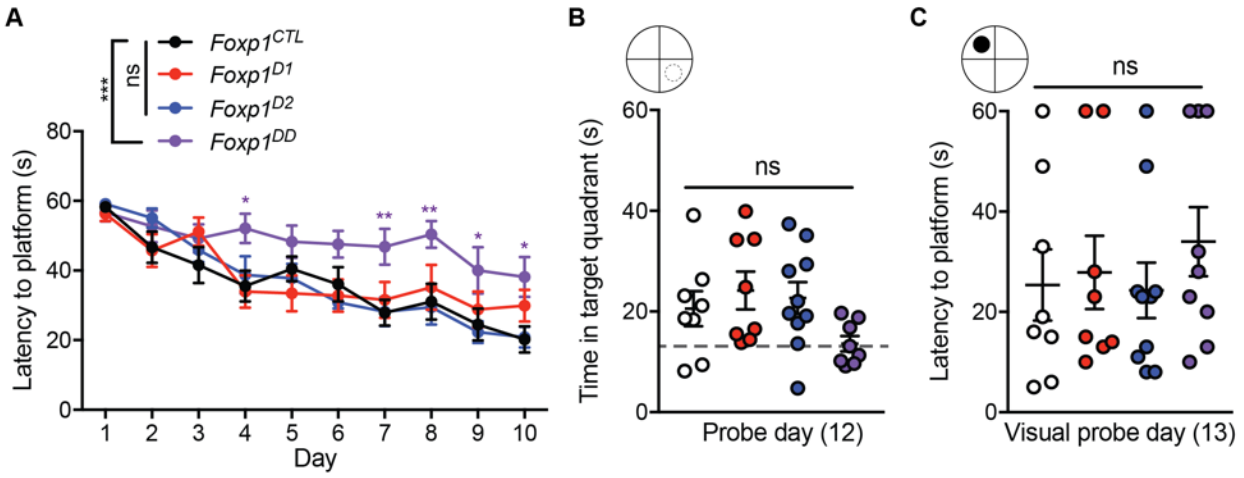

A) The latency to reach a hidden platform during 10 training days in the Morris water maze task across all *Foxp1 cKO* strains. Data are represented as mean ± SEM with n=8 for *Foxp1*^{CTL}, 10 for *Foxp1*^{D2}, 7 for *Foxp1*^{D1}, and 8 for *Foxp1*^{DD}. *p<0.05, **p<0.01, ***p<0.0001, two-way ANOVA with Sidak's multiple comparisons test. (**B**) Probe day measurement of time spent in the target quadrant (northeast) for each mouse for 60 seconds once platform was removed. (**C**) Visual probe day measurements of each mouse to reach a platform that is visible. P-values were calculated using a one-way ANOVA with Dunnett's multiple comparisons test.

FIGURE 4.7. Social interaction and grooming behaviors

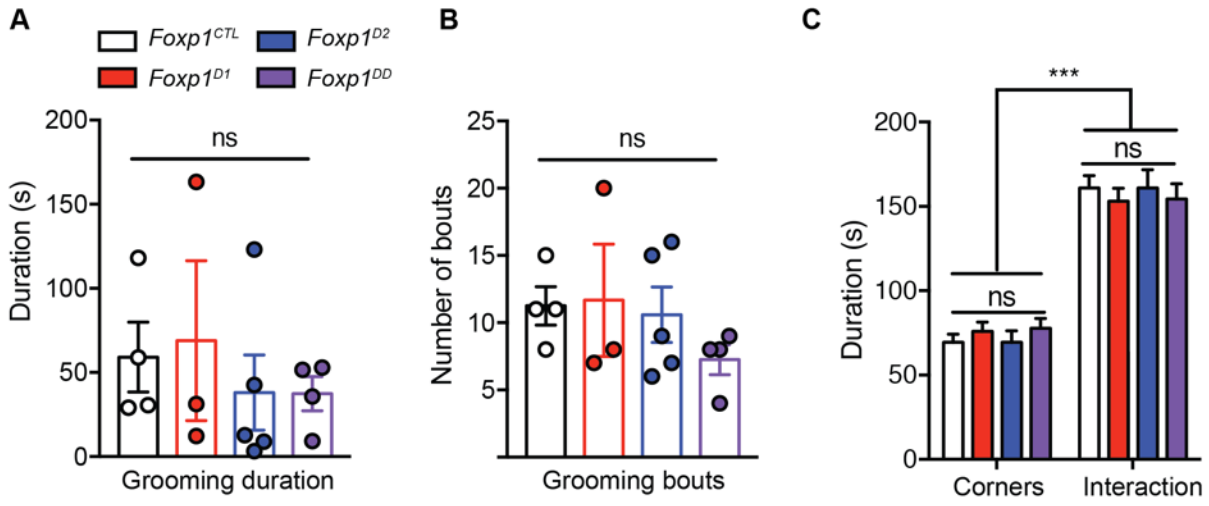

A) Total duration of grooming behavior and (**B**) number of grooming bouts scored within a 10 minutes recording for all *Foxp1 cKO* mice. Data are represented as mean ± SEM with n=4for *Foxp1*^{CTL}, 5 for *Foxp1*^{D2}, 3 for *Foxp1*^{D1}, and 4 for *Foxp1*^{DD}. ***p<0.0001, one-way ANOVA with Dunnett's multiple comparisons test. (**C**) Average time spent in the corners or interaction zone, with a target mouse, across *Foxp1 cKO* mice. Data are represented as mean ± SEM with n=20 for *Foxp1*^{CTL}, 8 for *Foxp1*^{D2}, 20 for *Foxp1*^{D1}, and 14 for *Foxp1*^{DD}. P-values measured using a two-way ANOVA with Sidak's multiple comparisons test.

FIGURE 4.8. Acute and chronic treatment with Aripiprazole does not improve rotarod performance in *Foxp1^{D2}* mice.

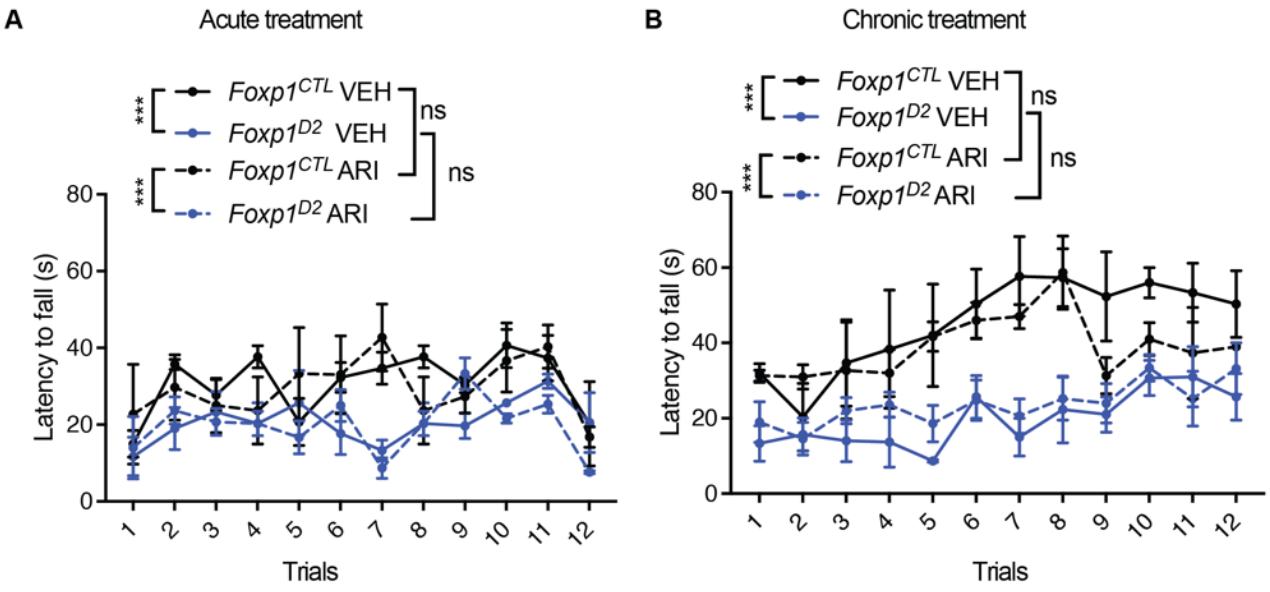

A) Mice received an acute intraperitoneal injection (IP) of 3mg/kg of aripiprazole (ARI) or vehicle control (VEH, 5% DMSO in saline solution) was administered 30min before testing and on all three days of testing (4 trials/day) on the accelerating rotarod. **B**) Mice received a chronic IP injection (3mg/kg) of ARI or vehicle control for 7 consecutive days before (and on) testing days. Data are represented as mean ± SEM, N=3/genotype for (A), N=3-5/genotype (B). ***P<0.0001, two-way ANOVA with Sidak's multiple comparisons.

FIGURE 4.9. Other drugs tested to rescue *Foxp1^{D2}* rotarod deficits

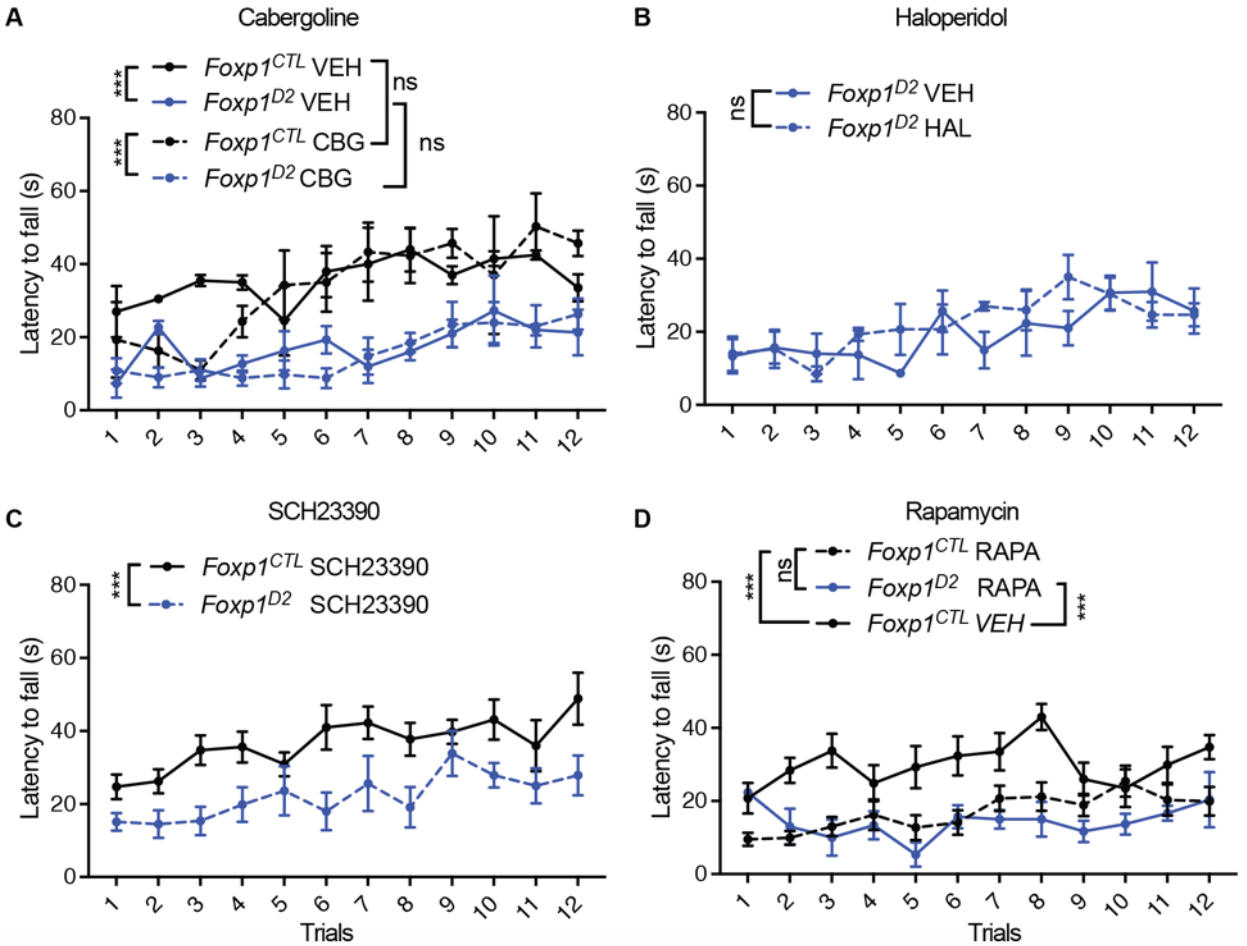

A) Mice received an acute intraperitoneal injection (IP) of 3mg/kg of cabergoline (CBG) or vehicle control (VEH, 5% DMSO in saline solution) was administered 1hr before testing and on all three days of testing (4 trials/day) on the accelerating rotarod. N=3 for *Foxp1^{CTL}*, 3 for *Foxp1^{D2}*. (**B**) Mice received a chronic IP injection (1mg/kg) of haloperidol (HAL) or vehicle control for 14 consecutive days before (and on) testing days. N=3 for *Foxp1^{CTL}*, 3 for *Foxp1^{D2}*. (**C**) Mice received an acute IP injection (0.02mg/kg) of SCH23390 30min before testing each day. N=8/genotype. **D**) Mice received IP injections (6mg/kg) of rapamycin (RAPA) everyday starting at P7 until testing at P47. Data are represented as

mean ± SEM, N=8 for *Foxp1*^{CTL} VEH and *Foxp1*^{CTL} RAPA, 3 for *Foxp1*^{D2} RAPA. ***P<0.0001, two-way ANOVA with Sidak's multiple comparisons.

FIGURE 4.10. Cloning a Cre-dependent AAV-Foxp1 plasmid for rescue experiments

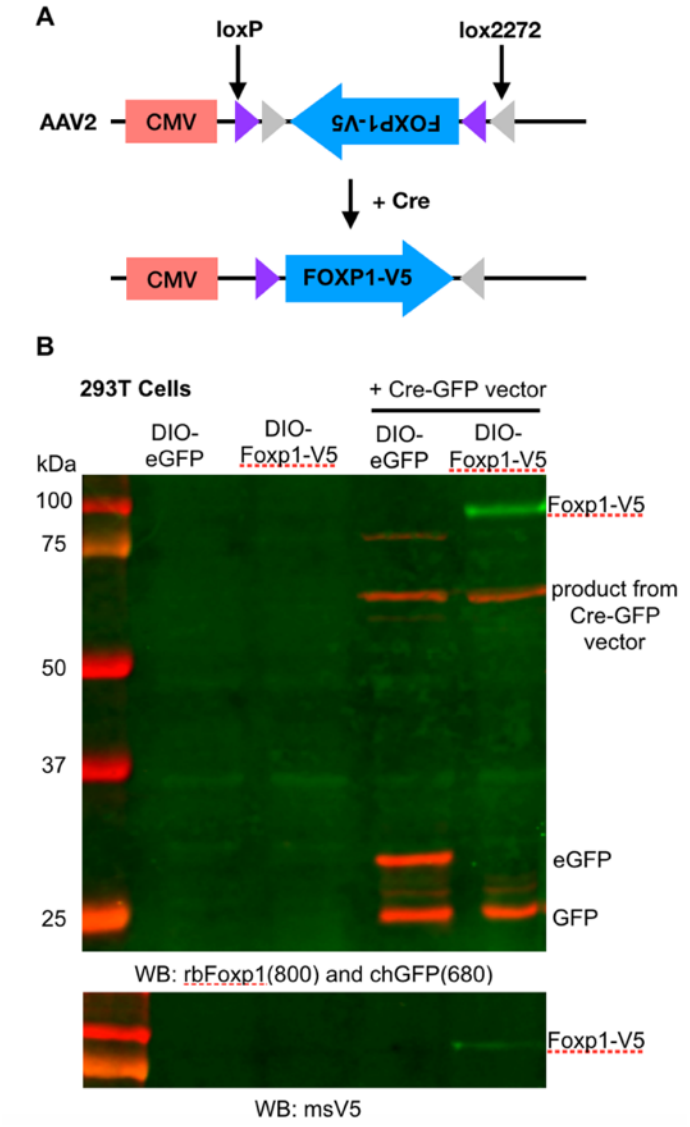

A) Schematic of a double-floxed-inverse orientation (DIO) AAV vector with a mouse Foxp1A-V5 region that becomes flipped and transcribed under the CMV promoter in the presence of Cre. **B**) Western blot of protein harvested from 293T cells transfected with a DIO-eGFP vector (control) or DIO-Foxp1-V5 in the absence or presence of a Cre-GFP vector. Foxp1 expression (green) only appears in the lane with DIO-Foxp1-V5 expression

co-transfected with the Cre plasmid. Bottom panels show the same samples probed the a V5 antibody to verify the expression of the V5 tag.

METHODS

Immunohistochemistry

Adults animals between 8-12 weeks of age were anesthetized with 80-100mg/kg of Euthasol (UTSW Animal Resources Center Veterinary Drug Services) and perfused with ice-cold PBS (~30ml) followed immediately by 4% PFA in PBS (~30ml). Brains were stored in 4% PFA overnight then transferred to 30% sucrose for 48 hours. 35um coronal or sagittal slices were made using a SM2000 R sliding microtome (Leica) and free-floating sections were stored in PBS with 0.01% sodium azide. Slices were washed with TBS and incubated for 30min in 3% hydrogen peroxide in PBS, washed, then incubated in 30min in 3M glycine in 0.4% Triton-X, TBS. Slices were incubated in primary antibodies overnight at 4C, washed, and incubated in secondary antibodies for 1hr at room temperature. Slices were washed then mounted onto slides and allowed to dry overnight. Sections were incubated in DAPI solution (600nM in PBS) on the slide for 5 minutes and washed 3X with PBS. Sections were allowed to dry before mounting coverslips using Prolong Diamond Antifade Mountant.

Imaging and Analysis

Images were collected using a Zeiss Confocal laser scanning microscope (LSM880) and all image quantification was performed using Fiji image processing package. For Darrp32 and NeuN quantification, 20X z-stack images of dorsolateral, dorsomedial, and ventral striatum were taken within one hemisphere of four separate striatal sections from anterior to posterior per animal (3 images/section, 4 sections/animal, at least 3 animals/genotype).

All images were taken within approximately similar sections across samples. Maximum projection images were quantified within a 1024x1024 pixel field of view across all images and averaged per section. For interneuron and Ki67 quantification, Zeiss Axioscan.Z1 20X images were taken of four separate striatal section from anterior to posterior per animal (4 sections/animals, at least 3 animals/genotype). Total number of interneurons were quantified within both hemispheres. Ki67+ cells along both ventricles from both hemispheres were quantified. Differences between genotypes were assessed using a one-way ANOVA with multiple comparisons.

Antibodies

The following primary antibodies were used for either immunoblots (IB) or immunohistochemistry (IHC) experiments: chicken anti-GFP (1:1,000, Aves Labs, GFP-1010), cleaved-Caspase 3 (Cell Signaling, 1:500), rabbit polyclonal anti-DARPP32 (1:1,000, Millipore, AB1778), mouse monoclonal anti-FOXP1 (1:500, Abcam, ab32010), rabbit polyclonal anti-FOXP1 (IHC:1:1,000, IB: 1:5,000 (Spiteri et al., 2007), goat polyclonal anti-Calretinin (1:1000, Millipore AB1550), mouse anti-Pvalb (1:500, Millipore MAB1572), goat anti-ChAT (1:500, Millipore AB144P), rabbit anti-NPY (1:1000, Immunostar, 22940), rabbit anti-SST (1:500, Immunostar, 20067) goat anti-nNOS (1:500, Abcam1376), rabbit anti-Ki67 (1:500, abcam15580), mouse anti-V5 (1:1000, Invitrogen R960-25). All IHC following secondary antibodies were used at a 1:1,000 dilutions Alexa Fluor 488 Donkey Anti-Chicken IgG (Thermo Fisher, 703-545-155), Alexa Fluor 555 Donkey Anti-Goat IgG (Thermo Fisher, A-21432), Alexa Fluor 647 Donkey Anti-Rabbit IgG (Thermo Fisher, 711-605-152), Alexa Fluor 647 Donkey Anti-Mouse IgG (Thermo

Fisher, A-31571). For IB, the following secondary antibodies were used at a 1:10,000 dilution: IRDye 800CW Donkey anti-Rabbit IgG (Licor, 925-32213) and IRDye 680RD Donkey anti-Mouse IgG (Licor, 925-68071).

Behavior

Psychostimulant response

Mice were placed in a 55cm x 55cm x 36cm open field arena for 30 minutes followed by an IP injection of cocaine (10mg/kg) solution in 0.9% saline as previously described (Kumar et al., 2013). LimeLight software was used for behavioral recording. Velocity (cm/min) was measured for 90 min total. Baseline is the 30 minutes before injection and locomotor response is the 30-60min period. Velocity measurements is binned by minute. The response was calculated by dividing the response by the baseline velocity for each mouse and then normalize by the average response/genotype.

Morris Water Maze

The water maze consisted of a 1.2-m-diameter circular pool filled with opaque, white tempera-paint-dyed 23°C water. Black and white visual cues were placed around the room containing the pool. A 10 cm circular plexiglas escape platform was submerged in one of the quadrants of the pool, ~1 cm below the surface. For training, mice were placed into the pool in one of four starting locations randomly ordered (north, south, east, or west) and allowed to swim until they found the platform. Mice were left on the platform for 5 s before being removed. If the mouse could not find the platform within 60 seconds, they were guided manually to the platform and given 5 s to rest before removal. Mice received four training trials per day for 10 days and were placed in temporary cages between the training trials of a particular day. On probe day (day 12), the escape platform was removed

and mice were allowed to swim in the pool for 60s. Animals were recorded by a video camera centered above the pool using ANY-Maze software (Stoelting). The latency to reach the escape platform was quantified for each mouse during the 10 day training period and, for the probe test, the amount of time spent in the escape platform quadrant (northeast) was quantified.

Social Interaction

Adult mice were placed individually in an open-field arena (44 x 44 cm with walls 30 cm high) and allowed to explore for 5 min. A small plastic chamber (the interaction box, 8.5 x 4.5 cm) was placed along one wall of the arena. the test mouse was removed after 5 min and a novel mouse (same sex and strain as the test mouse) placed into the interaction box. The test mouse was returned and allowed to explore for another 5 min. Small holes in the interaction box allow the mice to see, hear, and smell each other. The test mouse was monitored recorded using the Ethovision 3.0 (Noldus) software. The amount of time the test mouse spent in the interaction zone (within 8 cm of the box) and the time spent in the four corners of the arena (9 x 9 cm each) were analyzed.

Grooming behaviors

Each mouse was individually placed in a fresh cage and allowed to acclimate to the new environment for 30min. A video camera was placed on the side of the cage and the mouse was recorded for 10min. Duration of time spent grooming and number grooming bouts were manually scored by blinded to genotype.

Rotarod

Following previously published methods (Araujo et al., 2015), mice (8-12 weeks) were acclimated to the testing room for 30min before placed in one lane of a 5-lane accelerating

rotarod (Series 8 ITCC Life Science rotarod). The textured drum within the individual lanes was programed to accelerate from acceleration from 4-40 rpm within a maximum time frame of 300 sec. Each mouse was positioned facing away from the experimenter. Latency to fall was recorded once the trial was initiated. Manual activation of the sensors occurred when an animal made a full rotation holding onto the drum. Animals received four trials per day (20min intervals) with lanes cleaned between animals with NPD over the course of three consecutive days.

Pharmacology experiments

Mice used for these experiments were from *D2*$^{Cre/+}$*; Foxp1*$^{flox/flox}$ and *D2*$^{eGFP/+}$*; Foxp1*$^{flox/flox}$ cross. Mice tested were all *D2*$^{eGFP/+}$ positive. Aripiprazole (3mg/kg) (Batista et al., 2016; Hara et al., 2017; Viana et al., 2013), cabergoline (3mg/kg) (Tsuchioka et al., 2015), haloperidol (1mg/kg) (Bateup et al., 2010), and SCH23390 (0.02mg/kg) (Lee et al., 2018) were dissolved in pure DMSO and diluted with 0.9% saline to a 5% final volume. Stock solutions were made fresh, daily before injections. Rapamycin (6mg/kg) was dissolved in pure EtOH as 50mg/ml stock solution and stored in -80C. Rapamycin working solutions (1mg/ml) were made by diluting stock solutions to a final volume in 5% Tween 80 and 5% PEG solutions (Tsai et al., 2012). For acute administration, IP injections were given either 30min (aripiprazole, haloperidol, SCH223390) or 1hr (cabergoline) before following the rotorod protocol. Chronic administration consisted of daily IP injection of 3mg/kg injections of aripiprazole 7 days prior and during rotarod testing. For haloperidol, chronic administration consisted of a daily IP injection (1mg/kg) for 14 days prior and during rotarod testing. For rapamycin, IP injections (6mg/kg) began at postnatal day 7 every MWF for 6 weeks, until testing at 7 weeks (no injections on testing days).

Cloning AAV-DIO-Foxp1-V5 construct

Using a previously described plasmid backbone (Xu and Südhof, 2013) (pAAV-CMV-flip-GFP-2a-TeNT) to replace GFP-2a-TeNT with musFoxp1 isoform A with a V5 tag.

Foxp1-V5 amplification primers with AgeI and BamHI restriction digest sites:

Primer Name:	Sequence
musFoxp1-AgeI-PCR F	taagcaACCGGTatgatgcaagaatctgggtctgagacaaaaagtaacggatcagccatccagaacgggtcc
musFoxp1-V5-BamHI- PCR R	gaatcgGGATCCCGTAGAATCGAGACCGAGGAGAGGGTTAGGGATAGGCTTACCctccatgtcctcatttac

Confirmed AAV backbone plasmid by digesting plasmid DNA (1ug) with AgeI and BamHI to check fragment pattern: In .2ml PCR tube, mixed the following: 0.5ul of AgeI and BamHI, 5ul of SmartCutter Buffer, 2ul of plasmid (~2ug), and 43ul MBG water. Incubated at 37C in thermocycler overnight. Ran out on 1% agarose gel. Expected fragment sizes: (bp) 512, 772, 943, and 4885

Amplifying musFoxp1-V5 insert from pCMV26-Foxp1 plasmid: Used the following mix: 22.5ul of Accuprime pfx supermix, 1.5ul of F/R 10uM Primer mix, 150ng of plasmid (~0.5ul of 1:20 of PCMV26) and incubated in the following PCR program: 95C for 2min, 25x (95C for 15sec, 65C for 45sec, 68C for 2min 20sec), 68C for 2min, 4C hold

Digesting insert and backbone vector and purifying: In .2ml PCR tube, mixed the following: 0.5ul of AgeI and BamHI, 5ul of SmartCutter Buffer, 2ul of plasmid (~2ug) or all of PCR product, and MBG water up to 50ul. Incubate at 37C overnight. Run out on 1% agarose gel.

Ligation of insert and backbone vector: In .2ml PCR tube, mixed the following: 50ng of vector backbone, 250ng insert, 2ul 10X T4 ligation buffer, 1ul T4 LIGASE, Up to 20ul H2O, heat inactivate rxns at 65C for 10min. Transformed ligation into Stbl3 cells and grew colonies on Amp plates at 30C. Miniprepped colonies using Qiagen kit and sequenced isolated DNA with musFoxp1 3'R primer (ACTGTGGTTGGCTGTTGTCA)

Testing AAV-DIO-musFoxp1-V5 expression in 293T cells: Plates were ~75% confluent when ready to transfect. 1 6-well plate is for Cre + AAV-DIO vectors and the other 6-well is for AAV-DIO vectors alone. Each well will have 3ug of DNA and at a ratio of 3:1 Fugene to DNA. Transfection mix/per condition: up to 450ul of DMEM media (no Anti-anti or FBS!), add 27ul of Fugene, 4.5ug of Cre plasmid, 4.5ug of AAV plasmids, mix by flicking tube, and let sit at RT for 15min in hood. Flick again and add Fugene/plasmid mix drop-wise to 293T cells in DMEM media.

Harvesting protein from 293T cells and immunoblotting:

Cellular lysates were obtained using lysis buffer containing 0.5% Nonidet P-40,1 mM PMSF, 0.1 mM Na_3VO_4, 50 mM NaF, 1 uM DTT, 2 µg/mL pepstatin, and 1 µg/mL leupeptin. Tissue samples were lysed in buffer containing 1% Igepal, 1 mM PMSF, 0.1 mM Na_3VO_4, 2 µg/mL pepstatin, and 1 µg/mL leupeptin. Protein concentrations were determined using a Bradford assay (Bio-Rad). A total of 35µg of each sample was run o a 10% gel and processed following standard protocols for both HRP-conjugated and fluorescent secondary antibodies.

CHAPTER 5: DISCUSSION AND IMPLICATIONS

FOXP1 is one of the top 10 ASD-associated genes and linked to pervasive neurodevelopmental comorbidities, including motor delay, speech delay, and intellectual disability. Studies have shown that Foxp1 is critical for global brain developmental pathways. However, the role of Foxp1 in the striatum had not been fully characterized or examined at a cell-type specific level. In this thesis, I have examined the molecular, functional, and behavioral consequences of deleting *Foxp1* from striatal projection neurons of the direct and indirect pathways. These findings further our understanding of the role of FoxP1 in brain development and will ultimately help to elucidate pathways or circuits to target for potential therapeutic intervention.

iSPNs are particularly vulnerable with *Foxp1* reduction

Hyperexcitability of iSPNs

A consistent feature across both *Foxp1* heterozygous and *Foxp1* iSPN-specific cKO mice is the selective vulnerability of iSPNs. In **Chapter 2**, we found that iSPNs with reduction of Foxp1 were significantly more excitable than iSPNs from control animals, with no measured difference in dSPNs. We highlight that potassium (K^+) channels likely regulate this phenotype given the enrichment of K^+-channels and subunits in the differentially expressed gene (DEG) analysis of the *Foxp1*$^{+/-}$ striatum from **Table 2.1**. We also found a significant decrease in amplitude of spontaneous excitatory postsynaptic

currents (sEPSCs) that suggests a possible decrease in postsynaptic AMPA receptors. In **Chapter 3**, we found that two-thirds of the iSPN population was reduced by complete loss of *Foxp1* (**Figure 3.2**). Molecularly, we found that numerous K^+-channels were significantly differentially expressed within iSPNs with deletion of Foxp1 (**Table 3.2**). There was a notable overlap in the *Foxp1*$^{+/-}$ and *Foxp1*^{D2} iSPN DEGs for the following K^+-channels: *Kcnab1*, *Kcnc2*, *Kcnip1*, *Kcnip2*, *Kcnj3*, *Kcnk2*, and *Kcnmb2*. When compared to DEGs within dSPNs in *Foxp1*^{D1} mice, only *Dpp10*, a Kv4.2 binding protein, was significantly reduced. These results indicate that significant potassium channel dysregulation is occurring specifically within iSPNs. An important question remains: can the hyperexcitability of iSPNs can be directly linked to a shared behavioral deficit in *Foxp1*$^{+/-}$ and *Foxp1*^{D2} cKO animals, such as the increase in open field activity observed in both strains?

Several studies have published the effects of directly stimulating iSPNs and dSPNs in the striatum using Cre-dependent channel rhodopsin constructs (Kravitz et al., 2010, Lobo et al., 2010). Stimulation of iSPNs in the dorsomedial striatum caused hypoactive rodent behaviors, such as freezing and less ambulation, whereas stimulation of dSPNs in the same region induced hyperactivity (Kravitz et al., 2010). Optogenetic stimulation of iSPNs and dSPNs in the nucleus accumbens (ventral region) did not alter locomotor behaviors (Lobo et al., 2010). However, another study that examined the overexpression D2Rs in the ventral striatum and found this manipulation caused hyperactivity in mice (Gallo et al., 2015). Ablation of iSPNs throughout most of the dorsal and ventral striatum also increased locomotor activity (Durieux et al., 2009), which is similar to what we observe with reduction of Foxp1. Therefore, the striatal subregion in which iSPNs are

being manipulated has an important impact on behavior. This evidence suggests the signaling pathways within iSPNs of *Foxp1 KO* and *Foxp1^{D2}* mice are fundamentally dysfunctional and not just an overactivation of an intact indirect pathway. Additionally, the loss of iSPNs in *Foxp1^{D2}* mice is more severe in the dorsal striatum compared to the ventral regions (**Figure 3.2**), suggesting sub-regional differences in the role of Foxp1 in the striatum. A direct test of whether striatal iSPN hyperexcitability increases the locomotor activity in *Foxp1 KO* and *cKO* mice would be to use an optogenetic or DREADD-based approach and attempt to decrease the activity of iSPNs to rescue activity behavior in particular regions of the striatum (e.g., dorsal lateral, dorsal medial, or ventral regions).

Loss of iSPNs with complete deletion of Foxp1

The significant reduction of iSPNs within *Foxp1^{D2}* mice raises a couple of questions: first, how are striatal iSPNs lost? And second, why do a small population of iSPNs still remain? To begin answering these questions, I have identified from my scRNA-seq results (discussed in **Chapter 3)** that there are distinct populations of iSPNs and dSPNs that correspond to both matrix i/dSPNs or striosome i/dSPNs. Additionally, a recently described population of SPNs, termed “eSPNs”, clusters separately from canonical d/iSPN clusters (**Figure 3.2**). SPNs are also at different maturation stages within the postnatal striatum. Therefore, Foxp1 might be critical for the specification of a distinct iSPN subpopulation. Given that two thirds of striatal iSPNs are lost with deletion of *Foxp1*, I hypothesized that Foxp1 was likely important for specifying either matrix or striosomal iSPNs. To test this, I examined whether the remaining iSPN (r-iSPNs) locate

to the matrix or striosome compartments (**Figure 3.3)** and found that r-iSPNs largely aggregate along the striosome-matrix border.

By examining the differentially expressed genes in *Foxp1*^{D2} and *Foxp1*^{DD} iSPNs relative to control iSPNs, I found that top markers for eSPNs were upregulated, while both striosome and matrix iSPN markers were downregulated (**Figure 3.4A, E**). eSPNs were also more abundant as a percentage of total cells with loss of Foxp1 across all genotypes (**Figure 3.2G**). These results suggest that Foxp1 functions normally to repress eSPN identity and that remaining iSPNs have become more "eSPN"-like. A caveat is that eSPNs have yet to be characterized morphologically or functionally and their spatial location within the striatum in relation to the striosome-matrix mosaic is currently unknown. Importantly, both *Foxp2* and *Six3* are upregulated in the remaining iSPN populations of both *Foxp1*^{D2} and *Foxp1*^{DD} samples. *Six3* is a critical transcription factor for specifying iSPNs and *Foxp2* could be playing a compensatory role with loss of Foxp1 within this iSPN subpopulation (further discussed below).

Another explanation for the missing and remaining iSPNs in *Foxp1*^{D2} mice and their unique localization pattern could be that deletion of *Foxp1* alters the expression of genes involved in cell migration and motility. Recent studies have shown that matrix SPNs, particularly late-born matrix cells, exhibit repulsive migratory behavior by extending and retracting processes to avoid striosomal patches and aggregating with each other (Hagimoto et al., 2017; Tinterri et al., 2018). Striosome SPNs displayed attracting migratory behaviors to clusters (Hagimoto et al., 2017). Moreover, iSPNs specifically exhibit dynamic multidirectional migration patterns and rely on dSPNs to properly intermix within dSPN-rich striatal (Tinterri et al., 2018). Gene ontology analyses of iSPN-specific

DEGs regulated by Foxp1 show both upregulated and downregulated genes are enriched for categories such as cell motility and cell-cell adhesion (**Chapter 3**). For example, the most upregulated gene in *Foxp1*^{D2} iSPNs is *Unc5D* (Unc-5 netrin receptor D) that functions as a repulsive axon-guidance receptor for Netrin-1. Unc5D also binds with high affinity to FLRT2 (fibronectin and leucine-rich transmembrane protein-2), a protein important for cell adhesion and neurite outgrowth. FLRT2 is enriched in the striosome SPNs of both pathways in *Foxp1*^{CTL} samples population within my scRNA-seq data (**Figure 3.3B-C**) and within postnatal and adult striatal eSPNs (Saunders et al., 2018). Unc5d is not highly expressed in control iSPNs, therefore a significant upregulation of Unc5D in *Foxp1*^{D2} iSPNs could act as a repulsive cue to Flrt2-expressing striosomal neurons and therefore explain the aggregation along the striosomal border. Moreover, both *Unc5d* and *Flrt2* are upregulated in dSPNs specifically in *Foxp1*^{D1} and *Foxp1*^{DD} samples, which could be a mechanism by which striosome compartments are generally disrupted across genotypes. Interestingly, *Unc5D* and *Flrt3*, another FLRT-protein, are both upregulated in *Foxp1*$^{+/-}$ mice. Striosome-matrix architecture has not been analyzed in *Foxp1*$^{+/-}$ mice and I would hypothesize there would be structural differences.

Finally, Foxp1 could be critical for either iSPN survival or proliferation as other reasonable explanations for the decrease iSPNs observed in *Foxp1*^{D2} mice. While the possibility of iSPN cell-death was thoroughly discussed in **Chapter 4**, it is important to mention that Foxp1 has been linked to Huntington's disease (HD), a neurodegenerative disorder characterized by loss of lower-layer cortical neurons and striatal spiny projection neurons. iSPNs are particularly vulnerable in HD (Sebastianutto et al., 2017). Two mouse models of HD have shown that iSPNs are the first to degenerate, preceded by

hyperexcitability and loss of dendritic arborization (Sebastianutto et al., 2017). Reduction of FoxP1 has been found in post-mortem caudate samples from HD patients and in mouse models of HD. FOXP1 can also directly interact with mutant huntingtin protein. However, whether reduction of Foxp1 is a mechanism of pathology in HD or just a byproduct of striatal neuronal loss remains unclear. Therefore, cell-death cannot be ruled out as a potential mechanism of iSPN loss with deletion of *Foxp1*, especially given the data from **Figure 4.2**. Importantly, however, I have not found any molecular evidence, such as DEGs and gene ontology analyses from my dataset, that point to neurodegenerative or inflammatory pathways being activated with deletion of *Foxp1*. This could be a matter of experimental timing and analyzing gene expression data from younger (embryonic) and older timepoints (>6 months) within *Foxp1*^{D2} mice would help better understand whether molecular pathways involved in cell-death are activated over development.

A decrease in the proliferation of iSPNs with loss of Foxp1 could also explain the reduction of this subpopulation. Evidence from our scRNA-seq data suggests that loss of Foxp1 reduces the population of neurogenic progenitors (**Figure 3.1G-J**). In the literature, however, loss of Foxp1 has not been shown to affect the proliferation of E14.5 striatal embryonic neurons *in vitro* (Precious et al., 2016) or E14.5 cortical neurons *in vivo* (Li et al., 2015). In adult mice, I found a significant increase in Ki67^{+} cells along the lateral ventricle in *Foxp1*^{DD} mice, but no change within *Foxp1*^{D1} and *Foxp1*^{D2} *cKO* animals (**Figure 4.3**). However, staining with Ki67 or labelling cells with BrdU at embryonic timepoints would answer this question directly.

Using the pseudobulk analysis pipeline, I also examined differentially expressed genes regulated by Foxp1 within every cell-type of *Foxp1 cKO* cell-types in my scRNA-seq data. Surprisingly, significant DEGs were found in all cell-types, including *Mki67* (transcript for Ki67). *Mki67* was upregulated in oligodendrocyte precursor cells (OPCs) in *Foxp1^{D2} cKO* samples and upregulated in both astrocytes and microglia within *Foxp1^{D1} cKO* samples (**Table 5.2**). No change in *Mki67* was found in either SPNs, neurogenic progenitors, or other progenitors. This suggests that manipulation of Foxp1 in SPNs induces gene expression changes in glial populations. A deeper analysis of other cell-types (e.g., non-SPNs) within this single-cell data and follow-up experimentation will be needed to better understand the full impact of non-cell autonomous changes with SPN-specific *Foxp1* deletion.

Given the possibility that Foxp1 might alter the specification, migration, proliferation, or survival of iSPNs, future experiments will be needed to uncover the exact mechanism by which iSPNs are lost. An important step toward identifying this mechanism will be using a Cre-dependent fluorescent reporter strain (e.g., Rosa26Sor$^{eGFP/loxP}$ mice) crossed into *Foxp1^{D1}* and *Foxp1^{D2}* mice (**Figure 5.1**). Using these mice, we can permanently tag any Cre expressing cell and will be able to determine whether: 1) iSPN numbers are truly reduced or if they are being specified into another cell-type and 2) if iSPN are migrating to another location. Moreover, detection of when this mechanism occurs over development could be examined by harvesting embryonic timepoints and quantifying the number eGFP+ cells in the striatum and possibly other regions.

Cell-type specific molecular targets of Foxp1 and compensation by Foxp2/4

An important approach to finding cell-type specific Foxp1 targets was the use of high-throughput single-cell RNA-sequencing (reviewed in **Appendix A**). This relatively new and rapidly developing technology was invaluable for the ability to examine both changes in striatal cellular composition and the cell-autonomous transcriptional changes occurring in dSPNs and iSPNs, respectively, with deletion of *Foxp1*. Importantly, this tool also allowed for the detection of non-cell autonomous gene expression changes in all striatal cell-types. Using a pseudobulk analysis (discussed in Chapter 3), I found that iSPNs of *Foxp1*^{D2} mice had nearly 5X more differentially expressed genes than in dSPNs of *Foxp1*^{D1} mice (**Figure 3.4**). This was interesting given our *Foxp1*$^{+/-}$ striatal bulk RNA-seq data, where we found significantly more genes DEGs enriched for dSPNs markers compared to iSPN markers (**Figure 2.2**). However, in the bulk RNA-seq data, we were unable to attribute these DEGs to distinct cell-types. Using scRNA-seq, we found that DEGs enriched in both direct and indirect pathways were downregulated in both iSPNs and dSPNs with deletion of *Foxp1*, while eSPN subtype markers were upregulated (**Figure 3.4**). Interestingly, *Foxp2* is one of the top 5 marker genes of eSPNs and is highly expressed in dSPN populations and striosomal iSPNs (**Figure 3.2** and **Supplemental Figure 3.2**). Moreover, *Foxp2* is upregulated in iSPNs with deletion of *Foxp1*. These findings raise the possibility that Foxp2 might compensate for loss of Foxp1 in dSPNs, which could explain why dSPNs are grossly unaffected with deletion of *Foxp1*.

As discussed in **Chapter 1**, mutations in FoxP2 are known to alter striatal activity patterns in rodents and humans (Liégeois et al., 2003). Work from Rui Costa and Simon Fisher's labs have shown that mice with a heterozygous Foxp2-KE mutations (R552H) had higher rates of striatal activity, deficits on the rotarod, and aberrant striatal firing

during a motor-skills learning tasks (French et al., 2012; Groszer et al., 2008). Interestingly, striatal-specific *Foxp2 cKO* mice, using the *Rgs9-Cre* strain, did not have overt motor-learning deficits on the rotorod, but displayed more subtle motor-skills deficits in lever pressing and coordination.

To answer whether Foxp2 compensates for Foxp1 in dSPNs, characterizing the deletion of both proteins in dSPNs will be important. I have started crossing *Foxp1*$^{loxP/loxP}$ and *Foxp2*$^{loxP/loxP}$ conditional strains to obtain floxed alleles of both transcription factors on one strain. Crossing these double floxed animals to D1-Cre (and D2-Cre) driver strains and performing behavioral experiments, such as open field and rotarod, will help identify whether behavioral compensation occurs with deletion of one or both proteins in dSPNs and iSPNs. Moreover, using scRNA-seq to find the downstream molecular targets regulated by both Foxp1 and Foxp2 will help understand shared and unique molecular pathway underlying these behavioral changes. While *Foxp4* expression drops steeply during postnatal development (**Figure 1.3**), another interesting possibility could be that Foxp4 compensates embryonically for loss of Foxp1 in dSPNs. Foxp4 overlaps with Foxp1 and Foxp2 expression in the developing striatum, however, it remains unknown whether Foxp4 expression is enriched within a distinct SPN subtypes. Therefore, examining the contribution of Foxp4 the development of the striatum will be an important future direction in the FOXP field.

Common circuits disrupted across *Foxp1 KO* and *cKO* mouse models

A goal in characterizing the role Foxp1 in the murine brain has been to uncover the circuits that might underlie behavioral deficits relevant to phenotypes observed in *FOXP1* syndrome. Individuals with *FOXP1* mutations have a range of

neurodevelopmental disorder-associated behaviors, including autism or autistic features, motor and speech delay, hyperactivity, motor coordination deficits, and intellectual disability. To determine concordance to human disease, all *Foxp1 KO* and *cKO* strains undergo a variety of behaviors paradigms designed to test patient-relevant phenotypes. First, we tested a Foxp1 heterozygous model that likely resembles Foxp1 dosage levels in human mutations. We found that *Foxp1*$^{+/-}$ mice had significantly altered pup ultrasonic vocalizations. *Foxp1*$^{+/-}$ pups produced fewer calls, calls were lower in frequency (or pitch), and the call structure was altered (**Figure 2.4**). These mice also exhibited: hyperactivity, contextual and cued fear-conditioned learning deficits, and reduced forelimb and hindlimb grip strength. In order to examine which brain regions or circuits might regulate these behavior deficits, our lab turned to *Foxp1 cKO* strains where we can restrict the deletion of *Foxp1* to distinct brain regions or cell-types.

With cortical and hippocampal deletion of *Foxp1*, the *Emx-Foxp1 cKO* strain had broad deficits in social, motor, and spatial-learning (see **Appendix B**). With the *Foxp1*$^{+/-}$ mice, they shared an increase in hyperactivity, reduced number of pup vocalizations, and reduced forelimb and hindlimb grip strength (Araujo et al., 2017; Usui et al., 2017a). Testing *Foxp1*^{D1} mice, where *Foxp1* is deleted from lower cortical layers V-VI and direct pathway SPNs, the overlap of phenotypes with both *Foxp1*$^{+/-}$ and *Emx-Foxp1 cKO* mice becomes restricted to reduced number of pup vocalizations (**Figure 3.6**). *Foxp1*^{D1} and *Foxp1*$^{+/-}$ mice overlap in contextual fear conditioning (FC) deficits (**Figure 3.6**), whereas no FC deficits were found with hippocampal and cortical deletion of *Foxp1*. Moreover, *Foxp1*^{D1} and *Emx-Foxp1 cKO* mice shared deficits in nesting behavior (Figure 3.6) (Araujo et al., 2017). We can then narrow down likely circuits mediating USV call number

to disruption of cortico-striatal circuitry and contextual fear conditioning to striatal direct pathway dysfunction, where *Foxp1* dosage is important for both behaviors. While contextual fear conditioning is classically associated with hippocampal and amygdalar circuits, restricted ablation striatal dSPNs have been shown to mediate contextual fear memory formation (Ikegami et al., 2014b). With complete loss of *Foxp1*, cortico-striatal circuit dysfunction leads to nesting behavior deficits, suggesting that some compensatory mechanisms are happening in *Foxp1*$^{+/-}$ mice.

Foxp1$^{+/-}$, *Emx-Foxp1,* and *Foxp1*^{D2} *cKO* mice all share a hyperactivity phenotype. In *Foxp1*^{D2} mice, Foxp1 is specifically deleted from indirect pathway SPNs suggesting that cortico-indirect pathways circuits could mediate this behavior. *Foxp1*^{D2} mice have loss of iSPNs most strikingly in the dorsal medial and lateral striatal regions. The dorsolateral region receives dense projections from the motor and sensorimotor cortex, which might be disrupted with loss of Foxp1 (Hunnicutt et al., 2016). Electrophysiological experiments in the cortex of *Foxp1 KO* or *cKO* mice have not yet been published, but such experiments would be helpful for better understanding the mechanism of cortico-striatal circuit dysfunction. Additionally, thalamic inputs onto cortex could be disrupted within *Foxp1 KO* and *cKO* models since thalamocortical inputs are a “read-out” of cortico-basal ganglia activity. Thalamic nuclei receiving inputs from the basal ganglia (GPi and SNr) send dense projections back to the motor cortex. Thus, cortical and striatal deletion of *Foxp1* could disrupt multiple circuits within the cortico-thalamo-basal ganglia loop.

Interestingly, *Foxp1*^{D1}, *Foxp1*^{D2}, *Foxp1*^{DD}, and *Foxp1*$^{+/-}$ mice all shared a common deficit in cued fear-conditioning recall. Our analysis of SPN projection patterns in *Foxp1 cKO* mice showed that iSPNs in *Foxp1*^{D2} mice had fewer projections to the GPe and that

dSPNs in *Foxp1*^{D2} mice had significantly fewer dSPN projections onto the GPi (**Figure 3.5** and **Supplemental Figure 3.5**). No significant disruptions in dSPN projections in *Foxp1*^{D1} mice were found, indicating a non-cell autonomous effect on dSPNs in *Foxp1*^{D2} mice. This suggests the most likely circuits mediating the cued FC response arise from dysfunctional inputs onto the striatal SPNs and not from downstream SPN signaling. The striosome-matrix architecture preferentially receives inputs from limbic structures, such as the bed nucleus of the stria terminalis (Smith et al., 2016). Disorganization of the striosome-matrix compartments, which is observed in all genotypes at postnatal day 9 (**Figure 3.3**), could disrupt the patterning of inputs onto the striatum. Striosome-matrix organization is more unorganized in *Foxp1*^{D1} mice and dSPNs receive preferential inputs from the amygdala, which could explain why *Foxp1*^{D1} mice also have deficits in contextual FC. Examining the striosome-matrix organization in *Foxp1*$^{+/-}$ mice would be important to confirm given the overlapping FC behaviors. Tracing inputs from the amygdala and analyzing their striosome-matrix projection patterning in the striatum of *Foxp1*$^{+/-}$ and striatal *Foxp1 cKO* mice would address this possibility.

Future experimental systems and therapeutic directions

From a clinical perspective, an important future direction for the Foxp1 field will be to develop better tools for more translational studies. For example, generating mice with patient-relevant *Foxp1* mutations will provide valuable insight into Foxp1 function, much like the Foxp2 patient-mutation mouse models. In tandem with these translational mouse tools, using induced pluripotent stem cells (iPSCs) derived from patients with FOXP1 mutations will help scientists better pinpoint disrupted molecular pathways and ultimately

lead to better therapeutic development. From my research, I have found that DR2 expressing SPN are particularly vulnerable to reduction or complete loss of *Foxp1*. While my limited testing of drugs targeting the dopaminergic system did not work, a more exhaustive investigation into potential drugs targeting this neuromodulatory system might be helpful in eventually treating the motor deficits seen in FOXP1 syndrome. There are several Foxp1-regulated genes identified from my single-cell differential gene expression analyses that could be targeted for future pharmacological intervention, such as the adenosine receptor 2A (*Adora2a*), components of the activin A complex (*Acvr1*), or phosphodiesterase 1A (*Pde1a*) regulated pathways.

From a basic science perspective, the development of better tools to target unique cell-types identified in scRNA-seq studies will be an important future direction for the field of neuroscience. A lesson from the many scRNA-seq studies is that a cell-type is not defined by the expression of a single gene, but rather the unique combination of several genes. Therefore, the current tools we use to target cell-types will need to be further adapted, such as combining the use of flippase and cre-recombinases to better target distinct populations. We could then use these tools to manipulate Foxp1 within distinct subtypes of the striatum, such as striosome and matrix d/iSPNs. Future studies of Foxp1 function in other brain regions, such as the thalamus and deep cerebellar nuclei, will be also be important to connect circuits to behaviors. Moreover, *Foxp1* is expressed at the transcript level in non-neuronal cells in the brain, such as microglia. Understanding whether 1) Foxp1 protein is expressed in microglia and 2) the role of Foxp1 in microglia are important future directions to comprehensive understanding to cell-types and circuits that are affected with Foxp1 loss-of-function.

FIGURE 5.1. Rosa$^{eGFP\text{-}lox}$ mice crossed into *Foxp1^{D2}* mice to label all Cre^{+} cells

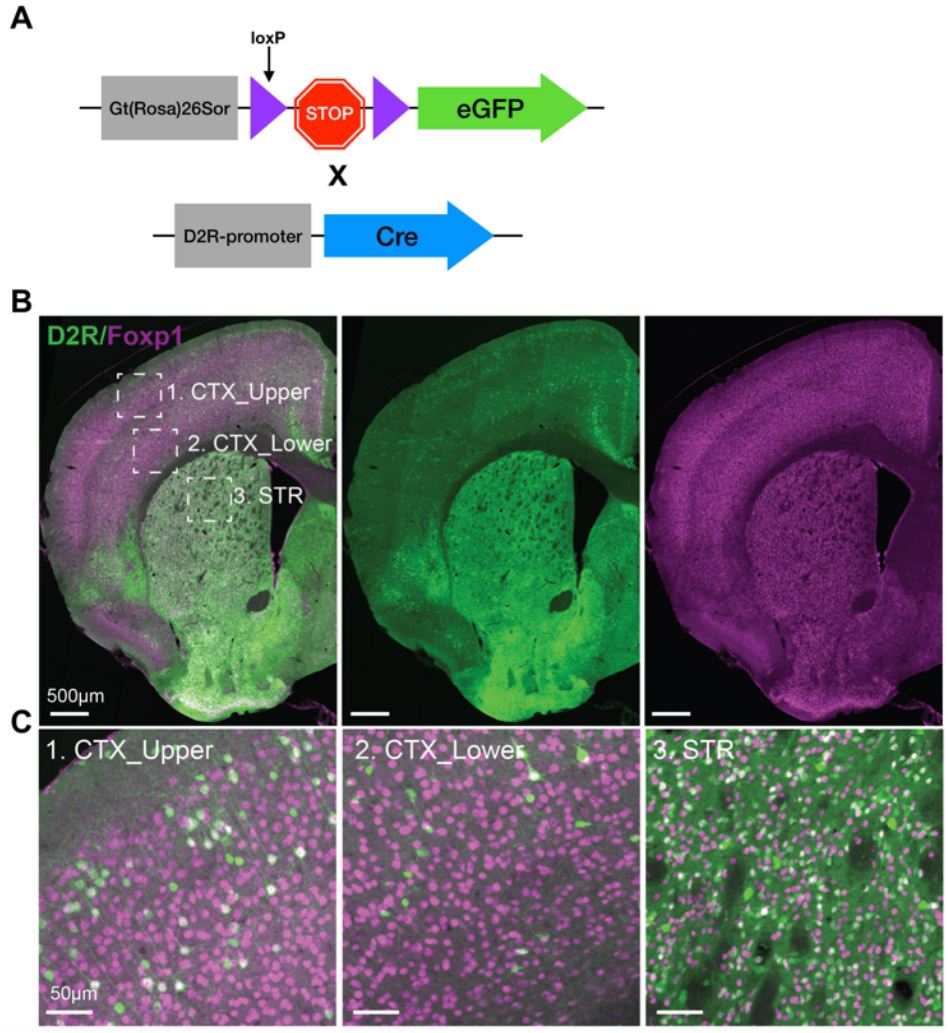

A) Schematic of a knockin Gt(Rosa)26Sor mouse strain with a floxed stop before the eGFP coding sequence. When crossed into a Cre-reporter strain (e.g., the D2R-Cre line), eGFP will be expressed in all Cre^{+} cells. **B**) Immunohistochemistry for eGFP (green) and Foxp1 (purple) in *D2-Cre; Rosa$^{eGFP\text{-}lox}$; Foxp1$^{flox/+}$* showing colocalization of Foxp1 and Cre^{+} cells in the cortex and striatum.

FIGURE 5.2. Pseudobulk DEG analysis for all cell-types in striatal scRNA-seq data

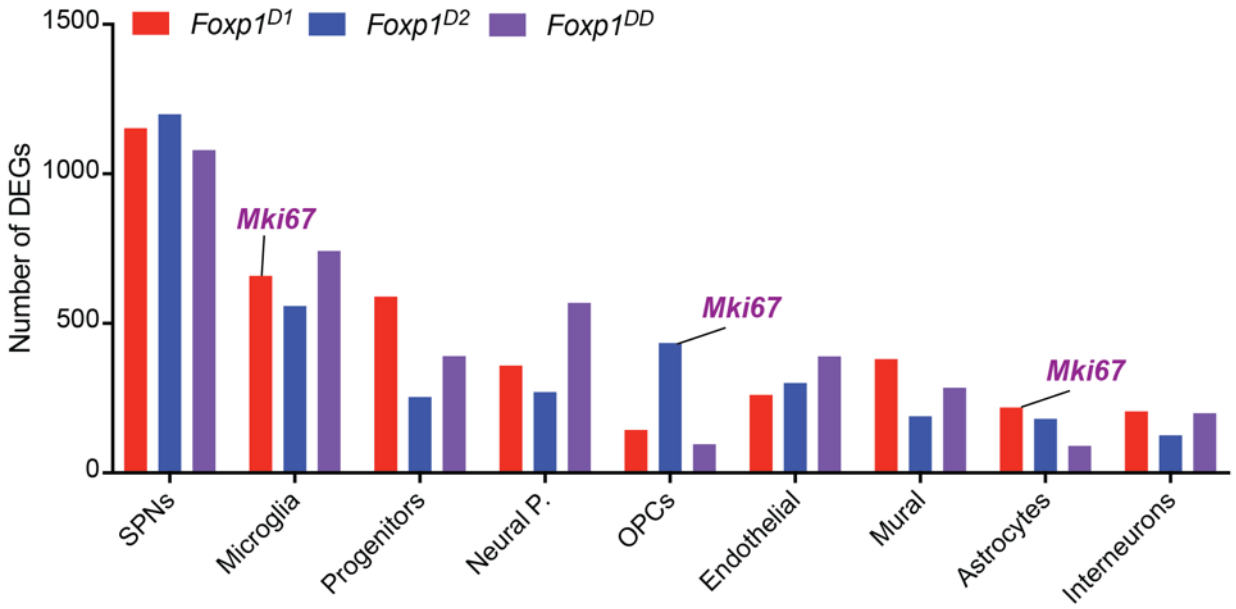

Number of differentially expressed genes found in a pseudobulk analysis of all cell-types within P9 striatal scRNA-seq data across all Foxp1 cKO samples relative to control samples. *Mki67* transcript is upregulated within indicated *Foxp1 cKO* samples and cell-types.

REFERENCES

Ade, K.K., Janssen, M.J., Ortinski, P.I., and Vicini, S. (2008). Differential tonic GABA conductances in striatal medium spiny neurons. J. Neurosci. *28*, 1185–1197.

Ade, K.K., Wan, Y., Chen, M., Gloss, B., and Calakos, N. (2011). An Improved BAC Transgenic Fluorescent Reporter Line for Sensitive and Specific Identification of Striatonigral Medium Spiny Neurons. Front Syst Neurosci *5*, 32.

Adegbola, A.A., Cox, G.F., Bradshaw, E.M., Hafler, D.A., Gimelbrant, A., and Chess, A. (2015). Monoallelic expression of the human FOXP2 speech gene. Proc. Natl. Acad. Sci. U.S.a. *112*, 6848–6854.

Agakidis, C., Agakidou, E., Sarafidis, K., Papoulidis, I., Xinias, I., and Farmaki, E. (2019). Immune Dysregulation, Polyendocrinopathy, Enteropathy, X-Linked Syndrome Associated With a Novel Mutation of FOXP3 Gene. Front Pediatr *7*, 20.

Aggleton, J.P., and Christiansen, K. (2015). The subiculum: the heart of the extended hippocampal system. Progress in Brain Research *219*, 65–82.

Anderson, S.A., Qiu, M., Bulfone, A., Eisenstat, D.D., Meneses, J., Pedersen, R., and Rubenstein, J.L. (1997). Mutations of the homeobox genes Dlx-1 and Dlx-2 disrupt the striatal subventricular zone and differentiation of late born striatal neurons. Neuron *19*, 27–37.

Andrews, S. (2010). FastQC: a quality control tool for high throughput sequence data.

Araujo, D.J., Anderson, A.G., Berto, S., Runnels, W., Harper, M., Ammanuel, S., Rieger, M.A., Huang, H.-C., Rajkovich, K., Loerwald, K.W., et al. (2015). FoxP1 orchestration of ASD-relevant signaling pathways in the striatum. Genes & Development *29*, 2081–2096.

Araujo, D.J., Toriumi, K., Escamilla, C.O., Kulkarni, A., Anderson, A.G., Harper, M., Usui, N., Ellegood, J., Lerch, J.P., Birnbaum, S.G., et al. (2017). Foxp1 in Forebrain Pyramidal Neurons Controls Gene Expression Required for Spatial Learning and Synaptic Plasticity. J. Neurosci. *37*, 10917–10931.

Arlotta, P., Molyneaux, B.J., Jabaudon, D., Yoshida, Y., and Macklis, J.D. (2008). Ctip2 Controls the Differentiation of Medium Spiny Neurons and the Establishment of the Cellular Architecture of the Striatum. Journal of Neuroscience *28*, 622–632.

Bacchetta, R., Barzaghi, F., and Roncarolo, M.-G. (2018). From IPEX syndrome to FOXP3 mutation: a lesson on immune dysregulation. Ann. N. Y. Acad. Sci. *1417*, 5–22.

Bacon, C., Schneider, M., Le Magueresse, C., Froehlich, H., Sticht, C., Gluch, C., Monyer, H., and Rappold, G.A. (2015). Brain-specific Foxp1 deletion impairs neuronal development and causes autistic-like behaviour. Molecular Psychiatry *20*, 632–639.

Bandukwala, H.S., Wu, Y., Feuerer, M., Chen, Y., Barboza, B., Ghosh, S., Stroud, J.C., Benoist, C., Mathis, D., Rao, A., et al. (2011). Structure of a domain-swapped FOXP3 dimer on DNA and its function in regulatory T cells. Immunity *34*, 479–491.

Bateup, H.S., Santini, E., Shen, W., Birnbaum, S., Valjent, E., Surmeier, D.J., Fisone, G., Nestler, E.J., and Greengard, P. (2010). Distinct subclasses of medium spiny neurons differentially regulate striatal motor behaviors. Proc. Natl. Acad. Sci. U.S.a. *107*, 14845–14850.

Batista, L.A., Viana, T.G., Silveira, V.T., Aguiar, D.C., and Moreira, F.A. (2016). Effects of aripiprazole on caffeine-induced hyperlocomotion and neural activation in the striatum. Naunyn Schmiedebergs Arch. Pharmacol. *389*, 11–16.

Becht, E., McInnes, L., Healy, J., Dutertre, C.-A., Kwok, I.W.H., Ng, L.G., Ginhoux, F., and Newell, E.W. (2018). Dimensionality reduction for visualizing single-cell data using UMAP. Nat. Biotechnol. *37*, 38–44.

Bello, E.P., Casas-Cordero, R., Galiñanes, G.L., Casey, E., Belluscio, M.A., Rodríguez, V., Noaín, D., Murer, M.G., and Rubinstein, M. (2016). Inducible ablation of dopamine D2 receptors in adult mice impairs locomotion, motor skill learning and leads to severe parkinsonism. Molecular Psychiatry *22*, 595–604.

Belton, E., Salmond, C.H., Watkins, K.E., Vargha-Khadem, F., and Gadian, D.G. (2003). Bilateral brain abnormalities associated with dominantly inherited verbal and orofacial dyspraxia. Hum Brain Mapp *18*, 194–200.

Bennett, C.L., and Ochs, H.D. (2001). IPEX is a unique X-linked syndrome characterized by immune dysfunction, polyendocrinopathy, enteropathy, and a variety of autoimmune phenomena. Curr. Opin. Pediatr. *13*, 533–538.

Bennett, C.L., Christie, J., Ramsdell, F., Brunkow, M.E., Ferguson, P.J., Whitesell, L., Kelly, T.E., Saulsbury, F.T., Chance, P.F., and Ochs, H.D. (2001). The immune dysregulation, polyendocrinopathy, enteropathy, X-linked syndrome (IPEX) is caused by mutations of FOXP3. Nat Genet *27*, 20–21.

Bergsland, M., Werme, M., Malewicz, M., Perlmann, T., and Muhr, J. (2006). The establishment of neuronal properties is controlled by Sox4 and Sox11. Genes & Development *20*, 3475–3486.

Berke, J.D. (2011). Functional properties of striatal fast-spiking interneurons. Front Syst Neurosci *5*, 45.

Boulanger-Bertolus, J., Rincón-Cortés, M., Sullivan, R.M., and Mouly, A.-M. (2017). Understanding pup affective state through ethologically significant ultrasonic vocalization frequency. Sci. Rep. *7*, 13483.

Brunkow, M.E., Jeffery, E.W., Hjerrild, K.A., Paeper, B., Clark, L.B., Yasayko, S.A., Wilkinson, J.E., Galas, D., Ziegler, S.F., and Ramsdell, F. (2001). Disruption of a new

forkhead/winged-helix protein, scurfin, results in the fatal lymphoproliferative disorder of the scurfy mouse. Nat Genet *27*, 68–73.

Butler, A., Hoffman, P., Smibert, P., Papalexi, E., and Satija, R. (2018). Integrating single-cell transcriptomic data across different conditions, technologies, and species. Nat. Biotechnol. *36*, 411–420.

Carr, C.W., Moreno-De-Luca, D., Parker, C., Zimmerman, H.H., Ledbetter, N., Martin, C.L., Dobyns, W.B., and Abdul-Rahman, O.A. (2010). Chiari I malformation, delayed gross motor skills, severe speech delay, and epileptiform discharges in a child with FOXP1 haploinsufficiency. European Journal of Human Genetics *18*, 1216–1220.

Castellucci, G.A., McGinley, M.J., and McCormick, D.A. (2016). Knockout of Foxp2 disrupts vocal development in mice. Sci. Rep. *6*, 23305.

Cembrowski, M.S., Wang, L., Lemire, A.L., Copeland, M., DiLisio, S.F., Clements, J., and Spruston, N. (2018). The subiculum is a patchwork of discrete subregions. Elife *7*, 65.

Cembrowski, M.S., Wang, L., Sugino, K., Shields, B.C., and Spruston, N. (2016). Hipposeq: a comprehensive RNA-seq database of gene expression in hippocampal principal neurons. Elife *5*, e14997.

Cepeda, C., André, V.M., Yamazaki, I., Wu, N., Kleiman-Weiner, M., and Levine, M.S. (2008). Differential electrophysiological properties of dopamine D1 and D2 receptor-containing striatal medium-sized spiny neurons. Eur. J. Neurosci. *27*, 671–682.

Chang, J., Gilman, S.R., Chiang, A.H., Sanders, S.J., and Vitkup, D. (2014). Genotype to phenotype relationships in autism spectrum disorders. Nat Neurosci *18*, 191–198.

Chapman, K.Z., Ge, R., Monni, E., Tatarishvili, J., Ahlenius, H., Arvidsson, A., Ekdahl, C.T., Lindvall, O., and Kokaia, Z. (2015). Inflammation without neuronal death triggers striatal neurogenesis comparable to stroke. Neurobiology of Disease *83*, 1–15.

Charng, W.-L., Karaca, E., Akdemir, Z.C., Gambin, T., Atik, M.M., Gu, S., Posey, J.E., Jhangiani, S.N., Muzny, D.M., Doddapaneni, H., et al. (2016). Exome sequencing in mostly consanguineous Arab families with neurologic disease provides a high potential molecular diagnosis rate. BMC Med Genomics *9*, 1–14.

Chen, C., Lee, G.A., Pourmorady, A., Sock, E., and Donoghue, M.J. (2015a). Orchestration of Neuronal Differentiation and Progenitor Pool Expansion in the Developing Cortex by SoxC Genes. J. Neurosci. *35*, 10629–10642.

Chen, Y., Chen, C., Zhang, Z., Liu, C.-C., Johnson, M.E., Espinoza, C.A., Edsall, L.E., Ren, B., Zhou, X.J., Grant, S.F.A., et al. (2015b). DNA binding by FOXP3 domain-swapped dimer suggests mechanisms of long-range chromosomal interactions. Nucleic Acids Res. *43*, 1268–1282.

Chu, Y.-P., Chang, C.-H., Shiu, J.-H., Chang, Y.-T., Chen, C.-Y., and Chuang, W.-J. (2011). Solution structure and backbone dynamics of the DNA-binding domain of FOXP1: insight into its domain swapping and DNA binding. Protein Sci. *20*, 908–924.

Cirillo, L.A., and Zaret, K.S. (2007). Specific interactions of the wing domains of FOXA1 transcription factor with DNA. J. Mol. Biol. *366*, 720–724.

Clark, K.L., Halay, E.D., Lai, E., and Burley, S.K. (1993). Co-crystal structure of the HNF-3/fork head DNA-recognition motif resembles histone H5. Nature *364*, 412–420.

Coe, B.P., Stessman, H.A.F., Sulovari, A., Geisheker, M.R., Bakken, T.E., Lake, A.M., Dougherty, J.D., Lein, E.S., Hormozdiari, F., Bernier, R.A., et al. (2019). Neurodevelopmental disease genes implicated by de novo mutation and copy number variation morbidity. Nat Genet *51*, 106–116.

Coe, B.P., Witherspoon, K., Rosenfeld, J.A., van Bon, B.W.M., Vulto-van Silfhout, A.T., Bosco, P., Friend, K.L., Baker, C., Buono, S., Vissers, L.E.L.M., et al. (2014). Refining analyses of copy number variation identifies specific genes associated with developmental delay. Nat Genet *46*, 1063–1071.

Corbin, J.G., Gaiano, N., Machold, R.P., Langston, A., and Fishell, G. (2000). The Gsh2 homeodomain gene controls multiple aspects of telencephalic development. Development *127*, 5007–5020.

Costa, R.H., Grayson, D.R., and Darnell, J.E. (1989). Multiple hepatocyte-enriched nuclear factors function in the regulation of transthyretin and alpha 1-antitrypsin genes. Molecular and Cellular Biology *9*, 1415–1425.

Crittenden, J.R., and Graybiel, A.M. (2011). Basal Ganglia disorders associated with imbalances in the striatal striosome and matrix compartments. Front Neuroanat *5*, 59.

Crittenden, J.R., Tillberg, P.W., Riad, M.H., Shima, Y., Gerfen, C.R., Curry, J., Housman, D.E., Nelson, S.B., Boyden, E.S., and Graybiel, A.M. (2016). Striosome-dendron bouquets highlight a unique striatonigral circuit targeting dopamine-containing neurons. Proc. Natl. Acad. Sci. U.S.a. *113*, 11318–11323.

Cui, G., Jun, S.B., Jin, X., Pham, M.D., Vogel, S.S., Lovinger, D.M., and Costa, R.M. (2013). Concurrent activation of striatal direct and indirect pathways during action initiation. Nature *494*, 238–242.

Dasen, J.S., De Camilli, A., Wang, B., Tucker, P.W., and Jessell, T.M. (2008). Hox repertoires for motor neuron diversity and connectivity gated by a single accessory factor, FoxP1. Cell *134*, 304–316.

Day, M., Wokosin, D., Plotkin, J.L., Tian, X., and Surmeier, D.J. (2008). Differential excitability and modulation of striatal medium spiny neuron dendrites. J. Neurosci. *28*, 11603–11614.

Deacon, R.M.J. (2006). Assessing nest building in mice. Nat Protoc *1*, 1117–1119.

Demontis, D., Walters, R.K., Martin, J., Mattheisen, M., Als, T.D., Agerbo, E., Baldursson, G., Belliveau, R., Bybjerg-Grauholm, J., Bækvad-Hansen, M., et al. (2019). Discovery of the first genome-wide significant risk loci for attention deficit/hyperactivity disorder. Nat Genet *51*, 63–75.

Dobin, A., Davis, C.A., Schlesinger, F., Drenkow, J., Zaleski, C., Jha, S., Batut, P., Chaisson, M., and Gingeras, T.R. (2013). STAR: ultrafast universal RNA-seq aligner. Bioinformatics *29*, 15–21.

Durieux, P.F., Bearzatto, B., Guiducci, S., Buch, T., Waisman, A., Zoli, M., Schiffmann, S.N., and de Kerchove d'Exaerde, A. (2009). D2R striatopallidal neurons inhibit both locomotor and drug reward processes. Nat Neurosci *12*, 393–395.

Ehrman, L.A., Mu, X., Waclaw, R.R., Yoshida, Y., Vorhees, C.V., Klein, W.H., and Campbell, K. (2013). The LIM homeobox gene Isl1 is required for the correct development of the striatonigral pathway in the mouse. Proc. Natl. Acad. Sci. U.S.a. *110*, E4026–E4035.

Ernst, A., Alkass, K., Bernard, S., Salehpour, M., Perl, S., Tisdale, J., Possnert, G., Druid, H., and Frisén, J. (2014). Neurogenesis in the Striatum of the Adult Human Brain. Cell *156*, 1072–1083.

Feng, X., Ippolito, G.C., Tian, L., Wiehagen, K., Oh, S., Sambandam, A., Willen, J., Bunte, R.M., Maika, S.D., Harriss, J.V., et al. (2010). Foxp1 is an essential transcriptional regulator for the generation of quiescent naive T cells during thymocyte development. Blood *115*, 510–518.

Ferland, R.J., Cherry, T.J., Preware, P.O., Morrisey, E.E., and Walsh, C.A. (2003). Characterization of Foxp2 and Foxp1 mRNA and protein in the developing and mature brain. J. Comp. Neurol. *460*, 266–279.

Feuk, L., Kalervo, A., Lipsanen-Nyman, M., Skaug, J., Nakabayashi, K., Finucane, B., Hartung, D., Innes, M., Kerem, B., Nowaczyk, M.J., et al. (2006). Absence of a paternally inherited FOXP2 gene in developmental verbal dyspraxia. The American Journal of Human Genetics *79*, 965–972.

Fischbach, G.D., and Lord, C. (2010). The Simons Simplex Collection: a resource for identification of autism genetic risk factors. Neuron *68*, 192–195.

Fisher, S.E., Vargha-Khadem, F., Watkins, K.E., Monaco, A.P., and Pembrey, M.E. (1998). Localisation of a gene implicated in a severe speech and language disorder. Nat Genet *18*, 168–170.

Fong, W.L., Kuo, H.-Y., Wu, H.-L., Chen, S.-Y., and Liu, F.-C. (2018). Differential and Overlapping Pattern of Foxp1 and Foxp2 Expression in the Striatum of Adult Mouse Brain. Neuroscience *388*, 214–223.

French, C.A., Jin, X., Campbell, T.G., Gerfen, E., Groszer, M., Fisher, S.E., and Costa, R.M. (2012). An aetiological Foxp2 mutation causes aberrant striatal activity and alters plasticity during skill learning. Molecular Psychiatry *17*, 1077–1085.

French, C.A., Groszer, M., Preece, C., Coupe, A.-M., Rajewsky, K., and Fisher, S.E. (2007). Generation of mice with a conditional Foxp2 null allele. Genesis *45*, 440–446.

French, C.A., Vinueza Veloz, M.F., Zhou, K., Peter, S., Fisher, S.E., Costa, R.M., and De Zeeuw, C.I. (2019). Differential effects of Foxp2 disruption in distinct motor circuits. Molecular Psychiatry *24*, 447–462.

Friedman, A., Homma, D., Gibb, L.G., Amemori, K.-I., Rubin, S.J., Hood, A.S., Riad, M.H., and Graybiel, A.M. (2015). A Corticostriatal Path Targeting Striosomes Controls Decision-Making under Conflict. Cell *161*, 1320–1333.

Fröhlich, H., Rafiullah, R., Schmitt, N., Abele, S., and Rappold, G.A. (2017). Foxp1 expression is essential for sex-specific murine neonatal ultrasonic vocalization. Hum. Mol. Genet. *26*, 1511–1521.

Fuccillo, M.V. (2016). Striatal Circuits as a Common Node for Autism Pathophysiology. Front Neurosci *10*, 27.

Fujita, E., Tanabe, Y., Shiota, A., Ueda, M., Suwa, K., Momoi, M.Y., and Momoi, T. (2008). Ultrasonic vocalization impairment of Foxp2 (R552H) knockin mice related to speech-language disorder and abnormality of Purkinje cells. Proc. Natl. Acad. Sci. U.S.a. *105*, 3117–3122.

Gallo, E.F., Salling, M.C., Feng, B., Morón, J.A., Harrison, N.L., Javitch, J.A., and Kellendonk, C. (2015). Upregulation of dopamine D2 receptors in the nucleus accumbens indirect pathway increases locomotion but does not reduce alcohol consumption. Neuropschopharmacology *40*, 1609–1618.

García-Avilés, Á., Albert-Gascó, H., Arnal-Vicente, I., Elhajj, E., Sanjuan-Arias, J., Sanchez-Perez, A.M., and Olucha-Bordonau, F. (2015). Acute oral administration of low doses of methylphenidate targets calretinin neurons in the rat septal area. Front Neuroanat *9*, 33.

Garel, S., Marín, F., Grosschedl, R., and Charnay, P. (1999). Ebf1 controls early cell differentiation in the embryonic striatum. Development *126*, 5285–5294.

Gerfen, C.R., and Bolam, J.P. (2016). The Neuroanatomical Organization of the Basal Ganglia. Handbook of Behavioral Neuroscience *24*, 3–32.

Gerfen, C.R., and Surmeier, D.J. (2011). Modulation of Striatal Projection Systems by Dopamine. Annu. Rev. Neurosci. *34*, 441–466.

Gertler, T.S., Chan, C.S., and Surmeier, D.J. (2008). Dichotomous anatomical properties of adult striatal medium spiny neurons. J. Neurosci. *28*, 10814–10824.

Gokce, O., Stanley, G.M., Treutlein, B., Neff, N.F., Camp, J.G., Malenka, R.C., Rothwell, P.E., Fuccillo, M.V., Südhof, T.C., and Quake, S.R. (2016). Cellular Taxonomy of the Mouse Striatum as Revealed by Single-Cell RNA-Seq. CellReports *16*, 1126–1137.

Gong, S., Doughty, M., Harbaugh, C.R., Cummins, A., Hatten, M.E., Heintz, N., and Gerfen, C.R. (2007). Targeting Cre recombinase to specific neuron populations with bacterial artificial chromosome constructs. J. Neurosci. *27*, 9817–9823.

Gong, S., Zheng, C., Doughty, M.L., Losos, K., Didkovsky, N., Schambra, U.B., Nowak, N.J., Joyner, A., Leblanc, G., Hatten, M.E., et al. (2003). A gene expression atlas of the central nervous system based on bacterial artificial chromosomes. Nature *425*, 917–925.

Gorski, J.A., Talley, T., Qiu, M., Puelles, L., Rubenstein, J.L.R., and Jones, K.R. (2002). Cortical excitatory neurons and glia, but not GABAergic neurons, are produced in the Emx1-expressing lineage. J. Neurosci. *22*, 6309–6314.

Graveland, G.A., research, M.D.B., 1985 The frequency and distribution of medium-sized neurons with indented nuclei in the primate and rodent neostriatum. Elsevier.

Groszer, M., Keays, D.A., Deacon, R.M.J., de Bono, J.P., Prasad-Mulcare, S., Gaub, S., Baum, M.G., French, C.A., Nicod, J., Coventry, J.A., et al. (2008). Impaired synaptic plasticity and motor learning in mice with a point mutation implicated in human speech deficits. Curr. Biol. *18*, 354–362.

Hachigian, L.J., Carmona, V., Fenster, R.J., Kulicke, R., Heilbut, A., Sittler, A., Pereira de Almeida, L., Mesirov, J.P., Gao, F., Kolaczyk, E.D., et al. (2017). Control of Huntington's Disease-Associated Phenotypes by the Striatum-Enriched Transcription Factor Foxp2. CellReports *21*, 2688–2695.

Hagimoto, K., Takami, S., Murakami, F., and Tanabe, Y. (2017). Distinct migratory behaviors of striosome and matrix cells underlying the mosaic formation in the developing striatum. J. Comp. Neurol. *525*, 794–817.

Hamdan, F.F., Daoud, H., Rochefort, D., Piton, A., Gauthier, J., Langlois, M., Foomani, G., Dobrzeniecka, S., Krebs, M.-O., Joober, R., et al. (2010). De novo mutations in FOXP1 in cases with intellectual disability, autism, and language impairment. Am. J. Hum. Genet. *87*, 671–678.

Hannenhalli, S., and Kaestner, K.H. (2009). The evolution of Fox genes and their role in development and disease. Nat Rev Genet *10*, 233–240.

Hara, Y., Ago, Y., Taruta, A., Hasebe, S., Kawase, H., Tanabe, W., Tsukada, S., Nakazawa, T., Hashimoto, H., Matsuda, T., et al. (2017). Risperidone and aripiprazole alleviate prenatal valproic acid-induced abnormalities in behaviors and dendritic spine density in mice. Psychopharmacology (Berl.) *234*, 3217–3228.

Hashemi, E., Ariza, J., Rogers, H., Noctor, S.C., and Martínez-Cerdeño, V. (2018). The Number of Parvalbumin-Expressing Interneurons Is Decreased in the Prefrontal Cortex in Autism. Cereb. Cortex *28*, 690–690.

Heiman, M., Schaefer, A., Gong, S., Peterson, J.D., Day, M., Ramsey, K.E., Suárez-Fariñas, M., Schwarz, C., Stephan, D.A., Surmeier, D.J., et al. (2008). A translational profiling approach for the molecular characterization of CNS cell types. Cell *135*, 738–748.

Hisaoka, T., Nakamura, Y., Senba, E., and Morikawa, Y. (2010). The forkhead transcription factors, Foxp1 and Foxp2, identify different subpopulations of projection neurons in the mouse cerebral cortex. Neuroscience *166*, 551–563.

Horn, D., Kapeller, J., Rivera-Brugués, N., Moog, U., Lorenz-Depiereux, B., Eck, S., Hempel, M., Wagenstaller, J., Gawthrope, A., Monaco, A.P., et al. (2010). Identification of FOXP1 deletions in three unrelated patients with mental retardation and significant speech and language deficits. Hum. Mutat. *31*, E1851–E1860.

Hu, H., Wang, B., Borde, M., Nardone, J., Maika, S., Allred, L., Tucker, P.W., and Rao, A. (2006). Foxp1 is an essential transcriptional regulator of B cell development. Nat Immunol *7*, 819–826.

Hunnicutt, B.J., Jongbloets, B.C., Birdsong, W.T., Gertz, K.J., Zhong, H., and Mao, T. (2016). A comprehensive excitatory input map of the striatum reveals novel functional organization. Elife *5*, 9497.

Hurst, J.A., Baraitser, M., Auger, E., Graham, F., and Norell, S. (1990). An extended family with a dominantly inherited speech disorder. Dev Med Child Neurol *32*, 352–355.

Iafrate, A.J., Feuk, L., Rivera, M.N., Listewnik, M.L., Donahoe, P.K., Qi, Y., Scherer, S.W., and Lee, C. (2004). Detection of large-scale variation in the human genome. Nat Genet *36*, 949–951.

Ikegami, M., Uemura, T., Kishioka, A., Sakimura, K., and Mishina, M. (2014). Striatal dopamine D1 receptor is essential for contextual fear conditioning. Sci. Rep. *4*, 1–10.

Iossifov, I., O'Roak, B.J., Sanders, S.J., Ronemus, M., Krumm, N., Levy, D., Stessman, H.A., Witherspoon, K.T., Vives, L., Patterson, K.E., et al. (2014). The contribution of de novo coding mutations to autism spectrum disorder. Nature *515*, 216–221.

Jin, C., Marsden, I., Chen, X., and Liao, X. (1999). Dynamic DNA contacts observed in the NMR structure of winged helix protein-DNA complex. J. Mol. Biol. *289*, 683–690.

Kang, H.J., Kawasawa, Y.I., Cheng, F., Zhu, Y., Xu, X., Li, M., Sousa, A.M.M., Pletikos, M., Meyer, K.A., Sedmak, G., et al. (2011). Spatio-temporal transcriptome of the human brain. Nature *478*, 483–489.

Kelly, S.M., Raudales, R., He, M., Lee, J.H., Kim, Y., Gibb, L.G., Wu, P., Matho, K., Osten, P., Graybiel, A.M., et al. (2018). Radial Glial Lineage Progression and Differential Intermediate Progenitor Amplification Underlie Striatal Compartments and Circuit Organization. Neuron *99*, 345–361.e4.

Kent, W.J., Sugnet, C.W., Furey, T.S., Roskin, K.M., Pringle, T.H., Zahler, A.M., and Haussler, D. (2002). The human genome browser at UCSC. Genome Res. *12*, 996–1006.

Kim, E.J., Battiste, J., Nakagawa, Y., and Johnson, J.E. (2008). Ascl1 (Mash1) lineage cells contribute to discrete cell populations in CNS architecture. Molecular and Cellular Neuroscience *38*, 595–606.

Konopka, G., and Roberts, T.F. (2016). Insights into the Neural and Genetic Basis of Vocal Communication. Cell *164*, 1269–1276.

Koós, T., and Tepper, J.M. (1999). Inhibitory control of neostriatal projection neurons by GABAergic interneurons. Nat Neurosci *2*, 467–472.

Kozorovitskiy, Y., Saunders, A., Johnson, C.A., Lowell, B.B., and Sabatini, B.L. (2012). Recurrent network activity drives striatal synaptogenesis. Nature *485*, 646–650.

Kravitz, A.V., Freeze, B.S., Parker, P.R.L., Kay, K., Thwin, M.T., Deisseroth, K., and Kreitzer, A.C. (2010). Regulation of parkinsonian motor behaviours by optogenetic control of basal ganglia circuitry. Nature *466*, 622–626.

Kreitzer, A.C., and Malenka, R.C. (2007). Endocannabinoid-mediated rescue of striatal LTD and motor deficits in Parkinson's disease models. Nature *445*, 643–647.

Kumar, V., Kim, K., Joseph, C., Kourrich, S., Yoo, S.-H., Huang, H.-C., Vitaterna, M.H., de Villena, F.P.-M., Churchill, G., Bonci, A., et al. (2013). C57BL/6N Mutation in Cytoplasmic FMRP interacting protein 2 Regulates Cocaine Response. Science *342*, 1508–1512.

Laffin, J.J.S., Raca, G., Jackson, C.A., Strand, E.A., Jakielski, K.J., and Shriberg, L.D. (2012). Novel candidate genes and regions for childhood apraxia of speech identified by array comparative genomic hybridization. Genet. Med. *14*, 928–936.

Lai, C.S., Fisher, S.E., Hurst, J.A., Levy, E.R., Hodgson, S., Fox, M., Jeremiah, S., Povey, S., Jamison, D.C., Green, E.D., et al. (2000). The SPCH1 region on human 7q31: genomic characterization of the critical interval and localization of translocations associated with speech and language disorder. The American Journal of Human Genetics *67*, 357–368.

Lai, C.S., Fisher, S.E., Hurst, J.A., Vargha-Khadem, F., and Monaco, A.P. (2001). A forkhead-domain gene is mutated in a severe speech and language disorder. Nature *413*, 519–523.

Lai, C.S.L., Gerrelli, D., Monaco, A.P., Fisher, S.E., and Copp, A.J. (2003). FOXP2 expression during brain development coincides with adult sites of pathology in a severe speech and language disorder. Brain *126*, 2455–2462.

Lai, E., Prezioso, V.R., Smith, E., Litvin, O., Costa, R.H., and Darnell, J.E. (1990). HNF-3A, a hepatocyte-enriched transcription factor of novel structure is regulated transcriptionally. Genes & Development *4*, 1427–1436.

Le Fevre, A.K., Taylor, S., Malek, N.H., Horn, D., Carr, C.W., Abdul-Rahman, O.A., O'Donnell, S., Burgess, T., Shaw, M., Gecz, J., et al. (2013). FOXP1 mutations cause intellectual disability and a recognizable phenotype. Am. J. Med. Genet. *161A*, 3166–3175.

Lee, Y., Kim, H., Kim, J.-E., Park, J.-Y., Choi, J., Lee, J.-E., Lee, E.-H., and Han, P.-L. (2018). Excessive D1 Dopamine Receptor Activation in the Dorsal Striatum Promotes Autistic-Like Behaviors. Mol. Neurobiol. *55*, 5658–5671.

Lennon, P.A., Cooper, M.L., Peiffer, D.A., Gunderson, K.L., Patel, A., Peters, S., Cheung, S.W., and Bacino, C.A. (2007). Deletion of 7q31.1 supports involvement of FOXP2 in language impairment: clinical report and review. Am. J. Med. Genet. *143A*, 791–798.

Li, H., Handsaker, B., Wysoker, A., Fennell, T., Ruan, J., Homer, N., Marth, G., Abecasis, G., and Durbin, R. (2009). The Sequence Alignment/Map format and SAMtools. Bioinformatics *25*, 2078–2079.

Li, S., Weidenfeld, J., and Morrisey, E.E. (2003). Transcriptional and DNA Binding Activity of the Foxp1/2/4 Family Is Modulated by Heterotypic and Homotypic Protein Interactions. Molecular and Cellular Biology *24*, 809–822.

Li, M., Santpere, G., Imamura Kawasawa, Y., Evgrafov, O.V., Gulden, F.O., Pochareddy, S., Sunkin, S.M., Li, Z., Shin, Y., Zhu, Y., et al. (2018). Integrative functional genomic analysis of human brain development and neuropsychiatric risks. Science *362*, 7615.

Li, S., Wang, Y., Zhang, Y., Lu, M.M., DeMayo, F.J., Dekker, J.D., Tucker, P.W., and Morrisey, E.E. (2012). Foxp1/4 control epithelial cell fate during lung development and regeneration through regulation of anterior gradient 2. Development *139*, 2500–2509.

Li, S., Weidenfeld, J., and Morrisey, E.E. (2004a). Transcriptional and DNA binding activity of the Foxp1/2/4 family is modulated by heterotypic and homotypic protein interactions. Molecular and Cellular Biology *24*, 809–822.

Li, S., Zhou, D., Lu, M.M., and Morrisey, E.E. (2004b). Advanced cardiac morphogenesis does not require heart tube fusion. Science *305*, 1619–1622.

Li, X., Xiao, J., Fröhlich, H., Tu, X., Li, L., Xu, Y., Cao, H., Qu, J., Rappold, G.A., and Chen, J.-G. (2015). Foxp1 regulates cortical radial migration and neuronal morphogenesis in developing cerebral cortex. PLoS ONE *10*, e0127671.

Liao, Y., Smyth, G.K., and Shi, W. (2014). featureCounts: an efficient general purpose program for assigning sequence reads to genomic features. Bioinformatics *30*, 923–930.

Liégeois, F., Baldeweg, T., Connelly, A., Gadian, D.G., Mishkin, M., and Vargha-Khadem, F. (2003). Language fMRI abnormalities associated with FOXP2 gene mutation. Nat Neurosci *6*, 1230–1237.

Lobo, M.K., Covington, H.E., Chaudhury, D., Friedman, A.K., Sun, H., Damez-Werno, D., Dietz, D.M., Zaman, S., Koo, J.W., Kennedy, P.J., et al. (2010). Cell type-specific loss of BDNF signaling mimics optogenetic control of cocaine reward. Science *330*, 385–390.

Lobo, M.K., Karsten, S.L., Gray, M., Geschwind, D.H., and Yang, X.W. (2006a). FACS-array profiling of striatal projection neuron subtypes in juvenile and adult mouse brains. Nat Neurosci *9*, 443–452.

Lobo, M.K., Yeh, C., and Yang, X.W. (2008). Pivotal role of early B-cell factor 1 in development of striatonigral medium spiny neurons in the matrix compartment. J. Neurosci. Res. *86*, 2134–2146.

Long, J.E., Swan, C., Liang, W.S., Cobos, I., Potter, G.B., and Rubenstein, J.L.R. (2009). Dlx1&2 and Mash1 transcription factors control striatal patterning and differentiation through parallel and overlapping pathways. J. Comp. Neurol. *512*, 556–572.

Lu, K.-M., Evans, S.M., Hirano, S., and Liu, F.-C. (2014). Dual role for Islet-1 in promoting striatonigral and repressing striatopallidal genetic programs to specify striatonigral cell identity. Proc. Natl. Acad. Sci. U.S.a. *111*, E168–E177.

Lu, M.M., Li, S., Yang, H., and Morrisey, E.E. (2002). Foxp4: a novel member of the Foxp subfamily of winged-helix genes co-expressed with Foxp1 and Foxp2 in pulmonary and gut tissues. Mech. Dev. *119 Suppl 1*, S197–S202.

MacDermot, K.D., Bonora, E., Sykes, N., Coupe, A.-M., Lai, C.S.L., Vernes, S.C., Vargha-Khadem, F., McKenzie, F., Smith, R.L., Monaco, A.P., et al. (2005). Identification of FOXP2 truncation as a novel cause of developmental speech and language deficits. The American Journal of Human Genetics *76*, 1074–1080.

Malach, R., and Graybiel, A.M. (1986). Mosaic architecture of the somatic sensory-recipient sector of the cat's striatum. Journal of Neuroscience *6*, 3436–3458.

Martín-Ibáñez, R., Pardo, M., Giralt, A., Miguez, A., Guardia, I., Marion-Poll, L., Herranz, C., Esgleas, M., Garcia-Díaz Barriga, G., Edel, M.J., et al. (2017). Helios expression

coordinates the development of a subset of striatopallidal medium spiny neurons. Development *144*, 1566–1577.

Maze, I., Chaudhury, D., Dietz, D.M., Schimmelmann, Von, M., Kennedy, P.J., Lobo, M.K., Sillivan, S.E., Miller, M.L., Bagot, R.C., Sun, H., et al. (2014). G9a influences neuronal subtype specification in striatum. Nat Neurosci *17*, 533–539.

Meerschaut, I., Rochefort, D., Revençu, N., Pètre, J., Corsello, C., Rouleau, G.A., Hamdan, F.F., Michaud, J.L., Morton, J., Radley, J., et al. (2017). FOXP1-related intellectual disability syndrome: a recognisable entity. J. Med. Genet. *54*, 613–623.

Miller, J.A., Ding, S.-L., Sunkin, S.M., Smith, K.A., Ng, L., Szafer, A., Ebbert, A., Riley, Z.L., Royall, J.J., Aiona, K., et al. (2014). Transcriptional landscape of the prenatal human brain. Nature *508*, 199–206.

Modat, M., Cash, D.M., Daga, P., Winston, G.P., Duncan, J.S., and Ourselin, S. (2014). Global image registration using a symmetric block-matching approach. J Med Imaging (Bellingham) *1*, 024003.

Moralli, D., Nudel, R., Chan, M.T.M., Green, C.M., Volpi, E.V., Benítez-Burraco, A., Newbury, D.F., and García-Bellido, P. (2015). Language impairment in a case of a complex chromosomal rearrangement with a breakpoint downstream of FOXP2. Mol Cytogenet *8*, 36.

Murugan, M., Harward, S., Scharff, C., and Mooney, R. (2013). Diminished FoxP2 Levels Affect Dopaminergic Modulation of Corticostriatal Signaling Important to Song Variability. Neuron *80*, 1464–1476.

Mutlu-Albayrak, H., and Karaer, K. (2019). Vocal cord immobility as a cause of aphonia in a child with 3p13p12 deletion syndrome encompassing FOXP1 gene. International Journal of Pediatric Otorhinolaryngology *117*, 179–181.

O'Roak, B.J., Deriziotis, P., Lee, C., Vives, L., Schwartz, J.J., Girirajan, S., Karakoc, E., MacKenzie, A.P., Ng, S.B., Baker, C., et al. (2011). Exome sequencing in sporadic autism spectrum disorders identifies severe de novo mutations. Nat Genet *43*, 585–589.

Oh, S.W., Harris, J.A., Ng, L., Winslow, B., Cain, N., Mihalas, S., Wang, Q., Lau, C., Kuan, L., Henry, A.M., et al. (2016). A mesoscale connectome of the mouse brain. Nature *508*, 207–214.

Onorati, M., Castiglioni, V., Biasci, D., Cesana, E., Menon, R., Vuono, R., Talpo, F., Laguna Goya, R., Lyons, P.A., Bulfamante, G.P., et al. (2014). Molecular and functional definition of the developing human striatum. Nat Neurosci *17*, 1804–1815.

Palka, C., Alfonsi, M., Mohn, A., Cerbo, R., Guanciali Franchi, P., Fantasia, D., Morizio, E., Stuppia, L., Calabrese, G., Zori, R., et al. (2012). Mosaic 7q31 deletion involving FOXP2 gene associated with language impairment. Pediatrics *129*, e183–e188.

Palumbo, O., D'Agruma, L., Minenna, A.F., Palumbo, P., Stallone, R., Palladino, T., Zelante, L., and Carella, M. (2013). 3p14.1 de novo microdeletion involving the FOXP1 gene in an adult patient with autism, severe speech delay and deficit of motor coordination. Gene *516*, 107–113.

Pariani, M.J., Spencer, A., Graham, J.M., and Rimoin, D.L. (2009). A 785kb deletion of 3p14.1p13, including the FOXP1 gene, associated with speech delay, contractures, hypertonia and blepharophimosis. European Journal of Medical Genetics *52*, 123–127.

Pearson, C.A., Moore, D., Tucker, H., Dekker, J., Hu, H., Miquelajáuregui, A., and Novitch, B. (2018). Foxp1 controls neural stem cell competence and bias towards deep layer cortical fate. bioRxiv 386276.

Peixoto, R.T., Wang, W., Croney, D.M., Kozorovitskiy, Y., and Sabatini, B.L. (2016). Early hyperactivity and precocious maturation of corticostriatal circuits in Shank3B(-/-) mice. Nat Neurosci *19*, 716–724.

Petryszyn, S., Beaulieu, J.-M., Parent, A., and Parent, M. (2014). Distribution and morphological characteristics of striatal interneurons expressing calretinin in mice: a comparison with human and nonhuman primates. J. Chem. Neuroanat. *59-60*, 51–61.

Precious, S.V., Kelly, C.M., Reddington, A.E., Vinh, N.N., Stickland, R.C., Pekarik, V., Scherf, C., Jeyasingham, R., Glasbey, J., Holeiter, M., et al. (2016). FoxP1 marks medium spiny neurons from precursors to maturity and is required for their differentiation. Exp. Neurol. *282*, 9–18.

Ragan, T., Kadiri, L.R., Venkataraju, K.U., Bahlmann, K., Sutin, J., Taranda, J., Arganda-Carreras, I., Kim, Y., Seung, H.S., and Osten, P. (2012). Serial two-photon tomography for automated ex vivo mouse brain imaging. Nat. Methods *9*, 255–258.

Rapanelli, M., Frick, L.R., and Pittenger, C. (2017). The Role of Interneurons in Autism and Tourette Syndrome. Trends in Neurosciences *40*, 397–407.

Reuter, M.S., Riess, A., Moog, U., Briggs, T.A., Chandler, K.E., Rauch, A., Stampfer, M., Steindl, K., Gläser, D., Joset, P., et al. (2017). FOXP2 variants in 14 individuals with developmental speech and language disorders broaden the mutational and clinical spectrum. J. Med. Genet. *54*, 64–72.

Revishchin, A.V., Okhotin, V.E., and Pavlova, G.V. (2010). New Calretinin-Positive Cells with Polymorphous Spines in the Mouse Forebrain during Early Postnatal Ontogeny. Neurosci Behav Physi *40*, 833–840.

Rice, G.M., Raca, G., Jakielski, K.J., Laffin, J.J., Iyama-Kurtycz, C.M., Hartley, S.L., Sprague, R.E., Heintzelman, A.T., and Shriberg, L.D. (2012). Phenotype of FOXP2 haploinsufficiency in a mother and son. Am. J. Med. Genet. *158A*, 174–181.

Rieger, M.A., and Dougherty, J.D. (2016). Analysis of within Subjects Variability in Mouse Ultrasonic Vocalization: Pups Exhibit Inconsistent, State-Like Patterns of Call Production. Front Behav Neurosci *10*, 182.

Rousso, D.L., Gaber, Z.B., Wellik, D., Morrisey, E.E., and Novitch, B.G. (2008). Coordinated actions of the forkhead protein Foxp1 and Hox proteins in the columnar organization of spinal motor neurons. Neuron *59*, 226–240.

Rousso, D.L., Pearson, C.A., Gaber, Z.B., Miquelajáuregui, A., Li, S., Portera-Cailliau, C., Morrisey, E.E., and Novitch, B.G. (2012). Foxp-mediated suppression of N-cadherin regulates neuroepithelial character and progenitor maintenance in the CNS. Neuron *74*, 314–330.

Royer, L.A., Weigert, M., Günther, U., Maghelli, N., Jug, F., Sbalzarini, I.F., and Myers, E.W. (2015). ClearVolume: open-source live 3D visualization for light-sheet microscopy. Nat. Methods *12*, 480–481.

Saleem, R.A., Banerjee-Basu, S., Berry, F.B., Baxevanis, A.D., and Walter, M.A. (2003). Structural and functional analyses of disease-causing missense mutations in the forkhead domain of FOXC1. Hum. Mol. Genet. *12*, 2993–3005.

Sano, H., Yasoshima, Y., Matsushita, N., Kaneko, T., Kohno, K., Pastan, I., and Kobayashi, K. (2003). Conditional ablation of striatal neuronal types containing dopamine D2 receptor disturbs coordination of basal ganglia function. J. Neurosci. *23*, 9078–9088.

Satterstrom, F.K., Kosmicki, J.A., Wang, J., Breen, M.S., De Rubeis, S., An, J.-Y., Peng, M., Collins, R.L., Grove, J., Klei, L., et al. (2018). Novel genes for autism implicate both excitatory and inhibitory cell lineages in risk. bioRxiv 484113.

Saunders, A., Macosko, E.Z., Wysoker, A., Goldman, M., Krienen, F.M., de Rivera, H., Bien, E., Baum, M., Bortolin, L., Wang, S., et al. (2018). Molecular Diversity and Specializations among the Cells of the Adult Mouse Brain. Cell *174*, 1015–1030.e1016.

Sebastianutto, I., Cenci, M.A., and Fieblinger, T. (2017). Alterations of striatal indirect pathway neurons precede motor deficits in two mouse models of Huntington's disease. Neurobiology of Disease *105*, 117–131.

Shema, R., Kulicke, R., Cowley, G.S., Stein, R., Root, D.E., and Heiman, M. (2015). Synthetic lethal screening in the mammalian central nervous system identifies Gpx6 as a modulator of Huntington’s disease. Proceedings of the National Academy of Sciences *112*, 268–272.

Shriberg, L.D., Ballard, K.J., Tomblin, J.B., Duffy, J.R., Odell, K.H., and Williams, C.A. (2006). Speech, prosody, and voice characteristics of a mother and daughter with a 7;13 translocation affecting FOXP2. J. Speech Lang. Hear. Res. *49*, 500–525.

Shu, W., Yang, H., Zhang, L., Lu, M.M., and Morrisey, E.E. (2001). Characterization of a new subfamily of winged-helix/forkhead (Fox) genes that are expressed in the lung and act as transcriptional repressors. Journal of Biological Chemistry *276*, 27488–27497.

Shu, W., Cho, J.Y., Jiang, Y., Zhang, M., Weisz, D., Elder, G.A., Schmeidler, J., De Gasperi, R., Sosa, M.A.G., Rabidou, D., et al. (2005). Altered ultrasonic vocalization in mice with a disruption in the Foxp2 gene. Proceedings of the National Academy of Sciences *102*, 9643–9648.

Silverman, J.L., Yang, M., Lord, C., and Crawley, J.N. (2010). Behavioural phenotyping assays for mouse models of autism. Nature Publishing Group *11*, 490–502.

Siper, P.M., De Rubeis, S., Trelles, M.D.P., Durkin, A., Di Marino, D., Muratet, F., Frank, Y., Lozano, R., Eichler, E.E., Kelly, M., et al. (2017). Prospective investigation of FOXP1 syndrome. Molecular Autism *8*, 57.

Skene, N.G., and Grant, S.G.N. (2016). Identification of Vulnerable Cell Types in Major Brain Disorders Using Single Cell Transcriptomes and Expression Weighted Cell Type Enrichment. Front Neurosci *10*, 16.

Smith, J.B., Klug, J.R., Ross, D.L., Howard, C.D., Hollon, N.G., Ko, V.I., Hoffman, H., Callaway, E.M., Gerfen, C.R., and Jin, X. (2016). Genetic-Based Dissection Unveils the Inputs and Outputs of Striatal Patch and Matrix Compartments. Neuron *91*, 1069–1084.

Smith, T.S., Heger, A., and Sudbery, I. (2017). UMI-tools: Modelling sequencing errors in Unique Molecular Identifiers to improve quantification accuracy. Genome Res. *27*, gr.209601.116–gr.209601.499.

Sollis, E., Deriziotis, P., Saitsu, H., Miyake, N., Matsumoto, N., Hoffer, M.J.V., Ruivenkamp, C.A.L., Alders, M., Okamoto, N., Bijlsma, E.K., et al. (2017). Equivalent missense variant in the FOXP2 and FOXP1 transcription factors causes distinct neurodevelopmental disorders. Hum. Mutat. *38*, 1542–1554.

Sollis, E., Graham, S.A., Vino, A., Froehlich, H., Vreeburg, M., Dimitropoulou, D., Gilissen, C., Pfundt, R., Rappold, G.A., Brunner, H.G., et al. (2016). Identification and functional characterization of de novo FOXP1variants provides novel insights into the etiology of neurodevelopmental disorder. Hum. Mol. Genet. *25*, 546–557.

Sommer, C., Straehle, C., Koethe, U., and Hamprecht, F.A. (2011). Ilastik: Interactive learning and segmentation toolkit. pp. 230–233.

Song, H., Makino, Y., Noguchi, E., and Arinami, T. (2015). A case report of de novo missense FOXP1 mutation in a non-Caucasian patient with global developmental delay and severe speech impairment. Clin Case Rep *3*, 110–113.

Spiteri, E., Konopka, G., Coppola, G., Bomar, J., Oldham, M., Ou, J., Vernes, S.C., Fisher, S.E., Ren, B., and Geschwind, D.H. (2007). Identification of the transcriptional

targets of FOXP2, a gene linked to speech and language, in developing human brain. Am. J. Hum. Genet. *81*, 1144–1157.

Stessman, H.A.F., Xiong, B., Coe, B.P., Wang, T., Hoekzema, K., Fenckova, M., Kvarnung, M., Gerdts, J., Trinh, S., Cosemans, N., et al. (2017). Targeted sequencing identifies 91 neurodevelopmental-disorder risk genes with autism and developmental-disability biases. Nat Genet *49*, 515–526.

Stroud, J.C., Wu, Y., Bates, D.L., Han, A., Nowick, K., PAAbo, S., Tong, H., and Chen, L. (2006). Structure of the forkhead domain of FOXP2 bound to DNA. Structure *14*, 159–166.

Takahashi, K., Liu, F.-C., Hirokawa, K., and Takahashi, H. (2003). Expression of Foxp2, a gene involved in speech and language, in the developing and adult striatum. J. Neurosci. Res. *73*, 61–72.

Takahashi, K., Liu, F.-C., Hirokawa, K., and Takahashi, H. (2008). Expression of Foxp4 in the developing and adult rat forebrain. J. Neurosci. Res. *86*, 3106–3116.

Takata, A., Miyake, N., Tsurusaki, Y., Fukai, R., Miyatake, S., Koshimizu, E., Kushima, I., Okada, T., Morikawa, M., Uno, Y., et al. (2018). Integrative Analyses of De Novo Mutations Provide Deeper Biological Insights into Autism Spectrum Disorder. CellReports *22*, 734–747.

Talkowski, M.E., Rosenfeld, J.A., Blumenthal, I., Pillalamarri, V., Chiang, C., Heilbut, A., Ernst, C., Hanscom, C., Rossin, E., Lindgren, A.M., et al. (2012). Sequencing chromosomal abnormalities reveals neurodevelopmental loci that confer risk across diagnostic boundaries. Cell *149*, 525–537.

Tam, W.Y., Leung, C.K.Y., Tong, K.K., and Kwan, K.M. (2011). Foxp4 is essential in maintenance of Purkinje cell dendritic arborization in the mouse cerebellum. Neuroscience *172*, 562–571.

Tamura, S., Morikawa, Y., Iwanishi, H., Hisaoka, T., and Senba, E. (2004). Foxp1 gene expression in projection neurons of the mouse striatum. Nsc *124*, 261–267.

Tamura, S., Morikawa, Y., Iwanishi, H., Hisaoka, T., and Senba, E. (2003). Expression pattern of the winged-helix/forkhead transcription factor Foxp1 in the developing central nervous system. Gene Expression Patterns *3*, 193–197.

Tang, B., Becanovic, K., Desplats, P.A., Spencer, B., Hill, A.M., Connolly, C., Masliah, E., Leavitt, B.R., and Thomas, E.A. (2012). Forkhead box protein p1 is a transcriptional repressor of immune signaling in the CNS: implications for transcriptional dysregulation in Huntington disease. Hum. Mol. Genet. *21*, 3097–3111.

Tasic, B., Menon, V., Nguyen, T.N., Kim, T.K., Jarsky, T., Yao, Z., Levi, B., Gray, L.T., Sorensen, S.A., Dolbeare, T., et al. (2016). Adult mouse cortical cell taxonomy revealed by single cell transcriptomics. Nat Neurosci *19*, 335–346.

Taverna, S., Ilijic, E., and Surmeier, D.J. (2008). Recurrent collateral connections of striatal medium spiny neurons are disrupted in models of Parkinson's disease. J. Neurosci. *28*, 5504–5512.

Tecuapetla, F., Jin, X., Lima, S.Q., and Costa, R.M. (2016). Complementary Contributions of Striatal Projection Pathways to Action Initiation and Execution. Cell *166*, 703–715.

Tecuapetla, F., Koós, T., Tepper, J.M., Kabbani, N., and Yeckel, M.F. (2009). Differential dopaminergic modulation of neostriatal synaptic connections of striatopallidal axon collaterals. J. Neurosci. *29*, 8977–8990.

Tepper, J.M., Sharpe, N.A., Koós, T.Z., and Trent, F. (1998). Postnatal development of the rat neostriatum: electrophysiological, light- and electron-microscopic studies. Dev. Neurosci. *20*, 125–145.

Tepper, J.M., Koós, T., Ibanez-Sandoval, O., Tecuapetla, F., Faust, T.W., and Assous, M. (2018). Heterogeneity and Diversity of Striatal GABAergic Interneurons: Update 2018. Front Neuroanat *12*, 91.

Thevenon, J., Monnier, N., Callier, P., Dieterich, K., Francoise, M., Montgomery, T., Kjaergaard, S., Neas, K., Dixon, J., Dahm, T.L., et al. (2014). Delineation of the 3p14.1p13 microdeletion associated with syndromic distal limb contractures. Am. J. Med. Genet. *164A*, 3027–3034.

Thibault, D., Loustalot, F., Fortin, G.M., Bourque, M.-J., and Trudeau, L.-É. (2013). Evaluation of D1 and D2 dopamine receptor segregation in the developing striatum using BAC transgenic mice. PLoS ONE *8*, e67219.

Tinterri, A., Menardy, F., Diana, M.A., Lokmane, L., Keita, M., Coulpier, F., Lemoine, S., Mailhes, C., Mathieu, B., Merchan-Sala, P., et al. (2018). Active intermixing of indirect and direct neurons builds the striatal mosaic. Nature Communications *9*, 4725.

Tomblin, J.B., O'Brien, M., Shriberg, L.D., Williams, C., Murray, J., Patil, S., Bjork, J., Anderson, S., and Ballard, K. (2009). Language features in a mother and daughter of a chromosome 7;13 translocation involving FOXP2. J. Speech Lang. Hear. Res. *52*, 1157–1174.

Toresson, H., Potter, S.S., and Campbell, K. (2000). Genetic control of dorsal-ventral identity in the telencephalon: opposing roles for Pax6 and Gsh2. Development *127*, 4361–4371.

Tsai, K.-L., Huang, C.-Y., Chang, C.-H., Sun, Y.-J., Chuang, W.-J., and Hsiao, C.-D. (2006). Crystal structure of the human FOXK1a-DNA complex and its implications on the diverse binding specificity of winged helix/forkhead proteins. Journal of Biological Chemistry *281*, 17400–17409.

Tsai, P.T., Hull, C., Chu, Y., Greene-Colozzi, E., Sadowski, A.R., Leech, J.M., Steinberg, J., Crawley, J.N., Regehr, W.G., and Sahin, M. (2012). Autistic-like behaviour and cerebellar dysfunction in Purkinje cell Tsc1 mutant mice. Nature *488*, 647–651.

Tsuchioka, A., Oana, F., Suzuki, T., Yamauchi, Y., Ijiro, T., Kaidoh, K., and Hiratochi, M. (2015). Duration of drug action of dopamine D2 agonists in mice with 6-hydroxydopamine-induced lesions. Neuroreport *26*, 1126–1132.

Tunstall, M.J., Oorschot, D.E., Kean, A., and Wickens, J.R. (2002). Inhibitory interactions between spiny projection neurons in the rat striatum. J. Neurophysiol. *88*, 1263–1269.

Turner, S.J., Hildebrand, M.S., Block, S., Damiano, J., Fahey, M., Reilly, S., Bahlo, M., Scheffer, I.E., and Morgan, A.T. (2013). Small intragenic deletion in FOXP2 associated with childhood apraxia of speech and dysarthria. Am. J. Med. Genet. *161A*, 2321–2326.

Turner, T.N., Coe, B.P., Dickel, D.E., Hoekzema, K., Nelson, B.J., Zody, M.C., Kronenberg, Z.N., Hormozdiari, F., Raja, A., Pennacchio, L.A., et al. (2017a). Genomic Patterns of De Novo Mutation in Simplex Autism. Cell *171*, 710–722.e712.

Turner, T.N., Yi, Q., Krumm, N., Huddleston, J., Hoekzema, K., F Stessman, H.A., Doebley, A.-L., Bernier, R.A., Nickerson, D.A., and Eichler, E.E. (2017b). denovo-db: a compendium of human de novo variants. Nucleic Acids Res. *45*, D804–D811.

Urreizti, R., Damanti, S., Esteve, C., Franco-Valls, H., Castilla-Vallmanya, L., Tonda, R., Cormand, B., Vilageliu, L., Opitz, J.M., Neri, G., et al. (2018). A De Novo FOXP1 Truncating Mutation in a Patient Originally Diagnosed as C Syndrome. Sci. Rep. *8*, 694.

Usui, N., Araujo, D.J., Kulkarni, A., Co, M., Ellegood, J., Harper, M., Toriumi, K., Lerch, J.P., and Konopka, G. (2017a). Foxp1 regulation of neonatal vocalizations via cortical development. Genes & Development *31*, 2039–2055.

Usui, N., Co, M., Harper, M., Rieger, M.A., Dougherty, J.D., and Konopka, G. (2017b). Sumoylation of FOXP2 Regulates Motor Function and Vocal Communication Through Purkinje Cell Development. Biological Psychiatry *81*, 220–230.

Vargha-Khadem, F., Watkins, K.E., Price, C.J., Ashburner, J., Alcock, K.J., Connelly, A., Frackowiak, R.S., Friston, K.J., Pembrey, M.E., Mishkin, M., et al. (1998). Neural basis of an inherited speech and language disorder. Proceedings of the National Academy of Sciences *95*, 12695–12700.

Vargha-Khadem, F., Watkins, K., Alcock, K., Fletcher, P., and Passingham, R. (1995). Praxic and nonverbal cognitive deficits in a large family with a genetically transmitted speech and language disorder. Proceedings of the National Academy of Sciences *92*, 930–933.

Vargha-Khadem, F., Gadian, D.G., Copp, A., and Mishkin, M. (2005). FOXP2 and the neuroanatomy of speech and language. Nat Rev Neurosci *6*, 131–138.

Vernes, S.C., MacDermot, K.D., Monaco, A.P., and Fisher, S.E. (2009). Assessing the impact of FOXP1 mutations on developmental verbal dyspraxia. European Journal of Human Genetics *17*, 1354–1358.

Vernes, S.C., Newbury, D.F., Abrahams, B.S., Winchester, L., Nicod, J., Groszer, M., Alarcón, M., Oliver, P.L., Davies, K.E., Geschwind, D.H., et al. (2008). A functional genetic link between distinct developmental language disorders. N. Engl. J. Med. *359*, 2337–2345.

Vernes, S.C., Nicod, J., Elahi, F.M., Coventry, J.A., Kenny, N., Coupe, A.-M., Bird, L.E., Davies, K.E., and Fisher, S.E. (2006). Functional genetic analysis of mutations implicated in a human speech and language disorder. Hum. Mol. Genet. *15*, 3154–3167.

Vernes, S.C., Oliver, P.L., Spiteri, E., Lockstone, H.E., Puliyadi, R., Taylor, J.M., Ho, J., Mombereau, C., Brewer, A., Lowy, E., et al. (2011). Foxp2 regulates gene networks implicated in neurite outgrowth in the developing brain. PLoS Genet *7*, e1002145.

Viana, T.G., Almeida-Santos, A.F., Aguiar, D.C., and Moreira, F.A. (2013). Effects of aripiprazole, an atypical antipsychotic, on the motor alterations induced by acute ethanol administration in mice. Basic Clin. Pharmacol. Toxicol. *112*, 319–324.

Vuillaume, M.L., Cogné, B., Jeanne, M., Boland, A., Ung, D.C., Quinquis, D., Besnard, T., Deleuze, J.F., Redon, R., Bézieau, S., et al. (2018). Whole genome sequencing identifies a de novo 2.1 Mb balanced paracentric inversion disrupting FOXP1 and leading to severe intellectual disability. Clinica Chimica Acta *485*, 218–223.

Waclaw, R.R., Ehrman, L.A., Merchan-Sala, P., Kohli, V., Nardini, D., and Campbell, K. (2017). Foxo1 is a downstream effector of Isl1 in direct pathway striatal projection neuron development within the embryonic mouse telencephalon. Mol. Cell. Neurosci. *80*, 44–51.

Wall, N.R., La Parra, De, M., Callaway, E.M., and Kreitzer, A.C. (2013). Differential innervation of direct- and indirect-pathway striatal projection neurons. Neuron *79*, 347–360.

Wang, B., Lin, D., Li, C., and Tucker, P. (2003). Multiple Domains Define the Expression and Regulatory Properties of Foxp1 Forkhead Transcriptional Repressors. Journal of Biological Chemistry *278*, 24259–24268.

Wang, B., Waclaw, R.R., Allen, Z.J., Guillemot, F., and Campbell, K. (2009). Ascl1 is a required downstream effector of Gsx gene function in the embryonic mouse telencephalon. Neural Dev *4*, 5.

Wang, B., Weidenfeld, J., Lu, M.M., Maika, S., Kuziel, W.A., Morrisey, E.E., and Tucker, P.W. (2004). Foxp1 regulates cardiac outflow tract, endocardial cushion morphogenesis and myocyte proliferation and maturation. Development *131*, 4477–4487.

Watkins, K.E., Dronkers, N.F., and Vargha-Khadem, F. (2002a). Behavioural analysis of an inherited speech and language disorder: comparison with acquired aphasia. Brain *125*, 452–464.

Watkins, K.E., Vargha-Khadem, F., Ashburner, J., Passingham, R.E., Connelly, A., Friston, K.J., Frackowiak, R.S.J., Mishkin, M., and Gadian, D.G. (2002b). MRI analysis of an inherited speech and language disorder: structural brain abnormalities. Brain *125*, 465–478.

Weigel, D., and Jäckle, H. (1990). The fork head domain: a novel DNA binding motif of eukaryotic transcription factors? Cell *63*, 455–456.

Weigel, D., Jürgens, G., Küttner, F., Seifert, E., and Jäckle, H. (1989). The homeotic gene fork head encodes a nuclear protein and is expressed in the terminal regions of the Drosophila embryo. Cell *57*, 645–658.

Wiehagen, K.R., Corbo-Rodgers, E., Li, S., Staub, E.S., Hunter, C.A., Morrisey, E.E., and Maltzman, J.S. (2012). Foxp4 Is Dispensable for T Cell Development, but Required for Robust Recall Responses. PLoS ONE *7*, e42273.

Xu, W., and Südhof, T.C. (2013). A Neural Circuit for Memory Specificity and Generalization. Science *339*, 1290–1295.

Xu, X., Wells, A.B., O'Brien, D.R., Nehorai, A., and Dougherty, J.D. (2014). Cell Type-Specific Expression Analysis to Identify Putative Cellular Mechanisms for Neurogenetic Disorders. Journal of Neuroscience *34*, 1420–1431.

Xu, Z., Liang, Q., Song, X., Zhang, Z., Lindtner, S., Li, Z., Wen, Y., Liu, G., Guo, T., Qi, D., et al. (2018). SP8 and SP9 coordinately promote D2-type medium spiny neuron production by activating Six3 expression. Development *145*, dev165456.

Yamamoto-Shimojima, K., Okamoto, N., Matsumura, W., Okazaki, T., and Yamamoto, T. (2019). Three Japanese patients with 3p13 microdeletions involving FOXP1. Brain Dev. *41*, 257–262.

Yang, Z., You, Y., and Levison, S.W. (2008). Neonatal hypoxic/ischemic brain injury induces production of calretinin-expressing interneurons in the striatum. J. Comp. Neurol. *511*, 19–33.

Yun, K., Potter, S., and Rubenstein, J.L. (2001). Gsh2 and Pax6 play complementary roles in dorsoventral patterning of the mammalian telencephalon. Development *128*, 193–205.

Zeesman, S., Nowaczyk, M.J.M., Teshima, I., Roberts, W., Cardy, J.O., Brian, J., Senman, L., Feuk, L., Osborne, L.R., and Scherer, S.W. (2006). Speech and language impairment and oromotor dyspraxia due to deletion of 7q31 that involves FOXP2. Am. J. Med. Genet. *140*, 509–514.

Zhang, Q., Zhang, Y., Wang, C., Xu, Z., Liang, Q., An, L., Li, J., Liu, Z., You, Y., He, M., et al. (2016). The Zinc Finger Transcription Factor Sp9 Is Required for the Development of Striatopallidal Projection Neurons. CellReports *16*, 1431–1444.

Zhang, Y., Li, S., Yuan, L., Tian, Y., Weidenfeld, J., Yang, J., Liu, F., Chokas, A.L., and Morrisey, E.E. (2010). Foxp1 coordinates cardiomyocyte proliferation through both cell-autonomous and nonautonomous mechanisms. Genes & Development *24*, 1746–1757.

Zheng, G.X.Y., Terry, J.M., Belgrader, P., Ryvkin, P., Bent, Z.W., Wilson, R., Ziraldo, S.B., Wheeler, T.D., McDermott, G.P., Zhu, J., et al. (2017). Massively parallel digital transcriptional profiling of single cells. Nature Communications *8*, 14049.

Ziegler, S.F. (2006). FOXP3: of mice and men. Annu. Rev. Immunol. *24*, 209–226.

Zilina, O., Reimand, T., Zjablovskaja, P., Männik, K., Männamaa, M., Traat, A., Puusepp-Benazzouz, H., Kurg, A., and Ounap, K. (2012). Maternally and paternally inherited deletion of 7q31 involving the FOXP2 gene in two families. Am. J. Med. Genet. *158A*, 254–256.

APPENDIX A. Beyond bulk: a review of single cell transcriptomics methodologies and applications

APPENDIX B. Foxp1 in forebrain pyramidal neurons controls gene expression required for spatial learning and synaptic plasticity